UNITED STATES AIR FORCE
AIR UNIVERSITY
AIR FORCE INSTITUTE OF TECHNOLOGY
Wright-Patterson Air Force Base, Ohio

82 06 14 167

A COMPARATIVE ANALYSIS OF KALMAN FILTERS
USING A HYPERVELOCITY MISSILE SIMULATION

AFIT/GE/EE/81D-13   THESIS

Donald W. Capps   and   Donald C. Nelson
Capt   USAF   Capt   USAF

1981

A COMPARATIVE ANALYSIS OF KALMAN FILTERS
USING A HYPERVELOCITY MISSILE SIMULATION

THESIS

Presented to the Faculty of the School of Engineering

of the Air Force Institute of Technology

in Partial Fulfillment of the Requirements for the

Degree of Master of Science

by

Donald W. Capps, B.S.E.E.

Capt   USAF

and

Donald C. Nelson, B.E.E.

Capt   USAF

Graduate Engineering

December 1981

Preface

This project has provided us with a challenging and rewarding experience. The study was sponsored by the Armament Laboratory, Eglin, AFB, Florida.

We would like to express appreciation to our advisors, Lieutenant Colonel Robert Edwards, Peter Maybeck, and Capt. James Silverthorn. Each has provided us with the needed direction, insight, and technical expertise to allow us to complete the project.

Finally, we would like to thank our wives, Eunice and Donna, and children for their understanding, support, and patience during the long hours involved in this effort.

We would like to thank our typist, Mrs. Janice Roberts, for her skill in typing and proofing technical material.

ii

Table of Contents

Table of Contents

(Continued)

Table of Contents

(Continued)

List of Figures

List of Figures

(Continued)

List of Tables

List of Important Symbols and Abbreviations

Symbol	Description
a	missile acceleration components
A	1. aircraft 2. inertial acceleration
ATLOS	aircraft-to-target, line-of-sight
AZ	azimuth measurement
C	1. rotation matrix 2. drag coefficients
D	drag
EKF	Extended Kalman Filter
EL	elevation measurement
g	gravity
HVM	Hypervelocity Missile
$\hat{i}$	inertial coordinate frame
INS	Inertial Navigation System
$\hat{\underline{k}}$	MTLOS coordinate frame
K	Kalman filter gain matrix
$\hat{\ell}$	ATLOS coordinate frame
LOS	line-of-sight
m	mass
$\hat{m}$	missile velocity frame
M	1. missile 2. mach number

List of Important Symbols and Abbreviations

(continued)

Symbol	Description
MTLOS	missile-to-target, line-of-sight
n	1. time correlated noise 2. guidance law gain constant
P	filter's conditional covariance matrix
Q	descriptor of the strength of the dynamic driving noise
$\underline{r}$	position vector
R	position vector component
t	time
T	1. target 2. thrust
v	measurement noise with descriptor of strength R
V	velocity
w	white Gaussian noise
x	system state variables
x,y,z	components of position vector
z	measurement vector
τ	correlation time constant
Θ, Ψ, λ	Euler angle
ω	angular velocity vector

Abstract

A systematic procedure is used to design Kalman Filters for a hypervelocity missile system. The procedure includes truth model development, state space model formulation, filter tuning, and Monte Carlo analysis. The study is based upon a planar engagement of highly dynamic missile, a constant-velocity aircraft, and a stationary target. Two line-of-sight filters are developed using the rotating aircraft-to-target line-of-sight frame as a reference and two inertial filters are developed using an inertial frame reference. The angle between the aircraft-to-target line-of-sight and the aircraft-to-missile line-of-sight is the only physical measurement processed by the filters. Due to observability considerations, the inertial filters also process additional pseudo-measurements of range. The filters are compared by calculation of miss distance statistics, probability of kill, and computational loading.

A COMPARATIVE ANALYSIS OF KALMAN FILTERS
USING A HYPERVELOCITY MISSILE SIMULATION

I. INTRODUCTION

1.1 Background

The United States Department of Defense has stressed, especially during the last decade, air-to-surface weapon research and development. The motivation for this emphasis comes from a large escalation in the numbers and qualities of tanks deployed by the Warsaw Pact countries. The Soviet Union, in particular, is adding 5000 ground combat vehicles to its inventory each year (Ref. 4). Among these vehicles is the T-64/T-72 series of battle tanks which are superior in quality to any comparable system deployed by NATO (Ref. 4). The buildup in Soviet forces has generated a significant numerical advantage in tanks over the combined NATO forces. The United States and other NATO countries are preparing to meet this threat by relying on anti-tank guided weapons (ATGWs). There are two major development objectives of the types of weapons under consideration. The first is to design weapon systems that can penetrate the comparatively thin upper surfaces of a tank. The other is to use the U.S. advantage in micro-electronics to develop precision-guided munitions (PGMs) with high probabilities of kill. A weapon which has the potential to meet these criteria is the hypervelocity missile (HVM).

The HVM concept incorporates available technologies in the development of a complete weapon system. The objective of the HVM is to defeat advanced armored ground vehicles with small, low cost missiles. The missiles are launched from an advanced fighter aircraft such as an F-16 or A-10. The velocity of the missile is approximately 5000 feet per second and its maximum down-range launch distance is 15,000 feet. The lethal mechanism of the HVM is a nonexplosive,

kinetic energy penetrator. The speed of the missile and its mass results in the kinetic energy necessary to disable the target. A carbon-dioxide laser is deployed on the aircraft to provide simultaneous guidance information to multiple (up to 10) independently-targeted missiles.

Though the primary emphasis of the HVM concept involves achieving a target kill, cost effectiveness and aircraft survivability are primary concerns to the Air Force. Analyses conducted in the Armament Division at Eglin Air Force Base have demonstrated that the HVM shows promise as a future Air Force weapon system. The potential for enhanced aircraft survivability exists since one pass near a target is normally sufficient to disable it. The analyses also demonstrate that the low HVM cost should provide a more cost-effective system. In addition, the increase in kills per aircraft pass should decrease the cost per target killed. These advantages have prompted the Air Force to proceed with feasibility studies and tests to demonstrate the capabilities of the HVM.

1.2 Statement of Problem and Objectives

The tactical missile intercept problem deals with guiding the missile to the target, with imperfect knowledge of target and missile positions. The missile uses information provided by the sensors and the launching aircraft to estimate the necessary information for guidance. The objective of this thesis is to develop this estimation process for the HVM.

The assumption of perfect knowledge of quantities that describe a system is often inadequate. Uncertainties are inherent in any system and their neglect frequently results in degraded performance. Examples of uncertainties that exist in tactical missile engagement are inherent mathematical modeling errors, external disturbances, and measurement errors. These uncertainties are modeled as random

phenomena, thus leading to stochastic equations to describe the system. Stochastic estimation is a method of formulating a best guess of certain state variables of importance based upon noisy observations of the system. The Kalman Filter is the optimal stochastic estimation algorithm for linear dynamical systems subjected to Gaussian noise. Nonlinear systems can often be successfully treated by straight-forward extensions of the Kalman Filter (Ref. 2, 6, 8, 14).

The HVM system requires an extremely high accuracy in order to be an effective weapon. Uncertainties in the system have the potential to degrade performance and thereby thwart the achievement of the desired accuracy. The objective of this study is to design alternative Kalman Filters, which account for the system uncertainties, and to compare their performance in terms of state estimation accuracy, statistics of terminal miss distance, probability of kill, and computational requirements. Due to the use of a kinetic energy penetrator, the probability of kill is also a function of the angle of incidence of the missile with the target. This factor, however, is not modeled in this study since its inclusion has no effect on Kalman Filter design. The angle of incidence would be accounted for in the guidance law formulation, however; this is beyond the scope of this study.

A Kalman Filter is designed for the HVM system based on a systematic approach. The procedure is as follows (Ref. 9:341):

1. Develop and validate a truth model (a complete, complex mathematical model that portrays system behavior very accurately).

2. Generate a Kalman Filter based upon the total truth model. This filter is used as a benchmark of performance in judging other filters.

3. Propose simplified, reduced order system models by removing or combining states associated with nondominant effects, deleting weak cross-coupling terms, and employing approximations. Develop simplified

1-3

filters based on each model.

4. Conduct a covariance performance analysis of each proposed Kalman Filter being driven by measurements from the truth model of the real system. Then tune each filter to provide the best possible performance from each.

5. Perform a Monte Carlo analysis for the filters that show promise.

6. Conduct a performance/computer loading trade-off analysis and select a design; investigate square root and other forms of implementing the chosen design.

7. Implement the chosen design on the online computer to be used in the final system.

8. Perform checkout, final tuning, and operational test of the filter.

The first six steps of the procedure are pursued in this study. Though the approach is difficult and time-consuming, it is cost-effective in that it solves most of the design problems before actual hardware implementation takes place.

1.3 Organization

The six chapters of this thesis closely follow this design procedure. Chapter I provides background information and states the objectives of this study. In Chapter II the system truth model is developed with primary emphasis on the dominant dynamic characteristics of the system. Also included in this chapter are coordinate frame definitions and engagement scenario assumptions. Chapter III contains the development of the four Kalman Filters which are to be investigated. Chapter IV discusses the implementation of the models

into a computer simulation. In addition, truth model and filter validation are discussed. The analysis of the four filters is the topic of Chapter V. Conclusions and recommendations for further study are provided in Chapter VI.

II. SYSTEM TRUTH MODEL

2.1 Introduction

The system truth model representation is very important in Kalman Filter design and performance analysis. The fidelity of the truth model will have a direct effect on the accuracy of the performance analysis results. It is therefore imperative that models accurately represent system dynamics and other appropriate characteristics.

This chapter contains a truth model for a hypervelocity missile system. The truth model contains realistic models for the missile, target, aircraft, and their engagement profiles. The mathematical model represents the dominant dynamic characteristics, relationships that describe sampled-data measured outputs, and other functions of interest.

The truth model is developed based on a three-dimensional profile. Since the filters designed in Chapter III are limited to the vertical plane for simplicity, the truth model lateral motion components are set to zero.

These system models are used in a digital computer simulation to obtain true missile trajectories and miss distances, thus motivating the name "system truth model". Kalman Filters are developed in Chapter III and Monte Carlo analyses on the nonlinear models are performed to compare outputs from the truth model and the filters (Figure 2-1). The Monte Carlo analysis is used to estimate the statistics of filter state estimates versus the truth model states. Iterations of this analysis allows filter parameters to be tuned for best filter performance. The Kalman Filter is based on the truth model but is of lower order. Thus,

2-1
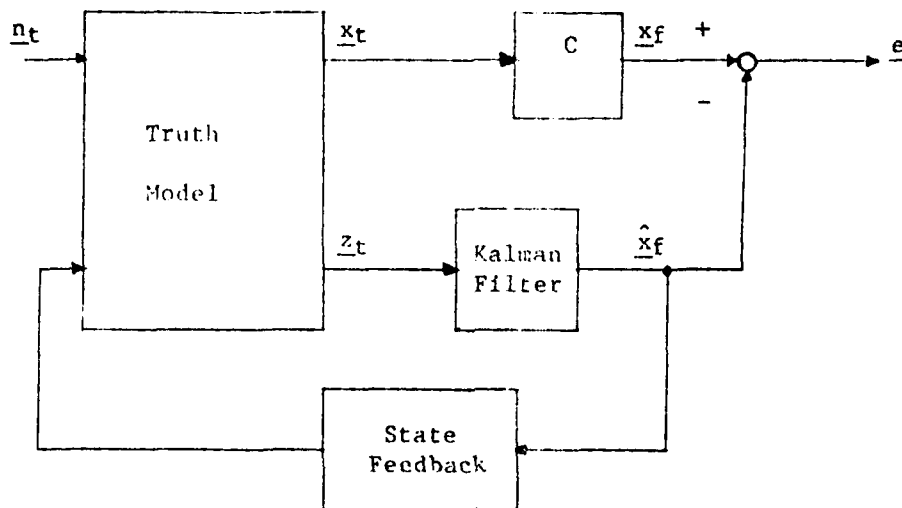
Figure 2-1. Truth Model and Filter
Relationship in Performance
Analysis

$\underline{x}_t$ = true states

$\underline{z}_t$ = measurement

$\underline{\hat{x}}_f$ = estimated states

$\underline{n}_t$ = noise added to truth model

C = conversion of truth model states to form and dimension of
filter states

$\underline{x}_f$ = truth model states in the form and dimension of the filter
states

$\underline{e}$ = errors in estimated states

2-2

to compare the truth model and filter states it is necessary to transform the true states to the form of the filter states. This transformation is indicated by "C" in Figure 2-1.

The system block diagram shown in Figure 2-2 depicts the major functional components and their input and output relationships. The truth model includes all blocks except the filter.

2.2 Coordinate Frames

The reference frames used in this study are the inertial, missile, target, aircraft, aircraft-to-target line-of-sight (ATLOS), and missile-to-target line-of-sight (MTLOS). Each frame is right-handed and orthogonal. Figure 2-3 depicts a planar view of the coordinate frames. Each is shown with its one and three axes in the plane of the page. The number two axis of each frame is not shown, but points out of the page. The inertial frame is an earth-fixed frame with $\hat{i}_1$ horizontal down range, $\hat{i}_2$ cross range, and $\hat{i}_3$ pointing down. It is fixed on the target at missile launch and remains at that location for the duration of flight. This frame is assumed inertially stationary due to the very short missile-target engagement time. The missile reference frame is fixed at the missile's center of gravity (M). The $\hat{m}_1$ axis lies along the missile velocity vector. The $\hat{m}_2$ and $\hat{m}_3$ axes are directed along the pitch (positive in up direction) and yaw (positive to the right) axes, respectively. Both the aircraft (A) and the target (T) are treated as point masses with $\hat{a}_1$ and $\hat{t}_1$ pointing in the direction of the aircraft velocity and target velocity, respectively. The other two axes are directed to the right of the velocity vector and down when the aircraft and target are traveling in a straight and level path parallel to the $\hat{i}_1$, $\hat{i}_2$ plane. The ATLOS frame is denoted by $\hat{\ell}_1$, $\hat{\ell}_2$, and $\hat{\ell}_3$ with the origin located at the target. This frame rotates with the line-of-sight between the aircraft and target, such that, $\hat{\ell}_1$ is always directed along this line. The $\hat{\ell}_2$ and $\hat{\ell}_3$

Figure 2-2. System Block Diagram
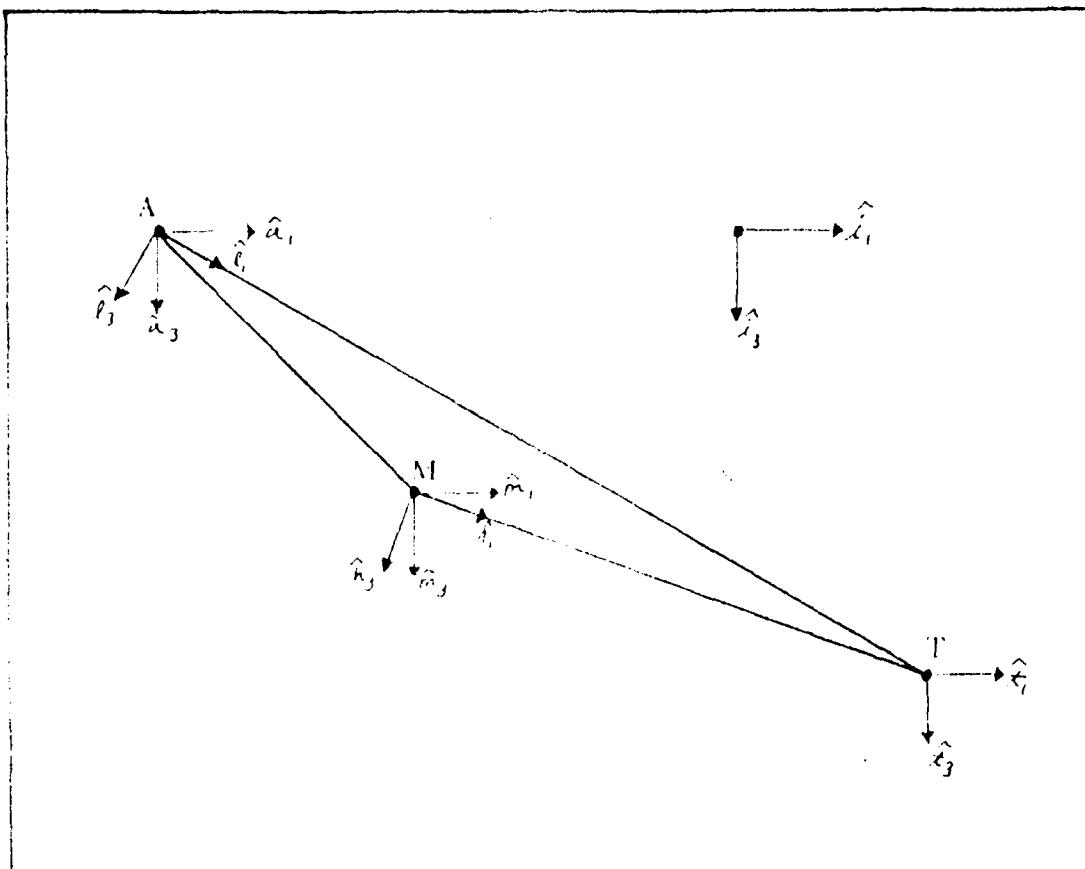
Figure 2-3. Coordinate Frames
(Aircraft, Missile, Target)

axes form the other orthogonal components, such that, $\hat{\ell}_2$ is directed to the right and $\hat{\ell}_3$ is directed down when the ATLOS is horizontal. The same type of orientation applies to the MTLOS frame with $\hat{k}_1$ originating from the missile center of gravity and pointing in the line-of-sight direction, $\hat{k}_2$ pointing to the right, and $\hat{k}_3$ pointing down. Appendix A contains angular relationships and coordinate transformations between the reference frames.

2.3 Missile Model

This section describes the missile and develops its three-degree-of-freedom dynamics. Included in the development is a simplified second-order model for the actuator/airframe attitude dynamics. Normally, the attitude dynamics would be developed in detail with consideration of a six-degree-of-freedom model. However, missile rotational dynamics are typically of a much higher frequency than the translational dynamics which the Kalman Filter estimates. Therefore, approximating the rotational dynamics has very little effect on the performance of the Kalman Filter and vice-versa. In addition, aerodynamic data describing a hypervelocity missile is proprietary and thus unavailable for general use. These data include vital information, such as moments of inertia and other aerodynamic data, which are needed for a six-degree-of-freedom simulation.

2.3.1 Assumptions. The type of missile used in this analysis is a highly maneuverable, short-range, tail fin controlled, air-to-surface missile. It is 3.5 in. in diameter and 72 in. long. The maximum lateral acceleration that the missile can command is assumed to be 100 g's (3,200 ft/sec^2) and its maximum flight time is 4.0 seconds. It is further assumed that the missile contains a strapdown inertial navigation system (INS) consisting of three accelerometers and three rate gyroscopes. The INS measures outputs of actual missile acceleration in the body frame and performs a coordinate transformation to get the accelerations in the inertial frame. It also provides angular rate information concerning the missile heading (Ψ) and flight path angle (Θ).

The missile is limited in the amount of knowledge it has at its disposal during and after launch. Initial aircraft and target state estimates are known, with some uncertainty, by the aircraft and are passed to the missile at launch. Once the missile has been launched, it continues to estimate these states through the use of a Kalman Filter. The missile receives measurements of azimuth (AZ) and elevation (EL) angles to use for updates in the filter. These measurements are obtained from a grid sensor model which is discussed in detail in the Measurement Model section of this chapter. A gimballed CO_2 laser projector on the aircraft generates a scanning signal which, based on the time between scan start and signal reception at the missile, determines azimuth and elevation. It is desired not to encode anything other than angle information onto this laser signal. Though this report is concerned only with the single target case, the actual system has to scan and track multiple targets (up to 10). To encode other information, as well as scan each target, presents a very burdensome, if not impossible, task for the aircraft laser generating system to handle. Once the measurement is obtained, the updated filter states are used by the guidance law to generate acceleration commands. The proposed states to be estimated in the onboard computer are discussed further in Chapter III.

The missile actuator and airframe attitude dynamics are assumed to be well represented by a second order system. In other words, the actual missile acceleration is modeled as a second order response to the commanded acceleration. This assumption has been used frequently in missile guidance analyses and is consistent with the level of modeling of this study (Ref. 2).

The missile is assumed to be a point mass in the three-degree-of-freedom dynamics development. In addition, the missile velocity vector and the longitudinal body direction are considered colinear, that is, there are zero angles of attack and sideslip. This assumption simplifies the dynamics development and is consistent with the three-

degree-of-freedom modeling. Also, the missile $\hat{m}_2$ axis remains in the horizontal plane throughout the engagement. This roll-stabilization assumption simplifies the development of the dynamics equations by eliminating roll-axis rotations. Other assumptions are discussed in the specific instance to which they apply.

   2.3.2 _Three-Degree-of-Freedom Dynamics Model_. The state equations which model the missile dynamics are developed in this section. Six equations are developed, with the necessary states, inputs, and parameters defined explicitly. The six states are

   $x_1 = x_{M/o}$, $\hat{i}_1$ component of missile position

   $x_2 = y_{M/o}$, $\hat{i}_2$ component of missile position

   $x_3 = z_{M/o}$, $\hat{i}_3$ component of missile position

   $x_4 = V_{M/o}$, magnitude of the missile velocity wrt pt 0

   $x_5 = \Psi$, missile heading angle

   $x_6 = \Theta$, missile flight path angle

In addition, variables and parameters that will affect the state relationships are

   T   = missile thrust

   D   = missile drag

   m   = missile mass

   g   = acceleration due to gravity

   a_L = missile lateral acceleration

   a_n = missile normal acceleration

   The acceleration due to gravity and thrust are considered constant. The acceleration due to gravity is the standard gravitational

2-8

acceleration of 32.17 ft/sec^2. It is assumed constant due to short flight time and range of the engagement. The thrust is also assumed constant, 5000 lb, for one second. The specific impulse of 5000 lb-sec generates the necessary impact velocity.

After one second, the thrust drops to zero resulting in a boost-coast trajectory if the flight time is greater than the thrust time. Missile drag, mass, lateral acceleration, and normal acceleration are variables that change with time. The establishment of models for each of these is discussed next.

The drag force on the missile is (Ref. 1:328):

$$D = \frac{1}{2} \rho V_M^2 S C_D \qquad (2-1)$$

where

ρ = density of the air

S = cross-sectional reference area

C_D = drag coefficient

V_M = velocity of the missile

The terms ρ and S are constants listed in Appendix D. The density of the air is assumed constant since the aircraft, missile, and target are within the same air mass. The cross-sectional area is the reference area for the coefficient of drag. The total coefficient of drag, C_D, is defined as

$$C_D = C_{DO} + C_{DI} \qquad (2-2)$$

where

C_{DO} = coefficient of zero-lift drag

C_{DI} = coefficient of induced drag

This expression can also be written as

$$C_D = C_{DO} + K C_L^2 \qquad (2-3)$$

2-9

where

K = inverse of the partial derivative of the coefficient of lift with respect to the angle of attack

C_L = coefficient of lift

The coefficient of zero-lift drag is approximated for a generic missile by (Ref. 5:22):

$$C_{DO} = \frac{2}{M} \qquad (2-4)$$

where

M = missile mach number

The mach number of the missile is calculated as

$$M = \frac{V_M}{V_S} \qquad (2-5)$$

where

V_S = constant speed of sound

The coefficient of induced drag is highly dependent on aerodynamic characteristics of the specific missile. Since these are unavailable and their inclusion only serves to change missile velocity, thus having minor effect on filter performance, the coefficient of induced drag is neglected.

The mass of the missile changes during the thrusting portion of the flight due to loss of fuel. The total missile mass is, therefore, modeled as a combination of the mass of the missile and the mass of the fuel.

$$m = m_M + k \, (t_T - t_F), \quad t_F \leq t_T \qquad (2-6)$$

or

$$m = m_M, \quad t_F > t_T \qquad (2-7)$$

2-10

where

m = total missile mass

m_M = mass of missile without fuel

$k = \dfrac{m_f}{t_T}$, fuel mass depletion rate at $t_F = 0$

m_f = total fuel mass

t_F = elapsed missile flight time

t_T = total missile thrust time

Thus as the missile thrusts, its mass will decrease at a constant rate until burn out. The mass will remain constant throughout the remainder of the flight.

The normal and lateral accelerations are the output of the actuator/airframe attitude dynamics model (Refer to Figure 2-2). The attitude response of the missile, due to acceleration commands from the guidance law, can be modeled by a second order system (Ref. 2). This lag comes from delays in the missile actuator and rotational dynamics to change the angle-of-attack which, in turn, produces the actual lateral and normal accelerations. The lateral and normal accelerations are generated based on

$$\frac{a_{ACT}}{a_{CMD}} = \frac{\omega_n^2}{s^2 + 2\zeta\,\omega_n s + \omega_n^2} \tag{2-8}$$

where

a_{ACT} = actual accelerations

a_{CMD} = commanded accelerations

ω_n = missile natural frequency

ζ = damping coefficient

The details of the computer implementation of this transfer function are contained in Appendix B.

Once the actual missile acceleration is generated, the missile position and velocity follow. This information is necessary to obtain relative information between the aircraft, target, and missile which is, in turn, applied to the measurement model to generate azimuth and elevation angles. These angles are used in the Kalman Filter as measurement updates. To obtain the missile position and velocity, both the inertial frame and the missile body frame are used. The inertial frame is to simplify obtaining relative position and velocity between the aircraft, target, and missile. Missile positions are expressed in the inertial frame in order to compare them directly with the aircraft and target position. The missile velocity state equations are defined in the missile body frame to minimize the number of vector rotations, since all aerodynamic forces are colinear with the body frame axes. Only one vector rotation is needed to rotate the missile velocity into the inertial frame for position state equations. Though there are many methods of generating state equations, using inertial position states and body frame velocity states is then a logical choice for this application.

Equations for missile position are developed by defining the missile position vector in the inertial frame. The derivative of this vector is then the velocity of the missile, expressed in the inertial frame. The velocity of the missile can also be expressed directly in the missile frame since it is, by definition, always in the $\hat{m}_1$ direction. This missile-frame velocity is then expressed in the inertial frame by a coordinate transformation. The two expressions for the inertial-frame velocity are then equated.

The equation for missile position with respect to point "o" expressed in the inertial frame is

$$\underline{r}_{M/o} = x_{M/o} \, \hat{i}_1 + y_{M/o} \, \hat{i}_2 + z_{M/o} \, \hat{i}_3 \tag{2-9}$$

Taking the derivative of (2-9) in the inertial frame yields

$$\dot{\underline{r}}_{M/o} = \dot{x}_{M/o}\,\hat{i}_1 + \dot{y}_{M/o}\,\hat{i}_2 + \dot{z}_{M/o}\,\hat{i}_3 \tag{2-10}$$

The zero angle-of-attack assumption allows the following equation for missile velocity:

$$\underline{V}^i_{M/o} = V_{M/o}\,\hat{m}_1 \tag{2-11}$$

where

$\underline{V}^i_{M/o}$ = missile velocity vector with respect to inertial frame

The transformation to the inertial frame results in the following equation:

$$\underline{V}^i_{M/o} = (V_{M/o}\cos\Theta\cos\Psi)\,\hat{i}_1 + (V_{M/o}\cos\Theta\sin\Psi)\,\hat{i}_2$$

$$- (V_{M/o}\sin\Theta)\,\hat{i}_3 \tag{2-12}$$

Since equations (2-10) and (2-12) are equivalent, the missile position state equations are

$$\dot{x}_1 = \dot{x}_{M/o} = V_{M/o}\cos\Theta\cos\Psi \tag{2-13}$$

$$\dot{x}_2 = \dot{y}_{M/o} = V_{M/o}\cos\Theta\sin\Psi \tag{2-14}$$

$$\dot{x}_3 = \dot{z}_{M/o} = -V_{M/o}\sin\Theta \tag{2-15}$$

The state equations for the missile velocity are developed next. The approach for a changing mass system is to use (Ref. 6):

$$\Sigma F = \tilde{m}\,\frac{dV}{dt} + \mu_i\,V_i - \mu_o\,V_o \tag{2-16}$$

2-13

where

$\bar{F}$ = system forces

$\tilde{m}$ = variable system mass

$\dfrac{dV}{dt}$ = rate of change of body velocity

μ_I, μ_o = rate of change of the input and output mass, respectively

V_i, V_o = velocities of the input and output particles, respectively

For this model V_i is zero. The thrust, V_o, and μ_o are constant and grouped into the thrust component of the forces. Thus equation (2-16) reduces to

$$\Sigma F = m \frac{dV}{dt} \qquad\qquad (2-17)$$

A free body diagram of the missile is set up to identify each of the system forces. These forces are then summed vectorally. Next, the acceleration of the missile, as seen by an observer in the inertial frame, is developed. The components of the forces and the components of acceleration times mass, which are in the same direction, are then equated.

The missile free body diagram is illustrated in Figure 2-4. The forces involved are the thrust, drag, normal, lateral, and gravitational forces. Thrust results from the boost provided by the solid propellant motor. The lateral force, L_2, is produced by horizontal plane steering commands which generate yaw motion. The normal force, L_N, is the result of pitch movement. Summing these forces

$$\Sigma \underline{F} = T\hat{m}_1 + L_2 \hat{m}_2 - L_N \hat{m}_3 - D\hat{m}_1 + mg \hat{i}_3 \qquad (2-18)$$

Transforming the $\hat{i}_3$ component by use of the direction cosine matrix from $\hat{I}$ to $\hat{m}$, C^{mi}, results in the following:

$$\Sigma \underline{F} = (T-D-mg \sin \theta) \hat{m}_1 + L_2\hat{m}_2 + (mg \cos \theta - L_N) \hat{m}_3 \qquad (2-19)$$

2-14
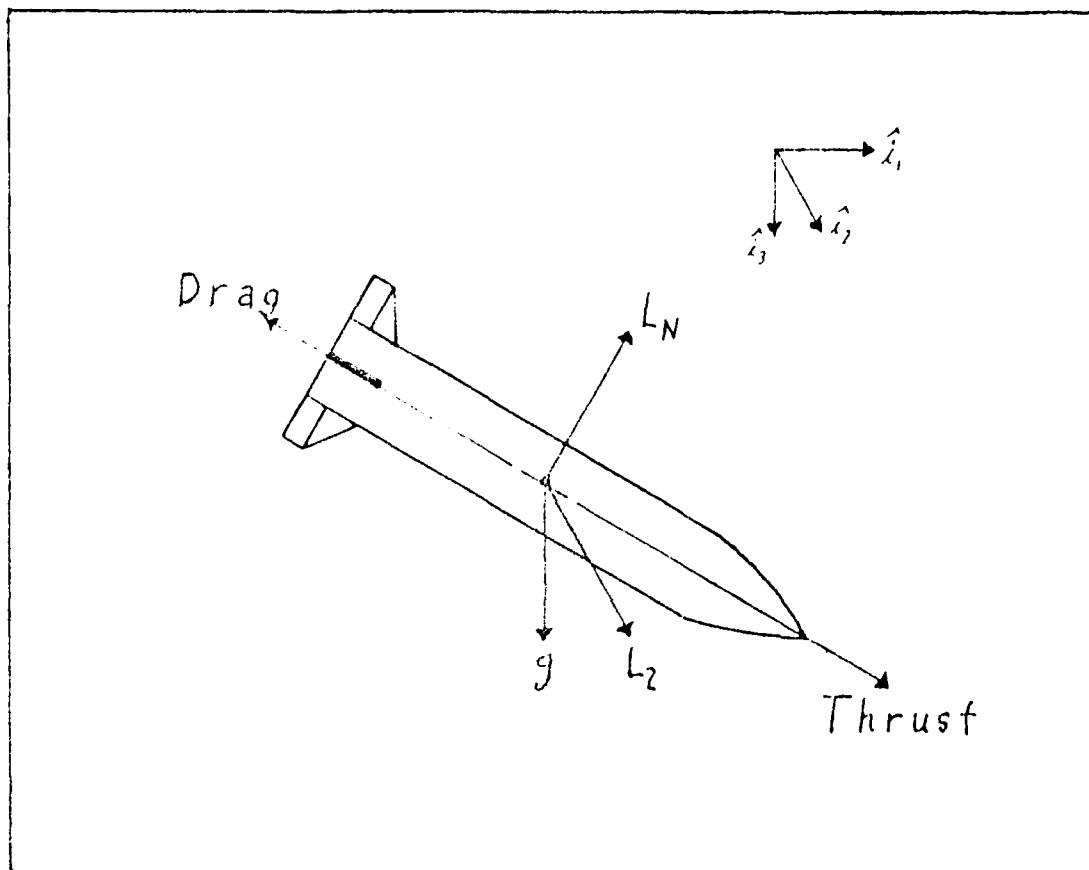
Figure 2-4. Missile Free Body Diagram

The acceleration of the missile as seen in the inertial frame is derived by taking the derivative of the equation (2-11), using the Theorem of Coriolis

$$A_{M/o}^i = \frac{{}^i d(\underline{V}_{M/o}^i)}{dt} = \frac{{}^m d\ (\underline{V}_{M/o}^i)}{dt} + (\underline{\omega}^{mi} \times \underline{V}_{M/o}^i) \tag{2-20}$$

where

$\underline{V}_{m/o}^i$ = as defined in equation (2-11)

$\dfrac{{}^m d(\ )}{dt}$ = derivative in the missile frame, $\hat{m}$

$\underline{\omega}^{mi}$ = rotation rate of the missile frame with respect to the inertial frame (Appendix A)

Therefore, coordinatizing this in the missile frame yields

$$A_{M/o}^i = \dot{V}_{M/o}\ \hat{m}_1 + (-\dot{\Psi} \sin \Theta\ \hat{m}_1 + \dot{\Theta}\ \hat{m}_2 + \dot{\Psi} \cos \Theta\ \hat{m}_3) \times V_{M/o}\hat{m}_1 \tag{2-21}$$

$$= \dot{V}_{M/o}\ \hat{m}_1 + \dot{\Psi}\ V_{M/o}\ \cos \Theta\ \hat{m}_2 - V_{M/o}\ \dot{\Theta}\ \hat{m}_3 \tag{2-22}$$

Equating colinear forces and accelerations results in the following missile velocity state equations:

$$\dot{x}_4 = \dot{V}_{M/o} = \frac{T-D}{m} - g \sin \Theta \tag{2-23}$$

$$\dot{x}_5 = \dot{\Psi} = \frac{L_2}{m\ V_{M/o} \cos \Theta} \tag{2-24}$$

$$\dot{x}_6 = \dot{\Theta} = \frac{L_n}{m\ V_{M/o}} - \frac{g \cos \Theta}{V_{M/o}} \tag{2-25}$$

2.4 Aircraft Model

2.4.1 Assumptions. The hypervelocity missiles will be deployed using a high performance aircraft, such as an F-16. The random accelerations of this type of aircraft are well represented by a first-order Gauss-Markov model in the inertial directions, with a correlation time constant of two seconds (Ref. 15). The aircraft also possesses a means of target acquisition and tracking. This system identifies the target and obtains range and angular position information. In addition, the aircraft is equipped with a carbon dioxide laser which scans the area in which the target and missile are located. These systems are discussed in more detail in the Measurement Model section.

2.4.2 Model. The aircraft dynamics are modeled by inertial position and velocity state equations. These states facilitate measurement modeling. The aircraft states are

$x_{A/o}$ = inertial aircraft position in $\hat{i}_1$ direction

$y_{A/o}$ = inertial aircraft position in $\hat{i}_2$ direction

$z_{A/o}$ = inertial aircraft position in $\hat{i}_3$ direction

$[V_{A/o}]_x$ = inertial velocity in $\hat{i}_1$ direction

$[V_{A/o}]_y$ = inertial velocity in $\hat{i}_2$ direction

$[V_{A/o}]_z$ = inertial velocity in $\hat{i}_3$ direction

and the state equations are

$$\dot{x}_{A/o} = [V_{A/o}]_x \qquad\qquad (2-26)$$

$$\dot{y}_{A/o} = [V_{A/o}]_y \qquad\qquad (2-27)$$

$$\dot{z}_{A/o} = [V_{A/o}]_z \qquad\qquad (2-28)$$

$$[\dot{V}_{A/o}]_x = [A_{A/o}]_x + n_1 \qquad\qquad (2-29)$$

2-17

$$[\dot{V}_{A/o}]y = [A_{A/o}]y + n_2 \tag{2-30}$$

$$[\dot{V}_{A/o}]z = [A_{A/o}]z + n_3 \tag{2-31}$$

where

$[A_{A/o}]x$, $[A_{A/o}]y$, $[A_{A/o}]z$ = aircraft inertial accelerations

n_1, n_2, n_3 = inertial, time-correlated
Gaussian noise (refer to the noise model section)

  The inertial accelerations are developed from the application of constant accelerations in the body axes. A transformation to the inertial frame, using the direction cosine matrix, C^{im}, develops $[A_{A/o}]x$, $[A_{A/o}]y$, and $[A_{A/o}]z$. A planar constant turn rate maneuver is generated by simultaneously applying a constant velocity in the $\hat{a}_1$ direction and a constant acceleration in one of the body axes perpendicular to the velocity. Thus, the aircraft has the capability of flying either with a constant acceleration or performing a planar constant turn rate maneuver.

2.5 Target Model

  2.5.1 Assumptions. Ground vehicles, for example tanks, are the types of targets for which these missiles are used. Current tanks are capable of turning against accelerations of 0.3 to 0.5 g's (Ref. 3). M60 tank accelerations are well-modeled by a first-order Gauss-Markov model in each horizontal direction. The correlation time constant associated with this model is 0.2 seconds (Ref. 4).

  2.5.2 Model. The target model is of the same form as the aircraft model. The states are inertial position and velocity as defined below.

 $x_{T/o}$ = inertial target position in $\hat{i}_1$ direction

 $y_{T/o}$ = inertial target position in $\hat{i}_2$ direction

 $z_{T/o}$ = inertial target position in $\hat{i}_3$ direction

$[V_{T/o}]x$ = inertial target velocity in $\hat{i}_1$ direction

$[V_{T/o}]y$ = inertial target velocity in $\hat{i}_2$ direction

$[V_{T/o}]z$ = inertial target velocity in $\hat{i}_3$ direction

The state equations are

$$\dot{x}_{T/o} = [V_{T/o}]x \tag{2-32}$$

$$\dot{y}_{T/o} = [V_{T/o}]y \tag{2-33}$$

$$\dot{z}_{T/o} = [V_{T/o}]z \tag{2-34}$$

$$[\dot{V}_{T/o}]x = [A_{T/o}]x + n_4 \tag{2-35}$$

$$[\dot{V}_{T/o}]y = [A_{T/o}]y + n_5 \tag{2-36}$$

$$[\dot{V}_{T/o}]z = [A_{T/o}]z + n_6 \tag{2-37}$$

where

$[A_{T/o}]x$, $[A_{T/o}]y$, $[A_{T/o}]z$ = nominal inertial target
accelerations (nominal time history for
simulation purposes)

n_4, n_5, n_6 = inertial, time-correlated
Gaussian noise (refer to Noise Model section)

The state equations are integrated by first-order Euler integration, as
in the aircraft model, since the equations are linear and the target
time constant of 0.2 seconds is much greater than the integration step
size of .02 seconds. The tank has the capability of standing still,
moving with a constant velocity, moving with a constant acceleration or
performing a constant turn rate maneuver. The maneuvers are
accomplished in the same manner as in the aircraft, that is, a constant
velocity is applied in the $\hat{t}_1$ direction and constant acceleration is
applied in the $\hat{t}_2$ direction. Thus motion of the target is restricted
to the $\hat{i}_1$, $\hat{i}_2$ plane.

2-19

2.6 Noise Model

Proposing shaping filters for a truth model is normally based upon extensive data analysis to determine the predominant error sources and their characteristics. The analysis provides autocorrelation and power spectral density data for which a mathematical model is developed to duplicate or at least closely approximate these characteristics. However, autocorrelation or power spectral density data for the hypervelocity missile system is not available for use in this report. Therefore, an aggregate noise model is used in the truth model and the error sources are not treated individually. The missile, aircraft, and target models are each corrupted in their body frame coordinates by a time-correlated, first-order Gauss-Markov noise added at the acceleration level.

Each of these scalar noises takes on the following form (Ref. 10:171-173):

$$\dot{n}(t) = -\frac{1}{\tau} n(t) + w(t) \tag{2-38}$$

where

τ = system correlation time constant

$w(t)$ = zero mean white Gaussian noise of strength Q_t

$n(o) = 0$

For the vector of scalar noises, this is

$$\dot{\underline{n}}(t) = \underline{F}\, \underline{n}(t) + \underline{G}\, \underline{w}(t) \tag{2-39}$$

where $\underline{F}$ is a diagonal matrix with elements $\frac{1}{\tau_i}$

and $\underline{G} = \underline{I}$,the identity matrix.

The equivalent discrete-time model is

$$\underline{n}(t_{i+1}) = \underline{\Phi}(t_{i+1}, t_i)\, \underline{n}(t_i) + \underline{w}_d(t_i) \tag{2-40}$$

2-20

where

$\Phi(t_{i+1}, t_i)$ = the state transition matrix that propagates
$\underline{n}$ from t_i to t_{i+1}

$\underline{w}_d(t_i)$ = discrete-time zero mean white Gaussian noise of
strength Q_d

Since noise model dynamics are time-invariant and the sample period of
.02 seconds is short compared to the missile time constant of 0.14 sec,
a first order approximation for the state transition matrix is used.

$$\underline{\Phi}(t_{i+1}, t_i) \cong \underline{I} + \underline{F}(t_i) \, [t_{i+1} - t_i] \qquad (2-41)$$

where

$\underline{F}(t_i)$ = evaluation sample of the dynamics matrix at
time t_i

In addition, a first-order approximation for the discrete-time white
Gaussian noise is

$$\underline{Q}_d \cong \underline{G} \, \underline{Q}_t \, \underline{G}^T \, [t_{i+1} - t_i] \qquad (2-42)$$

where

$\underline{G}$ = discrete sample of the dynamics driving
noise coefficient matrix

$\underline{Q}_d$ = discrete sample of the strength of the
dynamics driving noise, Q_t

For the simulation, it is desired to generate samples of the
discrete-time white Gaussian noise process, $\underline{w}_d(t_i)$, that has zero
mean and covariance

$$E[\underline{w}_d(t_i) \, \underline{w}_d^T(t_i)] = \underline{Q}_d \qquad (2-43)$$

This is done using a random number generator which generates
independent samples from populations of independent white Gaussian

noises, $\underline{w}_d{}'(t_i)$, with zero mean and covariance of identity. Thus $\underline{w}_d{}'(t_i)$ has autocorrelation

$$E[\underline{w}_d{}'(t_i)\ \underline{w}_d{}'(t_j)^T] = \begin{cases} \underline{I} & i=j \\ \underline{0} & i \neq j \end{cases} \tag{2-44}$$

Reference ten indicates that the truth model noise can be generated by

$$\underline{w}_d(t_i) = {}^C\!\sqrt{\underline{Q}_d}\ \underline{w}_d{}'(t_i) \tag{2-45}$$

where

$${}^C\!\sqrt{\underline{Q}_d} = \text{Cholesky square root of } \underline{Q}_d \text{ or any other matrix} \\ \text{square root method of } \underline{Q}_d$$

To show that this generates the appropriate characteristics, substitute equation (2-45) into equation (2-43) to get

$$E[\underline{w}_d(t_i)\ \underline{w}_d{}^T(t_i)] = E[\sqrt{\underline{Q}_d}\ \underline{w}_d{}'(t_i)\ \underline{w}_d{}'(t_i)^T \sqrt{\underline{Q}_d^T}] \tag{2-46}$$

Since the $\underline{Q}_d$ terms are not random, they can be moved outside the expectation to yield

$$E[\underline{w}_d(t_i)\ \underline{w}_d{}^T(t_i)] = \sqrt{\underline{Q}_d}\ E[\underline{w}_d{}'(t_i)\ \underline{w}_d{}'(t_i)^T] \sqrt{\underline{Q}_d^T} \tag{2-47}$$

Since the remaining expectation was defined as the identity matrix by equation (2-44)

$$E[\underline{w}_d(t_i)\ \underline{w}_d{}^T(t_i)] = \underline{Q}_d \tag{2-48}$$

which is the same as equation (2-43) and, therefore, equation (2-45) generates the discrete-time noise with desired chracteristics. (Ref. 10:408)

The values for $\underline{Q}_d$ are obtained by performing a steady state analysis on the system's conditional covariance matrix, $P(t)$. For the linear, continuous-time system, steady-state performance requires

$$\dot{\underline{P}}(t) = \underline{F}\ \underline{P}(t) + \underline{P}(t)\ \underline{F}^T + \underline{G}\ \underline{Q}\ \underline{G}^T = \underline{0} \qquad (2\text{-}49)$$

Using the first order approximation given by equation (2-42) and substituting into (2-49) yields

$$\underline{Q}_d = \frac{2}{\tau}\ \underline{P}_{ss}\ [t_{i+1} - t_i] \qquad (2\text{-}50)$$

where

$$\underline{P}_{ss} = \text{steady-state covariance}$$

Equation (2-50) can also be written as

$$\underline{Q}_d = \frac{2}{\tau}\ \sigma^2\ [t_{i+1} - t_i] \qquad (2\text{-}51)$$

where

$$\sigma = \text{standard deviation}$$

The required simulation noise parameters, σ and τ, are summarized in Table 2-1. These two parameters provide all the information needed for the simulation to use equations (2-40), (2-45), and (2-51). The aircraft is a high performance vehicle and the target is a tank. The values used for τ and σ are typical numbers that are representative of this class of problem (Ref. 4, 11). Since there is no data to indicate otherwise, the correlation time constants are assumed equal in all three directions.

Table 2-1

Simulation Statistics for Target, Aircraft, and Missile

Vehicle	Body Axis	Wn (rad/sec)	τ (sec)	σ (ft/sec²)	Qd (ft2/sec4)	Qd (ft/sec²)	Noise Source
Target	x	31.4	0.2	9.6	931.0	30.5	Maximum Acceleration *
	y	31.4	0.2	5.5	299.0	17.2	
	z	0.0	0.0	0.0	0.0	0.0	
Aircraft	x	3.0	2.1	0.0	0.0	0.0	Wind Buffeting
	y	3.0	2.1	0.1	9.3	3.1	
	z	3.0	2.1	0.1	9.8	3.1	
Missile	x	44.0	0.14	$10.4/m$	$1.6 \times 10^6 / m^2$	$1246.0/m$	Thrust Variation **
	y	44.0	0.14	.1	145.0	12.0	Wind
	z	44.0	0.14	.1	145.0	12.0	Buffeting

* The target z noise is a function of local terrain and is set to zero for this study.

** m = mass of missile, this noise source is set to zero for this study.

2-24

2.7 Measurement Model

A mathematical model for azimuth (AZ) and elevation (EL) is next developed as a measurement in the filter update. AZ and EL are angles that describe missile position relative to the aircraft-to-target line-of-sight (Figure 2-5). As mentioned in the Aircraft Model section, the aircraft has a target tracking system which acquires aircraft-to-target range and target position information. The aircraft also has a laser that scans the area in which both the target and missile are located. The missile is captured within the laser field-of-view shortly after launch and the target is always centered within the laser scan. Clocks on both the aircraft and missile are initialized at launch and assumed synchronized throughout the flight of the missile. The missile assumes that the aircraft precisely performs its function of centering the target on the laser scan field-of-view. Based upon this, the missile develops a grid model of the process performed by the aircraft (Figure 2-5).

The missile is aware of how many vertical scans the laser makes during a certain amount of time, with each vertical line on the grid corresponding to one vertical sweep of the laser. The laser signal is received by a tail-mounted sensor on the missile, with the total time from scan start to the moment of reception being the factor that determines the location of the missile on the grid. From the grid locations, the missile thus has a measurement of azimuth and elevation.

Associated with the measurement of azimuth and elevation are uncertainties. Tracking the target and centering it within the laser scan has uncertainty associated with it. Also, the timing process which sets up the missile grid model also contains uncertainties. The combination of these uncertainties is accounted for in the measurement model by the addition of a zero mean white Gaussian noise of strength 10^{-6} rad^2.
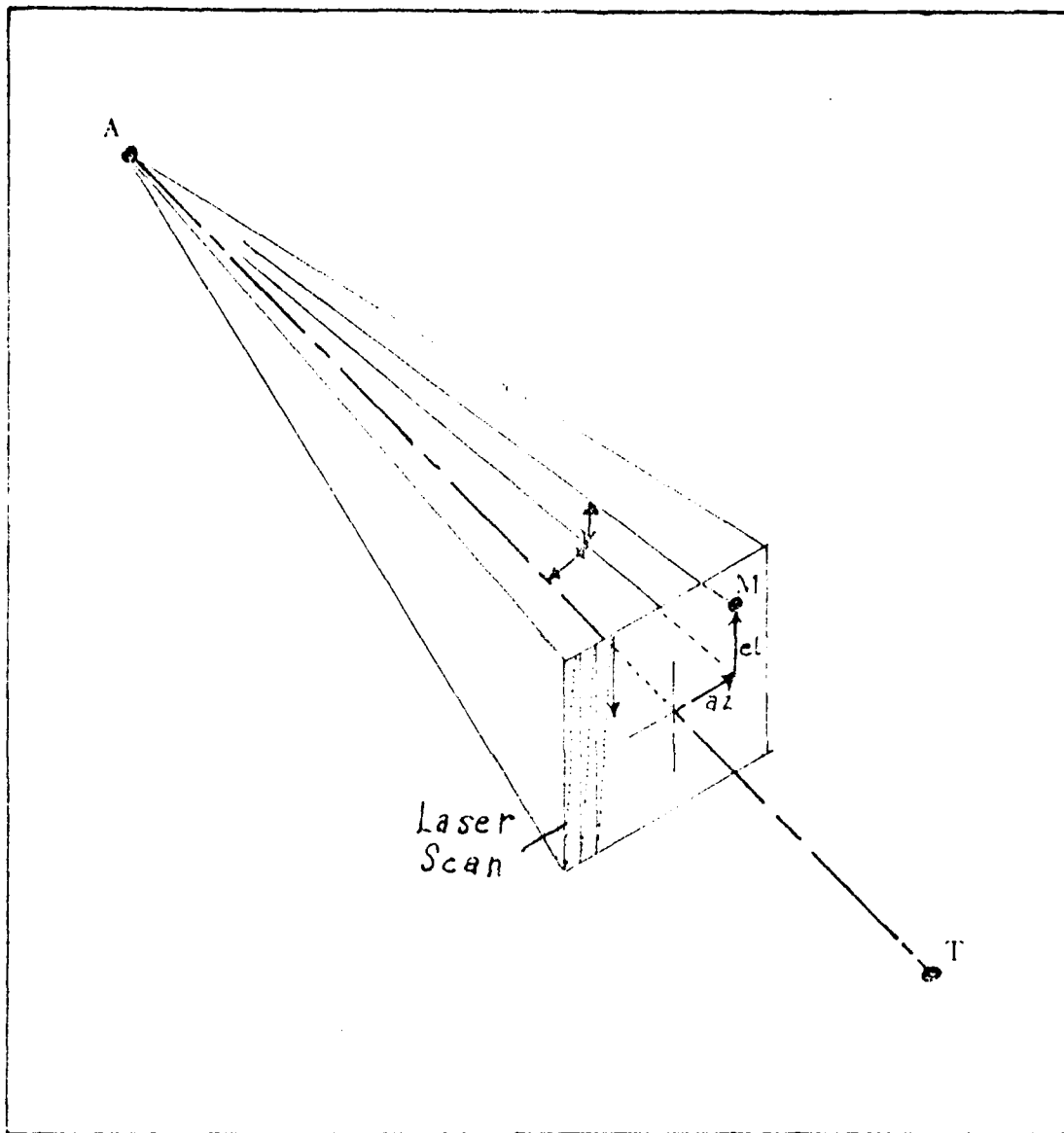
Figure 2-5. Laser Grid Scan and measurement
Scheme

2-26

The aircraft-to-target line-of-sight frame and the inertial frame components are used to generate truth model AZ and EL.

$$AZ = \sin^{-1} \left[\frac{(\text{projection of } \underline{r}_{M/A} \text{ onto } \hat{\ell}_2)}{(\underline{r}_{M/A})} \right] \qquad (2\text{-}52)$$

$$EL = \sin^{-1} \left[\frac{-(\text{projection of } \underline{r}_{M/A} \text{ onto } \hat{\ell}_3)}{(\underline{r}_{M/A})} \right] \qquad (2\text{-}53)$$

The projections onto $\hat{\ell}_2$ and $\hat{\ell}_3$ are found by transforming the missile-to-aircraft relative position from inertial to line-of-sight coordinates and choosing the appropriate components.

Using the direction cosine matrix, $[C^{\ell i}]$, in conjunction with the position of the missile with respect to the aircraft, $\underline{r}_{M/A}$, where

$$\underline{r}_{M/A} = x_{M/A} \, \hat{i}_1 + y_{M/A} \, \hat{i}_2 + z_{M/A} \, \hat{i}_3 \qquad (2\text{-}54)$$

$[C^{\ell i}]$ = inertial to aircraft-to-missile line-of-sight transformation matrix (Appendix A)

produces

$$\underline{r}_{M/A} = (x_{M/A} \cos \Theta_\ell \cos \Psi_\ell + y_{M/A} \cos \Theta_\ell \sin \Psi_\ell - z_{M/A} \sin \Theta_\ell) \, \hat{\ell}_1$$

$$+ (-x_{M/A} \sin \Psi_\ell + y_{M/A} \cos \Psi_\ell) \, \hat{\ell}_2$$

$$+ (x_{M/A} \sin \Theta_\ell \cos \Psi_\ell + y_{M/A} \sin \Theta_\ell \sin \Psi_\ell + z_{M/A} \cos \Theta_\ell) \, \hat{\ell}_3$$
$$(2\text{-}55)$$

The angles, Θ_ℓ and Ψ_ℓ, are not known yet and must be specified. This is done by first defining target-to-aircraft relative position as

$$\underline{r}_{T/A} = R_{T/A} \, \hat{\ell}_1 \qquad\qquad (2\text{-}56)$$

where

$$R_{T/A} = (x^2_{T/A} + y^2_{T/A} + z^2_{T/A})^{1/2} \qquad\qquad (2\text{-}57)$$

Then, since $[C^{\ell i}] = [C^{i\ell}]^T$

$$\begin{bmatrix} x_{T/A} \\ y_{T/A} \\ z_{T/A} \end{bmatrix} = [C^{\ell i}]^T \begin{bmatrix} R_{T/A} \\ 0 \\ 0 \end{bmatrix} \qquad\qquad (2\text{-}58)$$

Performing this operation results in three equations and three unknowns.

$$x_{T/A} = R_{T/A} \cos\Theta_\ell \cos\Psi_\ell \qquad\qquad (2\text{-}59)$$

$$y_{T/A} = R_{T/A} \cos\Theta_\ell \sin\Psi_\ell \qquad\qquad (2\text{-}60)$$

$$z_{T/A} = -R_{T/A} \sin\Theta_\ell \qquad\qquad (2\text{-}61)$$

From equation (2-61)

$$\Theta_\ell = \sin^{-1}\left[-\frac{z_{T/A}}{R_{T/A}} \right] \qquad\qquad (2\text{-}62)$$

and from equation (2-60)

$$\Psi_\ell = \sin^{-1}\left[\frac{y_{T/A}}{R_{T/A} \cos\Theta_\ell} \right] \qquad\qquad (2\text{-}63)$$

2-28

The equations for AZ and EL are thus completely specified by the following:

$$AZ = \sin^{-1} \frac{-x_{M/A} \sin \Psi_\ell + y_{M/A} \cos \Psi_\ell}{(x_{M/A}^2 + y_{M/A}^2 + z_{M/A}^2)^{1/2}} \tag{2-64}$$

$$EL = \sin^{-1} \frac{-(x_{M/A} \sin \Theta_\ell \cos \Psi_\ell + y_{M/A} \sin \Theta_\ell \sin \Psi_\ell + z_{M/A} \cos \Theta_\ell)}{(x_{M/A}^2 + y_{M/A}^2 + z_{M/A}^2)^{1/2}}$$

$$\tag{2-65}$$

2.8 Guidance Law

The guidance law accepts information concerning target and missile relative dynamics and generates acceleration commands to direct the missile to the target. The major guidance laws that are presently applicable to short-range tactical missiles are discussed in Reference 8. A comprehensive bibliography has also been included in this reference which readers can use for more in-depth study into the analysis of various guidance law schemes. The major guidance laws examined are line-of-sight, pursuit, proportional navigation, optimal linear, and others. The last category includes proposed guidance laws based, primarily, on differential game theory. These laws are still in the very early research and development stage and are not considered for possible implementation in this study. The first three are classical guidance laws, whereas, the fourth is a modern technique. Line-of-sight guidance can be further divided into two laws which differ, primarily, in how they are applied. These are beamrider and command to line-of-sight. The command to line-of-sight scheme typically uses a communications link from a controller to the missile. The controller tracks the missile, generates a line-of-sight to the target, and sends guidance signals to the missile. The beamrider concept, however, does not use a controller to track the missile. An air or ground station provides a line-of-sight to the target. The missile requires knowledge

2-29

of its position relative to the line-of-sight. It obtains line-of-sight information through a communications link with the controller and computes its position relative to the line-of-sight based on initial condition at launch. Pursuit guidance employs the technique of continually trying to keep the missile pointed at the target. There are two basic variations in this method. The first is attitude pursuit where the missile's longitudinal axis is directed at the target. The other is velocity pursuit where the missile's velocity vector is kept pointed at the target. Velocity pursuit exhibits much better performance than attitude pursuit, in terms of average terminal miss distance. Proportional navigation is a guidance scheme that attempts to null the missile-to-target line-of-sight rate, while closing in on the target. This puts the missile on a collision course with the target. Optimal linear guidance is based upon optimal control theory. Almost all of the work in this area is based on linear model dynamics, quadratic costs, and additive white Gaussian noise (LQG problem). It is implemented with an LQG controller and a Kalman Filter that generates state estimates.

Classical proportional navigation is the guidance law selected for this study. The target is an armored, ground vehicle which will be stationary or moving with a near constant velocity. For this type of target, proportional navigation has characteristics which favor it over the other schemes. Proportional navigation exhibits much better terminal miss distance performance than does pursuit guidance for targets moving with an acceleration less than 0.5 g's. Under these same conditions, line-of-sight guidance has a miss distance on the same order as proportional navigation; however, to implement it requires a complex controller, either on the aircraft or on the ground. Proportional navigation also has a much quicker reaction time and expends much less control energy in trying to reach the target. Thus, airframe and propulsion requirements are not nearly as stringent. For highly maneuverable accelerating targets, optimal guidance laws are superior to other laws in terms of miss distance performance.

However, a microcomputer is needed onboard the missile for
computational purposes. This significantly increases the complexity of
the system as well as creating more implementation problems. Since the
target is not highly maneuverable and the increased onboard complexity
is not desired, proportional navigation is more applicable. (Ref. 13)

The proportional navigation law commands a missile turning rate
which is proportional to the rate of change of the missile-to-target
line-of-sight angle (λ, refer to Figure 2-6). The defining scalar
equation is

$$a_{CMD} = n\ V_c\ \dot{\lambda} \qquad\qquad (2-66)$$

where

n = proportional navigation constant

V_c = closing velocity along the line-of-sight

$\dot{\lambda}$ = line-of-sight angle rate

Equation (2-66) can be extended to the vector case by simply using the
appropriate component of the missile-to-target line-of-sight rate
vector, $\underline{\omega}_{MTLOS}$, instead of $\dot{\lambda}$.

The closing velocity is the component of the velocity of the
missile with respect to the target along the missile-to-target line-of-
sight. This is computed by applying the dot product between the
velocity vector and a unit vector along the missile-to-target line-of-
sight.

That is

$$V_c = [\underline{V}_{T/M}^i] \cdot \frac{\underline{r}_{T/M}}{\left|\underline{r}_{T/M}\right|} \qquad\qquad (2-67)$$
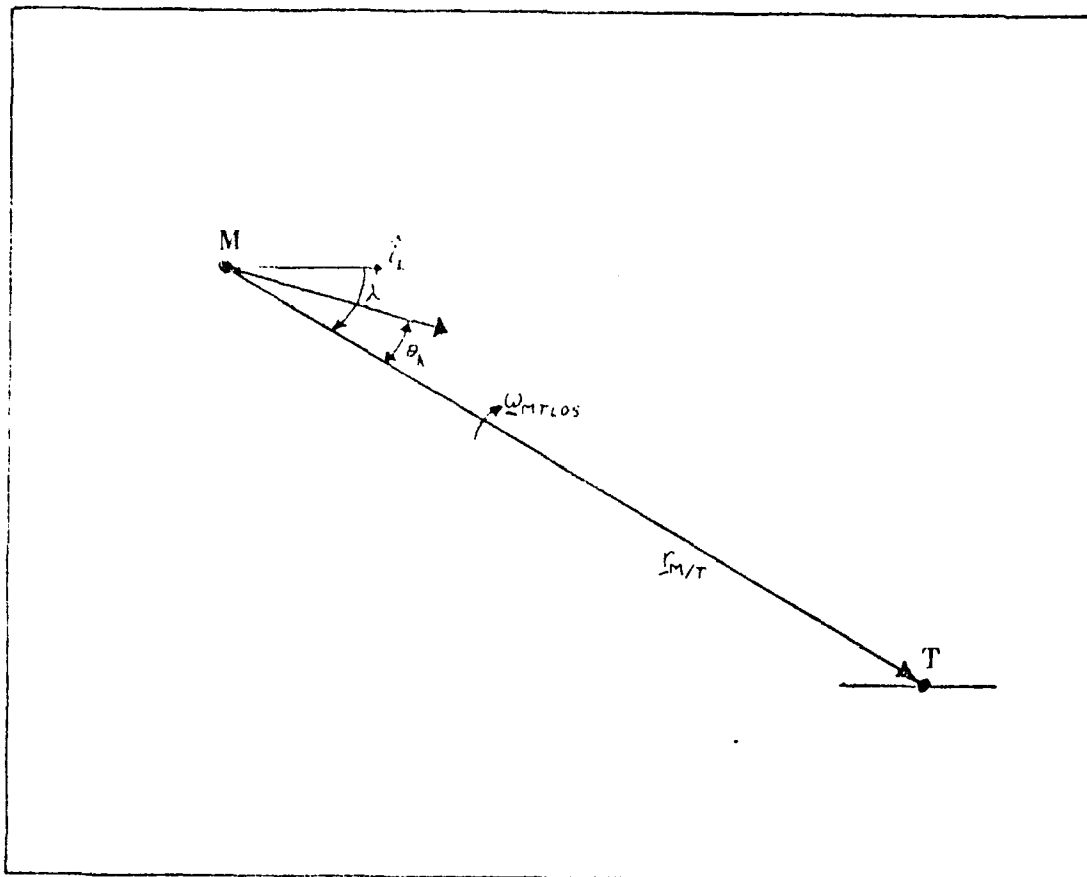
Figure 2-6. Missile-Target Planar Engagement
Scenario

using the expressions

$$\underline{r}_{T/M} = x_{T/M} \, \hat{i}_1 + y_{T/M} \, \hat{i}_2 + z_{T/M} \, \hat{i}_3 \qquad (2\text{-}68)$$

$$\underline{V}_{T/M} = \dot{x}_{T/M} \, \hat{i}_1 + \dot{y}_{T/M} \, \hat{i}_2 + \dot{z}_{T/M} \, \hat{i}_3 \qquad (2\text{-}69)$$

yields

$$V_c = \frac{(x_{T/M}) \, (\dot{x}_{T/M}) + (y_{T/M}) \, (\dot{y}_{T/M}) + (z_{T/M}) \, (\dot{z}_{T/M})}{(x_{T/M}{}^2 + y_{T/M}{}^2 + z_{T/M}{}^2)^{1/2}} \qquad (2\text{-}70)$$

The following development derives an expression for $\underline{\omega}_{MTLOS}$. Relating $\underline{V}^i_{T/M}$ between the $\hat{k}$ frame and $\hat{i}$ frame, via the Theorem of Coriolis, results in the following equation:

$$\underline{V}^i_{T/M} = \frac{{}^i d(\underline{r}_{T/M})}{dt} = \frac{{}^k d(\underline{r}_{T/M})}{dt} + (\underline{\omega}^{ki} \times \underline{r}_{T/M}) \qquad (2\text{-}71)$$

where

$\quad \underline{r}_{T/M} \quad$ = missile-to-target relative position

$\dfrac{{}^k d(\underline{r}_{T/M})}{dt}$ = rate of change of $\underline{r}_{T/M}$ as observed from the line-of-sight frame

$\quad \underline{\omega}^{ki}$ = rotation rate of the $\hat{k}$ frame with respect to the inertial frame

Since $\hat{k}_1$ is defined to point in the direction of the missile-to-target line-of-sight and the $\hat{k}$ frame rotates with the line-of-sight, the

2-33

rotation rate of the missile-to-target line-of-sight vector, $\underline{\omega}_{MTLOS}$, is equivalent to the rotation rate of the line-of-sight frame with respect to the inertial frame, $\underline{\omega}^{ki}$. Performing the cross product of $\underline{r}_{T/M}$ with both sides of equation (2-71) results in

$$\underline{r}_{T/M} \times \underline{v}^i_{T/M} = \underline{r}_{T/M} \times \frac{{}^k d(\underline{r}_{T/M})}{dt} + \underline{r}_{T/M} \times (\underline{\omega}^{ki} \times \underline{r}_{T/M})$$

(2-72)

where the expression $\underline{r}_{T/M} \times \dfrac{{}^k d(\underline{r}_{T/M})}{dt}$, is zero since both terms lie

along the missile-to-target line-of-sight. The triple cross product rule is defined by the following equation:

$$\underline{A} \times (\underline{B} \times \underline{C}) = (\underline{A} \cdot \underline{C}) \underline{B} - (\underline{A} \cdot \underline{B}) \underline{C}$$

(2-73)

Applying this to equation (2-73) results in

$$\underline{r}_{T/M} \times \underline{v}^i_{T/M} = (\underline{r}_{T/M} \cdot \underline{r}_{T/M}) \underline{\omega}_{MTLOS} - (\underline{r}_{T/M} \cdot \underline{\omega}_{MTLOS}) \underline{r}_{M/T}$$

(2-74)

The missile-to-target line-of-sight roll stabilization assumption allowed the selection of coordinate directions so that the term $\underline{r}_{T/M} \cdot \underline{\omega}_{MTLOS}$ is zero.

Thus, final form for the line-of-sight rotation is

$$\underline{\omega}_{MTLOS} = \frac{\underline{r}_{T/M} \times \underline{V}_{T/M}}{\left| \underline{r}_{T/M} \right|^2}$$

(2-75)

3-34

Therefore

$$\underline{\omega}_{MTLOS} = \frac{(L)\hat{i}_1 + (M)\hat{i}_2 + (N)\hat{i}_3}{(x^2_{T/M} + y^2_{T/M} + z^2_{T/M})} \qquad (2\text{-}76)$$

where

$$L = (y_{T/M})\,(\dot{z}_{T/M}) - (z_{T/M})\,(\dot{y}_{T/M})$$

$$M = (z_{T/M})\,(\dot{x}_{T/M}) - (x_{T/M})\,(\dot{z}_{T/M})$$

$$N = (x_{T/M})\,(\dot{y}_{T/M}) - (y_{T/M})\,(\dot{x}_{T/M})$$

Thus, the guidance law is completely specified with the various components of the equations being estimated states or parameters depending on the type of filter developed in Chapter III.

2.9 Summary

Truth models of the actual aircraft, missile, and target engagement scenario were developed in this chapter. The models include dynamics, a guidance law, and a measurement equation. The next step is to design a Kalman Filter which will accept azimuth and elevation measurements from the truth model and generate state estimates. These estimates inform the missile of its position and velocity relative to the aircraft and the target. They are then applied, along with INS estimates, to the guidance law to direct the missile to the target. The design of this filter is the topic of the next chapter.

III.   Kalman Filter Development

3.1 Introduction

3.1.1 Approach. The Kalman Filter is a digital computer algorithm
which uses the available discrete-time noisy measurements to estimate
certain desired variables. Since the analysis considered only the
vertical plane, elevation was the only angle measurement required. The
Kalman Filter processed this measurement and estimated relative
information between the aircraft, missile, and target. This chapter
contains a systematic procedure in developing full order and reduced
order filters. The full order filter performance was to be used as a
benchmark to which reduced order filters are compared. Selection of a
reduced order filter for actual implementation was a trade-off between
performance and on-board complexity.

Filter development first consisted of proposing models upon which
filter design could be based. The approach for each filter model was to
initially propose a set of state variables based upon kinematic
relationships. State equations, which contain both deterministic and
stochastic elements, were then developed. A measurement equation was
derived from the geometry of the engagement and expressed in terms of
the states. In addition, the guidance law must be able to perform its
function using the state estimates and launch data extrapolations.
Specific states were thus added based upon the requirements of the
guidance law and the measurement model. Models that show the most
promise for implementation were then selected and developed further.
Four separate filter design models were derived. Two of these models were
based upon polar coordinates and the other two were based upon cartesian

coordinates. Two of these four design models, one cartesian and one polar, were then selected for filter development and analysis.

3.1.2 Filter Model Selection. Due to the time limitation on this study, only two of the four filter models were selected for further analysis. Since there were two basic formulation methods, LOS and inertial, the initial decision was to choose one of each. Filter model L.1 was selected from the LOS choices. The L.1 model was based upon the ATLOS frame as a reference. On the other hand, the L.2 model was based upon the MTLOS frame as a reference. The ATLOS frame was much less dynamic than the MTLOS frame, therefore, numerical problems are less likely to appear.

Filter model I.1 is the inertial frame formulation selected for filter design and analysis. This model used aircraft-to-target and missile-to-target states. The corresponding measurement equation and guidance law depend only on state estimates. The I.2 model, however, estimates inertial aircraft and target states. The missile variables were assumed known through high quality INS data. However, the hypervelocity missile was designed to be very small so that many missiles can be deployed on each aircraft and the missiles were to be relatively inexpensive since they are destroyed upon impact. Therefore, the requirement for INS data was not desirable since a high-quality INS is both expensive and bulky.

3.1.3 Observability. For any proposed model, observability was a key issue. To be completely observable any change in an individual state variable must be distinguishable to the output measurement. In addition, any change in a particular state variable must be distinguishable in the output from a change in any other state variable. In the case of a Kalman Filter, the measurement update should have a distinguishable effect on each of the states. Also for a completely observable system the covariance will not grow unbounded.

An observability analysis was performed on each of the selected full order and reduced order filter models. The discrete-time observability matrix for time-invariant linear system models was constructed as follows:

$$\underline{M} \overset{\Delta}{=} [\underline{H}^T \vdots \underline{\phi}^T \underline{H}^T \vdots \cdots \vdots (\underline{\phi}^T)^{n-1} \underline{H}^T] \tag{3-1}$$

where

$\underline{\phi}$ = state transition matrix

$\underline{H}$ = measurement model coefficient matrix

The system is fully observable if the Matrix $\underline{M}$ is of rank equal to the state dimension. (Ref. 10:47)

3.1.4 Assumptions. For most of the models, the missile was assumed to have an INS, which provides missile total accelerations in the inertial frame:

$$\underline{A}_{INS} = a_1 \, \hat{i}_1 + a_3 \, \hat{i}_3 \tag{3-2}$$

In addition, the INS provides inertial velocities, $\dot{x}_{M/o}$ and $\dot{z}_{M/o}$, and positions, $x_{M/o}$ and $z_{M/o}$, by integration of the accelerations. These are assumed to be high quality data and are used as parameters in the measurement model and guidance law, as opposed to noise-corrupted measurements.

As discussed in the truth model, the aircraft obtains measurements of its range to the target. The aircraft also contains an INS which generates information of inertial accelerations, velocities, and positions. The INS information is passed to the missile at launch and then propagated by the missile based on constant aircraft and target acceleration assumptions.

There are two methods used to process the aircraft-to-target range. For the line-of-sight filter, the range was passed to the missile at launch and subsequently estimates within by the missile. This method was ruled out for the inertial filter due to observability problems not exhibited by the LOS filter. To obtain a fully observable inertial benchmark model, the aircraft-to-target range and the missile-to-target range are needed as measurements. The ranges were computed by the missile, with added uncertainties, and applied as pseudo-measurements to the filter.

3.2 Development of Line-Of-Sight Filters

3.2.1 Introduction. The filters developed in this section focus on equations of motion expressed in polar coordinates. This coordinate choice makes the equations of motion nonlinear due to the rotation of the reference frame. The equations developed here for the full order filter will also apply to the reduced order filters. While some of the variables in the full order filter are not used as states in the reduced order filter, they are propagated in time and treated as parameters in the filter and guidance law computations. The filter then assumes perfect knowledge of these parameters in this case. Pseudo-noise addition via tuning then accounts for the fact that these are not equal to true parameter values. With development in general form, the equations can be used directly to construct any of the reduced order filters.

3.2.2 Filter Model L.1. The equations of motion for this filter are expressed in polar coordinates based on the ATLOS line-of-sight reference frame with the origin remaining on the target. The state variables chosen are illustrated in Figure 3-1.
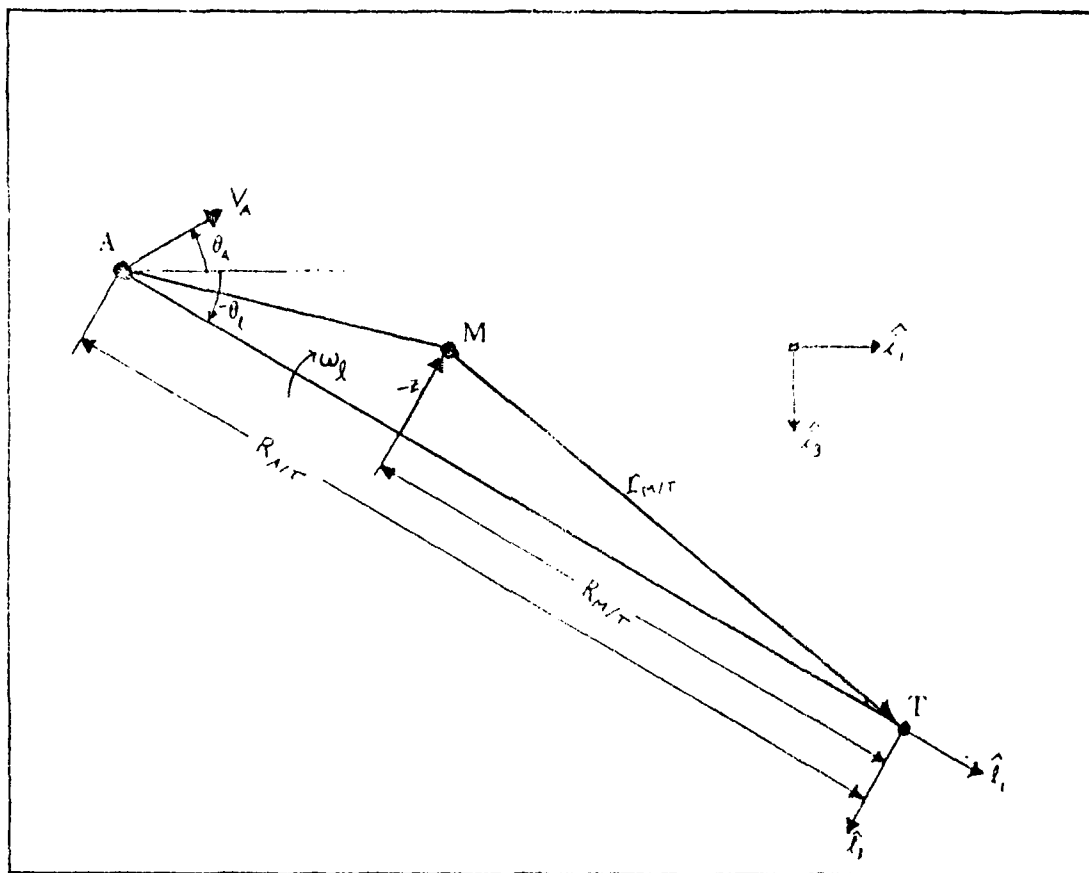
Figure 3-1.   Line-of-Sight Filter L.1 Variable
Description

The state variables are defined as

z = Distance of MSL below A/C-TO-TGT LOS

$\dot{z}$ = Velocity of MSL from A/C-TO-TGT LOS

$R_{M/T}$ = MSL-TO-TGT range along LOS

$\dot{R}_{M/T}$ = MSL-TO-TGT velocity along LOS

Θ_ℓ = elevation of the LOS with respect to horizon

$R_{A/T}$ = A/C-TO-TGT range along LOS

$V_{A/T}$ = A/C-TO-TGT velocity along LOS

And as a required parameter:

$\underline{\omega}^{\ell i}$ = rate of change of LOS

The $\omega^{\ell i}$ term can be included as a state variable under certain circumstances, but is more correctly treated here as a parameter. The coordinate frame as discussed in Section 2.2 is right-handed with $\hat{\ell}_1$ along the aircraft-to-target line-of-sight. The reference frame is roll stabilized with $\hat{\ell}_2$ along the horizontal plane and $\hat{\ell}_3$ downward completing the triad.

In deriving the equations of motion, let

$$\underline{\omega}^{\ell i} = - \omega_\ell \, \hat{\ell}_2 \tag{3-3}$$

$$\Theta_\ell = \Theta_\ell \, \hat{\ell}_2 \tag{3-4}$$

and

$$\underline{r}_{M/T} = R_{M/T} \, \hat{\ell}_1 + z \, \hat{\ell}_3 \tag{3-5}$$

The velocity of the missile can be obtained by taking the first derivative of $\underline{r}_{M/T}$ in the ℓ frame with respect to the inertial frame as defined by

$$\underline{V}^i_{M/T} = \frac{^i d}{dt} \, \underline{r}_{M/T} = \frac{^\ell d}{dt} \, \underline{r}_{M/T} + \underline{\omega}^{\ell i} \times \underline{r}_{M/T} \tag{3-6}$$

3-6

Which in terms of the state variables gives

$$\underline{V}^{\ell}_{M/T} = (\dot{R}_{M/T} - z\,\omega_\ell)\hat{\ell}_1 + (+\dot{z} + R_{M/T}\,\omega_\ell)\hat{\ell}_3 \tag{3-7}$$

Again, taking the derivative of velocity, using the Theorem of Coriolis, the acceleration is expressed as

$$\underline{A}^i_{M/T} = \frac{{}^i d}{dt}\,\underline{V}^i_{M/T} = \frac{{}^\ell d}{dt}\,\underline{V}^i_{M/T} + \underline{\omega}^{\ell i} \times \underline{V}^i_{M/T} \tag{3-8}$$

which yields

$$\underline{A}^i_{M/T} = (\ddot{R}_{M/T} - 2\,\dot{z}\,\omega_\ell - R_{M/T}\,\omega_\ell^2 + z\dot{\omega}_\ell)\hat{\ell}_1$$

$$+(\ddot{z} + 2\dot{R}_{M/T}\,\omega_\ell + R_{M/T}\,\dot{\omega}_\ell - z\omega_\ell^2)\hat{\ell}_3 \tag{3-9}$$

In the trajectory considered, the $\dot{\omega}$ and ω_ℓ^2 terms were found to be less than 2 percent of the larger terms and are considered neglible for the purposes of this development. However, they were used in the filter equations initially for completeness.

The outputs of the INS were considered to be high quality noise-free estimates of the missiles total acceleration expressed in inertial frame coordinates and expressed as:

$$\underline{A}^i_M = a_1\,\hat{i}_1 + a_2\,\hat{i}_2 + a_3\,\hat{i}_3 \tag{3-10}$$

The outputs of the INS were then rotated into the ℓ Frame Appendix A.

$$\underline{A}^i_M = (a_1\cos\Theta_\ell - a_3\sin\Theta_\ell)\,\hat{\ell}_1 + a_2\,\hat{\ell}_2 \tag{3-11}$$

$$+ (a_1\sin\Theta_\ell + a_3\cos\Theta_\ell)\,\hat{\ell}_3$$

The total acceleration of the missile with respect to the target is the difference of the missile's total acceleration and the target's total acceleration. However, since the missile's accelerations are much greater than those of the target, the relative missile-to-target

accelerations can be approximated by the missile's total accelerations. This assumption will permit equating $\underline{A}$ in equations (3-9) and (3-11) and grouping the vector components to yield:

$$\ddot{z} = -2\, R_{M/T}\, \dot{\omega}_\ell + a_1 \sin \Theta_\ell + a_3 \cos \Theta_\ell$$
$$- R_{M/T}\, \dot{\omega}_\ell + z\, \omega_\ell^2 \tag{3-12}$$

$$\ddot{R}_{M/T} = +2\, \dot{z}\omega_\ell + R_{M/T}\, \omega_\ell^2 + z\, \dot{\omega}_\ell - a_2 \cos \Theta_\ell + a_3 \sin \Theta_\ell \tag{3-13}$$

The expressions for Θ_ℓ and ω_ℓ are defined as

$$\dot{\Theta}_\ell = -\omega_\ell \tag{3-14}$$

$$\underline{\omega}^{\ell i} = \frac{\underline{r}_{A/T} \times \underline{V}_A}{r_{A/T}^{\ 2}} \tag{3-15}$$

where for the planar problem $\omega_\ell = \underline{\omega}^{\ell i}$

The velocity of the aircraft can be expressed in polar form as V_A at an angle of Θ_A above the horizon. If expressed in the LOS frame the aircraft velocity, V_A / Θ_A, becomes $V_{A/T}\, \hat{\ell}_1 +$ $V_A \tan(\Theta_\ell - \Theta_A)\hat{\ell}_3$ where $V_{A/T}$ and Θ_ℓ are states and Θ_A is assumed a constant. With this substitution, equation (3-15) becomes:

$$\underline{\omega}_\ell = \frac{(R_{A/T}\hat{\ell}_1) \times (V_{A/T}\, \hat{\ell}_1 + V_{A/T} \tan [\Theta_\ell - \Theta_A]\hat{\ell}_3)}{R_{A/T}^2} \tag{3-16}$$

which reduces to

$$\underline{\omega}_\ell = \frac{-V_{A/T} \tan(\Theta_\ell - \Theta_A)}{R_{A/T}}\, \hat{\ell}_2 \tag{3-17}$$

3-8

Note that the expression for ω_ℓ can be expressed as a function of three other states. In the case of the full order filter, ω_ℓ is computed as a parameter where needed. However, for the reduced order filter where any of the three variables needed for ω_ℓ are not states, ω_ℓ can itself be considered a potential state choice and can be obtained by taking the derivative of Θ_ℓ.

Taking the derivative of ω_ℓ can be simplified by using equation (3-20) and the approximation

$$V_{A/T} = V_A \cos(\Theta_\ell - \Theta_A) \tag{3-18}$$

where

V_A = the magnitude of the A/C velocity

$\dot{V}_A$ = 0 is assumed in this study

V_T = 0 is assumed

Then $\dot{\omega}_\ell$ becomes

$$\dot{\omega}_\ell = \frac{-V_{A/T}^2}{R_{A/T}^2} \tan(\Theta_\ell - \Theta_A) \tag{3-19}$$

Alternatively, $\dot{\omega}$ can be obtained in the simulation by

$$\dot{\omega}_\ell \approx [\omega_\ell(t_{i+1}) - \omega_\ell(t_i)]/(t_{i+1} - t_i) \tag{3-20}$$

since the rate of change of ω_ℓ will be small and relatively constant.

The aircraft accelerations were obtained in a similar fashion as that of the missile except without the INS inputs. Then the derivative of aircraft line-of-sight range yielding:

$$\dot{R}_{A/T} = V_{A/T} \tag{3-21}$$

3-9

Applying the Theorem of Coriolis to $R_{A/T}$ yields

$$\ddot{R}_{A/T} = +2 \; \dot{z}_{A/T} \; \omega_\ell + R_{A/T} \; \omega_\ell^2 + z_{A/T} \; \dot{\omega}_\ell \tag{3-22}$$

where

$$\dot{z}_{A/T} = \dot{R}_{A/T} \; \tan(\Theta_\ell - \Theta_A) \tag{3-23}$$

Substituting equation (3-23) into equation (3-22) and $z_{A/T} = 0$ by definition $\dot{\omega}_\ell$ negligible, $\ddot{R}_{A/T}$ is expressed in state variables

$$\ddot{R}_{A/T} = +2 \; \omega_\ell \; \dot{R}_{A/T} \; \tan(\Theta_\ell - \Theta_A) + R_{A/T} \; \omega_\ell^2 \tag{3-24}$$

The measurement equations for all of the LOS form filters considered here was given as

$$EL = \sin^{-1}\left[\frac{z}{R_{A/T} - R_{M/T}}\right] \tag{3-25}$$

The Proportional Navigation Guidance Law has the general form

$$A_{CMD} = n \; V_C \; \omega_{MTLOS} \tag{3-26}$$

where

A_{CMD} = commanded acceleration normal to LOS

n = gain constant

V_C = missile-to-target closing velocity

ω_{MTLOS} = rate of change of missile-to-target LOS

The gain constant is a term by which the user can "tune" the guidance law to optimize the overall performance of the algorithm for a given situation. This term typically has a range of approximately 3 to 5.

Using a lower number tends to produce larger accelerations toward the end of the trajectory. Increasing the gain term will bring the missile on course earlier in the flight while the velocity is lower.

The closing velocity was derived from

$$V_C = \frac{V^i_{-M/T} \cdot r_{-M/T}}{\left| r_{M/T} \right|} \tag{3-27}$$

and expressing this in terms of the state variables will yield:

$$V_C = \frac{R_{M/T} \dot{R}_{M/T} + z \dot{z}}{(R^2_{M/T} + z^2)^{1/2}} \tag{3-28}$$

For the air-to-surface scenario used here, it is reasonable to assume that $R_{M/T} \gg z$ and that $R_{M/T} \dot{R}_{M/T} \gg z \dot{z}$. With this assumption, the closing velocity can be approximated by the missile velocity along $\hat{\ell}_1$ as

$$V_C = \dot{R}_{M/T} \tag{3-29}$$

The expression for ω_{MTLOS} becomes a little more involved and was obtained from

$$\omega_{-MTLOS} = \frac{r_{M/T} \times V^i_{-M/T}}{\left| r_{M/T} \right|^2} \tag{3-30}$$

where $r_{M/T}$ and $V^i_{M/T}$ are defined in equation (3-5) and equation (3-7). As expressed in the state variables this cross product becomes

$$\omega_{MTLOS} = \left[\frac{\dot{z}}{R_{M/T}} - \omega_\ell - \frac{z \dot{R}_{M/T}}{R^2_{M/T}} + \frac{z^2 \omega_\ell}{R^2_{M/T}} \right] \hat{\ell}_2 \tag{3-31}$$

3-11

In this case the last term is very small with respect to the other terms and is neglected. The final expression for commanded acceleration is:

$$A_{CMD} = -n\left[\dot{R}_{M/T} \quad \frac{z}{R_{M/T}} - \omega_\ell - \frac{\dot{z} \, R_{M/T}}{R^2_{M/T}}\right] \tag{3-32}$$

3.2.3 Filter Model L.2. This filter model is depicted by Figure 3-2. The basic difference from the L.1 model is that the missile-to-target line-of-sight (MTLOS) frame, $\hat{k}$, is used to express positions and velocities. The model is developed in the same manner as the L.1 model and is, therefore, only summarized in terms of states, state equations, measurement model, and guidance law.

The proposed states are

$$x_1 = R_{M/T} = \text{as defined in Section 3.2.2} \tag{3-33}$$

$$x_2 = \dot{R}_{M/T} = \text{as defined in Section 3.2.2} \tag{3-34}$$

$$x_3 = \lambda = \text{missile-to-target line-of-sight angle} \tag{3-35}$$

$$x_4 = \omega_{MTLOS} = \lambda \text{ rate of change} \tag{3-36}$$

$$x_5 = \Theta_\ell = \text{as defined in Section 3.2.2} \tag{3-37}$$

$$x_6 = \omega_\ell = \text{as defined in Section 3.2.2} \tag{3-38}$$

The corresponding state equations are

$$\dot{x}_1 = x_2 \tag{3-39}$$

$$\dot{x}_2 = 2 \, x_4 \, x_2 \, \lambda' + x_1 \, x_4^2 + w_3 \sin x_3$$
$$-(a_1 + w_3) \cos x_3 + (a_3 + w_2) \sin x_3 \tag{3-40}$$

$$\dot{x}_3 = x_4 \tag{3-41}$$

$$\dot{x}_4 = \frac{-x_2^2}{x_1^2} - (a_1 + w_3) \sin(x_3) - (a_3 + w_2) \cos(x_3)$$
$$- w_1 \cos x_3 \tag{3-42}$$

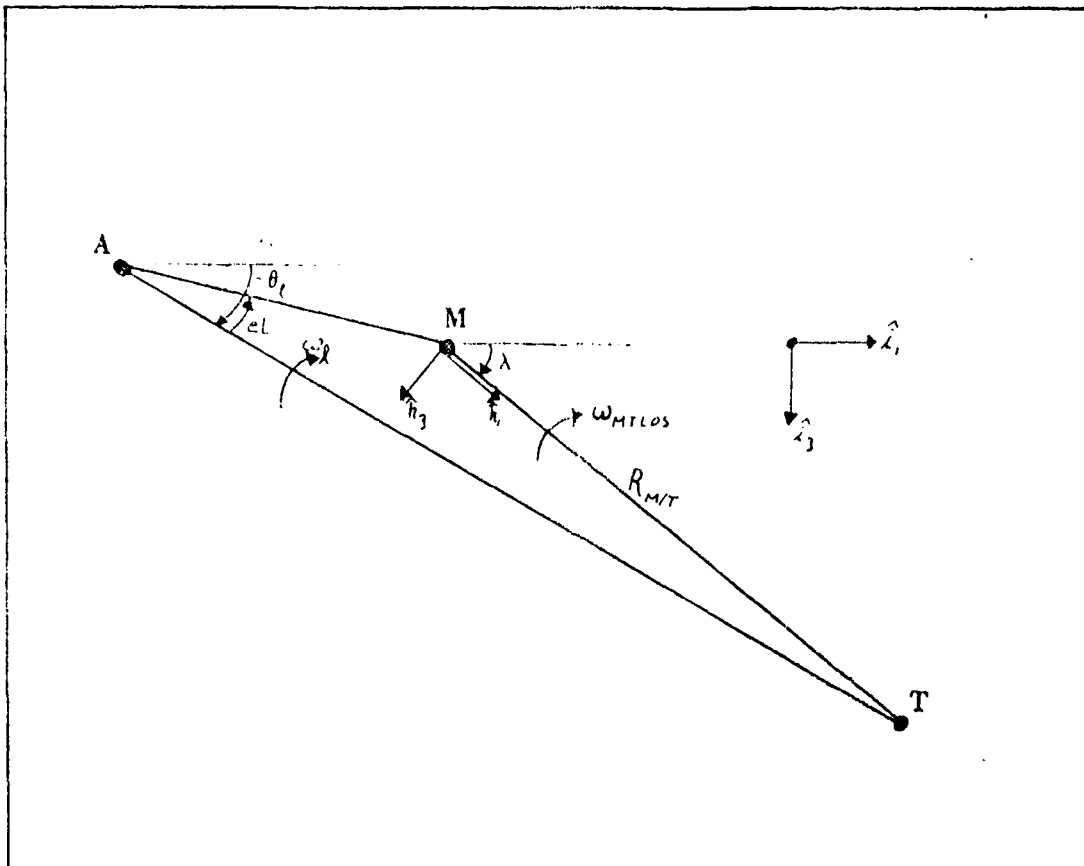$$\dot{x}_5 = x_6 \tag{3-43}$$

$$\dot{x}_6 = w_4 \tag{3-44}$$

3-12

Figure 3-2.   Line-of-Sight Filter L.2 Variable
Description

where

$$\lambda^\prime = \tan(\lambda - \Theta_k)$$

$$\Theta_k = \text{missile flight path angle}$$

$$a_1 \text{ and } a_3 = \text{missile INS total accelerations}$$

$$w_i = \text{as illustrated in Figure 3-3}$$

The measurement model is given as

$$EL = \sin^{-1}\left[\frac{x_1 \sin(x_5 - x_3)}{[(x_{M/o} - x_{A/o})^2 + (z_{M/o} - z_{A/o})^2]^{1/2}}\right] \tag{3-45}$$

where

$x_{M/o}$ and $z_{M/o}$ = missile INS inertial positions

$x_{A/o}$ and $z_{A/o}$ = aircraft inertial positions

The guidance law is

$$a_{CMD} = n(x_2)(x_4) \tag{3-46}$$

3.2.4 Kalman Filter. The above state equations and the measurement equation for filter L.1 were incorporated into an Extended Kalman Filter. The standard Kalman Filter could not be used because of the nonlinear dynamics. The Extended Kalman Filter was selected over the linearized filter to deal with whole valued states and to avoid the problem of selecting a nominal trajectory required for the linearized filter. The filter equations are repeated here for reference.

The system model is of the form:

$$\dot{\underline{x}}(t) = \underline{f}[x(t), \underline{u}(t), t] + \underline{G}(t) \underline{w}(t)$$

$$z(t_i) = h[x(t_i), t_i] + v(t_i)$$

where

$$E[w(t)] = 0$$

$$E[w(t) \, w(t+\tau)^T]^2 = \underline{Q}(t) \, \delta(\tau)$$

$$E[\underline{v}(t_i)] = 0 \tag{3-47}$$

$$E[\underline{v}(t_i)\ \underline{v}(t_j)] = \underline{R}(t)\ \delta(t_i - t_j)$$

The time propagation equations are:

$$\dot{\hat{\underline{x}}}(t/t_{i-1}) = \underline{f}(\hat{x}[t],\ \underline{u}[t],\ t) \tag{3-48}$$

$$\dot{\underline{P}}(t/t_{i-1}) = \underline{F}(t)\ \underline{P}(t/t_{i-1}) + \underline{P}(t/t_{i-1})\ \underline{F}^T(t)$$

$$+\ \underline{G}(t)\ \underline{Q}(t)\ \underline{G}^T(t) \tag{3-49}$$

where

$$\underline{F}(t) = \frac{\partial \underline{f}(x[t],\ \underline{u}[t],\ t)}{\partial \underline{x}}\ \Bigg|_{\underline{x}\ =\ \hat{x}(t_i/t_{i-1})} \tag{3-50}$$

The update equations being

$$\underline{K}(t_i) = \underline{P}(t_i^-)\ \underline{H}^T(t_i)\ [\underline{H}(t_i)\ \underline{P}(t_i^-)\ \underline{H}^T(t_i) + \underline{R}(t_i)]^{-1} \tag{3-51}$$

$$\underline{x}(t_i^+) = \hat{\underline{x}}(t_i^-) + \underline{K}(t_i)\ \underline{z}_i - h[\hat{x}(t_i),\ t] \tag{3-52}$$

$$\underline{P}(t_i^+) = \underline{P}(t_i^-) - \underline{K}(t_i)\ \underline{H}(t_i)\ \underline{P}(t_i^-) \tag{4-53}$$

where

$$\underline{H}(t_i) = \frac{\partial h(\underline{x}[t_i], t)}{\partial x_i}\ \Bigg|_{x_i\ =\ \hat{x}_i(t)} \tag{3-54}$$

The noise sources, ω_i, are illustrated in Figure 3-3 and are additive to the acceleration states as the time correlated Gaussian noise.
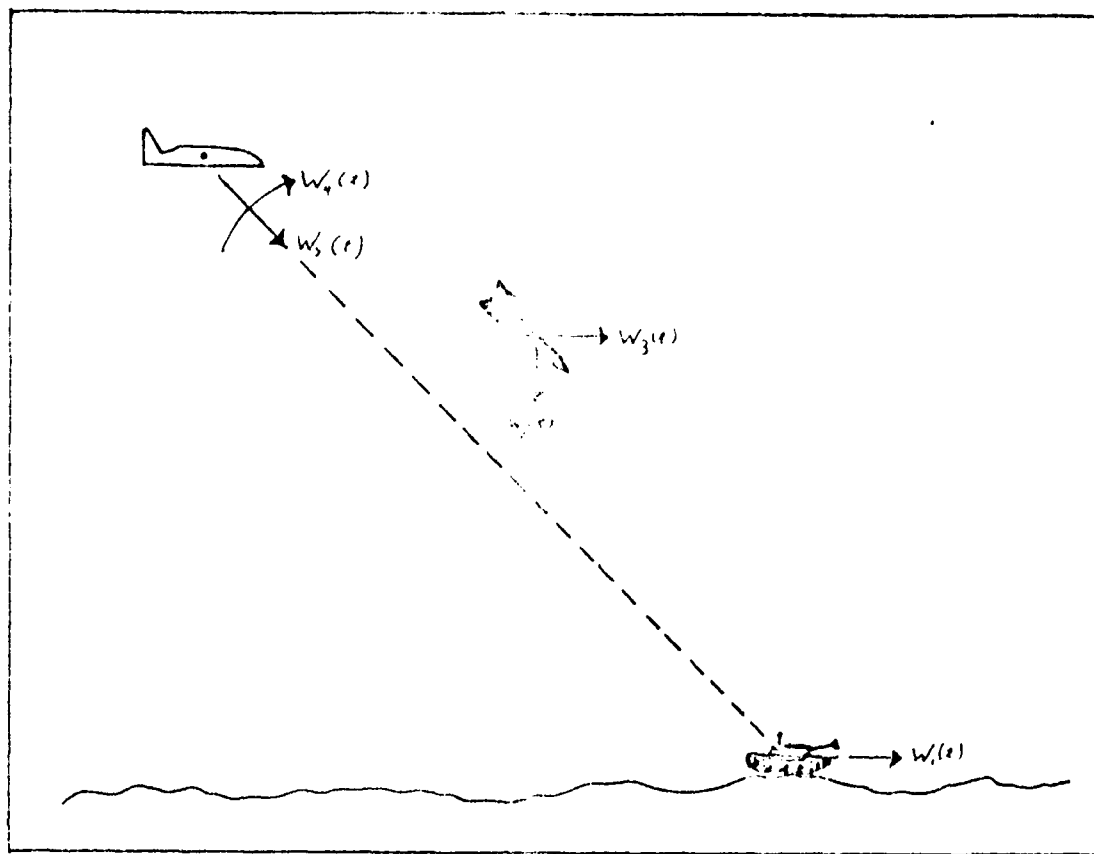
3-15

Figure 3-3. Line-of-Sight Filter Noise Sources

The state equations expressed in physical variables with the noise terms are summarized here:

$$\dot{x}(t) = \begin{bmatrix} \dot{z} \\[6pt] -2\,\dot{R}_{M/T}\,\omega_\ell + a_1\,\sin\Theta_\ell + a_3\,\cos\Theta_\ell \\[4pt] \qquad -R_{M/T}\,\dot{\omega}_\ell + z\,\omega_\ell^2 + (w_3 - w_1)\,\sin\Theta_\ell + w_2\,\cos\Theta_\ell \\[6pt] \dot{R}_{M/T} \\[4pt] 2\,\dot{z}\,\omega_\ell + R_{M/T}\,\omega_\ell^2 + z\dot{\omega}_\ell \\[4pt] \qquad + a_1\,\cos\Theta_\ell - a_3\,\sin\Theta_\ell \\[4pt] \qquad + z\dot{w} + (w_3 - w_1)\,\cos\Theta_\ell + w_2\,\sin\Theta_\ell \\[6pt] -\omega_\ell \\[6pt] \dot{R}_{A/T} \\[4pt] +2\omega_\ell\,\dot{R}_{A/T}\,\Theta' + R_{A/T}(\omega_\ell^2 + \dot{\omega}_\ell\,\Theta') + w_5 \\[4pt] \hline \\[-4pt] -2\,\dfrac{V_{A/T}^2\,\Theta'}{R_{A/T}^2} + w_4 \end{bmatrix}$$

and if ω_ℓ is needed:

$$\text{(3-55)}$$

where $\Theta' = \tan(\Theta_\ell - \Theta_A)$

A note here that in the full order filter, ω_ℓ is not a state to be estimated but a function of states to be estimated. However, the $w_4(t)$ term was used in the simulation to apply a minimal amount of noise to the z state covariance. This was needed to offset the negative trend caused by the cross coupling of other states into the z state as a result of Euler Integration errors. (Reference Section 5.2.1).

For the purposes of implementing $P(t_0)$ the selection of the variances at time t_0 was based on the knowledge of the states at the time of launch. At launch, the missile uncertainties are the same as those of the aircraft. The INS on the aircraft has a 1σ uncertainty

of 2-ft/sec in $\hat{x}$ and $\hat{z}$ (Ref. 11) and 0.5 milli-rad in attitude. The
tracker used is a Forward Looking Infra-Red (FLIR) class of Infra-Red
(IR) trackers with a 0.3 milli-rad angular accuracy and 150 ft in range.
These figures yield 1σ values for the following states.

$z \quad (0)^2 \qquad\qquad$ = Perfect knowledge of z at launch since missile is
$\qquad\qquad\qquad\qquad$ on ATLOS

$\dot{z} \quad (2 \text{ ft/sec})^2$ = Same as A/C

$R_{M/T} \ (150 \text{ ft})^2$ = From the tracker

$\dot{R}_{M/T} \ (2 \text{ ft/sec})^2$ = Same as A/C

$\Theta_\ell \quad (0.3 \text{ MRAD})^2$ = From the tracker

$\omega_\ell \quad (0.5/\text{sec})^2$ = z error/nominal range to TGT (if used)

$R_{A/T} \ (150 \text{ ft})^2$ = From the tracker

$R_{A/T} \ (2 \text{ ft/sec})^2$ = From A/C INS

These values serve as initial values for the filter testing.

The components of the propagation and update equations expressed
and developed above are summarized in Appendix C for reference.

3.2.5 Observability. The seven-state filter developed above
forms the basis of a number of reduced order filters. Many possible
combinations of states would appear to be suitable for implementation in
an estimator for the missile's guidance. The observability test
discussed earlier in this chapter was used to sort out potential
candidates. This test was first performed on the full order filter to
verify its validity. Various other combinations of states were checked
and summarized in Table 3-1. The z and $\dot{z}$ states were kept in each
filter since the measurement model and the guidance law are strongly
influenced by them.

It appears from Table 3-1 that ω decouples the $R_{M/T}$ and
$R_{A/T}$ measurements. Of the combinations listed in this table, some
could have increasing observability problems as ω goes to zero.

However, since the observability criteria was met with one measurement, additional measurements were not considered.

3.2.6 Reduced Order Filters. The state equations for the reduced order filters are essentially a subset of the state equations developed for the full order filter and presented in detail in Appendix C.1. The selection of state combinations was chosen to ensure observability as determined in Table 3-1. The initial implementation will be limited to 1 as the full order filter and 10 as the reduced order filter. Filter 10 was chosen since it estimates the missile states which have the greater effects on measurements and the guidance law as shown at the bottom of Table 3-1.

TABLE 3-1

LOS FILTER OBSERVABILITY SUMMARY

No.	z	$\dot{z}$	$R_{M/T}$	$\dot{R}_{M/T}$	Θ_ℓ	ω_ℓ	$R_{A/T}$	$V_{A/T}$	No. of States	$\omega \neq 0$	$\omega = 0$
1	X	X	X	X	X		X	X	7	7	6
2	X	X	X	X	X	X			6	6	4
3	X	X		X	X	X	X		6	6	5
4	X	X	X	X		X			5	5	3
5	X	X	X	X			X		5	4	2
6	X	X	X		X	X			5	4	4
7	X	X	X			X	X		5	4	4
8	X	X		X	X	X			5	5	4
9	X	X		X		X	X		5	5	4
10	X	X	X	X					4	4	2
11	X	X	X			X			4	3	3
12	X	X		X		X	X	X	4	4	3
13	X	X				X			4	4	4
14	X	X				X	X	X	4	4	4
15	X	X							4	4	3
	X		X				X		Measurement Model		
	X	X	X	X		X			Guidance Law		

NOTE: ω_ℓ is a function of Θ_ℓ, $R_{A/T}$, and $V_{A/T}$.

3.3 Development of Inertial Filters

3.3.1 Introduction. This section contains the development of
the I.1 filter model and the Kalman Filter based upon this model. The
I.2 model follows the same form of development as the I.1 model and is
presented in summary form. In addition, a reduced order filter model is
proposed and the corresponding filter derived. Observability
considerations also play a vital role in determining the final
configuration of this reduced order model.

3.3.2 Filter Model I.1. This filter model was based on an
inertial frame formulation of relative aircraft-to-target and
missile-to-target information. Since both the aircraft and the missile
travel much faster than the target, the target was assumed stationary in
developing the dynamics equations. Also, the aircraft was assumed to
have a constant velocity and altitude (feasible due to short missile
flight time) during the engagement. The dynamics equations are
developed based on these assumptions and acceleration uncertainties are
modeled as white Gaussian noises. The geometric relationships are
depicted in Figure 3-4.

The states are

$x_1 = x_{M/T} = \hat{i}_1$ component of missile position with respect to the target

$x_2 = \dot{x}_{M/T} = \hat{i}_1$ component of missile velocity with respect to the target

$x_3 = z_{M/T} = \hat{i}_3$ component of missile position with respect to the target

$x_4 = \dot{z}_{M/T} = \hat{i}_3$ component of missile velocity with respect to the target

$x_5 = x_{A/T} = \hat{i}_1$ component of aircraft position with respect to the target

$x_6 = \dot{x}_{A/T} = \hat{i}_1$ component of aircraft velocity with respect to the target

$x_7 = z_{A/T} = \hat{i}_3$ component of aircraft position with respect to the target

$x_8 = \dot{z}_{A/T} = \hat{i}_3$ component of aircraft position with respect to the target

3-20
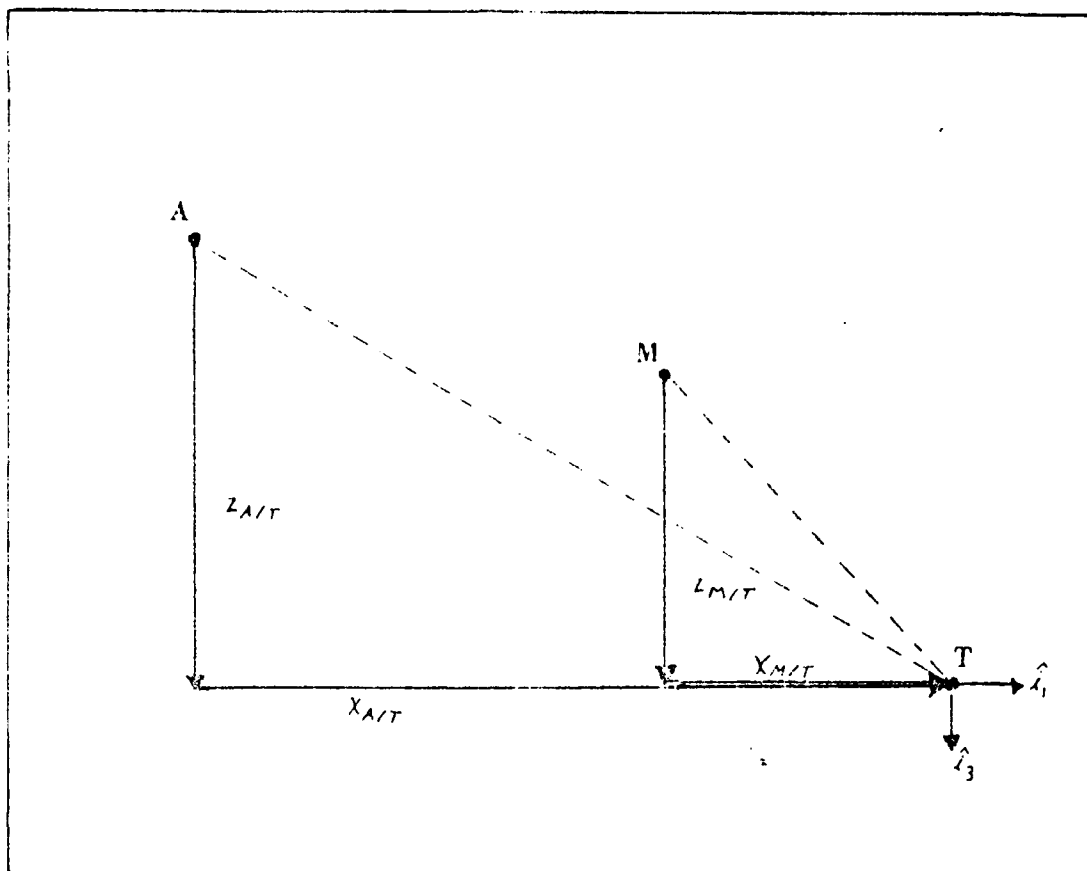
Figure 3-4. Inertial Filter I.1 Variable Description

An observability test was performed on the I.1 filter model and the results are summarized in Table 3-2. Using the angle only measurement of elevation results in unobservable states in the system. Moreover, by adding both missile-to-target range and aircraft-to-target range measurements, the system still is unobservable. To obtain a more observable system, the aircraft altitude $z_{A/T}$, and its rate of change, $\dot{z}_{A/T}$, were deleted as states from the dynamics model. The aircraft altitude, however, was needed in the measurement model and guidance law. This information was assumed to be passed from the aircraft to the missile at launch and extrapolated by the missile during flight. As in Table 3-3, only one unobservable state remains using the three measurements. This system was implemented with the one unobservable state, however, showed no significant degradation as a result. The ranges were passed from the aircraft to the missile at launch. Based upon this initial condition, the missile propagates the ranges, with uncertainty accounted for, and passes them to the filter as pseudo-measurements. This initial investigation incorporates white Gaussian noises to model the acceleration uncertainties. The addition of time-correlated uncertainty models is recommended for further study and comparisons.

The state equations are

$$\dot{x}_1 = x_2 \tag{3-56}$$

$$\dot{x}_2 = a_1 + w_1 + w_3 \tag{3-57}$$

$$\dot{x}_3 = x_4 \tag{3-58}$$

$$\dot{x}_4 = a_3 + w_2 + w_4 \tag{3-59}$$

$$\dot{x}_5 = x_5 \tag{3-60}$$

$$\dot{x}_6 = w_3 + w_5 \tag{3-61}$$

where

a_1, a_3 = INS inertial accelerations

w_1, w_2 = zero mean white Gaussian noise models for missile acceleration uncertainties

3-22

TABLE 3-2

Full Order Inertial Model Observability

Measurements	Number of Unobservable States
EL	6
EL, R_{AT}	4
EL, R_{MT}	4
EL, R_{MT}, R_{AT}	2

TABLE 3-3

Sixth Order Model Observability

Measurements	Number of Unobservable States
EL	4
EL, R_{AT}	3
EL, R_{MT}	2
EL, R_{MT}, R_{AT}	1

w_3, w_4 = zero mean white Gaussian noise models for inertial target acceleration uncertainties

w_5 = zero mean white Gaussian noise model for inertial aircraft acceleration uncertainties

The statistics of the initial conditions and the uncertainties are contained in Section 3.3.4.

The elevation measurement equation was derived from the geometry depicted in Figure 3-5.

$$-\tan(\Theta_\ell + EL) = \frac{z_{M/A}}{x_{M/A}} \tag{3-62}$$

where

$$z_{M/A} = z_{M/T} - z_{A/T} \tag{3-63}$$

$$x_{M/A} = x_{M/T} - z_{A/T} \tag{3-64}$$

Taking the inverse tangent of both sides of equation (3-62) and solving for elevation results in

$$EL = -\Theta_\ell - \tan^{-1}\left[\frac{z_{M/T} - z_{A/T}}{x_{M/T} - x_{A/T}}\right] \tag{3-65}$$

Also

$$-\tan(\Theta_\ell) = \frac{-z_{A/T}}{-x_{A/T}} \tag{3-66}$$

Solving this equation for Θ_ℓ and substituting into equation (3-65) yields

$$EL = \tan^{-1}\left[\frac{-z_{A/T}}{-x_{A/T}}\right] - \tan^{-1}\left[\frac{z_{M/T} - z_{A/T}}{x_{M/T} - x_{A/T}}\right] \tag{3-67}$$
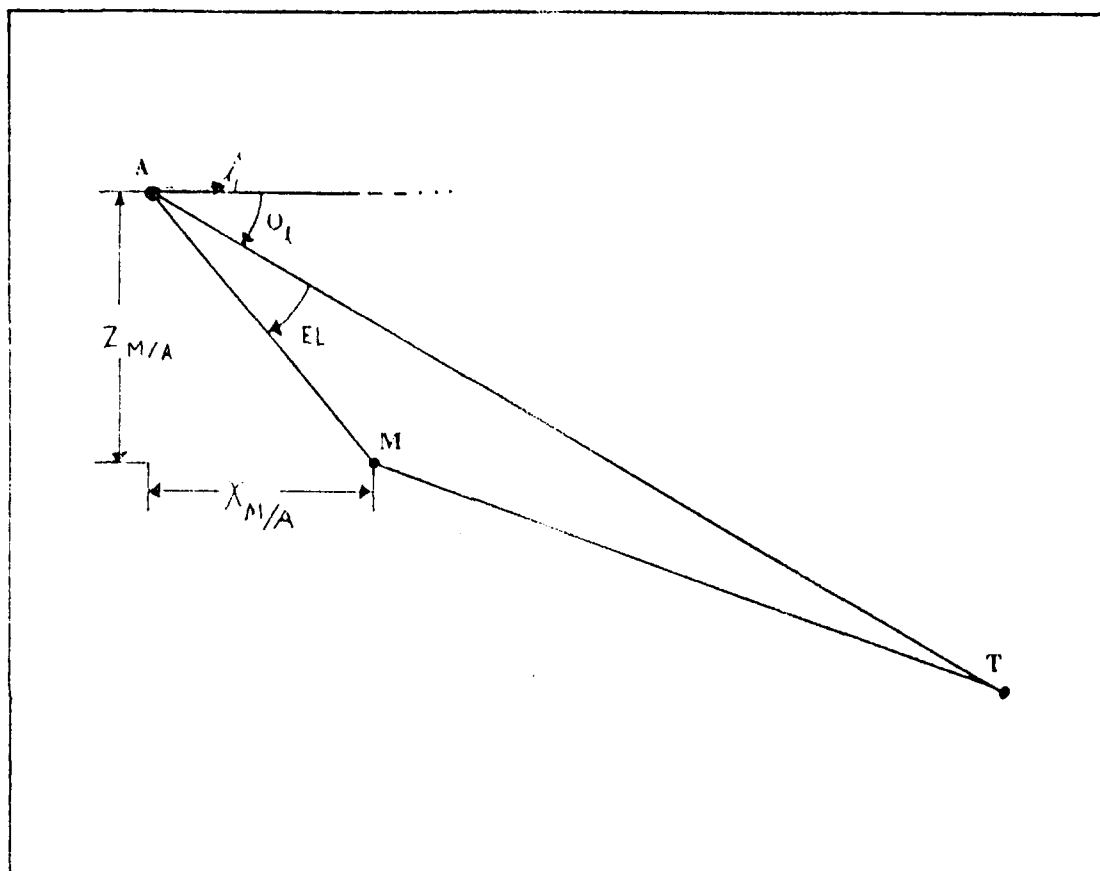
Figure 3-5.   Inertial Filter I.1 Measurement Model
Geometry

In terms of states this becomes

$$EL = \tan^{-1} \left[\frac{-z_{A/T}}{-x_5} \right] - \tan^{-1} \left[\frac{x_3 - z_{A/T}}{x_1 - x_5} \right] \qquad (3-68)$$

The aircraft-to-target range is

$$R_{AT} = (x_{A/T}^2 + z_{A/T}^2)^{1/2} \qquad (3-69)$$

and in terms of states becomes

$$R_{AT} = (x_5^2 + z_{A/T}^2)^{1/2} \qquad (3-70)$$

The missile-to-target range is

$$R_{MT} = (x_{M/T}^2 + z_{M/T}^2)^{1/2} \qquad (3-71)$$

which becomes

$$R_{MT} = (x_1^2 + x_3^2)^{1/2} \qquad (3-72)$$

Each of the three measurements are corrupted by noise prior to being received by the filter. The statistics of those noises and the method of processing the measurements are discussed in Section 3.3.4.

As discussed in the truth model, proportional navigation is the guidance law selected for this study. The law can be written as

$$A_{CMD} = n \, V_C \, \omega_{HTLOS} \qquad (3-26)$$

The closing velocity is determined by

$$V_C = \underline{V}_{M/T}^i \cdot \frac{\underline{r}_{M/T}}{\left| \underline{r}_{M/T} \right|} \qquad (3-27)$$

Substituting the planar expressions:

$$\underline{r}_{M/T} = x_{M/T}\ \hat{i}_1 + z_{M/T}\ \hat{i}_3 \tag{3-73}$$

$$\underline{v}^i_{M/T} = \dot{x}_{M/T}\ \hat{i}_1 + \dot{z}_{M/T}\ \hat{i}_3 \tag{3-74}$$

into equation (3-27) yields

$$V_C = \frac{(x_{M/T})\ (\dot{x}_{M/T}) + (z_{M/T})\ (\dot{z}_{M/T})}{(x^2_{M/T} + z^2_{M/T})\ 1/2} \tag{3-75}$$

In terms of states this becomes

$$V_C = \frac{(x_1)\ (x_2) + (x_3)\ (x_4)}{(x^2_1 + x^2_3)^{1/2}} \tag{3-76}$$

The MTLOS rate vector is expressed as

$$\underline{\omega}_{MTLOS} = \frac{\underline{r}_{M/T} \times \underline{v}^i_{M/T}}{\left|\underline{r}_{M/T}\right|^2} \tag{3-30}$$

Substituting equations (3-73) and (3-74) into equation (3-30) yields

$$\underline{\omega}_{MTLOS} = \left[\frac{(\dot{x}_{M/T})\ (z_{M/T}) - (x_{M/T})\ (\dot{z}_{M/T})}{(x^2_{M/T} + z^2_{M/T})}\right]\hat{\ell}_2 \tag{3-77}$$

Therefore

$$\omega_{MTLOS} = \frac{(\dot{x}_{M/T})\ (z_{M/T}) - (x_{M/T})\ (\dot{z}_{M/T})}{(x^2_{M/T} + z^2_{M/T})} \tag{3-78}$$

3-27

Therefore

$$\omega_{MTLOS} = \frac{(\dot{x}_{M/T})(z_{M/T}) - (x_{M/T})(\dot{z}_{M/T})}{(x_{M/T}^2 + z_{M/T}^2)} \tag{3-79}$$

In terms of states this becomes

$$\omega_{MTLOS} = \frac{(x_2)(x_3) - (x_1)(x_4)}{(x_1^2 + x_3^2)} \tag{3-80}$$

Thus in final form

$$A_{CMD} = n\left[\frac{(x_1)(x_2) + (x_3)(x_4)}{(x_1^2 + x_3^2)^{1/2}}\right]\left[\frac{(x_2)(x_3) - (x_1)(x_4)}{(x_1^2 + x_3^2)}\right] \tag{3-81}$$

3.3.3 Filter Model I.2. This filter model was based on a cartesian inertial coordinate formulation of aircraft and target variables and derived in a similar manner as the I.1 model above. Filter I.2 is summarized here in terms of states, state equations, measurement model and guidance law. The scenario is depicted in Figure 3-6. The missile has accurate knowledge of its own dynamics from the INS data. The filter estimates aircraft and target states. The deterministic dynamics equations are based upon a stationary target and a constant velocity, constant altitude aircraft.

Aircraft and target acceleration uncertainties are modeled as time correlated noises. The states are

$x_1 = x_{T/0} = \hat{i}_1$ component of target position

$x_2 = \dot{x}_{T/0} = \hat{i}_1$ component of target velocity

$x_3 = z_{T/0} = \hat{i}_3$ component of target position
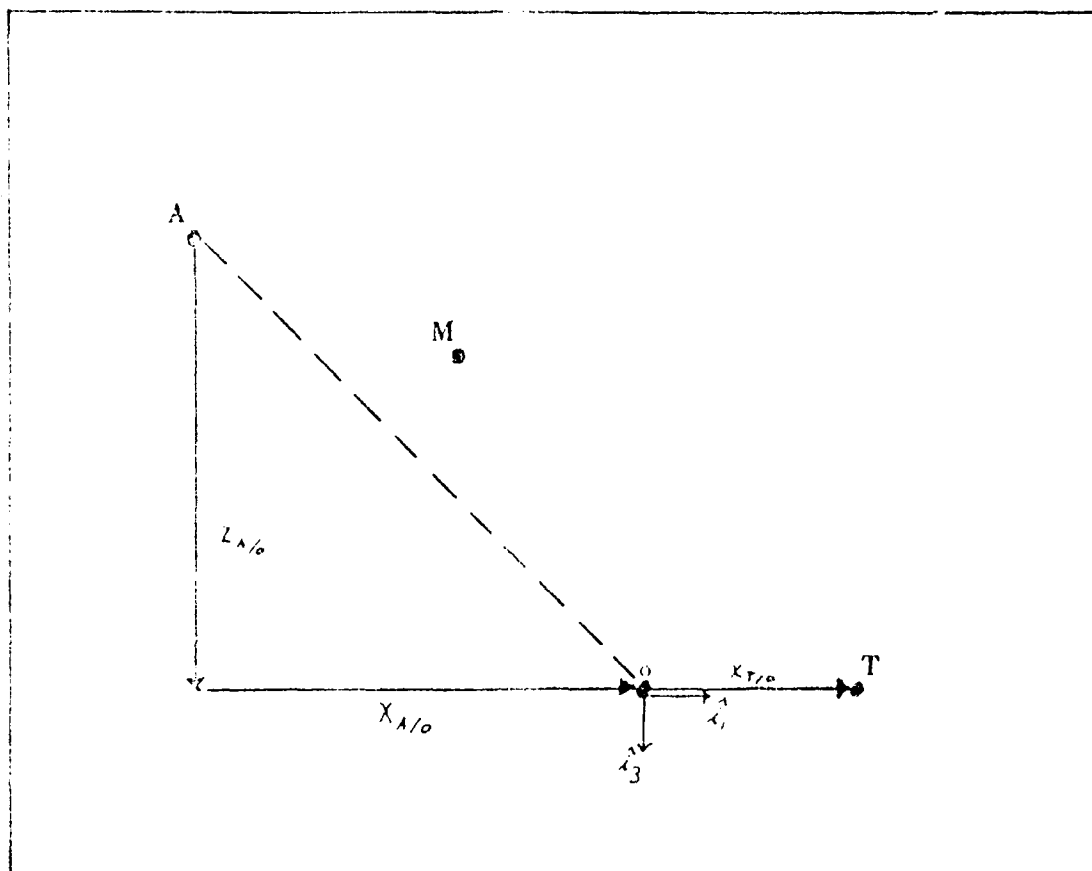
Figure 3-6. Inertial Fiiter I.2 Variable Description

$$x_4 = \dot{z}_{T/0} = \hat{i}_3 \text{ component of target velocity}$$

$$x_5 = x_{A/0} = \hat{i}_1 \text{ component of aircraft position}$$

$$x_6 = \dot{x}_{A/0} = \hat{i}_1 \text{ component of aircraft velocity}$$

$$x_7 = z_{A/0} = \hat{i}_3 \text{ component of aircraft position}$$

$$x_8 = \dot{z}_{A/0} = \hat{i}_3 \text{ component of aircraft velocity}$$

The corresponding state equations are

$$\dot{x}_1 = x_2 \qquad\qquad (3\text{-}82)$$

$$\dot{x}_2 = w_1 \qquad\qquad (3\text{-}83)$$

$$\dot{x}_3 = x_4 \qquad\qquad (3\text{-}84)$$

$$\dot{x}_4 = w_2 \qquad\qquad (3\text{-}85)$$

$$\dot{x}_5 = x_6 \qquad\qquad (3\text{-}86)$$

$$\dot{x}_6 = w_3 \qquad\qquad (3\text{-}87)$$

$$\dot{x}_7 = x_8 \qquad\qquad (3\text{-}88)$$

$$\dot{x}_8 = w_4 \qquad\qquad (3\text{-}89)$$

where

w_1 and w_2 = white Gaussian noise representing inertial target acceleration uncertainties

w_3 and w_4 = white Gaussian noise representing inertial aircraft acceleration uncertainties

The deterministic measurement model is

$$EL = \tan^{-1}\left[\frac{x_3 - x_7}{x_1 - x_5}\right] - \tan^{-1}\left[\frac{z_{M/0} - x_7}{x_{M/0} - x_5}\right] \qquad (3\text{-}90)$$

where

$x_{M/0}$ and $z_{M/0}$ = missile INS inertial position

The guidance law is

$$A_{CMD} = n \left[\frac{(x_{M/o} - x_1)(\dot{x}_{M/o} - x_2) + (z_{M/o} - x_3)(\dot{z}_{M/o} - x_4)}{[(x_{M/o} - x_1)^2 + (z_{M/o} - x_3)^2]^{1/2}} \right]$$

$$\left[\frac{(\dot{x}_{M/o} - x_2)(z_{M/o} - x_3) - (x_{M/o} - x_1)(\dot{z}_{M/o} - x_4)}{[(x_{M/o} - x_1)^2 + (z_{M/o} - x_3)^2]^{1/2}} \right] \quad (3-91)$$

where the following parameters are assumed available from the INS

$x_{M/o}$ and $z_{M/o}$ = as defined above

$\dot{x}_{M/o}$ and $\dot{z}_{M/o}$ = missile INS inertial velocities

3.3.4 Kalman Filter. An estimation algorithm is next developed based upon the I.1 model just described in Section 3.3.2. This filter estimates the states from noise corrupted observations of the real world. The optimal estimation algorithm for linear systems driven by white Gaussian noises is the Kalman Filter. For systems which are nonlinear, extensions of the Kalman Filter have been developed. A partial list of these extensions are the linearized Kalman Filter, the Extended Kalman Filter, the Modified Gaussian Second-Order Filter, and the Truncated Gaussian Second-Order Filter. The first two of these extensions linearize the system by using the first term of the Taylor series expansion about a nominal state trajectory. The remaining two are nonlinear techniques which use higher order terms of the Taylor series expansion to provide better modeling of the nonlinearities in the system.

The I.1 model has linear dynamics with nonlinear measurement equations. The linear dynamics model logically leads to an equivalent discrete-time model formulation and its corresponding time propagation equations. The nonlinear measurement equations motivate the use of the Extended Kalman Filter (EKF) equations. The EKF is the more widely used of the extensions to the linear Kalman Filter and is a good initial choice in solving the nonlinear estimation update problem because of the ease of implementation.

Examples of its use are contained in references 1, 3, 5, and 9. The EKF is superior to the linearized Kalman Filter in that it linearizes about current estimates of the states, as opposed to a reference trajectory. Higher order nonlinear filtering is a more complex alternative; therefore is only considered if the desired performance characteristics are not met by the EKF. The higher order filters are also more difficult and costly to implement than the EKF. For these reasons, they are not considered in this initial study.

The filter dynamics model in matrix form is

$$\dot{\underline{x}}(t) = \underline{F}\,\underline{x}(t) + \underline{B}\,\underline{u}(t) + \underline{G}\,\underline{w}(t) \qquad (3\text{-}92)$$

where

$$\underline{F} = \begin{bmatrix} 0 & 1 & 0 & 0 & 0 & 0 \\ 0 & 0 & 0 & 0 & 0 & 0 \\ 0 & 0 & 0 & 1 & 0 & 0 \\ 0 & 0 & 0 & 0 & 0 & 0 \\ 0 & 0 & 0 & 0 & 0 & 1 \\ 0 & 0 & 0 & 0 & 0 & 0 \end{bmatrix} \qquad (3\text{-}93) \qquad \underline{B} = \begin{bmatrix} 0 & 0 \\ 1 & 0 \\ 0 & 0 \\ 0 & 1 \\ 0 & 0 \\ 0 & 0 \end{bmatrix} \qquad (3\text{-}94)$$

$$\underline{G} = \begin{bmatrix} 0 & 0 & 0 & 0 & 0 \\ 1 & 0 & 1 & 0 & 0 \\ 0 & 0 & 0 & 0 & 0 \\ 0 & 1 & 0 & 1 & 0 \\ 0 & 0 & 0 & 0 & 0 \\ 0 & 0 & 1 & 0 & 1 \end{bmatrix} \qquad (3\text{-}95) \qquad \underline{u}(t) = \begin{bmatrix} a_1(t) \\ a_3(t) \end{bmatrix} \qquad (3\text{-}96)$$

$$
\underline{w}(t) = \begin{matrix} w_1(t) \\ w_2(t) \\ w_3(t) \\ w_4(t) \\ w_5(t) \end{matrix} \qquad\qquad (3\text{-}97)
$$

The initial condition $\underline{x}(t_0)$ is Gaussian with

$$
E[\underline{x}(t_0)] = \hat{\underline{x}}_0 \qquad\qquad (3\text{-}98)
$$

$$
E[\underline{x}(t_0)\, \underline{x}^T(t_0)^T] = \underline{P}_0 \qquad\qquad (3\text{-}99)
$$

where the actual values of $\hat{\underline{x}}_0$ and $\underline{P}_0$ are contained in Appendix C. The statistics of the dynamic driving noise are

$$
E[\underline{w}(t)] = 0 \qquad\qquad (3\text{-}100)
$$

$$
E[\underline{w}(t)\, \underline{w}(t')] = \underline{Q}(t)\, \delta(t - t') \qquad\qquad (3\text{-}101)
$$

where $\underline{Q}(t)$ is the strength of the dynamic driving noise, $\underline{w}(t)$. The noises are assumed to be uncorrelated which leads to

$$
\underline{Q}(t) = \begin{bmatrix} Q_1 & 0 & 0 & 0 & 0 \\ 0 & Q_2 & 0 & 0 & 0 \\ 0 & 0 & Q_3 & 0 & 0 \\ 0 & 0 & 0 & Q_4 & 0 \\ 0 & 0 & 0 & 0 & Q_5 \end{bmatrix} \qquad\qquad (3\text{-}102)
$$

where each strength corresponds to one of the individual uncertainties contained in equation (3-97) and depicted in Figure 3-7. As indicated in the figure, all of the uncertainties are assumed to be directed in inertial coordinates. The missile inertial acceleration uncertainties are denoted by w_1 and w_2. The target inertial acceleration uncertainties are denoted by w_3 and w_4. Since the aircraft states in the $\hat{I}_3$ direction have been deleted from the dynamics model, w_5 is the only aircraft inertial acceleration uncertainty that is modeled.

3-33
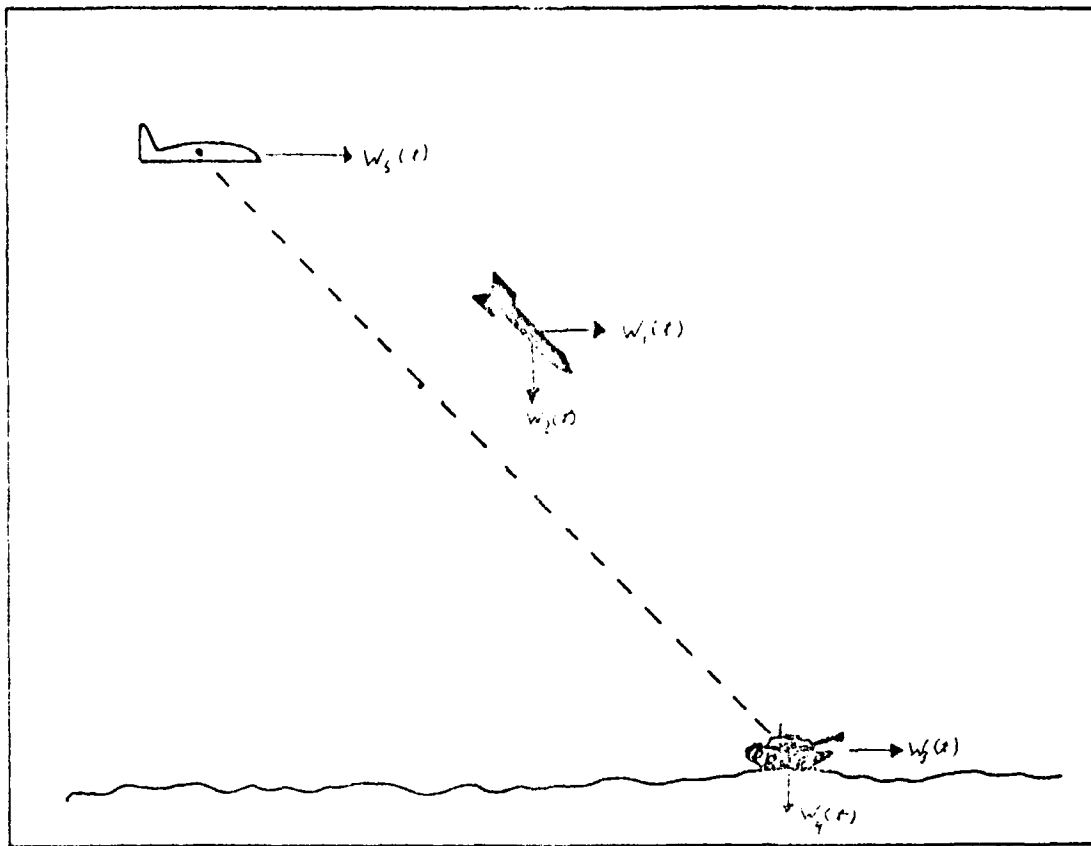
Figure 3-7.　Inertial Filter Noise Sources

The equation used to determine the strengths of the uncertainties is

$$Q_i = \frac{2}{\tau_i} \sigma_i^2 \tag{3-103}$$

The standard deviations, σ_i, and correlation times, τ_i, are listed in Table 2-1 and the corresponding strengths are contained in Appendix C.

Digital computer implementation motivates the equivalent discrete-time model

$$\underline{x}(t_{i+1}) = \underline{\Phi}(t_{i+1}, t_i) \, \underline{x}(t_i) + \underline{B}_d(t_i) \, \underline{u}(t_i) + \underline{w}_d(t_i) \tag{3-104}$$

where

$$E[\underline{w}_d(t_i)] = 0 \tag{3-105}$$

$$E[\underline{w}_d(t_i) \, \underline{w}_d^T(t_j)] = \left\{ \begin{array}{ll} Q_d(t_i) & t_i = t_j \\ 0 & t_i \neq t_j \end{array} \right\} \tag{3-106}$$

and the corresponding time propagation equations

$$\underline{\hat{x}}(t_i^-) = \underline{\Phi}(t_i, t_{i-1}) \, \underline{\hat{x}}(t_{i+1}^+) + \underline{B}_d(t_{i-1}) \, \underline{u}(t_{i-1}) \tag{3-107}$$

$$\underline{P}(t_i^-) = \underline{\Phi}(t_i, t_{i-1}) \, \underline{P}(t_{i-1}^+) \, \underline{\Phi}^T(t_i, t_{i-1}) + \underline{Q}_d(t_{i-1}) \tag{3-108}$$

where

$\quad \underline{\hat{x}}(t_i^-) =$ estimate of states just before update time, t_i

$\Phi(t_i, t_{i-1}) =$ discrete-time state transition matrix to propagate from time t_{i-1} to t_i

$\quad \underline{\hat{x}}(t_{i-1}^+) =$ estimate of states after update at time t_{i-1}

$\quad \underline{B}_d(t_{i-1}) =$ discrete-time input coefficient matrix

$\quad \underline{u}(t_{i-1}) =$ discrete-time samples of the accelerometer inputs

$\quad \underline{P}(t_i^-) =$ filter's conditional covariance matrix just before the update time, t_i

$\underline{P}(t_{i-1}^+)$ = filter's condition covariance matrix after the update at time t_{i-1}

$\underline{\Phi}^T(t_i,t_{i-1})$ = transpose of the discrete-time state transition matrix

$\underline{Q}_d(t_{i-1})$ = strength of the dynamic driving noise, $w_d(t_{i-1})$, at time t_{i-1}

First order approximations are used for the matrices $\underline{\Phi}(t_i,t_{i-1})$, $\underline{B}_d(t_{i-1})$, $\underline{\Phi}^T(t_i,t_{i-1})$, and $\underline{Q}_d(t_{i-1})$, since the dynamics equation is time-invariant and the sample period is short compared to the system time constants. These approximations are

$$\underline{\Phi}(t_i,t_{i-1}) \cong \underline{I} + \underline{F}(t_{i-1})\ [t_i - t_{i-1}] \tag{3-109}$$

$$\underline{B}_d(t_{i-1}) \cong \underline{B}(t_{i-1})\ [t_i - t_{i-1}] \tag{3-110}$$

$$\underline{Q}_d(t_{i-1}) \cong \underline{G}(t_{i-1})\ \underline{Q}(t_{i-1})\ \underline{G}^T(t_{i-1})\ [t_i - t_{i-1}] \tag{3-111}$$

With constant sample period, noise statistics, and dynamics equation coefficients, these matrices are computed initially and remain constant throughout a simulation run.

The actual matrices used for the full order filter are presented in Appendix C.

The measurement equations developed in Section 3.3.2 are each corrupted with a zero mean white Gaussian noise, $v(t_i)$, so that the form of the measurement model is

$$\underline{z}(t_i) = \underline{h}[\underline{x}(t_i),\ t_i] + \underline{v}(t_i) \tag{3-112}$$

where

$$\underline{h}[\underline{x}(t_i),t_i] = \begin{array}{l} \tan^{-1}\left[\dfrac{-z_A/T}{-x_5}\right] - \tan^{-1}\left[\dfrac{x_3 - z_A/T}{x_1 - x_5}\right] \\[2ex] (x_5^2 + z_A/T^2)^{1/2} \\[2ex] (x_1^2 + x_3^2)^{1/2} \end{array}$$

3-36

and

$$\underline{v}(t_i) = \begin{bmatrix} v_1(t_i) \\ v_2(t_i) \\ v_3(t_i) \end{bmatrix}$$

The statistics of the measurement noise are

$$E[\underline{v}(t_i)] = 0 \qquad\qquad (3\text{-}113)$$

$$E[\underline{v}(t_i)\ \underline{v}^T(t_j)] = \begin{cases} \underline{R}(t_i) & t_i = t_j \\ \underline{0} & t_i \neq t_j \end{cases} \qquad (3\text{-}114)$$

where

$$R(t_i) = \begin{bmatrix} R_1 & 0 & 0 \\ 0 & R_2 & 0 \\ 0 & 0 & R_3 \end{bmatrix} \qquad\qquad (3\text{-}115)$$

The elevation measurement noise strength, R_1, was based upon a standard deviation of .001 radians. Squaring this value yields an appropriate initial choice for R_1 of 10^{-6} radians squared.

The pseudo-measurements, R_{MT} and R_{AT}, were computed from filter state estimates rather than truth model measurements. The general form for these measurements is

$$\underline{z}' = \underline{h}'(\hat{\underline{x}}) \qquad\qquad (3\text{-}116)$$

To generate a statistical description of v', let

$$h'(\hat{\underline{x}}) = h'(\underline{x} + \underline{e}) \qquad\qquad (3\text{-}117)$$

where $\underline{e}$ is the filter errors and

$$\underline{h}'(\underline{x} + \underline{e}) \cong \underline{h}'(\underline{x}) + \underline{h}'(\underline{e}) \qquad\qquad (3\text{-}118)$$

then $\underline{h}'(e) = \underline{v}' \cong \underline{H}\ \underline{e}$.   Since the measurement, $\underline{z}'$, and the filter estimate of the measurement were both based on the filter states, the measurement uncertainty is zero. The covariance of the pseudo-measurement then becomes

$$E[\underline{v}'\ \underline{v}'^T] = E[H\ \underline{e}\ \underline{e}^T\ H^T] = \underline{R}' \qquad\qquad (3\text{-}119)$$

3-37

Since $E(\underline{e}\ \underline{e}^T) = \underline{P}$ then

$$\underline{R}' = \underline{H}\ \underline{P}\ \underline{H}^T \tag{3-120}$$

which is the strength of the pseudo-measurements.

The Extended Kalman Filter update equations are

$$\underline{K}(t_i) = \underline{P}(t_i^-)\ \underline{H}^T[t_i,\hat{\underline{x}}(t_i^-)]\ \left[\underline{H}[t_i,\hat{\underline{x}}(t_i^-)]\ \underline{P}(t_i^-)\ \underline{H}^T[t_i,\hat{\underline{x}}(t_i^-)] + \underline{R}(t_i)\right]^{-1} \tag{3-121}$$

$$\hat{\underline{x}}(t_i) = \hat{\underline{x}}(t_i^-) + \underline{K}(t_i)\ \left[\zeta(\underline{t}_i) - \hat{\underline{h}}[\underline{x}(t_i^-),\ t_i]\right] \tag{3-122}$$

$$\underline{P}(t_i^+) = \underline{P}(t_i^-) - \underline{K}(t_i)\ \underline{H}[t_i,\hat{x}(t_i^-)]\ \underline{P}(t_i^-) \tag{3-123}$$

where

$K(t_i)$ = gain matrix

$R(t_i)$ = measurement noise strength

$\hat{\underline{x}}(t_i^+)$ = state estimates after update at time, t_i

$\zeta(t_i)$ = true measurement vector at time, t_i

$\underline{h}[\underline{x}(t_i^-),t_i]$ = filter measurement calculation based on state state estimates at time t_i before update

$P(t_i^+)$ = filter's conditional covariance matrix after the update at time, t_i

and

$$H[t_i,\hat{\underline{x}}(t_i^-)] \triangleq \left. \frac{\partial h[\underline{x},\ t_i]}{\partial \underline{x}} \right|_{\underline{x}=\hat{\underline{x}}(t_i^-)} \tag{3-124}$$

The results of the above operation are listed in Appendix C for reference.

Batch processing and recursive processing are two methods used for incorporating measurements into the update equation at a given sample time. In batch processing, all measurements are simultaneously incorporated into the update equation. Recursive processing, on the other hand, accepts each measurement sequentially. After the first measurement and the corresponding update, the new state estimates and covariances are applied with no propagation stage in the update equation when the next measurement is processed. In this study, recursive processing of the measurements is used for the inertial Extended Kalman Filters.

The recursive form has qualities that make it preferable to batch for on-line processing. In an online situation, the computer allows only a finite amount of time for state estimation. It is possible to get cut off in the middle of incorporating the measurements and, therefore, lose all of the update. In recursive processing, however, at least some of the measurements could have been incorporated and the inherent benefits realized. Recursive processing also uses smaller matrices than batch and thus has simpler algorithms to compute.

For the Extended Kalman Filter, recursive processing has the potential for yielding better estimation performance than batch processing. The Extended Kalman Filter state estimates and covariances are iteratively computed based upon a relinearization about the state estimates each time they are computed. Batch processing the measurements, in this case, results in a single computation of the nominal trajectory at each update. The recursive method, however, computes more than one nominal at each up.ate time, with each successive computation being a better approximation than the previous one. The recursive method thus has the potential for yielding better results, especially when the most accurate measurements are processed first.

3.3.5 Filter Model I.3. Full-order filters are rarely incorporated as on-line estimators. These filters are to be used as benchmarks for comparison of reduced order filters. However, full-order filter models are often inappropriate as benchmarks because of observability problems. For this reason, the full-order, eight state model in this study was reduced to six states. In addition, full-order filters are a computational burden.

This section contains a reduced order filter model which is simply the I.1 filter model with the remaining aircraft states deleted. Since the missile is much more dynamic than either the aircraft or the target, accounting for missile acceleration uncertainties and estimating relative missile-to-target states is preferable. Therefore for this reduced order model, the relative aircraft-to-target states, x_5 and x_6, are deleted from the I.1 dynamics model. Since relative aircraft-to-target position and velocity are needed in the measurement model and the guidance law, they are assumed to be passed to the missile at launch and then extrapolated by the missile during flight. For the filter update, however, the filter's prediction of what the measurement will be includes these crude computations of relative aircraft-to-target positions. All errors between the actual measurements and the filter's prediction of the measurement are processed by the filter, however, these errors are also the result of unmodeled noises and errors in propagated parameters. This factor must be considered during the performance analysis of the filter.

The proposed states are the same as used in the I.1 filter model, but with a reduction in order. The corresponding matrices, initial condition statistics, and noise statistics are contained in Appendix C. The states, state equations, measurement model, and guidance law are

repeated (with appropriate modifications) for convenience to the
reader. The states are

$$x_1 = x_{M/T} = \hat{i}_1 \text{ component of relative missile-to-target position}$$

$$x_2 = \dot{x}_{M/T} = \hat{i}_1 \text{ component of relative missile-to-target velocity}$$

$$x_3 = z_{M/T} = \hat{i}_3 \text{ component of relative missile-to-target position}$$

$$x_4 = \dot{z}_{M/T} = \hat{i}_3 \text{ component of relative missile-to-target velocity}$$

and the state equations are

$$\dot{x}_1 = x_2 \qquad\qquad\qquad (3-125)$$

$$\dot{x}_2 = a_1 + w_1 + w_3 \qquad\qquad\qquad (3-126)$$

$$\dot{x}_3 = x_4 \qquad\qquad\qquad (3-127)$$

$$\dot{x}_4 = a_3 + w_2 + w_4 \qquad\qquad\qquad (3-128)$$

Observability analysis of this model (Table 3-4) reveals that in order
to have complete observability, a missile-to-target range measurement
is necessary in addition to the elevation measurement.

TABLE 3-4

Fourth Order Model Observability

Measurements	Number of Unobservable States
EL	2
EL, R_{MT}	0

3-41

The elevation measurement equation is

$$EL = \tan^{-1}\left[\frac{-z_{A/T}}{-x_{A/T}}\right] - \tan^{-1}\left[\frac{x_3 - z_{A/T}}{x_1 - x_{A/T}}\right] \tag{3-129}$$

The range measurement equation is

$$R_{M/T} = (x_1^2 + x_3^2)^{1/2} \tag{3-130}$$

The guidance law is

$$A_{CMD} = n\left[\frac{(x_1)(x_2) + (x_3)(x_4)}{(x_1^2 + x_3^2)^{1/2}}\right]\left[\frac{(x_2)(x_3) - (x_1(x_4)}{(x_1^2 + x_3^2)}\right] \tag{3-131}$$

3.4 Summary

The various filters that were considered for implementation were specified in this chapter. The filter development approach starts out with defining models upon which to base the filters. A model selection process then takes place in which models were chosen for implementation based upon their favorable characteristics. Two basic model formulations, LOS and inertial, are selected for further development and analysis. A reduced order model from each of these basic formulations was chosen principally by deleting states that have the least effect on the filter measurement prediction and the guidance law commands. Observability also played a key role in determining the final form of these models. State estimation algorithms were then proposed for each model based upon the dynamics equation and measurement model.

IV. SOFTWARE DEVELOPMENT AND VALIDATION

4.1 Introduction

A Software simulation was produced in conjunction with the developments in Chapter II and III to provide the means to evaluate the filters, guidance law, and dynamics models associated with the HVM scenario. The software for this simulation was developed in three phases: Truth Model Validation, Filter Validation, and Monte Carlo Incorporation.

4.2 Truth Model Implementation and Validation.

The overall flow of the program executive (Fig. 4-1), briefly described below, was developed based on the scenario diagram (Fig. 2-2) to control the timing and sequence of the simulation events. Some of the features and implementation methods are discussed here. All repetitive functions or events such as coordinate transforms, truth models, and filters, were committed to subroutines. The aircraft, missile, and target dynamics truth models were implemented as first order vector differential equations. Initially a predictor-corrector variable step size integration routine was used to propagate the states. For computational efficiency, the aircraft and target models were changed to Euler integration since the time constants associated with these two models are 2 seconds and .5 seconds, respectively, as compared to the .02 second sample period. This change reduced the run times by about 40 percent.

Dynamic driving noise was added to the three truth models and to the INS measurements. The INS noises were added as random bias since
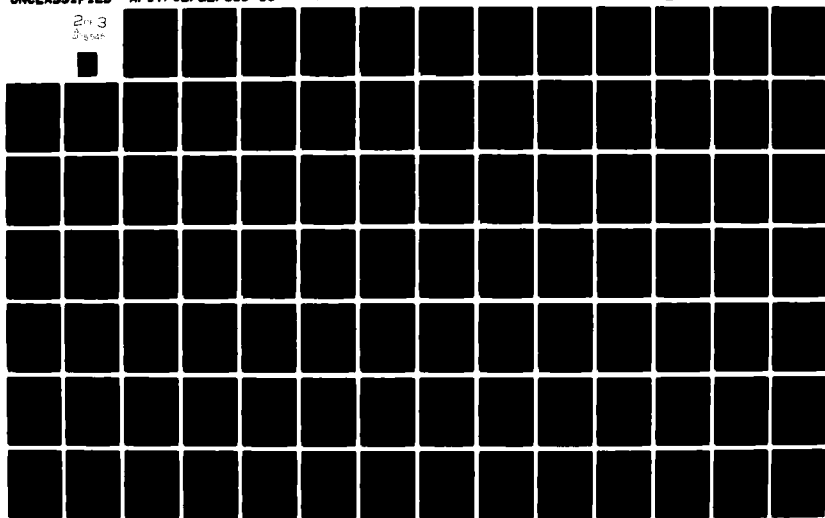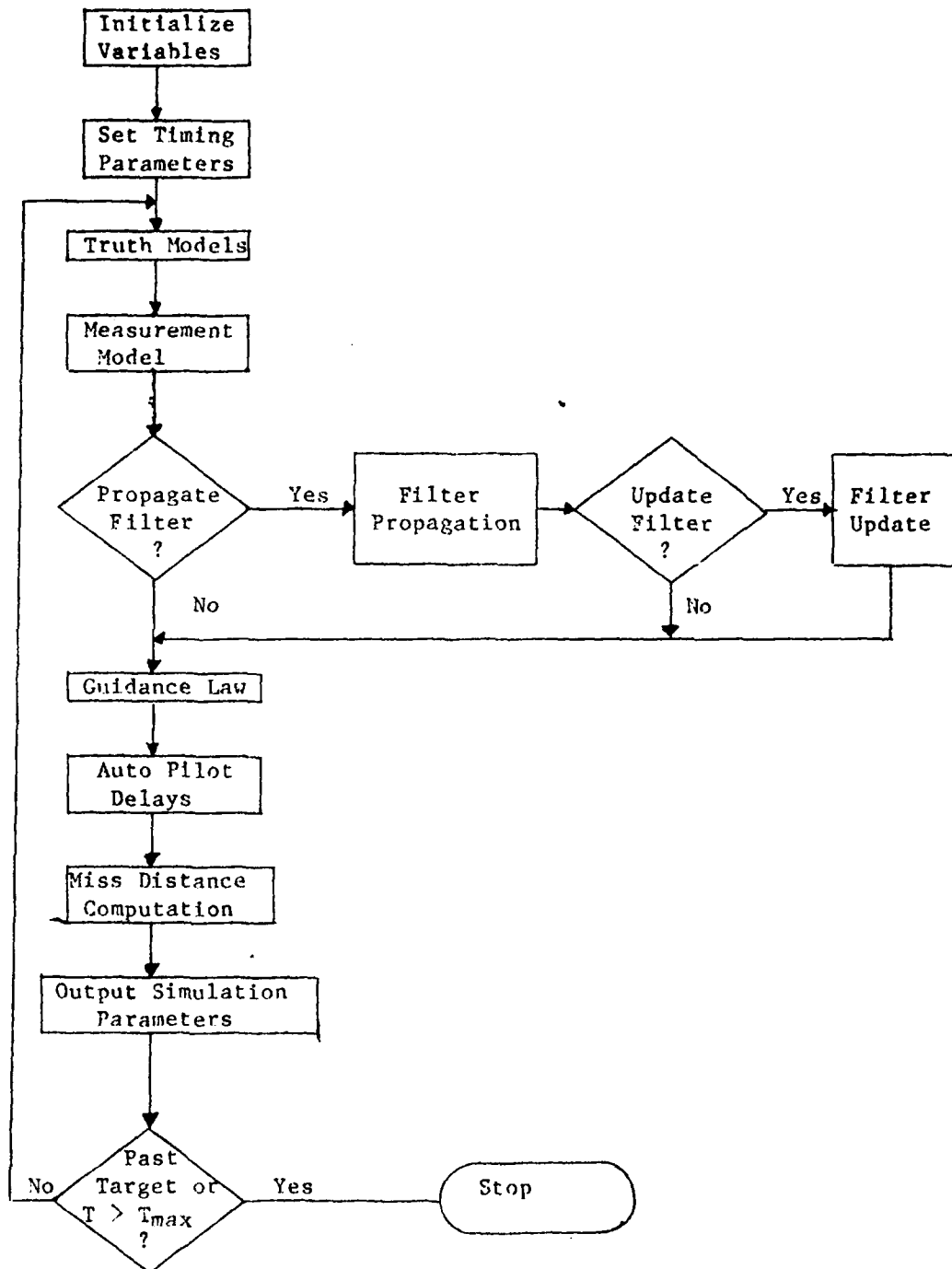
Figure 4-1   Single Mission Simulation Flow Diagram

4-2

the random walk phenomenon in the INS typically has correlation times
greater than 15 minutes while the missile has a flight time of less than
4 seconds. The dynamics truth model driving noise was added as time
correlated noise at the acceleration level. The simulated measurements
taken from the truth models are also corrupted by additive noise. The
initial test case filter is a "true state" filter whose states are
computed based upon the truth model rather than on an estimation
process. The values were used by the guidance law to compute the
desired accelerations which in turn were passed to a discrete time
second order lag (Appendix B.1). This lag models the delays in actuator
response and missile attitude response and outputs the missile's total
acceleration.

The initial test cases for the truth models are illustrated in
Fig. 4-2. These profiles exercised the lateral and vertical dynamics
and the guidance law to check for major implementation errors. To
further check the algorithms the commanded acceleration was fixed at
100 ft/sec/sec and propagated for .1 seconds. The change in position
and velocity compared with the closed form approximations with less than
5 percent error. Therefore, the truth model represented well the
intended trajectory.

4.3 Filter Implementation and Validation.

Valid truth models gave the needed foundation for implementing the
filters developed in Chapter III. The "true state" filter was replaced
by the filters designed and the dynamics restricted to the vertical
plane. In validating the filter for a given flight profile, the filter
was critiqued in two main areas. First was whether or not the dynamics
of the states responded according to the commanded accelerations as did
the truth model. And secondly, did the covariance matrix remain
positive semidefinite. This testing was accomplished without driving
noise added to the truth model states and without perturbed initial
conditions. As discussed in the filter evaluation (Section 5.2.1),

4-3
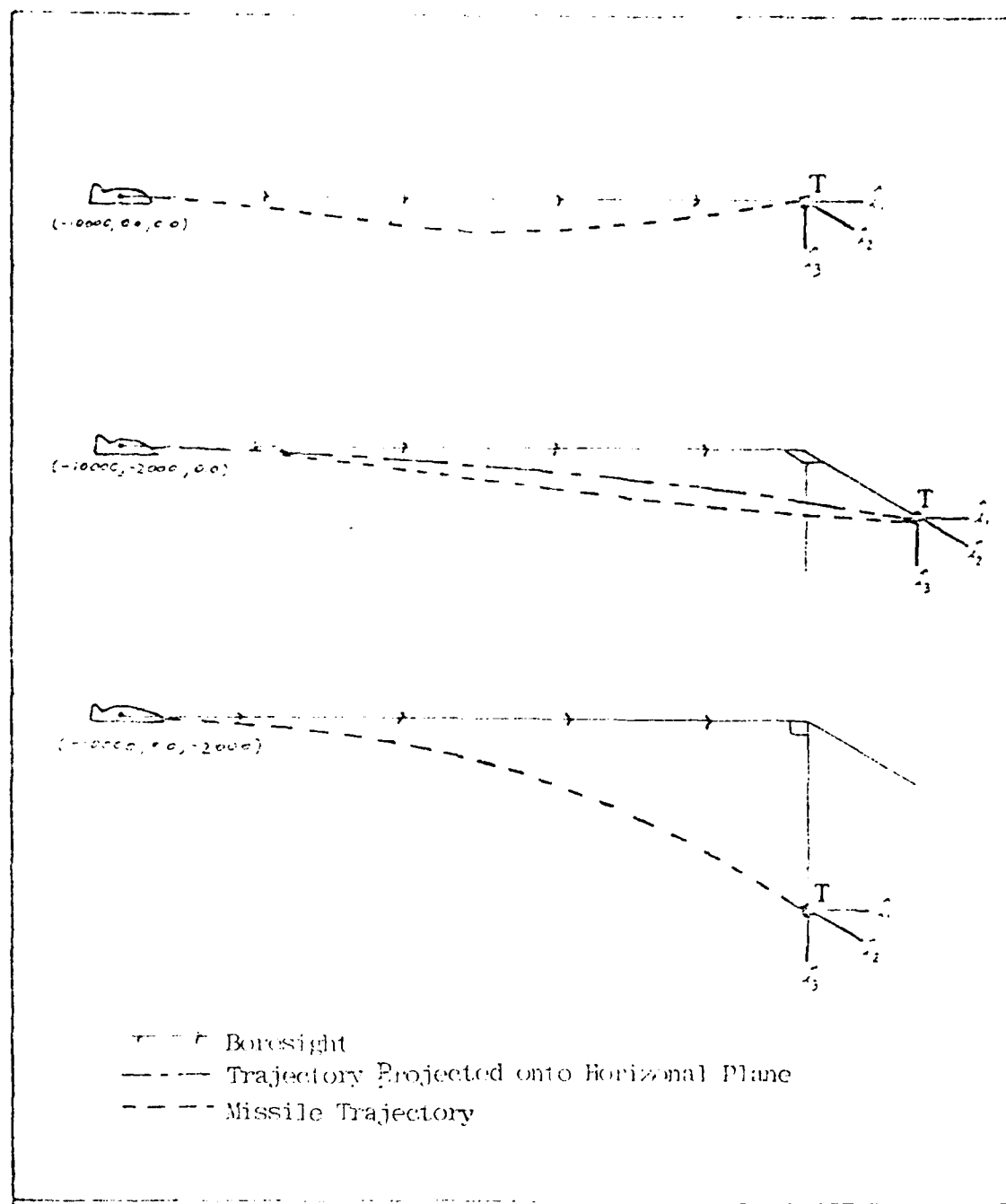
Figure 4-2. Test Flight Profiles

using Euler integration to propagate $\underline{P}(t)$ and the filter states produced numerical errors that seriously degraded the filter performance. The $\underline{P}$ matrix had diagonal elements that were becoming negative. The solution found was to add noise via the $\underline{Q}$ matrix to offset the integration errors. Some of the filter states were accumulating a growing bias due to the errors in Euler integration and the large dynamics input to the filter. These errors were reduced by as much as 50 percent by incorporating a trapezoidal integration into the state propagation portion of the filter.

4.4 Monte Carlo Incorporation.

Two changes were needed to convert this simulation into a full Monte Carlo program. The first was to add a case controller and second was to add an interface tape (Ref. 12) to take advantage of an existing Monte Carlo evaluation and plotting package (Ref. 3). The short case controller routine became the executive and calls the program developed above as a subroutine the specified number of times. Each call generates a full time history of the true missile states, filter state estimates, and filter covariance estimates based upon the same set of true initialization parameters but with different initial condition error, state dynamic noise, and measurement noise realizations in each case. The second change provides a composite output of a header and all case time histories in a format acceptable by the Monte Carlo evaluation routine developed at AFWAL. This post processor routine provides plots of designated parameters based upon the case time histories. These parameters include ensemble averages of filters and truth model states, means, and covariances.

4-5

V. ANALYSIS

5.1 Introduction.

The analysis of the filters covers two broad areas: issues of note that surfaced during filter development and filter performance. The filter development includes work done to produce working filters. Filter performance is demonstrated by probability of kill and computer loading comparisons. Another aspect of the performance considered is how well does the filter work with the guidance law. The LOS filter performance plots are Figures F-1 through F-32 in Appendix F and the Inertial filter performance plots are Figures F-33 through F-62.

5.2 Filter Development and Evaluation

5.2.1 LOS Filter. The initial trial runs on filter LOS.1 revealed a problem in the propagation and update of the $\underline{P}$ matrix. Since negative values were appearing on the diagonal, the covariance matrix was losing it's positive semi-definite nature. The following steps were taken to isolate the cause of the problem.

The negative values appeared on the diagonal shortly after the first update. So the first step was to rule out the possibility of numerical precision problems because of the large condition number, 10^{13}, of the initial $\underline{P}$ matrix and $\underline{R}$ value. The Joseph form of update has been shown to be less troubled by this (Ref. 10). However, there was no improvement or even change when this form of update was used indicating that the condition number was not the problem in the update.

The next step was to obtain the eigenvalues and eigenvectors of the covariance matrix to isolate when and where the problems began. An available routine using the QR algorithm was used to compute these quantities. By the third time propagation, one of the eigenvalues of the covariance matrix was going very slightly negative (-0.00019). At this point, the most likely explanations were either the Euler integration step size was too large with respect to the P matrix time constants or the large range of covariance matrix eigenvalues was inducing computational errors.

In pursuing the first possibility, the integration step size was reduced by a factor of 100, from 0.02 seconds to 0.0002 seconds. This produced a dramatic change for the better in the positive semi-definite nature of the covariance matrix but the very small negative eigenvalue nature persisted. The next improvement in the integration accuracy is to use a variable step size predictor-corrector type of integration. This integrator reduced the negative trend on the one diagonal element of the covariance matrix to almost 0. However, it is not practical to implement this type of algorithm in a missile computer. Also altering the P_0 matrix was attempted but only changed the time at which the diagonal elements went negative.

The four state filter (Filter I.3) also exhibited the same characteristics. Since four state filter is mathematically simpler to deal with, it was used to pursue other potential explanations.

To obtain the time constants of the $\dot{P}(t)$ equation it is necessary to formulate the $P \; F + F \; P^T$ expression, the homogenous form, with $G \; Q \; G^T$ term ignored at present. The F matrix used was taken from the propagation at $T = 0.02$ and the P matrix indexed to correspond to the elements in equation (5-4).

5-2

$$\underline{F} = \begin{bmatrix} 0 & 1 & d & 0 \\ 0 & 0 & 0 & c \\ 0 & 0 & 0 & 1 \\ 0 & a & b & 0 \end{bmatrix} \quad (5\text{-}1) \qquad \underline{P} = \begin{bmatrix} P_1 & P_2 & P_3 & P_4 \\ P_2 & P_5 & P_6 & P_7 \\ P_3 & P_6 & P_8 & P_9 \\ P_4 & P_7 & P_9 & P_{10} \end{bmatrix} \quad (5\text{-}2)$$

$$\underline{\dot{P}} = \begin{bmatrix} \boxed{1}\ 2(P_2 + d\,P_3) & \boxed{2}\ \text{--} & \boxed{3}\ \text{--} & \boxed{4}\ \text{--} \\ \boxed{2}\ cP_4 + P_5 + d\,P_6 & \boxed{5}\ 2\,cP_7 & \boxed{6}\ \text{--} & \boxed{7}\ \text{--} \\ \boxed{3}\ P_4 + P_6 + dP_8 & \boxed{6}\ P_7 + cP_9 & \boxed{8}\ 2\,P_9 & \boxed{9}\ \text{--} \\ \boxed{4}\ aP_2 + bP_3 + P_7 + dP_9 & \boxed{7}\ aP_5 + bP_6 + cP_{10} & \boxed{9}\ aP_5 + bP_6 + P_{10} & \boxed{10}\ 2(aP_7 + bP_9) \end{bmatrix}$$

$$(5\text{-}3)$$

Since $\underline{F}\,\underline{P} + \underline{P}\,\underline{F}^T$ is symmetric, there are only 10 unique elements. Thus equation (5-3) can be reconstructed to form a linear first order vector differential equation for these ten elements.

$$\begin{bmatrix} \dot{P}_1 \\ \dot{P}_2 \\ \cdot \\ \cdot \\ \cdot \\ \dot{P}_{10} \end{bmatrix} = \underline{F'} \begin{bmatrix} P_1 \\ P_2 \\ \cdot \\ \cdot \\ \cdot \\ P_{10} \end{bmatrix} \qquad (5\text{-}4)$$

5-3

where

$$
\underline{F}' =
\begin{bmatrix}
- & 2 & 2d & - & - & - & - & - & - & - \\
- & - & - & c & 1 & d & - & - & - & - \\
- & - & - & 1 & - & 1 & - & 8 & - & - \\
- & a & b & - & - & - & 1 & - & d & - \\
- & - & - & - & - & - & 2c & - & - & - \\
- & - & - & - & - & - & 1 & - & c & - \\
- & - & - & - & a & b & - & - & - & c \\
- & - & - & - & - & - & - & - & 2 & - \\
- & - & - & - & - & a & - & b & - & 1 \\
- & - & - & - & - & - & 2a & - & 2b & -
\end{bmatrix}
\qquad (5\text{-}5)
$$

and

$$a = -.0952$$

$$b = .00227$$

$$c = .0952$$

$$d = -.0476$$

$$- = 0.0$$

The eigenvalues of the $\underline{F}'$ matrix characterize the $\underline{P}$ matrix dynamics. For this case, 4 eigenvalues were 0.0, 2 pair at $0.0 \pm 0.0033j$, and one pair at $0.0 \pm 0.0066j$. All the non-zero roots are imaginary and of a very low frequency. Since the integrator step size is much less than the period of the low frequency components, the hypothesis of under sampling can be dismissed as the cause of the negative trend in the eigenvalues.

The other potential cause is the large difference in eigenvalues, in the covariance matrix. The solution was to scale the covariance matrix using a similarity transform to yield a $\underline{P}(t)$ with a good condition number. (Refs. 10 and 14) This basically states that for a given matrix there exists a matrix that can transform the state space to a new basis and thereby scale it. The transform matrix chosen was based upon the $\underline{P}(t_0)$. The expressions used to change the basis of the

state space are summarized in Appendix E.1 This transform produced a $\underline{P}(t)$, with a low condition number, that was propagated and then returned to the original state basis with virtually identical results. The expressions used to change the basis of the state space are summarized in Appendix E.1.

Up to this point, the problem in the full order filter has persisted through varying the integration step size, two integration methods, and a scaling of the covariance matrix. The problem in the reduced order filter has also persisted through varying the integration step size and setting the $\underline{Q}$ matrix to zero to see how the $\underline{P}$ matrix was propagating.

The $\underline{P}(t_o)$ matrix when combined with the state equation formulations as expressed in the F matrix, could be ill conditioned. This could be shown by one P matrix element propagating negative values into the diagonal elements. To verify this, both the $\underline{Q}$ matrix and the $\underline{P}(t_o)$ matrix are set to zero and only one of the $\underline{P}(t_o)$ diagonal terms was set to previously computed values per run. After propagating the $\underline{P}$ matrix, the P_{kk} element was increased by a small delta while another diagonal element was decreased by the same amount. The only exception was the P_{11} term which remained constant and did not couple into the other elements. As $P_{11}(t)$ remained constant on its own and it's associated $\underline{G} \, \underline{Q} \, \underline{G}^T$ element is 0, it tended to accumulate the small negative coupling. The Euler integration method was found to produce the negative trend (see Appendix E.2). The integration performed analytically in closed form, however, does not exhibit this problem.

The solution then, was to bias the P_{11} term artificially to counter the negative trend caused by this numerical method. In the simulation this bias was added through the $\underline{G} \, \underline{Q} \, \underline{G}^T$ expression. A bias value of .3 to .5 added to the P_{11} element was found to be sufficient for this formulation. The large time varying acceleration (thrust and commanded acceleration) acting on the missile also produced large errors in the states when using Euler integration. This effect can be

5-5

seen by the error trend in Figures F-1 and F-2 which were produced with
Euler integration and no driving noise in the truth model. The second
order effects were then included in the integration, now a trapezoidal
integration, to reduce the errors in propagating the states. This
improvement in accuracy is illustrated in comparing Figures F-3 and F-4
with Figures F-1 and F-2, respectively. Additional measurements were
not considered since the observability criteria was met without them.

5.2.2 Inertial Filter. The inertial filter development did not
exhibit difficulties in the filter covariance as did the LOS filter.
But a need for additional measurement information existed to meet
the observability criteria. The more dramatic effects of
incorporating the two pseudo-measurements (Section 3.3) are illustrated
in Figures F-33 and F-34 in the reduction of the covariance of the
x position of the aircraft. Also, there was a need for improved
integration in the state propagation as in the LOS filter. The
trapezoidal integration was implemented but did not operate properly.
This was a function of the coding rather than the algorithm, as verified
by decreasing the Euler integration step size by a factor of 10, from
.02 seconds to .002 seconds. This approach should approximate the
trapezoidal integration results at a .02 second step size, for purposes
of comparing the performance of the Inertial filter to that of the LOS
filter. This improvement is illustrated by comparing Figures F-37 and
F-38 with F-35 and F-36 respectively.

5.2.3 Tuning. The initial simulation runs were made with the
computed values of $\underline{P}(t_0)$ and $\underline{Q}$ as presented in Table 2-1 and with no
perturbations in the initial conditions. When the filter is properly
tuned, the mean and the standard deviation of the errors will remain
within the bounds set by the square root of the diagonals of the
covariance. If this is not the case, then the magnitudes of the $\underline{Q}$
element can be increased to realize the above criteria. As a starting
point, the $\underline{Q}$ values are based upon $\underline{P}(t_0)$ and the values of $\underline{Q}$ used in
the truth model for the dynamic driving noise. (Ref. Section 2.5) Error

5-6

statistics were taken from samples over 5 runs during the tuning process for the R_{MT} and Θ_ℓ states. The 5 runs would be sufficient to identify major difficulties. The initial Q values selected for the LOS filter allowed the standard deviation of the error to grow outside the standard deviations expected by the filter (Fig. F-5 and F-6). This was corrected by increasing the values of Q matrix which would increase $\underline{P}(t)$ and increase the relative weighting on the measurements in the state update.

For the LOS filter, the Q associated with $R_M/_T$ was increased by a factor of 10 to 1450 ft^2 and the Q for Θ_ℓ was set to 0.01 rad^2. These values brought the standard deviation of each state to within the bounds set by $\sqrt{P_{ii}(t)}$ of the filter. See Figures F-7 and F-8 for the LOS filter and Figures F-41 and F-42 for the inertial filter.

The dynamic driving noise was set to zero and bias noise terms were added to the initial conditions to evaluate the response of the filter to initial transients caused by errors in initial state estimates (Figures F-9 and F-10 and F-43 and F-44). Each initial condition error realization was computed by $\delta \underline{x}(t_o) = \sqrt[5]{\underline{P}(t_o)}\,\underline{w}$ where $\underline{w} \in N(\underline{0},\underline{I})$. The bias was added to the associated filter state at t_o. This check should reveal any divergent tendencies in the filter states.

The perturbed initial conditions and the propagation noise in the filter were both considered in the remainder of the performance evaluation of the filter. Also the number of runs per case is increased to 20 runs to provide larger sample space for the statistical analysis. Ref. Figures F-11 and F-12 and F-45 and F-46. During the analysis of the data plots in Appendix F it was necessary to exclude the radical transients after approximately 2.85 sec. Since all of the runs in a given Monte Carlo run will not complete at the same time, it was necessary to extend to final time to insure all the runs for the given case were completed.

The data plotted after the impact time then is of no value. As a final result the $\underline{Q}$ diagonal terms found for the LOS filter are:

3000	for Target x acceleration
1450	for Missile x acceleration
1450	for Missile z acceleration
5	for Missile z position
100	for A/C LOS acceleration
.01	for LOS Θ

and for the Inertial filter:

3000	for Target x acceleration
1000	for Missile x acceleration
1000	for Missile z acceleration
400	for A/C x acceleration

These values were derived only for a launch at 2000 ft altitude and 10,000 ft range. For other launch scenarios, additional study would be required to confirm the validity of these filter parameters.

5.2.4 Measurement Residual. The LOS filter exhibits a large measurement residual on the first few updates, on the order of .03 radians. This behavior is illustrated in Figure F-27 with no driving noise in the truth model and in Figure F-28 with driving noise and perturbed initial conditions. The magnitude of the residual should be less than 1 milli-radian. This error is a result of small perturbations in the z state when the aircraft-to-missile range is small that has a significant effect on filters estimate of the measurement at the first update. The most likely solution is to ignore the first measurement. This would be the case in a real world situation, since

the missile may not be within view of the laser grid scan until the
second or third update. The problem, however, does warrant further
investigation.

The inertial filter did not produce this large residual in
the elevation measurement, see Figures F-57 and F-58. The orientation
of the filter reference frame was not aligned with the reference frame
of the measurement, thus small errors in the states will effect both
the range along the missile-to-target LOS and the distance of the
missile off the LOS. This orientation would tend to reduce the overall
effects of the errors in the states on the measurement residual.

5.3 Filter Performance

5.3.1 Reduced Order Filter Performance. The reduced order
filters performed similarly to the full order filters, see Figures F-19
through F-22 and F-45 through F-48, as compared to Figures F-29 through
F-32 and F-59 through F-62, respectively. In some states the
performance was better as in Figure F-30 with respect to Figure F-20.
This improvement was expected since the parameters excluded from being
states had a negligible effect on the navigation solution. Also there
was improved observability as a result of removing some of the states
that have like orientation and dynamics as other states. This improves
the benefit of the measurement. The behavior of the covariance of the
$R_{A/T}$ does not agree with the behavior of the standard deviation of
the errors in Figure F-55. The probable cause of this is cross coupling
effects in the filter states and warrants further study.

5.3.2 Probability of Kill. At this point it is of value to
consider a figure of merit related to the probability of kill for a
missile equipped, in turn, with each of the filters in this study.
The mean and standard deviations are computed from the Monte Carlo run

miss distances of each flight for each case. These two values then
will characterize the Gaussian distribution of the hit area. Also
consider that the target vulnerability area can be modeled by a
probability of kill function which is a Gaussian-shaped distribution,
$f_T(x)$, with zero mean and standard deviation relative to the size of
the target. The area under this curve is scaled to be directly
proportional to a rectangular shaped function with magnitude of 1.0,
with a width relative to the size of the target, and centered on the
target. For this example let $\sigma_T = D/2$ where D is the diameter of the
target vulnerable area. The scale factor on the Gaussian curve is
chosen such that

$$\lim_{\sigma_T \to \infty} f_T(x) = 1 \qquad\qquad (5-6)$$

This occurs only if the scale factor is $2\pi \sigma_T$ as seen in
equation (5-7) for the target. The probability of damage is then the
marginal probability of the target distribution function and the missile
hit area which can be expressed as

$$f(x) = \frac{a}{2\pi s} e^{-d^2/s^2} \qquad\qquad (5-7)$$

where for the missile hit probability density

$$a = 1$$

$$s = \sigma_M$$

$$d = x - \zeta$$

$$\zeta = \text{mean of the miss distance}$$

and for the target vulnerable area

$$a = 2\pi \sigma_T$$

$$s = \sigma_T$$

$$d = x$$

5-10

Integrating over all x, the marginal probability will yield

$$P_K = \frac{\sigma_T}{\sigma_M^2 + \sigma_T^2)^{1/2}} \; e^{-\zeta^2/(\sigma_M^2 + \sigma_T^2)}$$ (5-8)

TABLE 5-1

MISSILE ACCURACY AS A FUNCTION OF THE FILTER TYPE

Filter	States	Miss Distance*		$P_K(\sigma_T = 5.0)$
		Mean	Std. Dev.	
LOS.1	7	.62	3.02	.89
LOS.2	4	.06	3.48	.82
INERT.1	6	-1.08	5.00	.69
INERT.2	4	-1.11	5.05	.68

* Miss distance based upon minimum missile-to-target range
with the launch from 10,000 ft range and 2000 ft altitude.

The LOS filter produced a probability of kill approximately 20%
better than the Inertial filter. This is due to the larger means and
standard deviations of the miss distance for the given scenario. Also
note that the reduced order filter performed within 4% of the larger
counterparts.

5.3.3 Computer Loading. Also of concern is whether or not the
desired filter can be implemented in an onboard computer. One aspect of
implementation is the computer work load requirements in terms of
operations per second for a given filter, integration interval size and
update rate. For the filters developed in this study, an algorithm was
derived for the LOS filter and one for the Inertial filter to give an
estimate of the number of operations performed per time propagations and

per update as a function of the number of filter states. The
operations were characterized into three groups: adds and subtracts,
multiplies and divides, and square roots and trigonometric functions.
This grouping permits better estimation of the timing requirements
needed for the chosen filter to run real time. The number of
operations per filter for time propagations and updates are given as:

TABLE 5-2

OPERATIONS REQUIRED FOR ONE TIME PROPAGATION AND

ONE UPDATE

LOS FILTER

	Time Propagations	Updates
Adds:	$2n^3 + n^2 + 38$	$n^3 + 3n^2 + 2n + m/2$
Multiplies:	$2n^3 + 4n^2 + 39$	$2n^3 + 2n^2 + 2n + m$
Square Roots:	$n + 5$	1

INERTIAL FILTER

	Time Propagations	Updates
Adds:	$6n + m$	$n^3 + 3n^2 + 2n + m + 2R - 2$
Multiplies:	$5n - 2$	$2n^3 + 2n^2 + 2n + 2m + 3R - 3$
Square Roots:	0	$m/2 + R$

where n = number of filter states

      m = total number of parameters propagated (8 in this study)

      R = number of measurements required per update

        1 for the LOS filters

        3 for the Inert.1 filter

        2 for Inert.2 and Inert.3 filters

Summarizing the above expressions will yield the following table

TABLE 5-3

NUMBER OF OPERATIONS PERFORMED BY FILTERS

| FILTER | FILTER OPERATIONS PER | | | | | |
| | Time Propagation | | | Update | | |
	Adds	Multiplies	Square Roots	Adds	Multiplies	Square Roots
LOS.1	1126	1351	14	724	1176	1
LOS.2	128	247	10	124	176	1
INERT.1	44	28	0	732	1199	7
INERT.2	32	18	0	134	193	6

Then using the following expression to get the time required per
time propagation and update respectively:

$$T_P = n_A \, t_A + n_M \, t_M + n_S \, t_S \tag{5-9a}$$

$$T_U = n'_A \, t_A + n'_M \, t_M + n'_S \, t_S \tag{5-9b}$$

where

    n = number of operations in the time propagation

    n' = number of operation in the update

    the subscripts a, m, and s refer to the groupings of adds,
    multiplies, and square roots, respectively

5-13

Reasonable values for the operation times for some smaller
state-of-the-art computers are

$$t_a = 2.1 \ \mu \ sec$$
$$t_m = 5.3 \ \mu \ sec$$
$$t_S = 60.0 \ \mu \ sec$$

Summarizing the above times and Table 5-3 will yield

TABLE 5-4

FILTER OPERATION TIMES

FILTER	FILTER OPERATION TIME (SEC) PER	
	Time Propagation	Update
LOS.1	.0110405	.0082476
LOS.2	.0022547	.0013276
INERT.1	.0002672	.0087511
INERT.2	.0001818	.0017447

The cases run in this study were with a time propagations rate of
50 Hertz and update rate of 10 Hertz. However, for this example let the
update rate be fixed at 10 Hertz and determine the maximum time
propagation rate as an integer multiple of the update rate.
Synchronizing the update with time propagations will simplify the timing
and sequencing task of the onboard executive. To determine this upper
limit, first multiply the time per update by the update rate and
subtract from one second. This remaining time is available for
propagating the filter states and is then divided by the time per
propagation. The resulting figure can then be rounded down to the next
multiple of the update rate giving the maximum

5-14

time propagation rate. This computation does not take into account the time required by the processor to perform other tasks, but does provide a meaningful measure of the impact of the filter on the onboard processor load requirements.

TABLE 5-5

MAXIMUM TIME PROPAGATION RATES

FILTER	Time for Ten Updates (Sec)	Time for Time Propagation (Sec)	Maximum Time Propagation Rate
LOS.1	.082476	.917524	83.1 or 80
LOS.2	.013276	.986724	473.6 or 430
INERT.1	.087511	.912489	3415.0 or 3410
INERT.2	.017447	.982443	5404.6 or 5400

There are two principle differences between the LOS filter and the inertial filter that affect the run times. First is that the LOS filter requires an Extended Kalman Filter structure for both time propagation and update. The Inertial filter is linear in the time propagation and uses the standard Kalman Filter structure there and the Extended Kalman Filter structure for the update. The second contributing factor is that the LOS filter has a reference coordinate frame that changes its orientation with time. This produces an addition computational burden by requiring the uses of trigonometric functions and addition square root operations.

5.4 Guidance Law

The proportional navigation guidance law performed equally well with each of the filters used in this study. However, the guidance law showed signs of instability as the missile closed in on the target.

The cause lies in using the missile-to-target range to compute the rate of change of the missile-to-target line-of-sight angle. Since the $R_{M/T}$ term is in the denominator of the expression, the commanded acceleration becomes increasingly sensitive as the range gets small. The standard deviation of the range error is on the order of 90 ft in the end game. This could cause the guidance law computation to produce very large numbers since the range estimate could in fact go through zero. The two potential cures for this are to use a time varying gain coefficient or to limit the missile-to-target range in the filter to a predetermined minimum. In this simulation this range was limited to a minimum of 100 ft.

The effect of varying the gain in the guidance law in illustrated in Figures F-61 through F-66. Another figure of merit, E_C, relating to the control energy commanded by

$$E_C = \int_{t_o}^{t_f} A_{CMC} \, dt \qquad (5\text{-}10)$$

The acceleration profile was not noticeably effected by changing the filters used in this simulation. The following table presents the effects of a range of gains in the guidance law to control energy and miss distance for the LOS filter.

TABLE 5-6

GUIDANCE LAW PERFORMANCE

Gain	CONTROL ENERGY		MISS DISTANCE		P_K
	Mean	Std. Dev.	Mean	Std. Dev.	
3	1292.9	112.9	-.99	6.97	.58
4	1117.5	114.3	.47	2.92	.86
5	1009.6	121.0	1.13	1.86	.90

The control energy commanded decreases as the gain increases but also note that the standard deviation increases, caused by increased sensitivity to perturbations in the filter states. The effect of the increasing gain also has a marked improvement in the standard deviation of miss distance. However, in looking at Figures F-64 through F-66, there is an increase in the instability in the end game as mentioned above. The probability of kill also increases with the gain. However, the improvement in P_K resulting from the gain changing from 4 to 5 is much less than from the gain changing from 3 to 4. With the tradeoffs involved, a gain of 4 would give the better improvement in P_K with only a modest degradation from the end game instabilities. The optimum configuration of gain, accepted miss distance and controls in the guidance law to limit the instability may vary as a function of launch scenario and warrants further study.

5.5 Summary

In the analysis of the filter developments, the method of integration proved to be of significant importance in both the stability of the filter covariance and the accuracy of the state estimates. The performance of the filter with respect to probability of kill and computer loading show both filters studied to be viable candidates for a weapon system simulated in this study. From this study, the use of a Kalman Filter as a state estimator onboard the HVM is a very feasible and viable approach to the guidance realization. Accompanying the filter, the guidance law selected becomes a recognized factor in the final performance of the missile.

VI. CONCLUSIONS AND RECOMMENDATIONS

6.1 Conclusions

A single missile-to-target trajectory was used in this study (Fig. 4.2). The scenario involves a stationary target and a constant-velocity aircraft. The missile, aircraft, and target are driven by time-correlated noise at the acceleration level.

Given these conditions, the following filter design analysis results were obtained:

1) The LOS filters exhibited a probability of kill on the order of 20 percent higher than the inertial filters. The major contributing factor is improved observability provided by the rotating reference frame in the LOS filter.

2) The probability of kill of the reduced order filters was within 4 percent of their full-order counterparts.

3) The six-state Inertial filter required additional measurement information to meet observability criteria. The additional measurements were generated as pseudo-measurements of air-to-target and missile-to-target range, expressed in terms of filter states and parameters. The pseudo-measurements provided reduced filter covariance in the aircraft-to-target states.

4) The eight-state LOS filter did not require the additional measurement information. However, as the rate of change of the aircraft-to-target line-of-sight approached zero, the filter exhibited reduced observability.

5) The Inertial filter required significantly fewer computations
   per time propagation (Ref. Figure 5-5). Since both filter types
   used the same update method, the number of computations per
   update were on the same order.

6) The use of Euler integration to propagate the filter states at
   a .02 second step time proved inadequate because of the large
   time-varying accelerations exhibited by the missile. A higher
   order integration scheme (trapezoidal) reduced the errors
   significantly.

Proportional navigation was the guidance law implemented for each
of the filters. A brief analysis of this guidance law for the LOS
filter and a single scenario (Figure 4-2) revealed the following:

1) The probability of kill improved as the guidance law gain, n,
   was increased.

2) The total control energy needed by the guidance law decreased as
   n was increased. The commanded accelerations were higher
   during thrust while the kinetic energy is lower thus reducing
   the needed course corrections later in flight.

3) The commanded accelerations demonstrated increased instability
   toward the end-game trajectory as n increased.

6.2 Recommendations

Suggestions for further study, as pertains to performance
analysis, are the following:

1) Maneuvers should be induced in both the aircraft and the
   target, and the robustness of the filters to these changes
   examined.

2) The INS data should be corrupted to improve modeling of the actual system that would be implemented. The performance analysis should be done again and comparisons made with the original system.

3) The recovery from initial conditions perturbations should be further investigated. A precomputed gain extended Kalman filter should be investigated if additional robustness is required.

4) The effects of varying propagation and update rates should be examined.

5) The Inertial filter pseudo-measurements of range should be replaced by real world measurements. The effect of encoding there true measurements onto the laser signal from the aircraft should be investigated by performance analysis and appropriate comparisons. This should also be done with the LOS filter for comparison.

The reduced order models used in this study are representative of many possible models. Further reduction in order as well as other combinations of filter states should be considered to obtain an optimum configuration. In conjunction with this, the white noise models for acceleration uncertainties in the filters should be replaced by Gauss-Markov models and the corresponding performance analyzed.

An error budget analysis is necessary to identify sources that can potentially degrade performance. Once these are determined, methods are used to reduce their effects. In order to accomplish the analysis it is necessary to

1) Modify the truth model by incorporating more exact models for the individual noise sources.

2) With an appropriate Kalman Filter in the system, turn off
each of the noises one at the time and obtain a comparison of
their effects on miss distance statistics.

Since the guidance law has a direct bearing on the performance of
navigation system, further study to optimize the guidance law should
include:

1) Other guidance law formulations.

2) Algorithms to handle potential angle-of-incidence difficulties.

3) Algorithms to avoid potential clobber (flight trajectory
hitting the ground before intercepting the target).

The simulation developed in this study provides a tool for further
analysis.

Bibliography

1. Blakelock, John H. Automatic Control of Aircraft and Missiles. New York: John Wiley and Sons, Inc., 1965.

2. Cusumano, Salvatore J. and Manuel De Ponte, Jr. An Extended Kalman Filter Fire Control System Against Air-to-Air Missiles M.S. thesis. Wright-Patterson Air Force Base, Ohio: Air Force Institute of Technology, February 1978.

3. Feldman, Richard E., Jerry G. Jensen, Staton H. Musick. SOFEPL: A Plotting Postprocessor for 'SOFE' User's Manual. AFWAL Technical Report 80-1109. Wright-Patterson AFB, Ohio: Avionics Laboratory, 1981.

4. Gibbs, Bruce P., and David W. Porter. "Development and Evaluation of an Adaptive Algorithm for Predicting Tank Motion", Proceeding of the 19th IEEE Conference on Decision and Control, 1:560-508 (December 1980).

5. Hewish, Mark. "Tactical-Missile Survey," International Defense Review, 13: 851-864 (1980).

6. Likens, Peter W. Elements of Engineering Mechanics. New York: McGraw-Hill Book Company, 1973.

7. Lutter, Robert N. Application of an Extended Kalman Filter to an Advanced Fire Control System. M.S. thesis. Wright-Patterson Air Force Base, Ohio: Air Force Institute of Technology, January 1977.

8. Maybeck, Peter S., "Performance Analysis of a Particularly Simple Kalman Filter", Journal of Guidance and Control, 1:391-396 (November 1978)

9. _____, "Stochastic Estimation and Control", Lecture notes, 1981.

10. _____, Stochastic Models, Estimation and Control. New York: Academic Press, 1979.

11. MIL-F-8785B(ASG). Flying Qualities of Piloted Airplanes. Washington: Department of the Air Force, August 1979.

12. Musick, Stanton H. "SOFE: A Generalized Digital Simulation for Optimal Filter Evaluation User's Manual", Technical Memorandum AFAL-TM-79-19, Revision A, November, 1978.

13. Pastrick, H.L., S.M. Seltzer, and M.E. Warren. "Guidance Laws for Short-Range Tactical Missiles", _Journal of Guidance and Control_, 4:98-108 (March 1981).

14. Reid, J. Gary. Lecture materials distributed in EE 5.10, Linear Systems and Digital Computation Methods. School of Engineering, Air Force Institute of Technology, Wright-Patterson AFB, 1980.

15. Worsley, William H., _Comparison of Three Extended Kalman Filters for Air-to-Air Tracking_. M.S. thesis. Wright-Patterson Air Force Base, Ohio: Air Force Institute of Technology, June 1980.

APPENDIX A

COORDINATE TRANSFORMATIONS

A.1 Inertial and Missile Frame Transformations

The missile body frame ($\hat{m}$) and the inertial frame ($\hat{i}$) are described in Chapter II. Based upon these definitions, the $\hat{m}$ frame differs from the $\hat{i}$ frame by first a rotation, Ψ, about the $\hat{i}_3$ axis to form an intermediate frame $\hat{h}$. Figure A-1 provides a top view of this situation, looking down onto the $\hat{i}_1$, $\hat{i}_3$ plane. Thus, the vector describing the rotation of the $\hat{h}$ frame with respect to the $\hat{i}$ frame is

$$\underline{\omega}^{hi} = \dot{\Psi}\ \hat{h}_3 = \dot{\Psi}\ \hat{e}_3 \qquad (A-1)$$

Resolving $\hat{h}$ into $\hat{i}$ components results in

$$\hat{h}_1 = \cos\ \Psi\ \hat{i}_1 + \sin\ \Psi\ \hat{i}_2 \qquad (A-2)$$

$$\hat{h}_2 = -\sin\ \Psi\ \hat{i}_1 + \cos\ \Psi\ \hat{i}_2 \qquad (A-3)$$

$$\hat{h}_3 = \hat{i}_3 \qquad (A-4)$$

Therefore, the direction cosine matrix which transforms from the $\hat{i}$ frame to the $\hat{h}$ frame is

$$[C^{hi}] = \begin{bmatrix} \cos\ \Psi & \sin\ \Psi & 0 \\ -\sin\ \Psi & \cos\ \Psi & 0 \\ 0 & 0 & 1 \end{bmatrix} \qquad (A-5)$$

The $\hat{m}$ frame next differs from the $\hat{i}$ frame by a rotation, Θ, about the $\hat{h}$ axis. Figure A-2 depicts a planar side view of the $\hat{h}_1$, $\hat{h}_3$ plane.

A-1
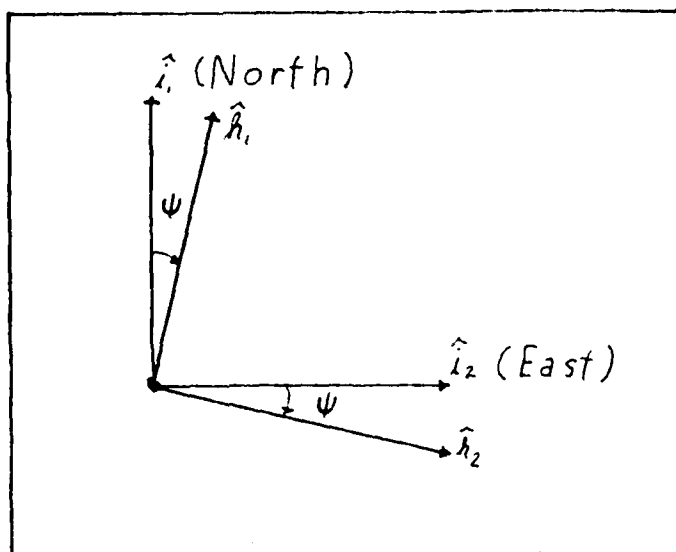
Figure A-1. Rotation about $\hat{i}_3$, $\hat{h}_3$
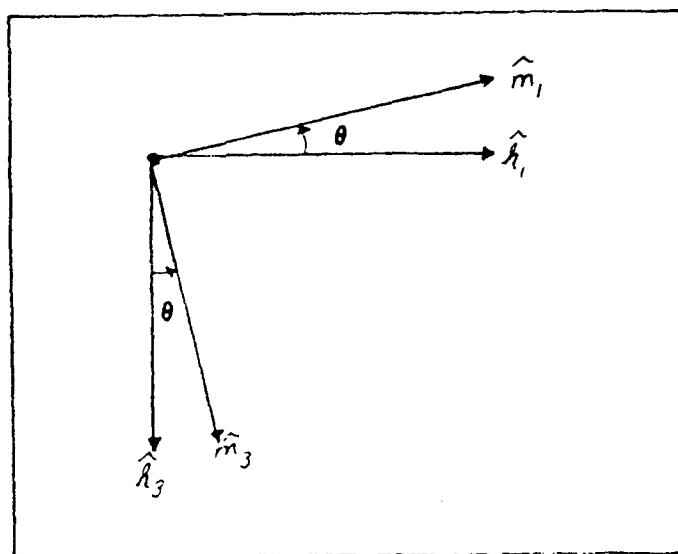
Figure A-2. Rotation about $\hat{h}_2$

The vector describing the rotation of the $\hat{m}$ frame with respect to the $\hat{h}$ frame is

$$\underline{\omega}^{mh} = \dot{\Theta}\,\hat{h}_2 = \dot{\Theta}\,\hat{m}_2 \qquad\qquad (A\text{-}6)$$

Therefore, the rotation of the $\hat{m}$ frame with respect to the $\hat{i}$ frame is

$$\underline{\omega}^{mi} = \underline{\omega}^{mh} + \underline{\omega}^{hi} \qquad\qquad (A\text{-}7)$$

Substituting (A-1) and (A-6) into (A-7) and expressing the result in the missile frame coordinates gives

$$\underline{\omega}^{mi} = -\dot{\Psi}\,\sin\Theta\,\hat{m}_1 + \dot{\Theta}\,\hat{m}_2 + \cos\Theta\,\hat{m}_3 \qquad\qquad (A\text{-}8)$$

Expressing $\hat{m}$ in terms of $\hat{h}$ results in

$$\hat{m}_1 = \cos\Theta\,\hat{h}_1 - \sin\Theta\,\hat{h}_3 \qquad\qquad (A\text{-}9)$$

$$\hat{m}_2 = \hat{h}_2 \qquad\qquad (A\text{-}10)$$

$$\hat{m}_3 = \sin\Theta\,\hat{h}_1 + \cos\Theta\,\hat{h}_3 \qquad\qquad (A\text{-}11)$$

Therefore, the direction cosine matrix which transform the $\hat{h}$ frame to the $\hat{m}$ frame is

$$[C^{mh}] = \begin{bmatrix} \cos\Theta & 0 & -\sin\Theta \\ 0 & 1 & 0 \\ \sin\Theta & 0 & \cos\Theta \end{bmatrix} \qquad\qquad (A\text{-}12)$$

Finally, the direction cosine matrix which transforms the $\hat{i}$ frame to the $\hat{m}$ frame is

$$[C^{mi}] = [C^{mh}][C^{hi}] \qquad\qquad (A\text{-}13)$$

$$= \begin{bmatrix} \cos\Theta\cos\Psi & \cos\Theta\sin\Psi & -\sin\Theta \\ -\sin\Psi & \cos\Psi & 0 \\ \sin\Theta\cos\Psi & \sin\Theta\sin\Psi & \cos\Theta \end{bmatrix}$$

For the two dimensional case which is implemented, in this study Ψ is zero and $[C^{mi}]$ reduces to equation (A-12).

A.2 Inertial and ATLOS Frame Transformations

The ATLOS frame is also described in Chapter II. Transformations between the inertial and the ATLOS frame are needed to compute true azimuth and elevation. The ATLOS-to-inertial transformation is identical in form to the missile-to-inertial transformation. The only difference is that Θ is replaced by Θ_ℓ and Ψ is replaced by Ψ_ℓ.

APPENDIX B

Simulation Implementation

B.1 Missile Attitude Response Model

The attitude response of the missile to commanded acceleration is modeled as a second order lag of the following form:

$$a_L = \frac{a_{CMDL}\ \omega_n^2}{s^2 + 2\ \zeta\omega_n\ s + \omega_n^2} \tag{B-1}$$

and

$$a_N = \frac{a_{CMDN}\ \omega_n^2}{s^2 + 2\zeta\omega_n s + \omega_n^2} \tag{B-2}$$

where in this study

a_{CMDL} = guidance law commanded lateral acceleration

a_{CMDN} = guidance law commanded normal acceleration

ζ = damping coefficient, .707

ω_n = missile natural frequency, 44 radians per second

The values for damping coefficient and missile natural frequency were selected as being representative numbers applicable to a highly maneuverable missile. (Ref. 15)

In state equation form, (B-1) and (B-2) are written as

$$\dot{x}(t) = \underline{A}\ \underline{x}(t) + \underline{B}\ \underline{u}(t) \tag{B-3}$$

$$\underline{y}(t) = \underline{H}\ \underline{x}(t) + \underline{D}\ \underline{u}(t) \tag{B-4}$$

B-1

where

$$\underline{A} = \begin{bmatrix} 0 & -1 \\ -\omega_n^2 & -2\zeta\omega_n \end{bmatrix}$$

$$\underline{B} = \begin{bmatrix} 0 \\ \omega_n^2 \end{bmatrix}$$

$$\underline{H} = [1 \quad 0]$$

$$\underline{D} = \begin{bmatrix} 0 \\ 0 \end{bmatrix}$$

$\underline{x}(t)$ = vector of state variables

$\underline{y}(t)$ = a_L and a_N

$\underline{u}(t)$ = a_{CMDL} and a_{CMDN}

Since this function will be called frequently and parameters will not normally be change after initialization, this model is implemented as a difference equation

$$\underline{x}(t_{i+1}) = \underline{\Phi}(t_{i+1}, t_i) \, \underline{x}(t_i) + \underline{B}_1 \, a_{CMD}(t_i) \qquad (B-5)$$

where

$\underline{\Phi}(t_{i+1}, t_i) = {}^{-1}[(S\underline{I} - \underline{A})^{-1}]$ = the inverse Laplace transform
of the inverse of the matrix $(S\underline{I} - \underline{A})$

$$\underline{B}_1 = \int_{t_i}^{t_{i+1}} \underline{\Phi}(t_{i+1}, t_i) \, B(t_i) \, dt$$

assuming that a_{CMD} is constant over the interval from t_i to t_{i+1}. Since the integration step size is fixed, the values used for $\underline{\Phi}$ and $\underline{B}_1$ are computed initially and remain constant during each computer run. This flexibility in the input parameters permits changing ω_n and ζ should the simulation later warrant such a change.

B-2

B.2 Euler Integration

The state equations that are integrated using the Euler integration technique use the following form

$$x(t_i) = x(t_{i-1}) + \dot{x}(t_{i-1}) \, \Delta t$$

where

$x(t_{i-1})$ = value of state at sample time (ti-1)

$\dot{x}(t_{i-1})$ = value of derivative of state at sample time (ti-1)

The Euler integration is used where the time constants associated with $x(t_{i-1})$ are relatively large with respect to the .02 second integration step time used.

B.3 Trapezoidal Integration

In the case of propagating the filter states, Euler integration did not provide the accuracy needed. The improved integration was implemented as a trapezoidal integration as

$$x(t_i) = x(t_{i-1}) + \frac{[\dot{x}(t_i) - \dot{x}(t_{i-1})] \, \Delta t}{2}$$

where the parameters are as defined above.

B-3

APPENDIX C

FILTER EQUATIONS

C.1 Line-of-Sight Coordinate Filter Equations

The state variables are referenced to the aircraft-to-target line-of-sight. See Figure 3-1.

The filter propagation equations are

$$\dot{\hat{\underline{x}}}(t) = \underline{f}[\hat{\underline{x}}(t_i), \underline{u}(t_i), t_i] + \underline{G}(t_i)\,\underline{w}(t_i) \tag{C-1}$$

$$\dot{\underline{P}}(t_i) = \underline{F}(t)\,\underline{P}(t_i) + \underline{P}(t_i)\,\underline{F}(t_i)^T + \underline{G}(t_i)\,\underline{Q}(t_i)\,\underline{G}^T(t_i) \tag{C-2}$$

The update equations are

$$\underline{K}(t_i) = \underline{P}(t_i^-)\,\underline{H}^T[t_i, \hat{\underline{x}}(t_i^-)]$$

$$\underline{H}[t_i, \hat{\underline{x}}(t_i^-)]\,\underline{P}(t_i^-)\,\underline{H}^T[t_i, \hat{\underline{x}}(t_i^-) + \underline{R}(t_i)]^{-1} \tag{C-3}$$

$$\hat{\underline{x}}(t_i^+) = \hat{\underline{x}}(t_i^-) + \underline{K}(t_i)\,\left\{\zeta(t_i) - \underline{h}[\underline{x}(t_i^-), t_i]\right\} \tag{C-4}$$

$$\underline{P}(t_i^+) = \underline{P}(t_i^-) - \underline{K}(t_i)\,\underline{H}[t_i, \hat{\underline{x}}(t_i^-)]\,\underline{P}(t_i^-) \tag{C-5}$$

State Variables

$$\dot{\underline{x}}(t) = \begin{bmatrix} z \\ \dot{z} \\ R_{M/T} \\ \dot{R}_{M/T} \\ \Theta_\ell \\ R_{A/T} \\ \dot{R}_{A/T} \\ \hdashline \omega_\ell \end{bmatrix} \quad \begin{array}{l} \text{missile position below LOS} \\ \text{missile velocity below LOS} \\ \text{missile position along LOS} \\ \text{missile velocity along LOS} \\ \text{inclination of LOS} \\ \text{aircraft position along LOS} \\ \text{aircraft velocity along LOS} \\ \text{rate of change of LOS, if used} \\ \quad \text{in reduced order filters} \end{array} \tag{C-6}$$

C-1

State Transition Equations

$$\underline{f}[\hat{\underline{x}}(t_i), \underline{u}(t), t] = \begin{bmatrix} \dot{z} \\[6pt] -2\,\dot{R}_{M/T}\,\omega_\ell + a_1 \sin\Theta_\ell + a_3 \cos\Theta_\ell \\[4pt] \qquad - R_{M/T}\,\dot{\omega}_\ell + z\,\omega_\ell^2 \\[6pt] \dot{R}_{M/T} \\[4pt] 2\,\dot{z}\,\omega_\ell + R_{M/T}\,\omega_\ell^2 + z\dot{\omega}_\ell \\[4pt] \qquad + a_1 \cos\Theta_\ell - a_3 \sin\Theta_\ell \\[6pt] -\omega_\ell \\[6pt] \dot{R}_{A/T} \\[4pt] +2\omega_\ell\,\dot{R}_{A/T}\,\Theta' + R_{A/T}(\omega_\ell^2 + \dot{\omega}_\ell\,\Theta') \\[6pt] \hline \\[-4pt] -2\,\dfrac{V_{A/T}^2\,\Theta'}{R_{A/T}^2} \end{bmatrix} \qquad (C\text{-}7)$$

and if ω_ℓ is needed:

where $\Theta' = \tan(\Theta_\ell - \Theta_A)$

Pertubations of the State Equations

$$\underline{F}(t) = \left[\begin{array}{cccccccc} 0. & 1. & 0. & 0. & 0. & 0. & 0. & 0. \\[4pt] \omega_\ell^2 & 0. & -\dot{\omega}_\ell & -2\omega_\ell & F_{25} & 0. & 0. & F_{28} \\[4pt] 0. & 0. & 0. & 1. & 0. & 0. & 0. & 0. \\[4pt] \dot{\omega}_\ell & 2\omega_\ell & \omega_\ell^2 & 0. & F_{45} & 0. & 0. & F_{48} \\[4pt] 0. & 0. & 0. & 0. & 0. & 0. & 0. & -1 \\[4pt] 0. & 0. & 0. & 0. & 0. & 0. & 1. & 0. \\[4pt] 0. & 0. & 0. & 0. & F_{75} & F_{76} & F_{77} & F_{78} \\[4pt] \hline \\[-4pt] 0. & 0. & 0. & 0. & F_{85} & F_{86} & F_{87} & 0. \end{array}\right]$$

where $\underline{x}$ is evaluated at $\underline{\ell}$

C-2

and

$$F_{25} = +a_1 \cos \Theta_\ell - a_3 \sin \Theta_\ell$$

$$F_{28} = -2 \dot{R}_{M/T} + 2 R_{M/T} \, \omega_\ell$$

$$F_{45} = -a_1 \sin \Theta_\ell - a_3 \cos \Theta_\ell$$

$$F_{48} = +2 \dot{z} + 2 R_{M/T} \, \omega_\ell$$

$$F_{75} = +(2 \, \omega_\ell \, \dot{R}_{A/T} + R_{A/T} \, \dot{\omega}_\ell) \, \sec^2 (\Theta_\ell - \Theta_A)$$

$$F_{76} = \omega_\ell^2 + \dot{\omega}_\ell \, \tan(\Theta_\ell - \Theta_A)$$

$$F_{77} = +2 \omega_\ell \tan (\Theta_\ell - \Theta_A)$$

$$F_{78} = +2 \dot{R}_{A/T} \tan (\Theta_\ell - \Theta_A) + 2 R_{A/T} \, \omega_\ell$$

$$F_{85} = \frac{-2 \, V_{A/T}^2}{R_{A/T}^2} \sec^2 (\Theta_\ell - \Theta_A)$$

$$F_{86} = \frac{+4 \, V_{A/T}^2}{R_{A/T}^3} \, \Theta'$$

$$F_{87} = \frac{-4 \, V_{A/T}}{R_{A/T}^2} \, \Theta'$$

and Θ' defined above in equation (C-7).

Measurement Model

$$h(t) = \sin^{-1} \left[\frac{z}{R_{A/T} - R_{M/T}} \right] \tag{C-9}$$

Pertubations of the Measurement Model

$$H(t) = \begin{bmatrix} \dfrac{A}{B} & 0 & \dfrac{zA}{B^2} & 0 & 0 & \dfrac{-zA}{B^2} & 0 \end{bmatrix} \tag{C-10}$$

C-3

where

$$A = \cfrac{1}{\left[1 - \left(\cfrac{z}{B}\right)^2\right]^{1/2}} \qquad \text{and} \quad B = (R_A/T - R_M/T)$$

Measurement Covariance

$$E[\underline{v}(t_i)] = 0$$

$$E[\underline{v}(t_i)\,\underline{v}^T(t_j)] = \begin{cases} \underline{R}\delta_{ij}(t) & i = j \\ 0 & i \neq j \end{cases} \tag{C-11}$$

Noise

$$G(t) = \begin{bmatrix} 0. & 0. & 0. & 1. & 0. \\ -\sin\Theta_\ell & \cos\Theta_\ell & \sin\Theta_\ell & 0. & 0. \\ 0. & 0. & 0. & 0. & 0. \\ -\cos\Theta_\ell & -\sin\Theta_\ell & \cos\Theta_\ell & 0. & 0. \\ 0. & 0. & 0. & 0. & 0. \\ 0. & 0. & 0. & 0. & 0. \\ 0. & 0. & 0. & 0. & 1. \end{bmatrix} \tag{C-12}$$

Strength of driving noise (Ref. Section 2.6 for Development of Values)

$$Q(t) = \begin{bmatrix} Q_1 & 0. & 0. & 0. & 0. \\ 0. & Q_2 & 0. & 0. & 0. \\ 0. & 0. & Q_3 & 0. & 0. \\ 0. & 0. & 0. & Q_4 & 0. \\ 0. & 0. & 0. & 0. & Q_5 \end{bmatrix} \tag{C-13}$$

C-4

The previous noise terms are associated with the following parameters:

Q_1 = horizontal target velocity

Q_2 = vertical missile velocity

Q_3 = horizontal missile velocity

Q_4 = change in ω due to A/C motion

Q_5 = $V_{A/T}$ due to A/C motion

For this filter the noise is implemented such that

$$\underline{Q}_d = \underline{G}(t)\ \underline{Q}(t)\ \underline{G}^T(t) \tag{C-14}$$

and

$$\underline{G}_d(t) = \underline{I}$$

Then Q_d can be expressed as

$Q_d(1,1) = 1.$

$Q_d(2,2) = Q_1 \sin^2 \Theta_\ell + Q_2 \cos^2 \Theta_\ell + Q_3 \sin^2 \Theta_\ell$

$Q_d(2,4) = (Q_1 - Q_2 + Q_3) \sin \Theta_\ell \cos \Theta_\ell$

$Q_d(4,2) = Q_d(2,4)$

$Q_d(4,4) = Q_1 \cos^2 \Theta_\ell + Q_2 \sin^2 \Theta_\ell + Q_3 \cos^2 \Theta_\ell$

$Q_d(7,7) = 1.$

all other components are zero

These values serve as initial values for P the filter testing.

$z = (0\ \text{ft})^2$ perfect knowledge of z at launch

$\dot{z} = (2\ \text{ft/sec})^2$ same as A/C

$R_{M/T} = (150\ \text{ft})^2$ from the tracker

$\dot{R}_{M/T} = (2\ \text{ft/sec})^2$ same as A/C

$\Theta_\ell = (.3 \text{ MRAD})^2$ from the tracker

$\omega = (0.5/\text{sec})^2$ z error/nominal range to TGT (if used)

$R_{A/T} = (150 \text{ ft})^2$ from tracker

$\dot{R}_{A/T} = (2 \text{ ft/sec})^2$ from A/C INS

C.2 Inertial Coordinate Filter Equations

Sixth Order Model. The filter propagation equations are:

$$\underline{\hat{x}}(t_i^-) = \underline{\Phi}(t_i, t_{i-1})\, \underline{x}(\hat{t}_{i-1}^+) + \underline{B}_d(t_{i-1})\, \underline{u}(t_{i-1}) \tag{C-15}$$

$$\underline{P}(t_i^-) = \underline{\Phi}(t_i, t_{i-1})\, \underline{P}(t_{i-1}^+)\, \underline{\Phi}^T(t_i, t_{i-1}) + \underline{Q}_d(t_{i-1}) \tag{C-16}$$

The update equations are

$$\underline{K}(t_i) = \underline{P}(t_i^-)\, \underline{H}^T[t_i, \underline{\hat{x}}(t_i^-)]$$

$$\left[\underline{H}[t_i, \underline{\hat{x}}(t_i^-)]\, \underline{P}(t_i^-)\, \underline{H}^T[t_i, \underline{\hat{x}}(t_i^-) + \underline{R}(t_i)] \right]^{-1} \tag{C-17}$$

$$\underline{\hat{x}}(t_i^+) = \underline{\hat{x}}(t_i^-) + \underline{K}(t_i)\quad \zeta(t_i) - \underline{h}[\underline{x}(t_i^-), t_i] \tag{C-18}$$

$$\underline{P}(t_i^+) = \underline{P}(t_i^-) - \underline{K}(t_i)\, \underline{H}[t_i, \underline{\hat{x}}(t_i^-)]\, \underline{P}(t_i^-) \tag{C-19}$$

The filter matrices are summarized as

$$\underline{F} = \begin{bmatrix} 0 & 1 & 0 & 0 & 0 & 0 \\ 0 & 0 & 0 & 0 & 0 & 0 \\ 0 & 0 & 0 & 1 & 0 & 0 \\ 0 & 0 & 0 & 0 & 0 & 0 \\ 0 & 0 & 0 & 0 & 0 & 1 \\ 0 & 0 & 0 & 0 & 0 & 0 \end{bmatrix} \quad (C\text{-}20) \qquad \underline{G} = \begin{bmatrix} 0 & 1 & 0 & 0 & 0 & 0 \\ 0 & 0 & 0 & 0 & 0 & 0 \\ 0 & 0 & 0 & 1 & 0 & 0 \\ 0 & 0 & 0 & 0 & 0 & 0 \\ 0 & 0 & 0 & 0 & 0 & 1 \\ 0 & 0 & 0 & 0 & 0 & 0 \end{bmatrix} \tag{C-21}$$

$$\underline{B} = \begin{bmatrix} 0 & 0 \\ 1 & 0 \\ 0 & 0 \\ 0 & 1 \\ 0 & 0 \\ 0 & 0 \end{bmatrix} \quad \text{(C-22)} \qquad \underline{Q} = \begin{bmatrix} Q_1 & 0 & 0 & 0 & 0 \\ 0 & Q_2 & 0 & 0 & 0 \\ 0 & 0 & Q_3 & 0 & 0 \\ 0 & 0 & 0 & Q_4 & 0 \\ 0 & 0 & 0 & 0 & Q_5 \end{bmatrix} \quad \text{(C-23)}$$

$$\underline{Q}_d(t_{i-1}) = \begin{bmatrix} 1 & t_i - t_{i-1} & 0 & 0 & 0 & 0 \\ 0 & 1 & 0 & 0 & 0 & 0 \\ 0 & 0 & 1 & t_i - t_{i-1} & 0 & 0 \\ 0 & 0 & 0 & 1 & 0 & 0 \\ 0 & 0 & 0 & 0 & 1 & t_i - t_{i-1} \\ 0 & 0 & 0 & 0 & 0 & 1 \end{bmatrix} \quad \text{(C-24)}$$

$$\underline{Q}_d(t_i) = \underline{G}\,\underline{Q}\,\underline{G}^T[t_i - t_{i-1}]$$

$$\underline{Q}_d(t_i) = \begin{bmatrix} 0 & 0 & 0 & 0 & 0 & 0 \\ 0 & \begin{array}{c}(Q_1 + Q_2) \\ (t_1 - t_{i-1})\end{array} & 0 & 0 & 0 & 0 \\ 0 & 0 & 0 & 0 & 0 & 0 \\ 0 & 0 & 0 & \begin{array}{c}(Q_2 + Q_4) \\ (t_1 - t_{i-1})\end{array} & 0 & 0 \\ 0 & 0 & 0 & 0 & 0 & 0 \\ 0 & 0 & 0 & 0 & 0 & \begin{array}{c}(Q_3 + Q_5) \\ (t_1 - t_{i-1})\end{array} \end{bmatrix} \quad \text{(C-25)}$$

C-7

The measurements available to this filter are

$$EL = \tan^{-1}\left[\frac{-x_7}{-x_5}\right] - \tan^{-1}\left[\frac{x_3 - x_7}{x_1 - x_5}\right] \tag{C-26}$$

$$R_{M/T} = (x_1^2 + x_3^2)^{1/2} \tag{C-27}$$

$$R_{A/T} = (x_5^2 + x_{A/T}^2)^{1/2} \tag{C-28}$$

The H-matrix partial derivatives are

$$H(1,2) = H(1,4) = H(1,6) = 0 \tag{C-29}$$

$$H(1,1) = \frac{x_3 - x_7}{(x_1 - x_5)^2 + (x_3 - x_7)^2} \tag{C-30}$$

$$H(1,3) = \frac{x_5 - x_1}{(x_1 - x_5)^2 + (x_3 - x_7)^2} \tag{C-31}$$

$$H(1,5) = \frac{x_7 - x_3}{(x_1 - x_5)^2 + (x_3 - x_7)^2} \tag{C-32}$$

$$H(2,2) = H(2,4) = H(2,5) = H(2,6) = 0 \tag{C-33}$$

$$H(2,1) = \frac{x_1}{(x_1^2 + x_3^2)^{1/2}} \tag{C-34}$$

C-8

$$H(2,3) = \frac{x_3}{(x_1^2 + x_3^2)^{1/2}} \qquad\qquad (C-35)$$

$$H(3,1) = H(3,2) = H(3,3) = H93,4) = H(3,6) = 0 \qquad (C-36)$$

$$H(3,5) = \frac{x_5}{(x_5^2 + x_{A/T}^2)^{1/2}} \qquad\qquad (C-37)$$

The measurement noise strength is represented by

$$\underline{R} = \begin{bmatrix} R_1 & 0 & 0 \\ 0 & R_2 & 0 \\ 0 & 0 & R_3 \end{bmatrix} \qquad\qquad (C-38)$$

The magnitudes of the noises are discussed in Chapter III.

Fourth Order Model. The filter equations are described in (C-15) through (C-19). The corresponding matrices are

$$\underline{F} = \begin{bmatrix} 0 & 1 & 0 & 0 \\ 0 & 0 & 0 & 0 \\ 0 & 0 & 0 & 1 \\ 0 & 0 & 0 & 0 \end{bmatrix} \quad (C-39) \qquad \underline{G} = \begin{bmatrix} 0 & 0 & 0 & 0 \\ 1 & 0 & 1 & 0 \\ 0 & 0 & 0 & 0 \\ 0 & 1 & 0 & 1 \end{bmatrix} \quad (C-40)$$

$$\underline{B} = \begin{bmatrix} 0 & 0 \\ 1 & 0 \\ 0 & 0 \\ 0 & 1 \end{bmatrix} \quad \text{(C-41)} \qquad \underline{\Phi}(t_1, t_{i-1}) = \begin{bmatrix} 1 & t_1 - t_{i-1} & 0 & 0 \\ 0 & 1 & 0 & 0 \\ 0 & 0 & 1 & t_1 - t_{i-1} \\ 0 & 0 & 0 & 1 \end{bmatrix} \quad \text{(C-42)}$$

$$\underline{B}_d(t_{i-1}) = \begin{bmatrix} 0 & 0 \\ t_i - t_{i-1} & 0 \\ 0 & 0 \\ 0 & t_i - t_{i-1} \end{bmatrix} \quad \text{(C-43)}$$

$$\underline{Q} = \begin{bmatrix} Q_1 & 0 & 0 & 0 \\ 0 & Q_2 & 0 & 0 \\ 0 & 0 & Q_3 & 0 \\ 0 & 0 & 0 & Q_4 \end{bmatrix} \quad \text{(C-44)}$$

$$\underline{Q}_d(t_1) = \underline{G} \; \underline{Q} \; \underline{G}^T [t_1 - t_{i-1}]$$

$$\underline{Q}_d(t) = \begin{bmatrix} 0 & 0 & 0 & 0 \\ 0 & (Q_1 + Q_3)(t_1 - t_{i-1}) & 0 & 0 \\ 0 & 0 & 0 & 0 \\ 0 & 0 & 0 & (Q_2 + Q_4)(t_1 - t_{i-1}) \end{bmatrix} \quad \text{(C-45)}$$

C-10

$$EL = \tan^{-1} \begin{bmatrix} -z_{A/T} \\ -x_{A/T} \end{bmatrix} - \tan^{-1} \begin{bmatrix} x_3 - z_{A/T} \\ x_1 - x_{A/T} \end{bmatrix} \qquad \text{(C-46)}$$

$$R_{M/T} = (x_1^2 + x_3^2)^{1/2} \qquad \text{(C-47)}$$

The H-matrix partial derivatives are

$$H(1,2) = H(1,4) = 0 \qquad \text{(C-48)}$$

$$H(1,1) = \frac{x_3 - z_{A/T}}{(x_1 - x_{A/T})^2 + (x_3 - z_{A/T})^2} \qquad \text{(C-49)}$$

$$H(1,3) = \frac{x_{A/T} - x_1}{(x_1 - x_{A/T})^2 + (x_3 - z_{A/T})^2} \qquad \text{(C-50)}$$

$$H(2,2) = H(2,4) = 0 \qquad \text{(C-51)}$$

$$H(2,1) = \frac{x_1}{(x_1^2 + x_3^2)^{1/2}} \qquad \text{(C-52)}$$

$$H(2,3) = \frac{x_3}{(x_1^2 + x_3^2)^{1/2}} \qquad \text{(C-53)}$$

The measurement noise strength is represented by

$$\underline{R} = \begin{bmatrix} R_1 & 0 \\ 0 & R_2 \end{bmatrix} \qquad \text{(C-54)}$$

C-11

APPENDIX D

SIMULATION PARAMETERS AND FLIGHT PROFILES

This appendix is a brief summary of the parameters, assumptions and flight profiles used in developing and running the simulation. The truth model developed in Chapter II has a three-dimensional capability while the filters developed in Chapter III are restricted to only two dimensions. The parameters listed below include information about all three dimensions but in the final implementation all parameters involving lateral motion were set to zero. (Ref. 11)

TABLE D-1

Aircraft Parameters Used

High dynamics air superiority fighter of the F15 class	
Natural frequency	3 rad/sec
Correlation time constant	2 sec
Constant velocity	500 ft/sec
Wind buffeting effects	3 ft/sec/sec
Maximum axial acceleration	64 ft/sec/sec
Maximum vertical acceleration	290 ft/sec/sec
Maximum lateral acceleration	290 ft/sec/sec
Onboard INS accuracy	4 ft/sec
IR tracker accuracy	3 milli-rad angular resolution and 150 ft range resolution

Only time correlated white Gaussian noise is added to the vertical and axial acceleration.

Missile Parameters Used:

Hyper-velocity missile	
Natural frequency	44.0 rad/sec during thrust 44.0 rad/sec after burnout
Correlation time constant	0.14 sec during thrust 0.14 sec after burnout
Damping coefficient	.707
Wind buffeting effects	3 ft/sec/sec
Maximum lift	3200 ft/sec/sec
Propulsion	solid propellant boost-coast profile
Thrust	5000 lbs
Thrust duration	1.0 sec
Flight duration	1.0 - 3.0 sec
Body size	3.5 inches diameter 72 inches in length
Body weight	26.7 lbs
Fuel weight	25.9 lbs
Drag coefficient	.35 during thrust .45 during coast
Air density	.0023 slugs/ft^3
Guidance law	proportional navigation (Ref. 2.5)

TABLE D.3

Target Parameters Used:

Highly maneuverable tank of the M1 class	
Natural frequency	31 rad/sec
Correlation time constant	.2 sec
Constant velocity	0 ft/sec
Maximum axial acceleration	29 ft/sec/sec
Maximum lateral acceleration	16 ft/sec/sec
Only time correlated noise is added to the axial acceleration.	

The following three flight profiles were used during the initial validation of the truth model to exercise the dynamics equations. The last of the three was used during the filter analysis as a typical mission profile with a down range distance of 10,000 ft and altitude of 2000 ft. Other variations of this last profile would include shortening the slant range and varying the angle between the aircraft velocity and target position.
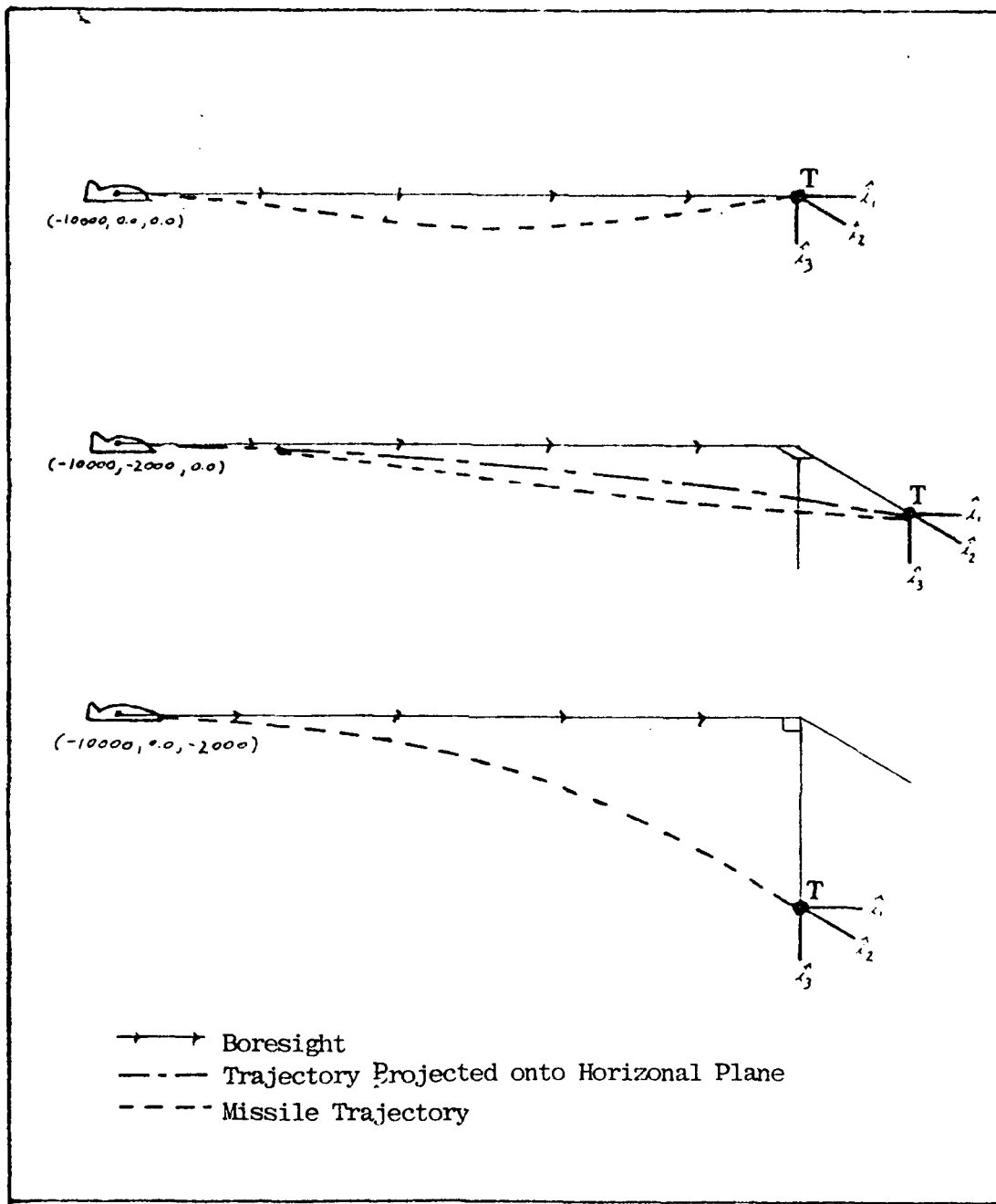
Figure D-1. Test Flight Profiles

D-4

APPENDIX E

FILTER ANALYSIS PROOFS

E-1 FORMULATION OF THE SIMILARITY TRANSFORM

In this case for the general equations

$$\dot{\underline{X}} = \underline{F}\ \underline{X} + \underline{B}\ \underline{U} \qquad (E-1)$$

$$\dot{\underline{P}} = \underline{F}\ \underline{P} + \underline{P}\ \underline{F}^T + \underline{G}\ \underline{Q}\ \underline{G}^T \qquad (E-2)$$

Let a transformation vector $\underline{T}$ be defined such that

$$\underline{X} = \underline{T}\ \underline{X}^* \qquad (E-3)$$

and $\quad \underline{X} = \underline{T}^{-1}\ \underline{X} \qquad (E-4)$

substituting E-3 and E-4 into E-1 and E-2 produces

$$\underline{T}\ \dot{\underline{X}}^* = \underline{F}\ \underline{T}\ \underline{X}^* + \underline{B}\ \underline{U} \qquad (E-5)$$

premultiplying by $\underline{T}^{-1}$ yields

$$\underline{X} = \underline{T}^{-1}\ \underline{F}\ \underline{T}\ \underline{X}^* + \underline{T}^{-1}\ \underline{B}\ \underline{U} \qquad (E-6)$$

and $\quad \dot{\underline{P}}^* = \underline{F}^*\underline{P}^* + \underline{P}^*\underline{F}^{T*} + \underline{G}^*\underline{Q}^*\underline{G}^{T*} \qquad (E-7)$

where $\underline{F}^* = \underline{T}^{-1}\ \underline{F}\ \underline{T} \qquad (E-8)$

$\underline{B}^* = \underline{T}^{-1}\ \underline{B} \qquad (E-9)$

$\underline{G}^* = \underline{T}^{-1}\ \underline{G} \qquad (E-10)$

$\underline{P}^* = \underline{T}^{-1}\ \underline{P}\ \underline{T} \qquad (E-11)$

These relationships are good only for constant $\underline{T}$. Also note that the similarity transform on the $\underline{F}$ matrix will preserve it's eigenvalues in a time response sense. For this problem, the scaling matrix $\underline{T}$ was chosen such that

$$\underline{T}_{ij} = \left\{ \begin{array}{ll} \dfrac{1}{P_{ij}(t_o)} & \text{for } i = j \\[2mm] 0 & \text{for } i \neq j \end{array} \right\} \qquad (E\text{-}12)$$

This would let $\underline{P}^*(t_o)$ be an identity matrix. Since $P(1,1)$ at $t=0$ was zero, $T(1)$ was set to 1 and later to that of $P(3,3)$ at $t=0$, which is a parameter of like dimensions. This scaling was done on the time propagations while the updates were turned off. The final result was that the scaled covariance matrix had the same problems with negative eigen-values than the original matrix.

E-2 FORMULATION OF ROOTS OF THE INTEGRATED COVARIANCE MATRIX

The Euler integration used on the covariance matrix can produce negative eigenvalues. This principle can be illustrated as follows. The $\underline{F}$ matrix in this example, as in the filter, has no real eigen-values. Now consider a second order system such that

$$\underline{F} = \begin{bmatrix} 0 & a \\ 0 & 0 \end{bmatrix} \qquad (E\text{-}13)$$

$$\underline{P}(t_o) = \begin{bmatrix} P_{11} & P_{12} \\ P_{12} & P_{22} \end{bmatrix} = \begin{bmatrix} 0 & 0 \\ 0 & b \end{bmatrix} \qquad (E\text{-}14)$$

and

$$\underline{\dot{P}} = \underline{F}\ \underline{P} + \underline{P}\ \underline{F}^T + \underline{G}\ \underline{Q}\ \underline{G}^T \qquad (E\text{-}15)$$

where in this case $\underline{G}\ \underline{Q}\ \underline{G}^T = 0$

First solve for $\underline{\dot{P}}$ in general form

$$\underline{\dot{P}} = \begin{bmatrix} 0 & ab \\ ab & 0 \end{bmatrix} \qquad (E\text{-}16)$$

E-2

Integrating $\underline{\dot{P}}$ using Euler integration, as in the simulation will yield

$$\underline{P} = \begin{bmatrix} P_{11} & P_{12} + ab\delta t \\ P_{12} + ab\delta t & P_{22} \end{bmatrix} \qquad (E-17)$$

Obtaining the characteristic equation from the form $(\lambda \underline{I} - \underline{P})$ and equation E-17 will yield

$$\lambda^2 - (P_{11} + P_{12})\ \lambda + (P_{11}\ P_{12} - (P_{12} + ab\delta t)^2)\ \lambda^o \qquad (E-18)$$

note that the λ^o term can become negative if $(P_{12} + ab\delta t)^2 > P_{11}$ P_{12} and will then produce a negative root. This is what was experienced in the simulation since P_{11} is small and is not driven by $\underline{Q}$.

Note however that this is using Euler integration and is only an approximation to the true solution in closed form. If you continue the above example and let $P_{11} = 0$, then equation E-16 can be expressed as

$$\underline{\dot{P}} = \begin{bmatrix} P_{11} & P_{12} \\ P_{12} & P_{22} \end{bmatrix} = \begin{bmatrix} 2aP_{12} & aP_{22} \\ aP_{22} & 0 \end{bmatrix} \qquad (E-19)$$

breaking up the components of the matrix and expressing them as vectors will yield

$$\begin{bmatrix} \dot{P}_{11} \\ \dot{P}_{12} \\ \dot{P}_{22} \end{bmatrix} = \begin{bmatrix} 0 & 2a & 0 \\ 0 & 0 & a \\ 0 & 0 & 0 \end{bmatrix} \begin{bmatrix} P_{11} \\ P_{12} \\ P_{22} \end{bmatrix} \qquad (E-20)$$

notice that $\underline{\dot{P}}_{22} = 0$ and let $P_{22} = b$, a constant in time. Then

$$\rightarrow \begin{bmatrix} P_{11} \\ P_{12} \end{bmatrix} = \begin{bmatrix} 0 & 2a \\ 0 & 0 \end{bmatrix} \begin{bmatrix} P_{11} \\ P_{12} \end{bmatrix} + \begin{bmatrix} 0 \\ ab \end{bmatrix} \qquad (E-21)$$

E-3

if $\ddot{P}_{12} = ab$, is a constant, it follows that

$$P_{12} = abt \qquad (E-22)$$

Since P_{12} is a growing function of time and if $\dot{P}_{11} = 2abP_{11} = 2a^2t$ it follows that

$$P_{11} = 2a^2\, bt^2 \qquad (F-23)$$

where

$$a^2 > 0$$

$$t^2 > 0$$

$$b > 0$$

then we can conclude that $P_{11} > 0$ also as was P_{22}.

The off diagonal terms may or may not be negative, but the diagonal terms will not become negative if $\underline{P}$ (t) is solved in closed form. The homogeneous portion of the solution to equation E-20 has the form

$$\dot{\underline{P}}(t) = e^{-At}\, P(t_o) \qquad (E-24)$$

where

$$\underline{A} = \begin{bmatrix} 0 & 2a & 0 \\ 0 & 0 & a \\ 0 & 0 & 0 \end{bmatrix} \qquad (E-25)$$

Since $\underline{A}$ is a matrix, equation E-24 can be solved by taking the inverse Laplace transform of $(S\,\underline{I} - \underline{A})$. This yields

$$\begin{bmatrix} P_{11}(t) \\ P_{12}(t) \\ P_{22}(t) \end{bmatrix} = \begin{bmatrix} 1 & 2at & 2a^2t^2 \\ 0 & 1 & at \\ 0 & 0 & 1 \end{bmatrix} \begin{bmatrix} P_{11}(t_o) \\ P_{12}(t_o) \\ P_{22}(t_o) \end{bmatrix} \qquad (E-26)$$

As above, P_{22} (t) is constant with time and P_{11} (t) and P_{12} (t) will increase positive with time.

E-4

APPENDIX F

KALMAN FILTER PERFORMANCE PLOTS

The plots in this section are a representation sampling of the state errors and covariances of the Kalman Filters developed in this study.

STATE 1, ERROR, STD. DEV., AND SORT COV.

Fig F-1. z State With Euler Integration and No Truth Model Noise

F-1
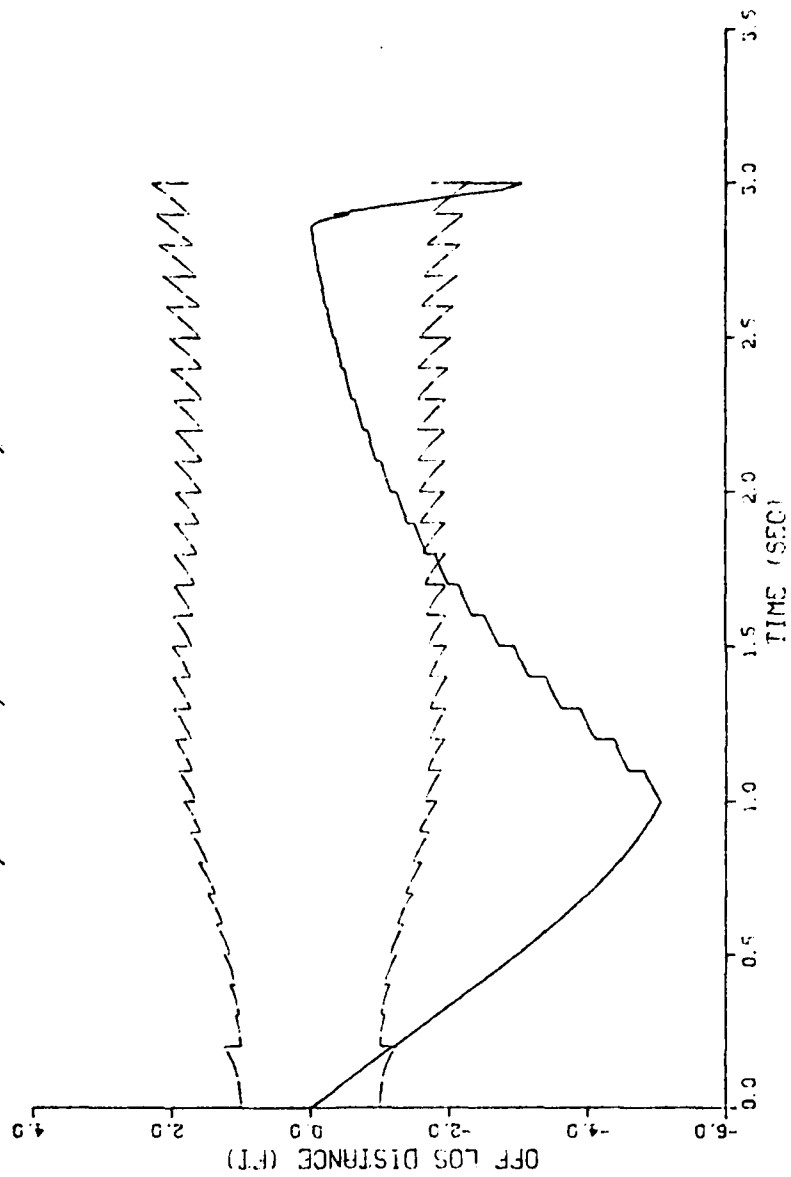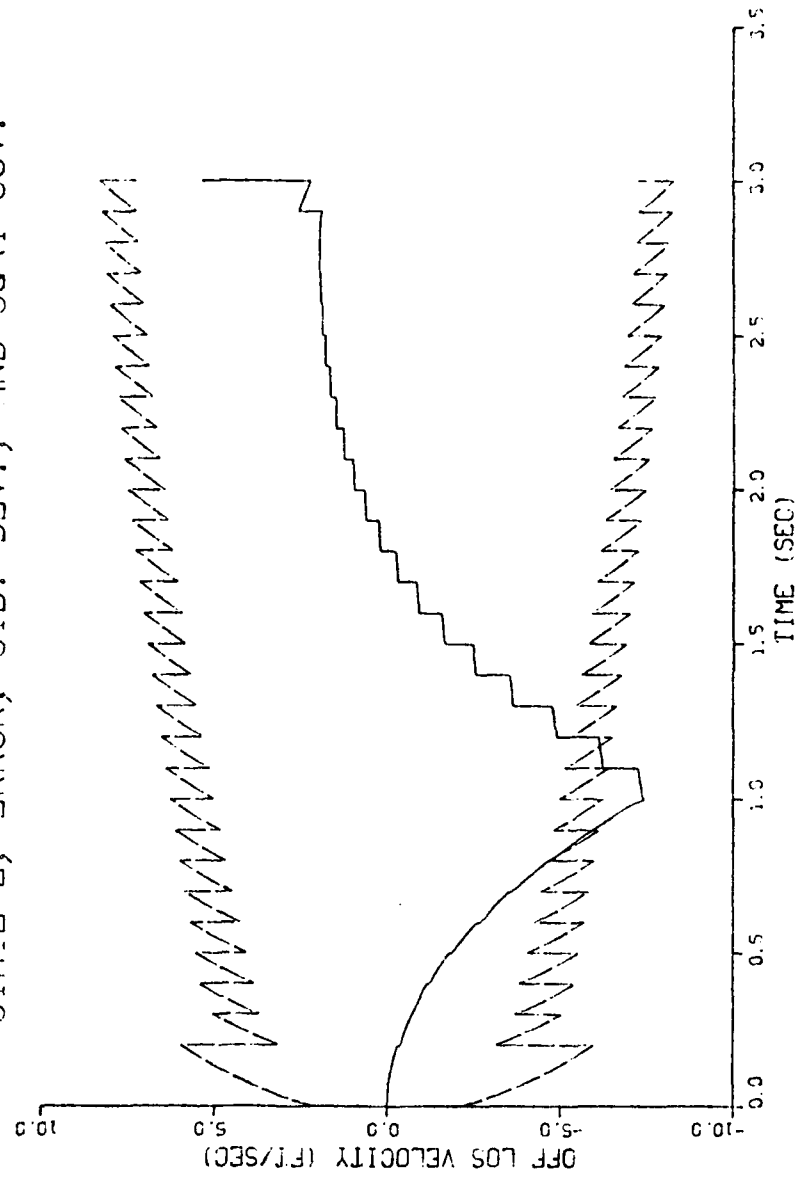
Fig F-2. $\dot{z}$ State With Euler Integration and No Truth Model Noise

F-2
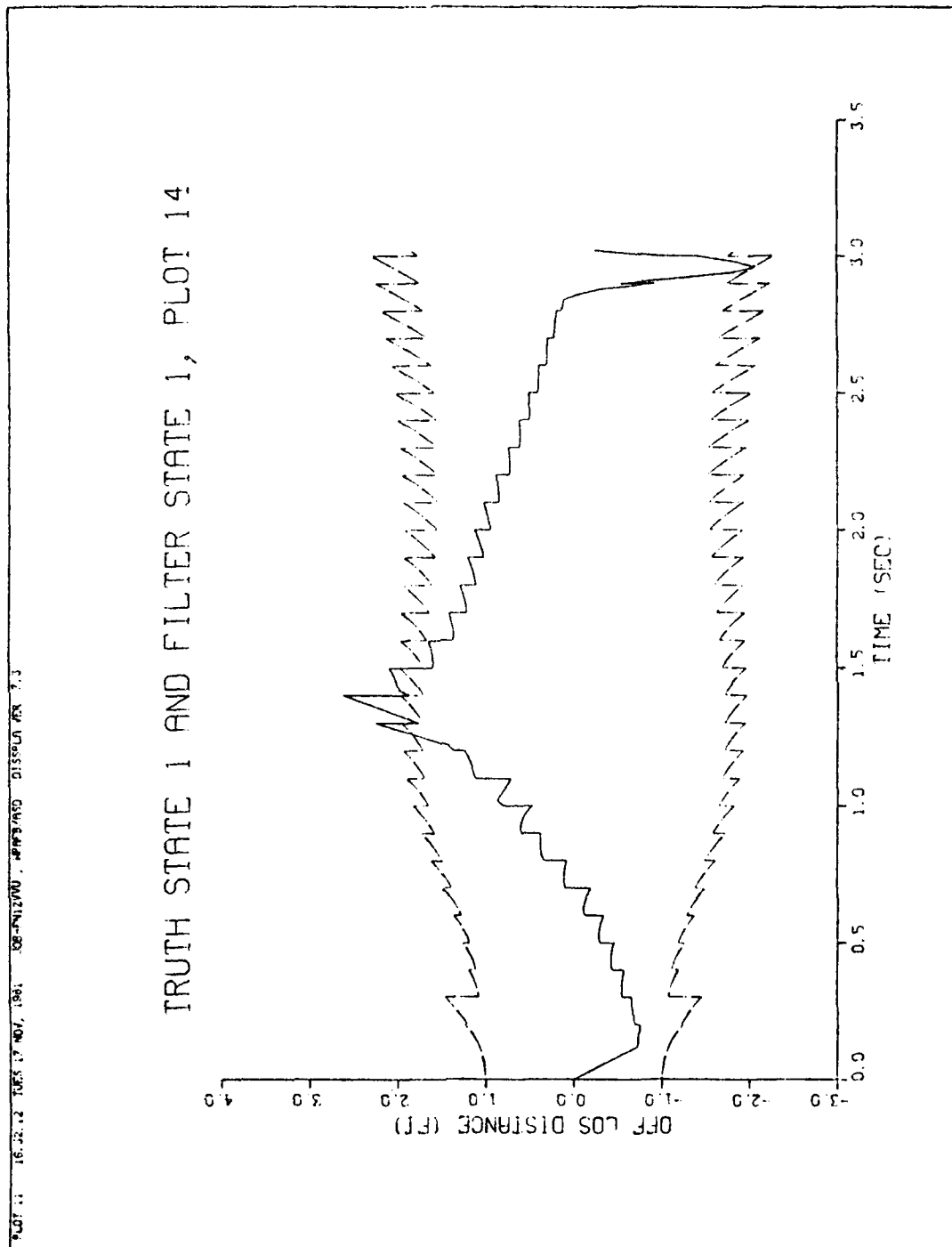
Fig F-3. z State With Trapezoidal Integration and No Truth Model Noise

Fig F-4. $\dot{z}$ State With Trapezoidal Integration and No Truth Model Noise
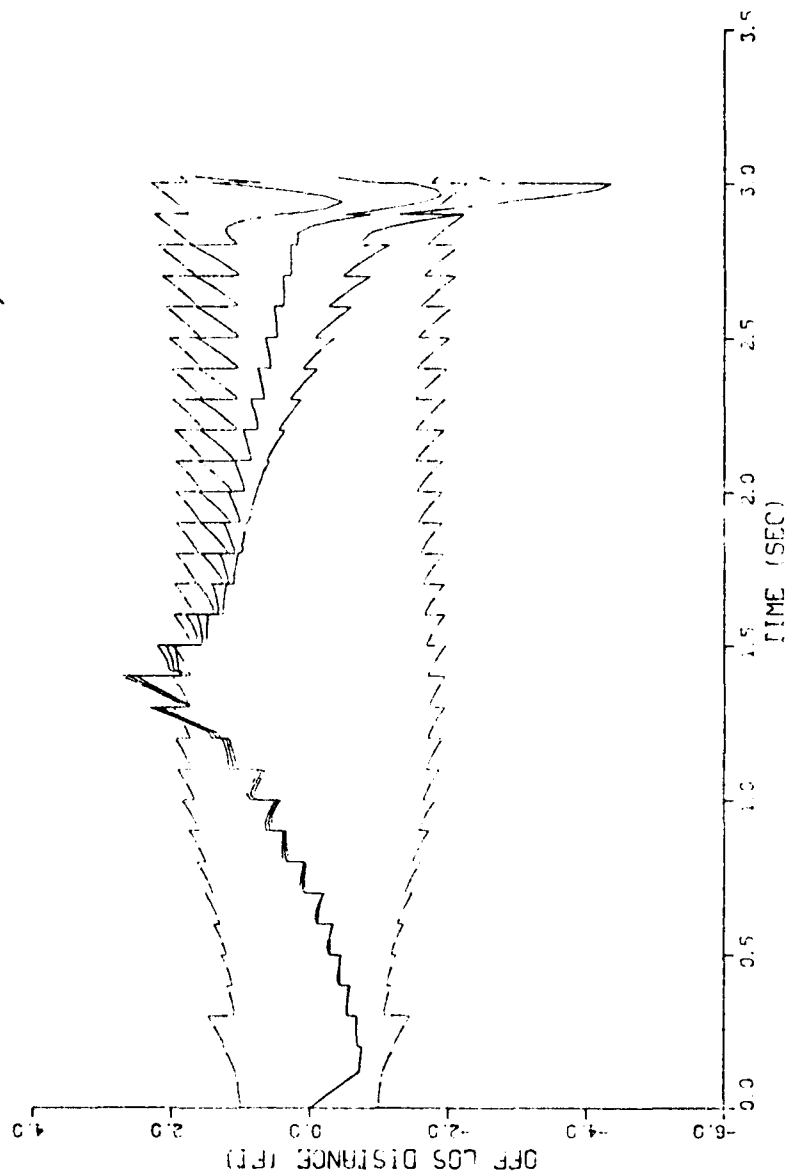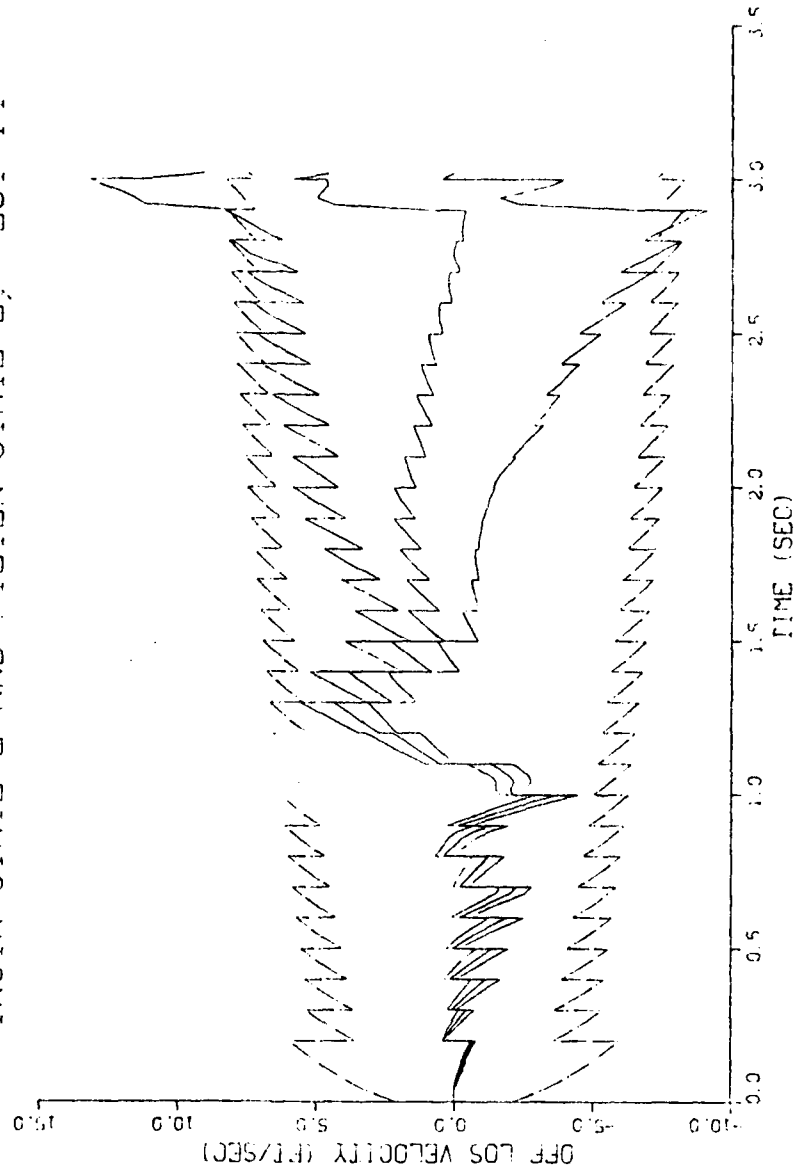
Fig F-5. z State With Computed $\underline{P}$, $\underline{Q}$ and Dynamic Driving Noise

Fig F-6. ż State With Computed $\underline{P}$, $\underline{Q}$ and Dynamic Driving Noise
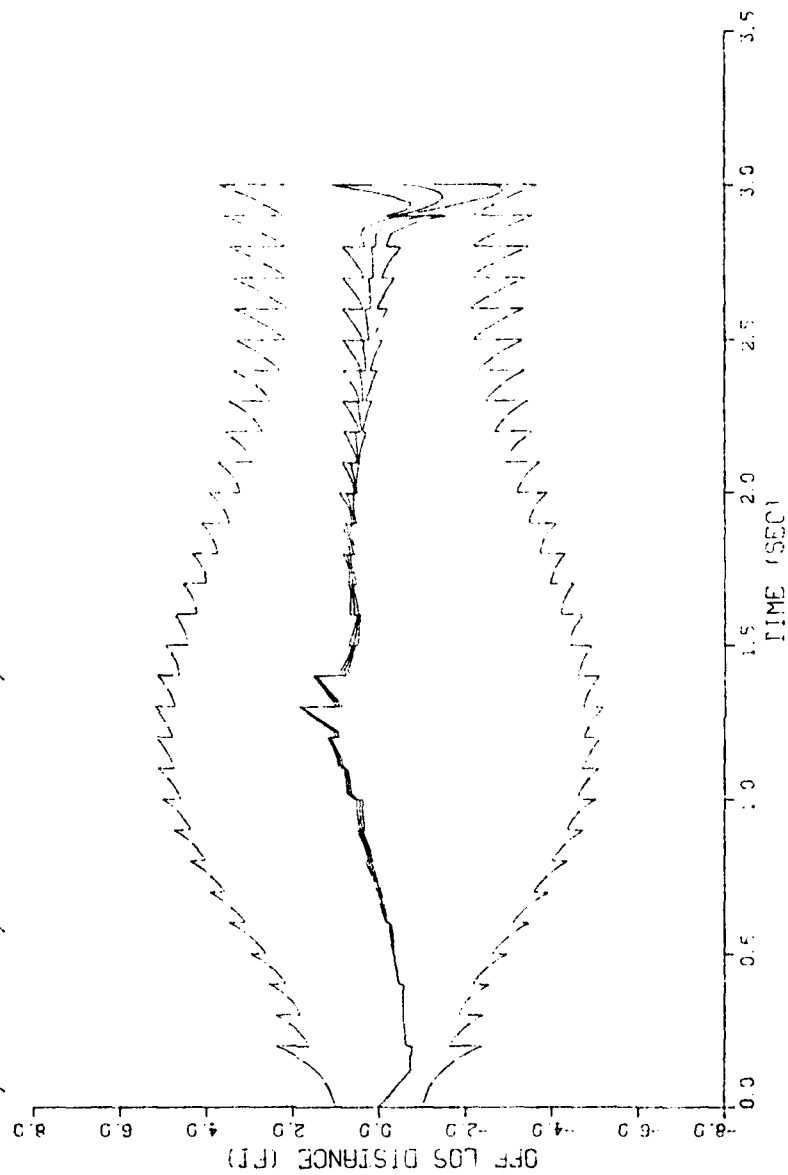
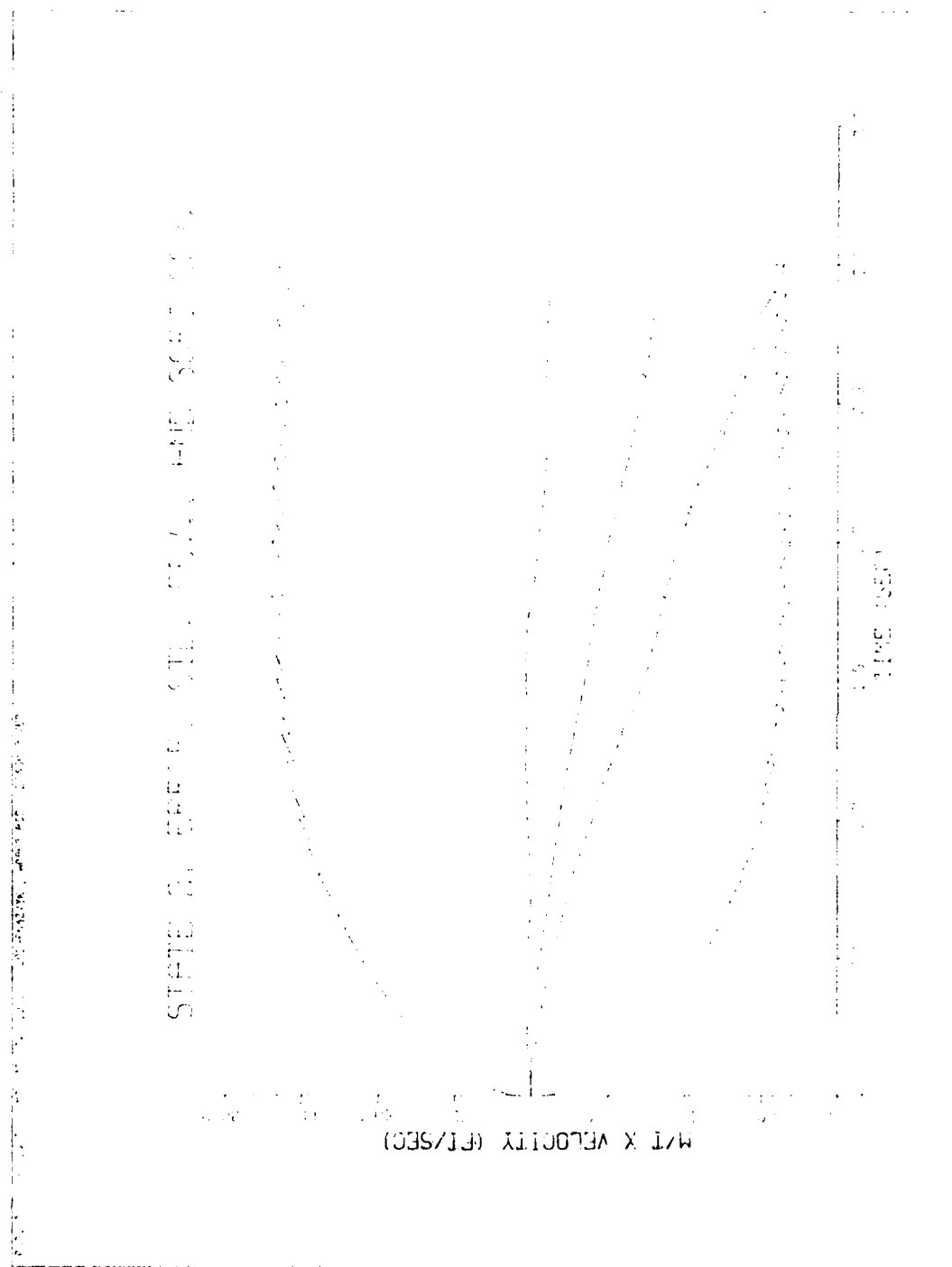Fig F-7. z State With Tuned Filter Q and Dynamic Driving Noise

STATE 2, ERROR, STD. DEV., AND SORT COV.

OFF LOS VELOCITY (FT/SEC)

TIME (SEC)

Fig F-8.   ż State With Tuned Filter Q and Dynamic Driving Noise

STATE 1, ERROR, STD. DEV., AND SQRT COV.

Fig F-9. z State With Tuned Filter Q and Perturbed Initial Conditions

F-9

STATE 2, ERROR, STD. DEV., AND SQRT COV.

TIME (SEC)

DFF LOS VELOCITY (FT/SEC)
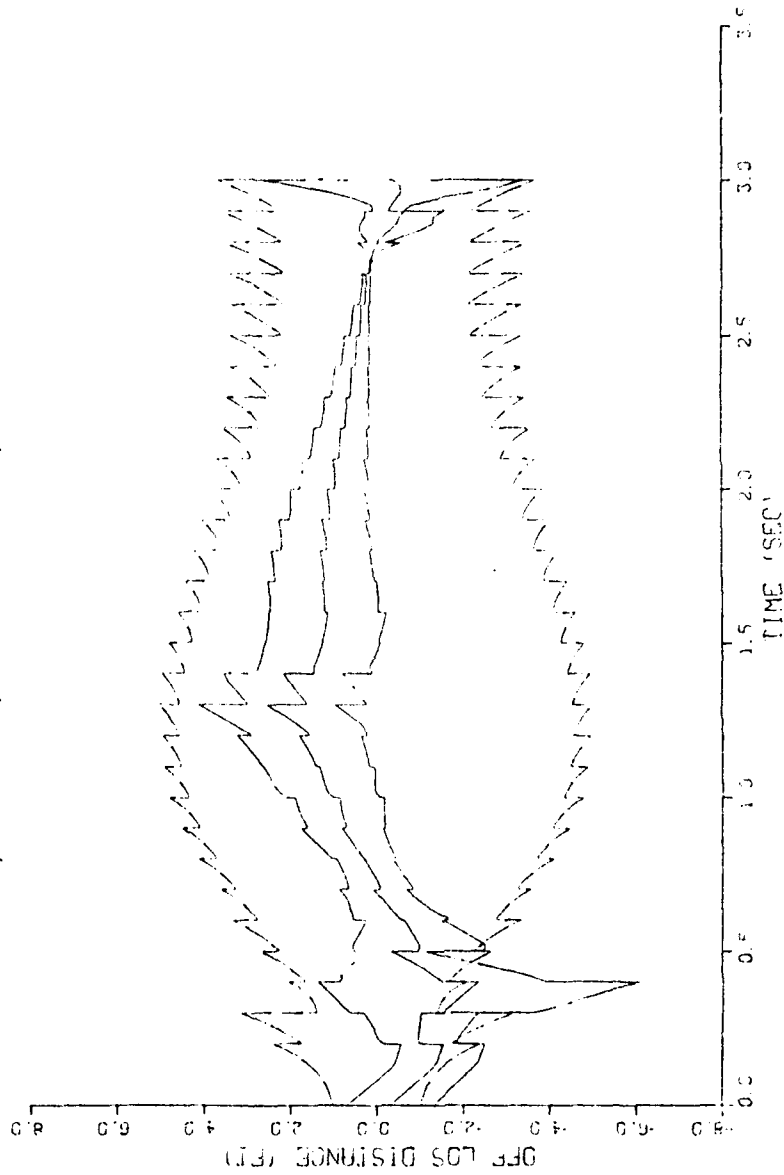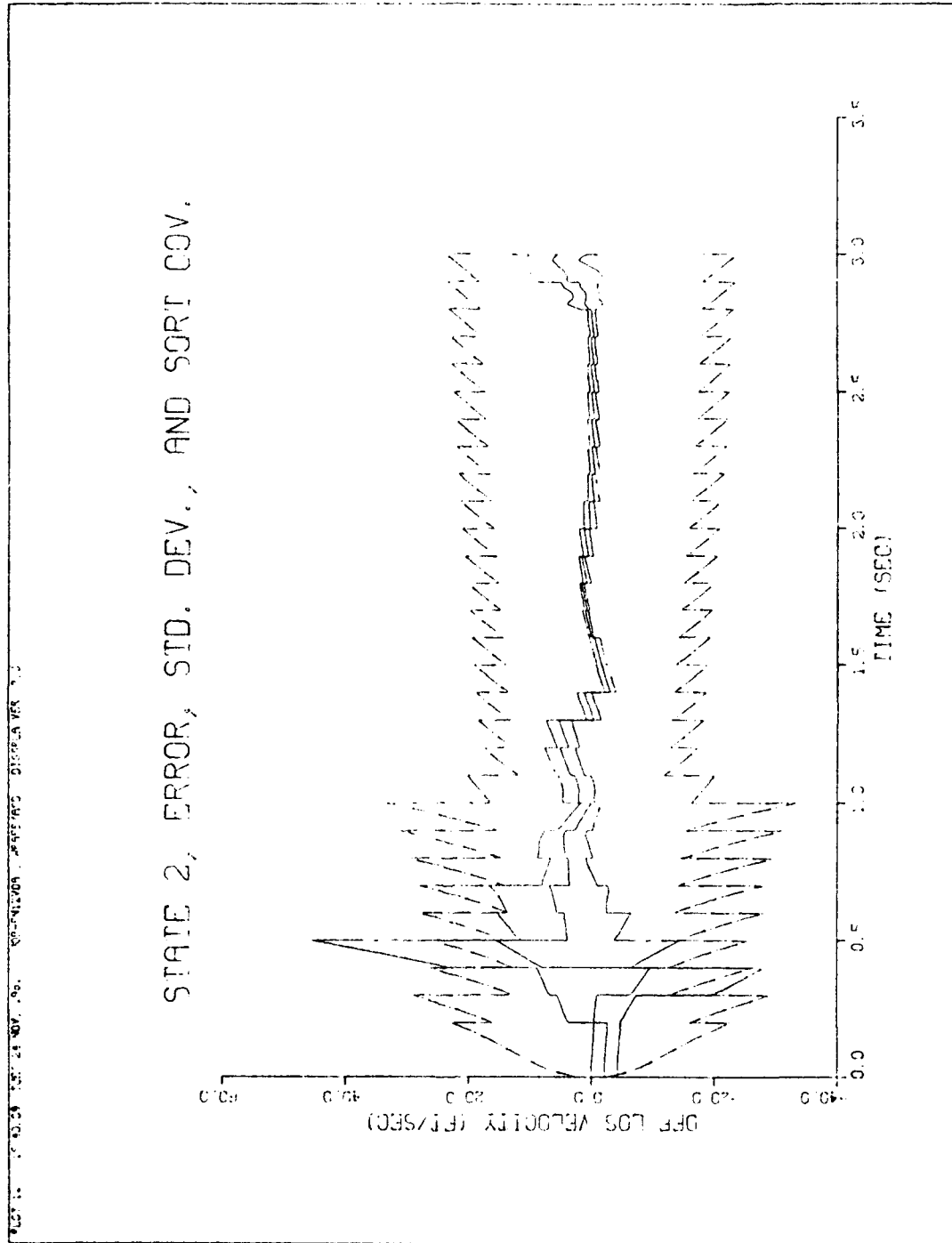
Fig F-10. $\dot{z}$ State With Tuned Filter Q and Perturbed Initial Conditions

F-10
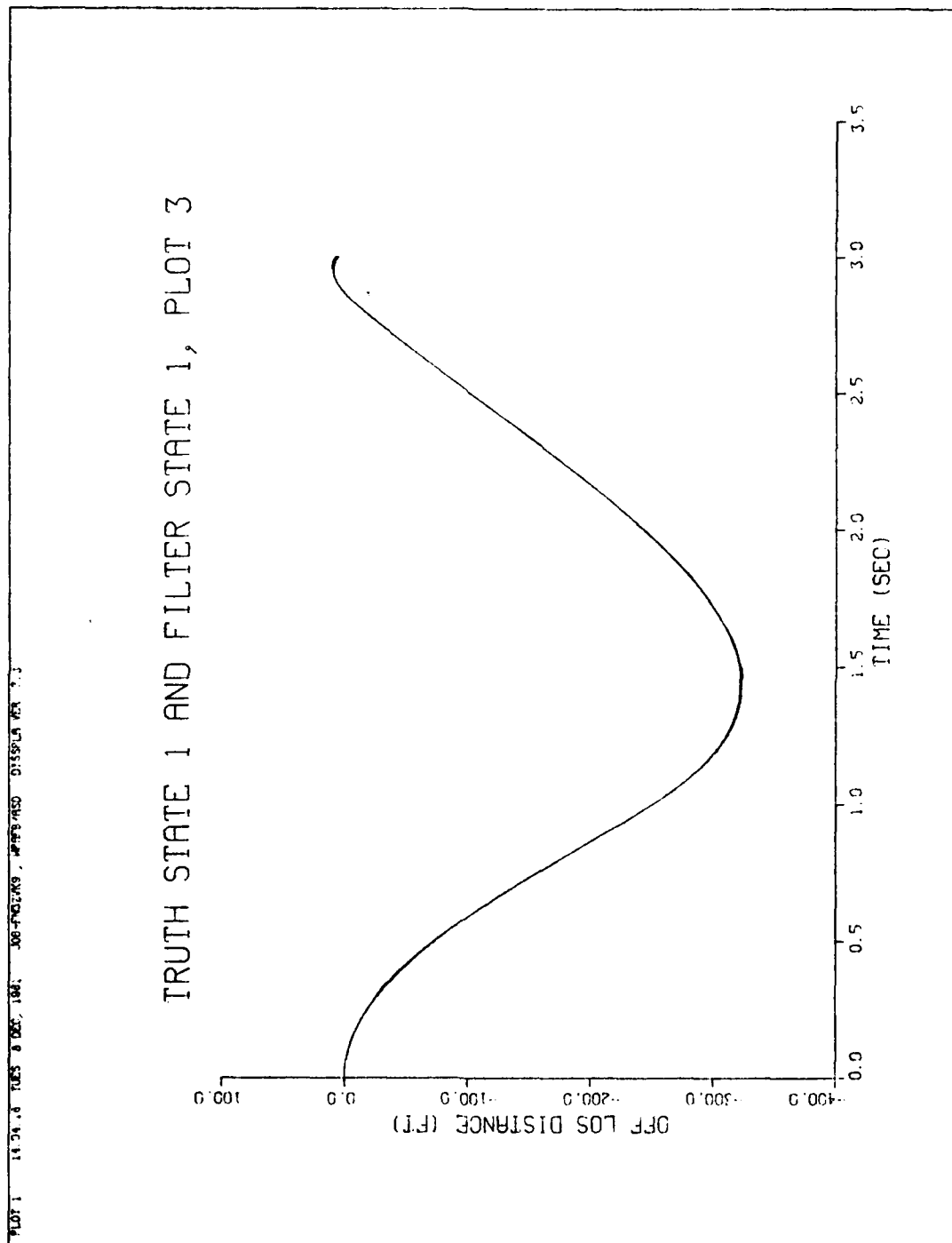
Fig F-11. z State Profile With Acquisition and Dynamic Driving Noise

F-11
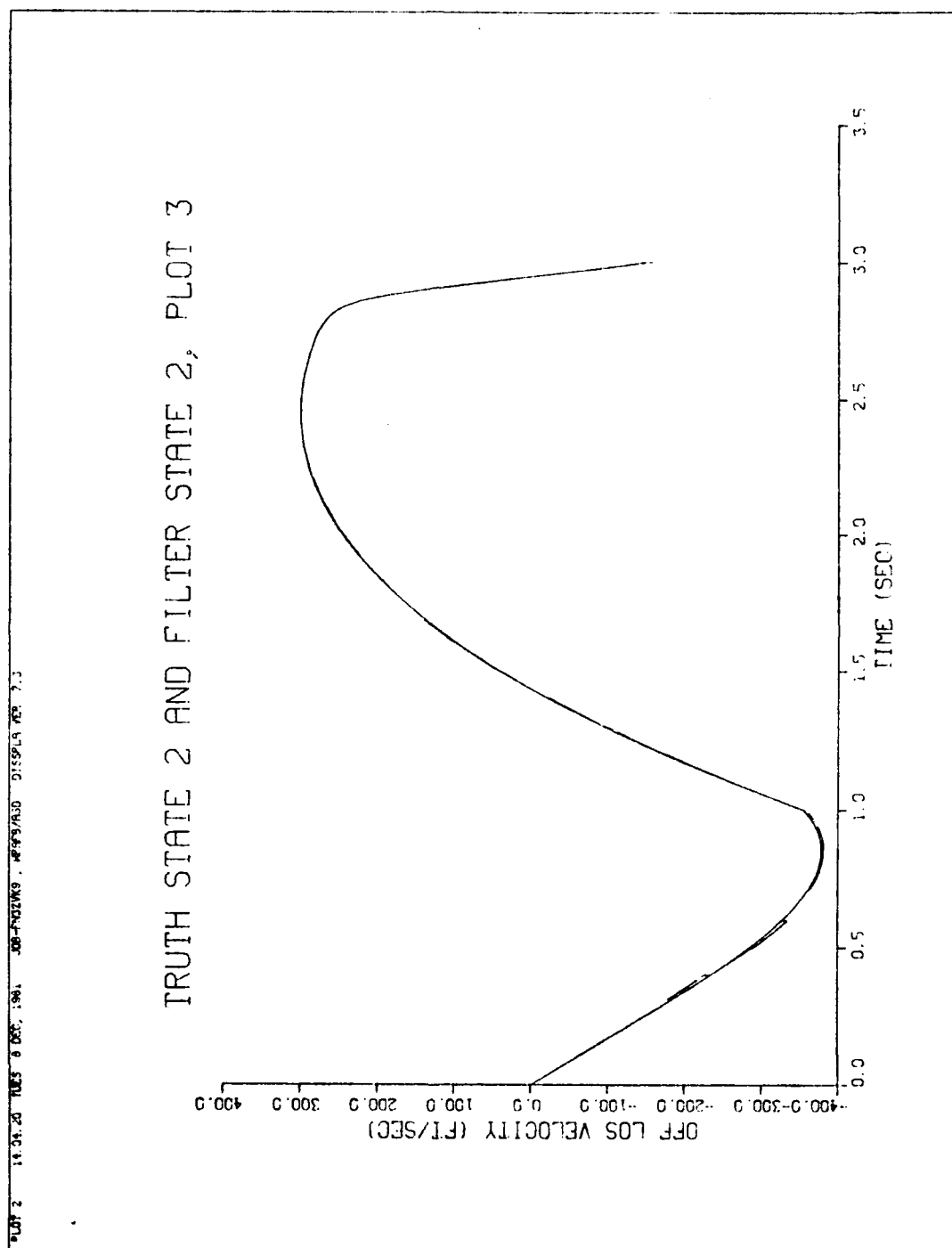
Fig F-12. z State Profile With Acquisition and Dynamic Driving Noise
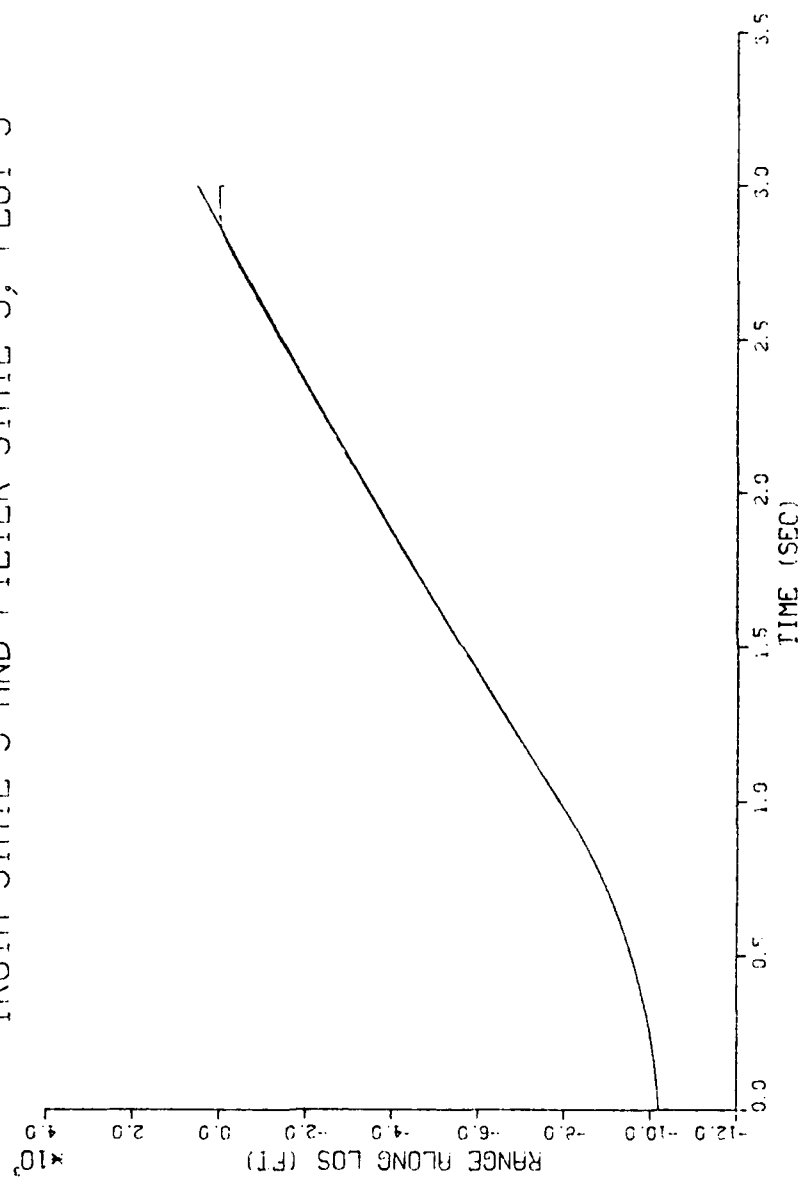
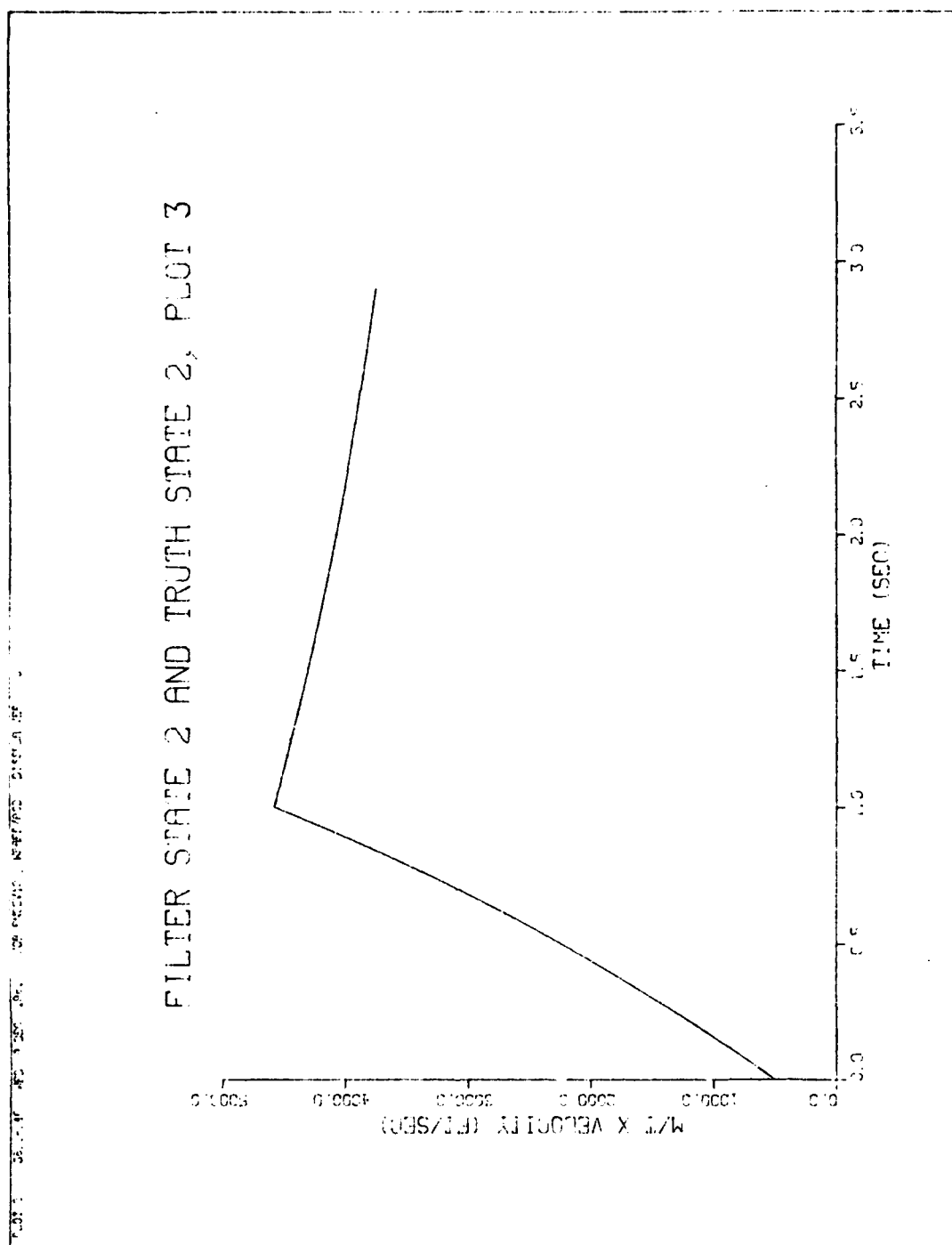Fig F-13. $R_{M/T}$ State Profile With Acquisition and Dynamic Driving Noise
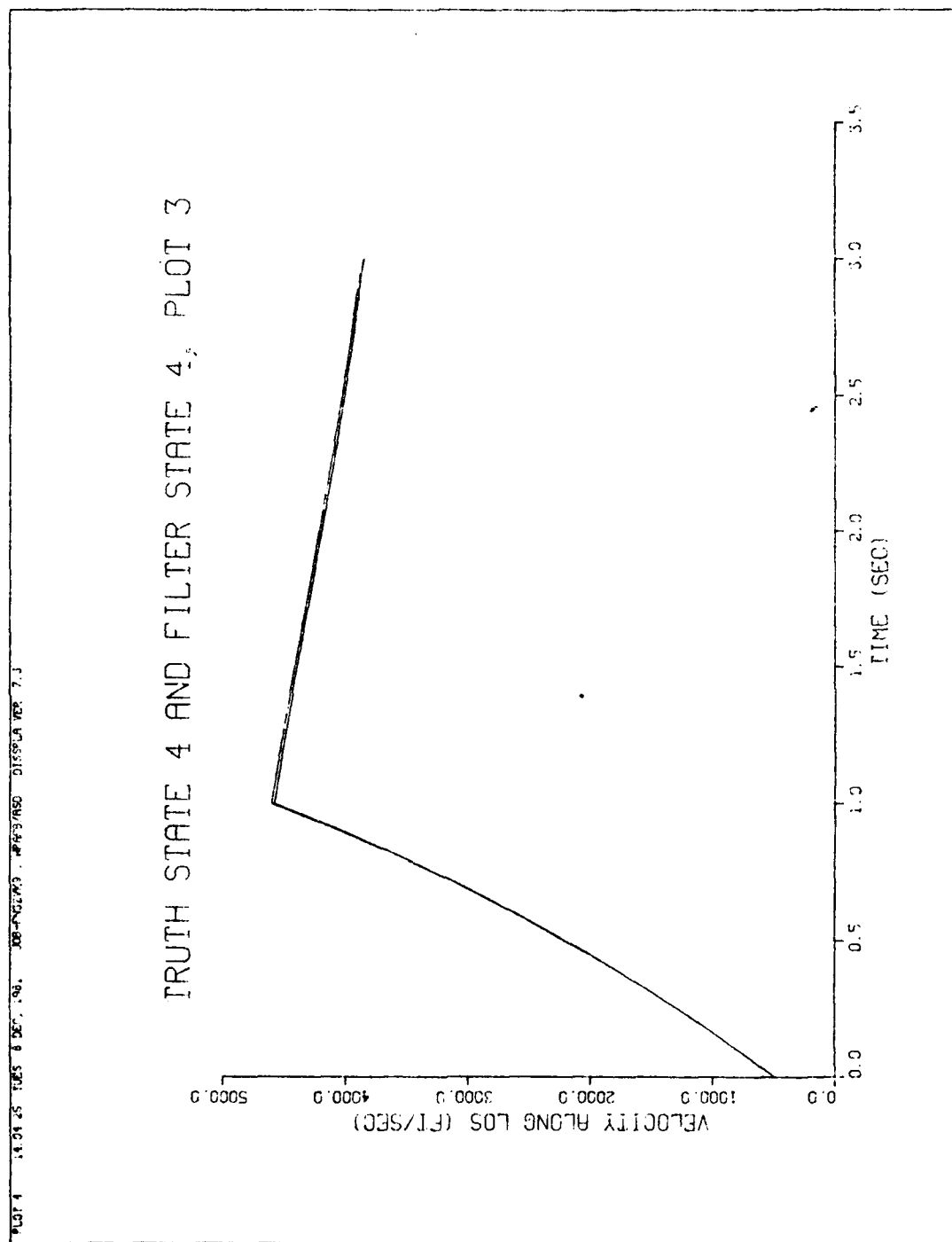
Fig F-14. $\dot{R}_{M/T}$ State Profile With Acquisition and Dynamic Driving Noise
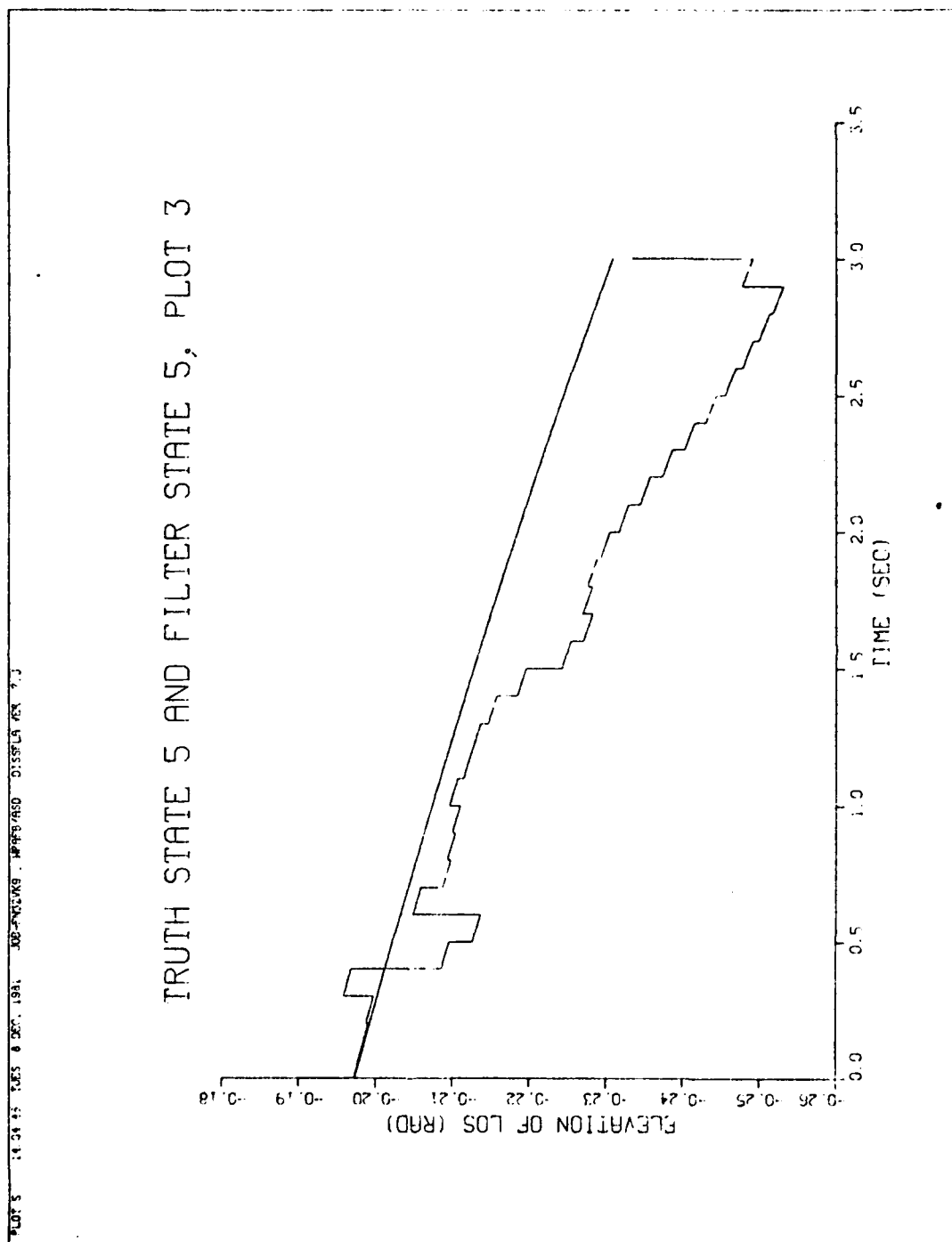
Fig F-15. 0 State Profile With Acquisition and Dynamic Driving Noise
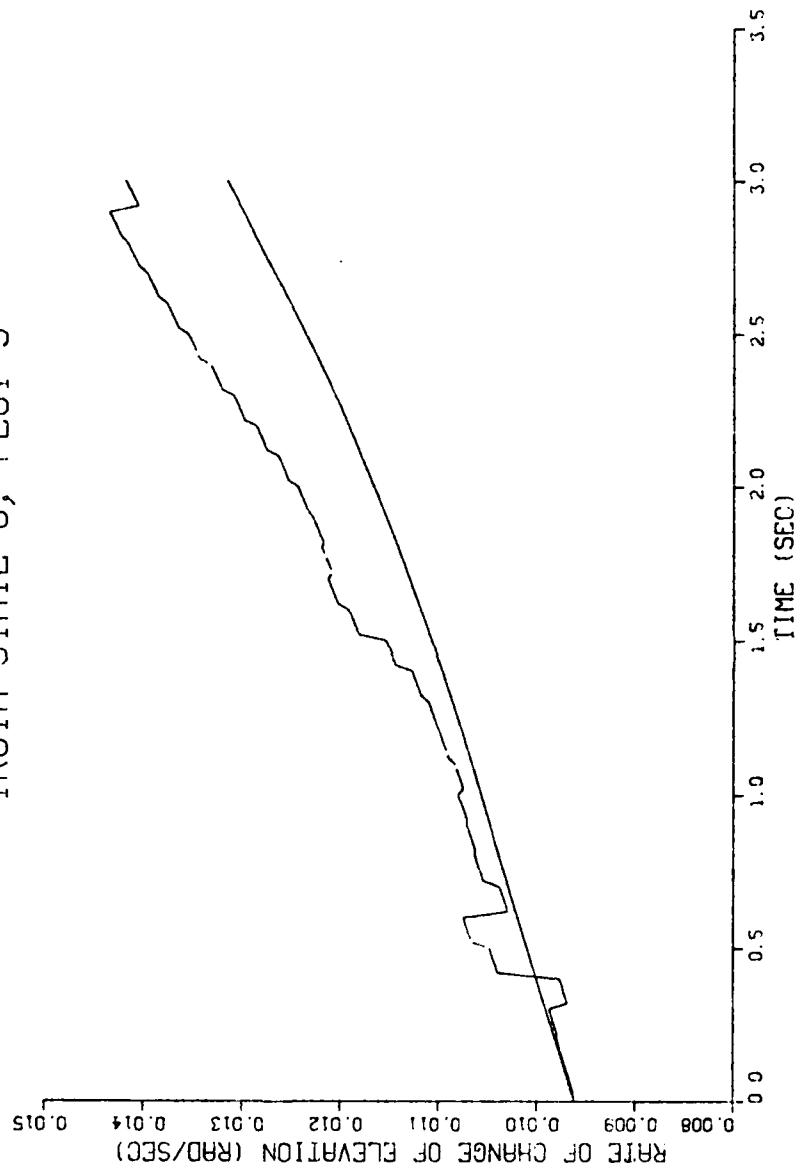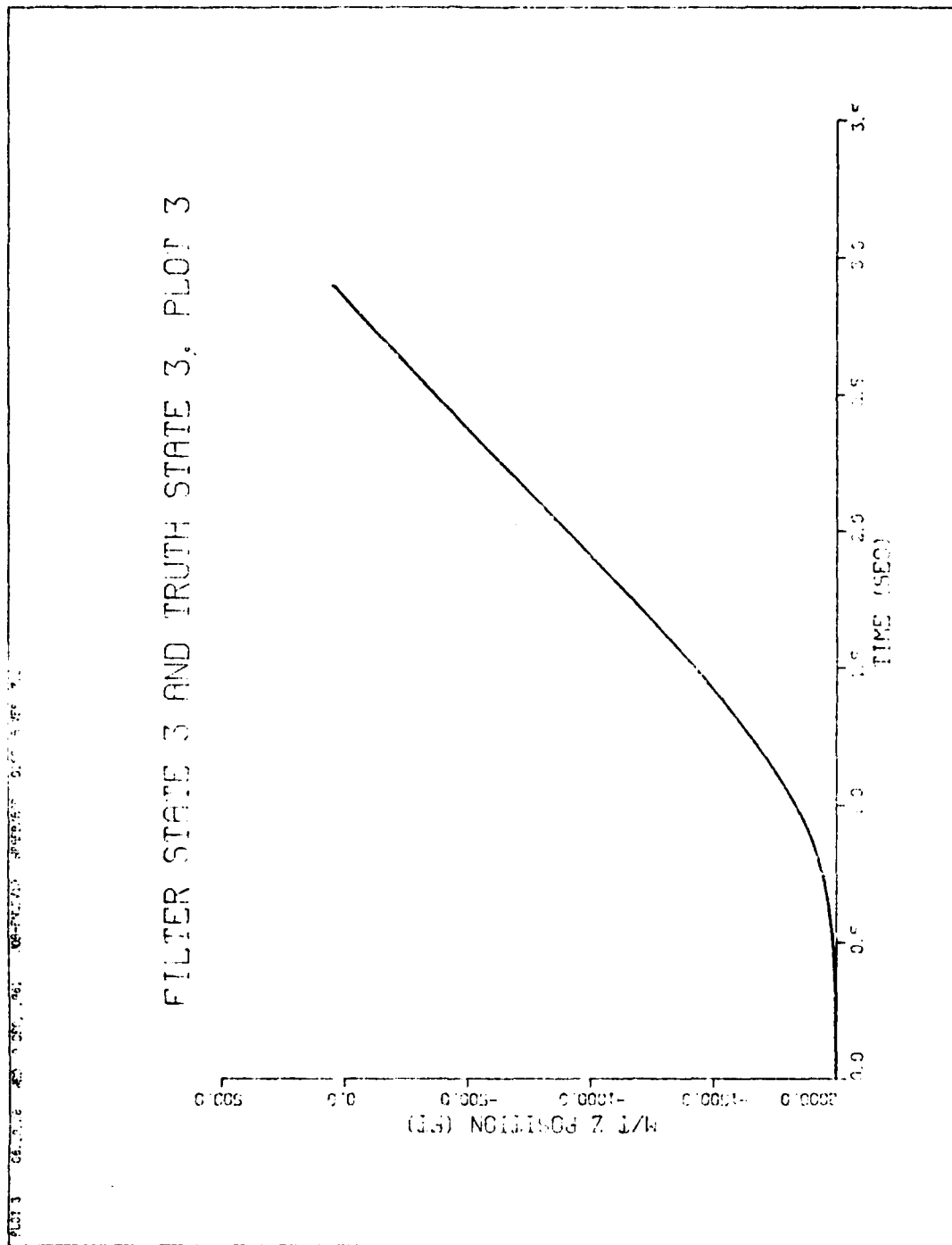
Fig F-16. ω Profile as a Computed Parameter
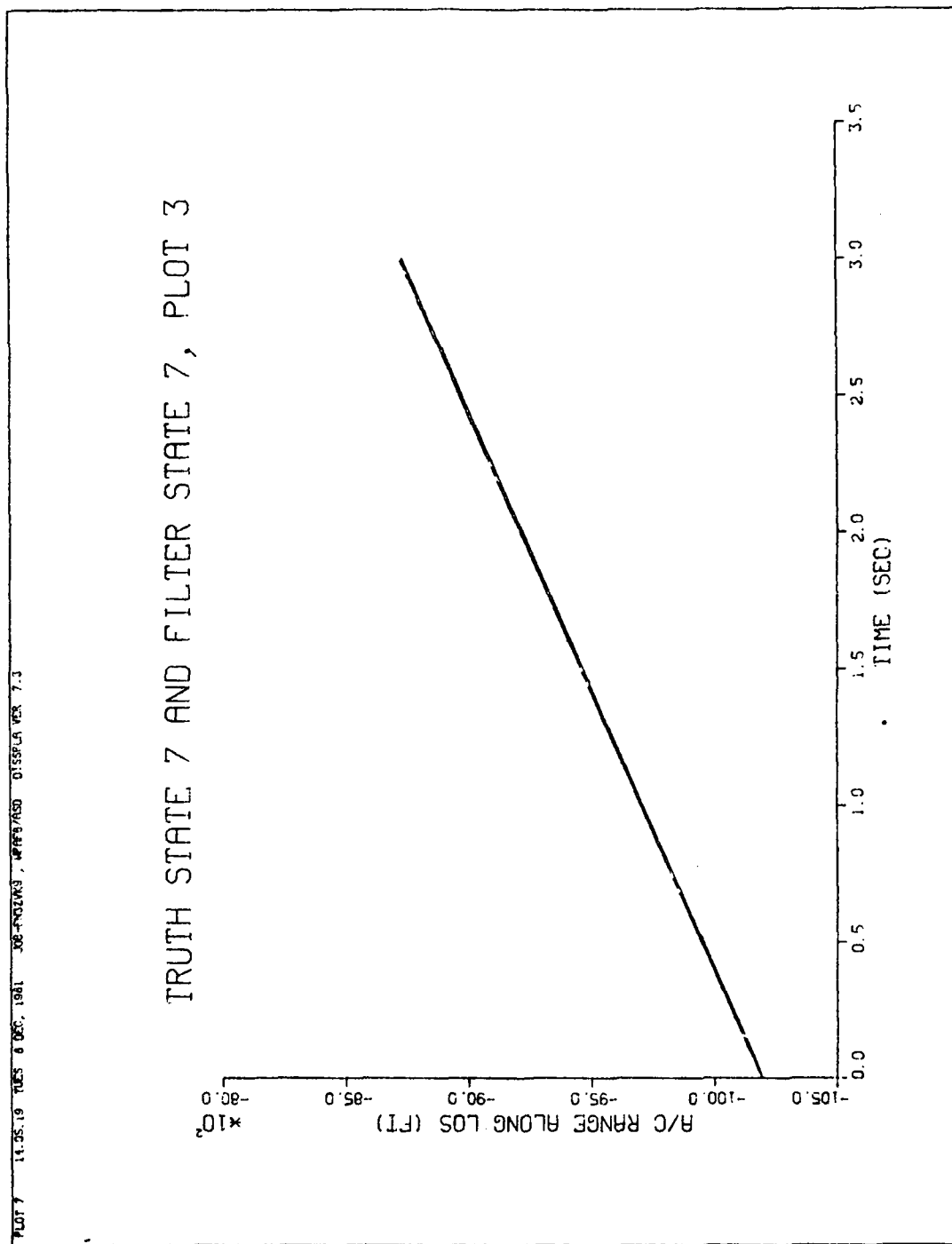
Fig F-17. $R_{A/T}$ State Profile With Acquisition and Dynamic Driving Noise
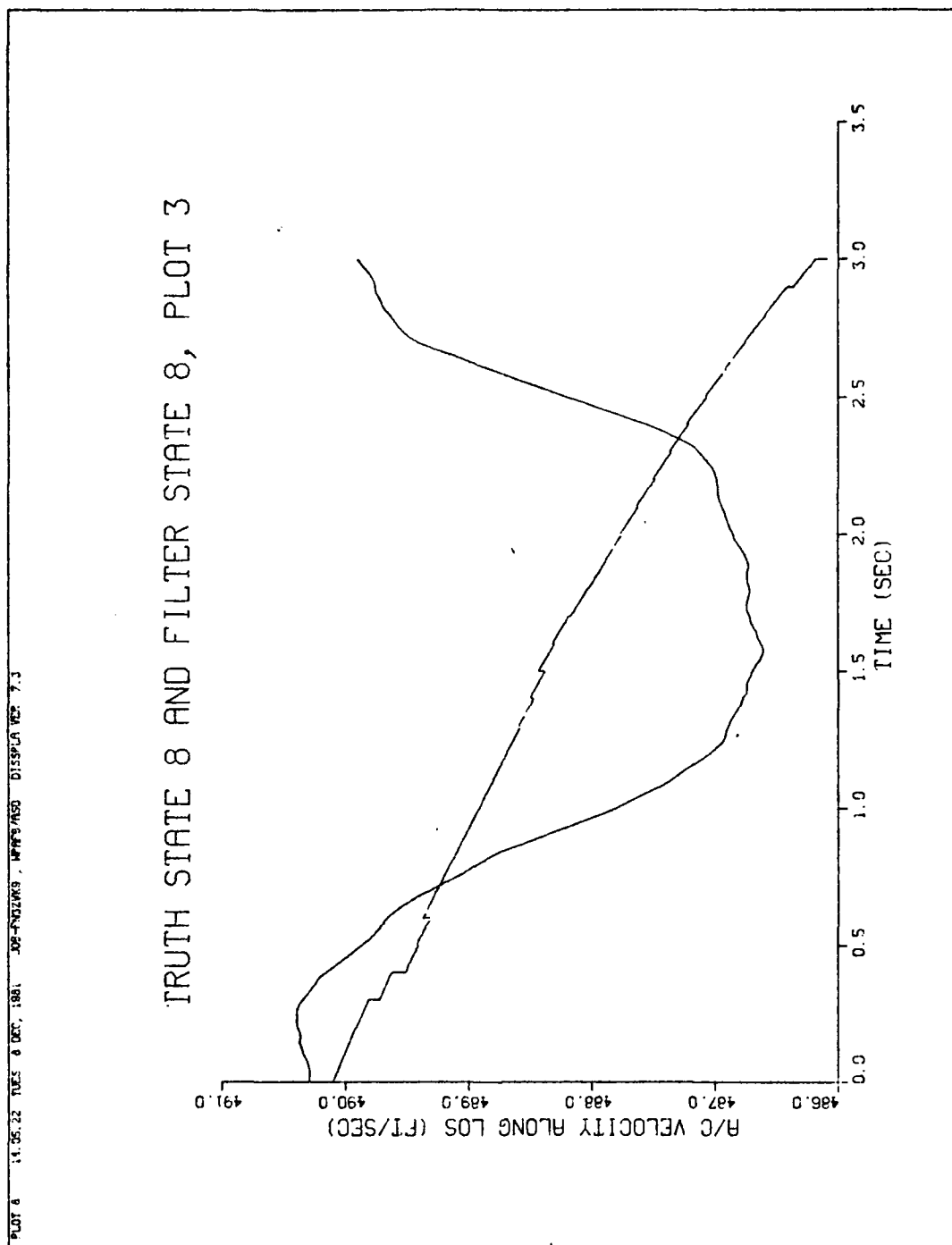
Fig F-18. $V_{A/T}$ State Profile With Acquisition and Dynamic Driving Noise

STATE 1, ERROR, STD. DEV., AND SORT COV.
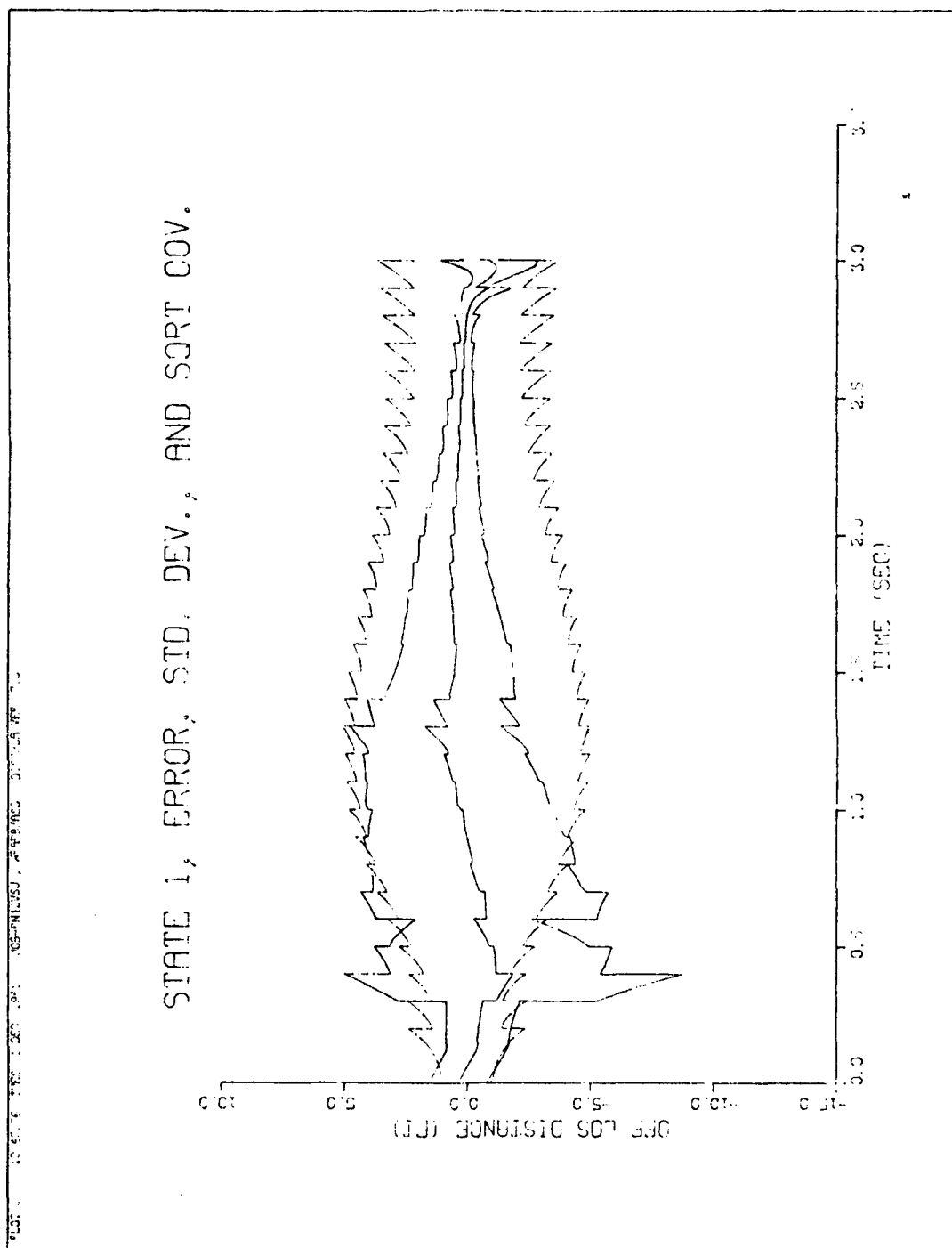
Fig F-19. z State Errors, Standard Deviation, and Filter Covariance

F-19

STATE 2. ERROR, STD. DEV., AND SORT COV.
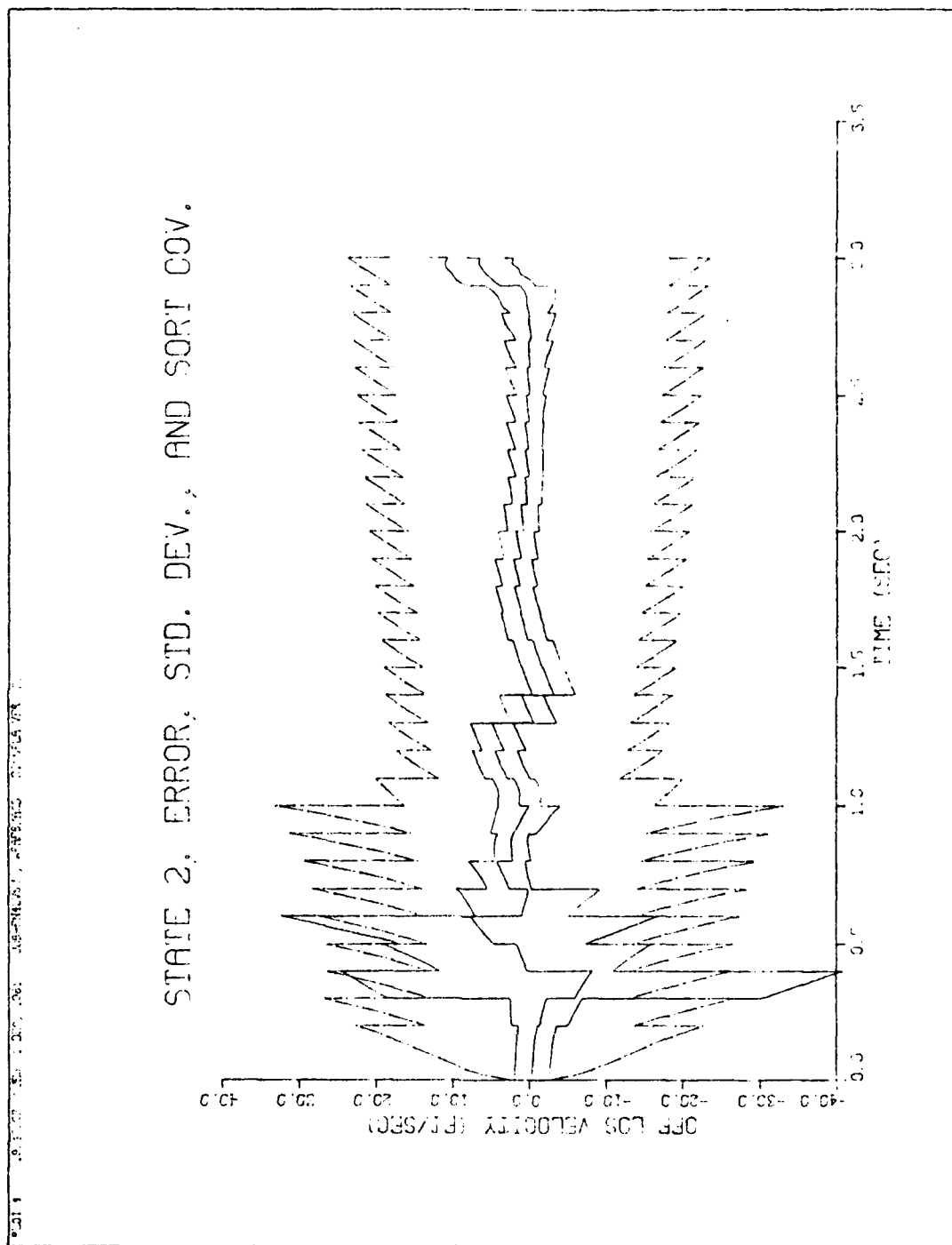
Fig F-20. ż State Errors, Standard Deviation, and Filter Covariance
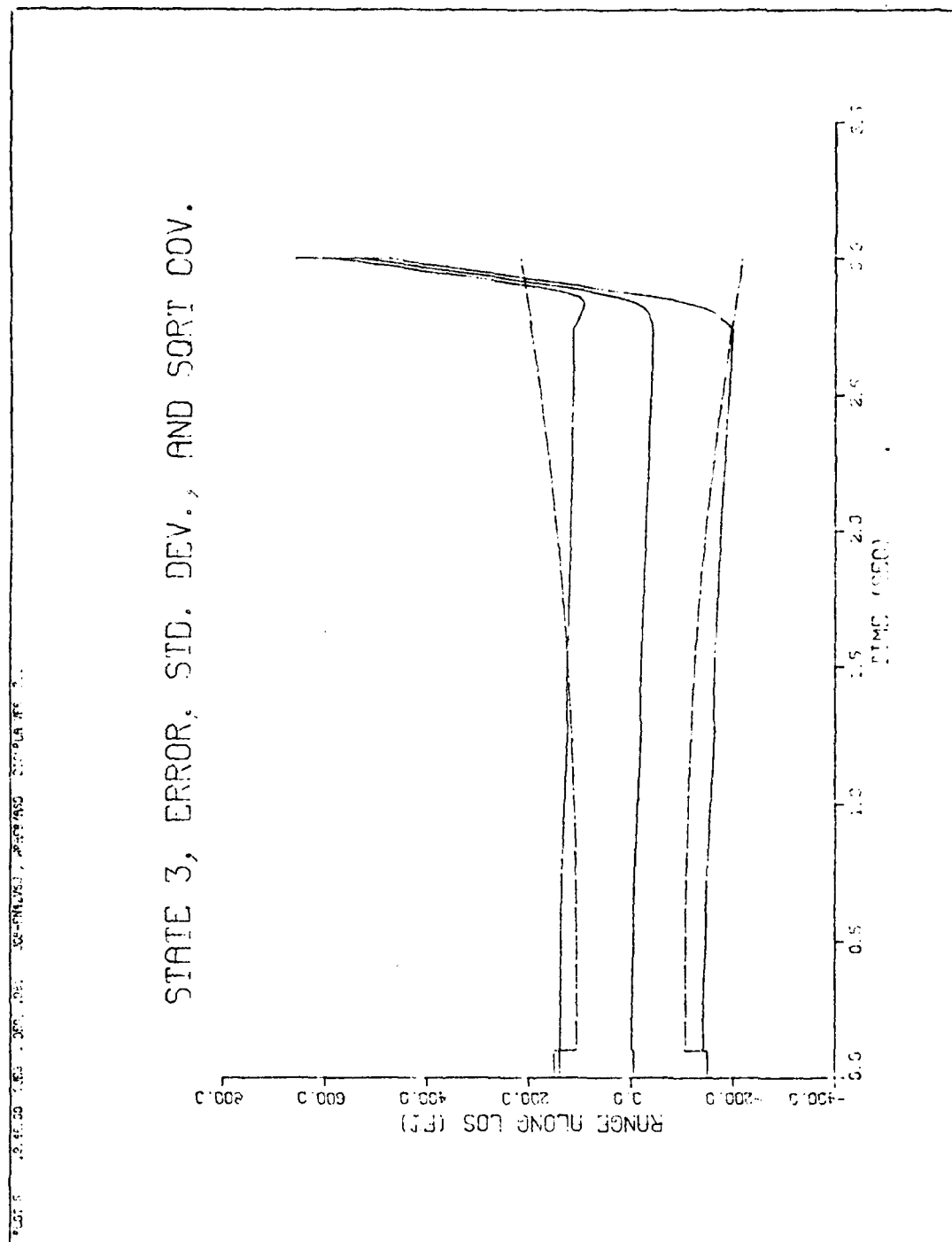
Fig F-21. $R_{M/T}$ State Errors, Standard Deviation, and Filter Covariance
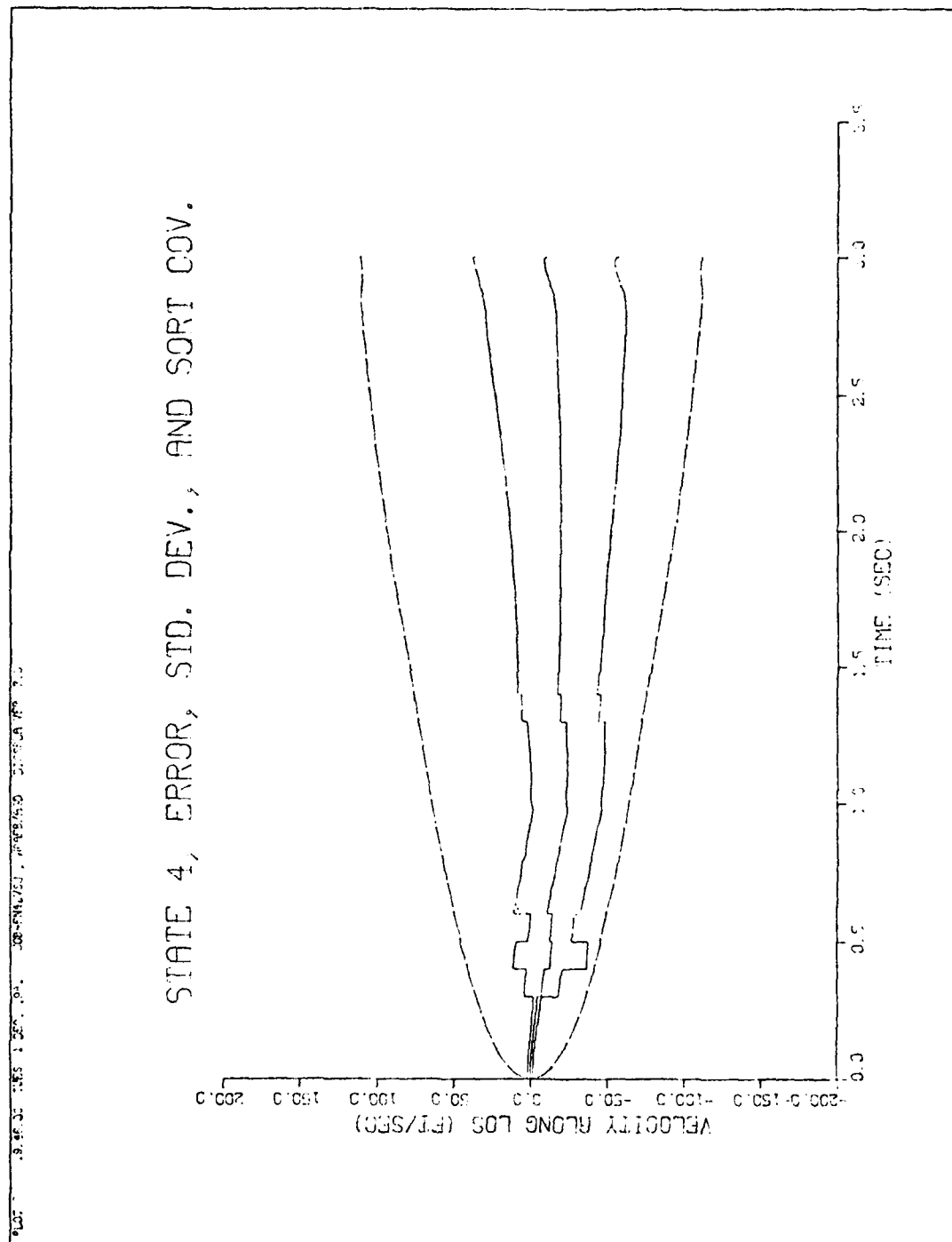
Fig F-22. $\dot{R}_{M/T}$ State Errors, Standard Deviation, and Filter Covariance
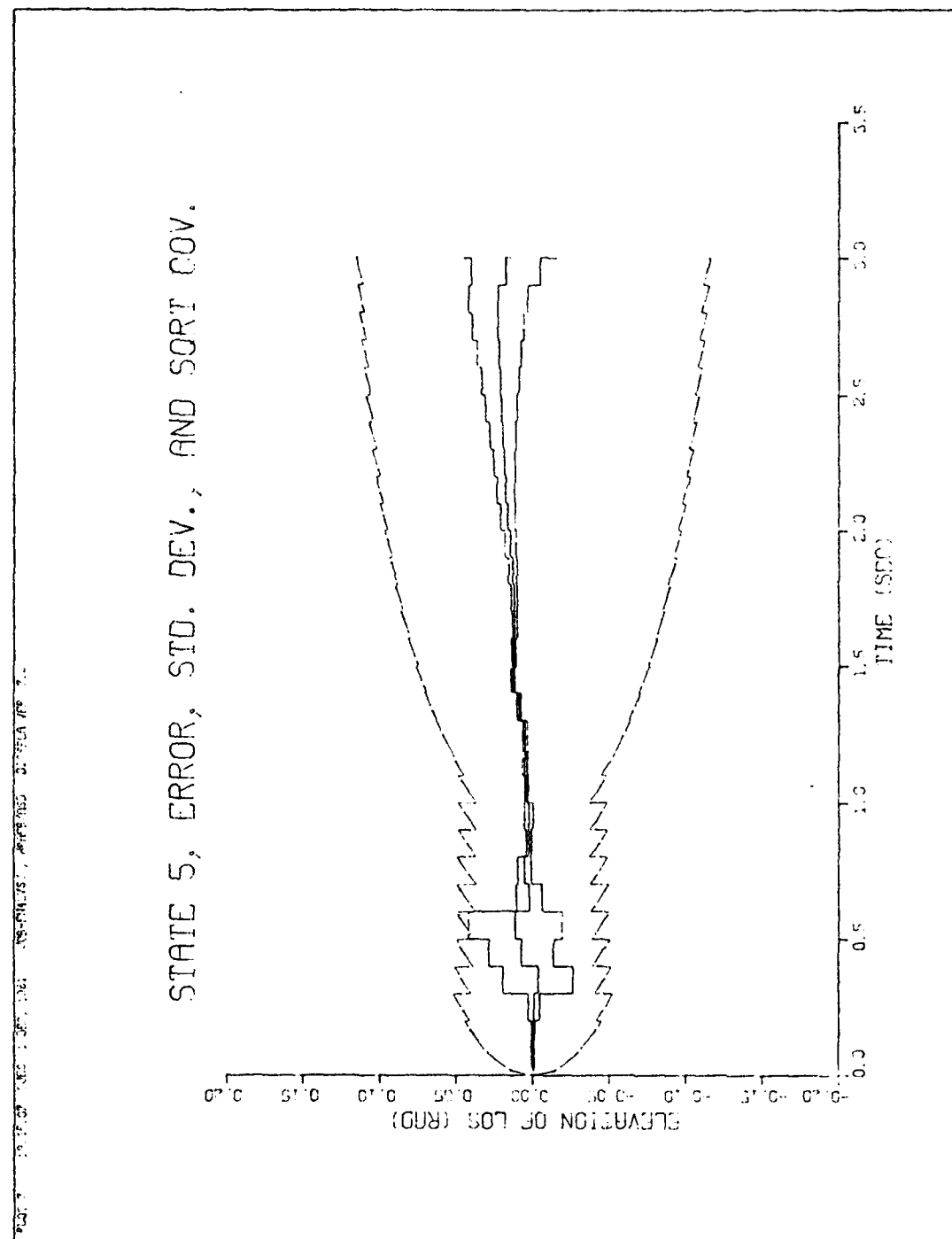
STATE 5, ERROR, STD. DEV., AND SORT COV.

ELEVATION OF LOS (RAD)

TIME (SEC)

Fig F-23. θ State Errors, Standard Deviation, and Filter Covariance

F-23

STATE 6, ERROR, STD. DEV., AND SQRT COV.
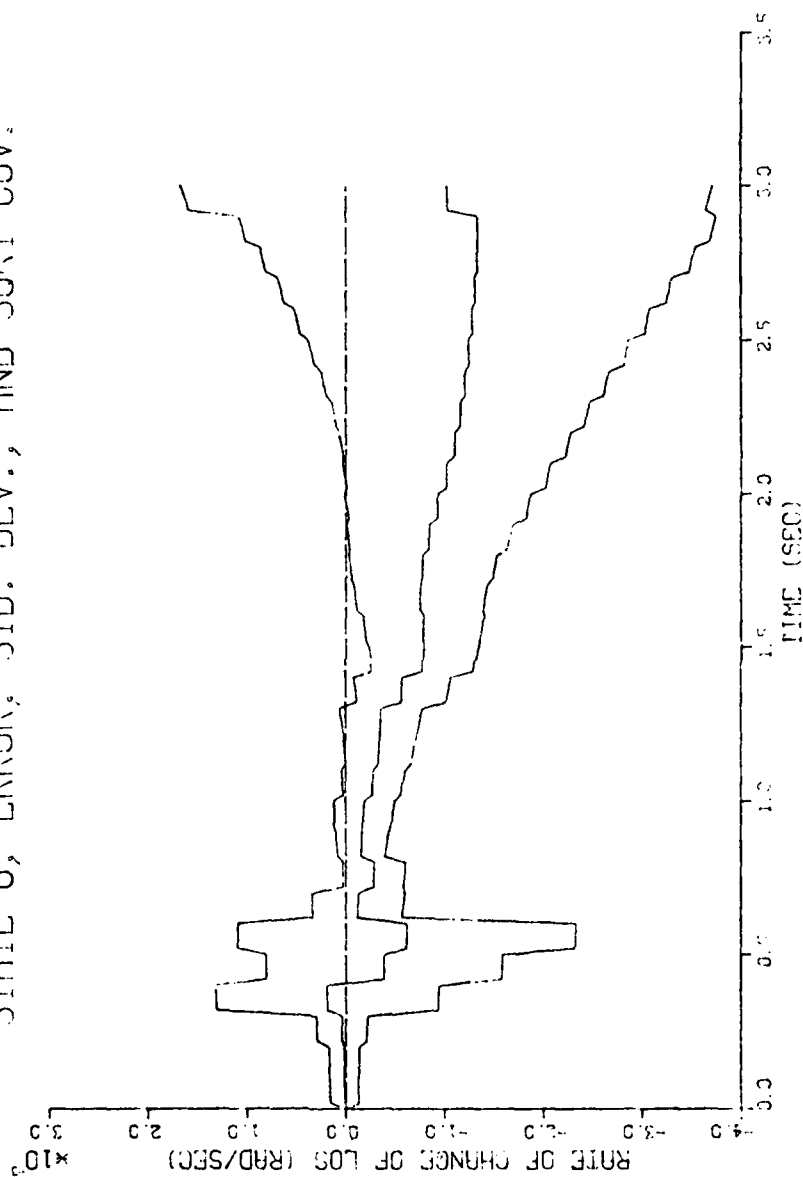
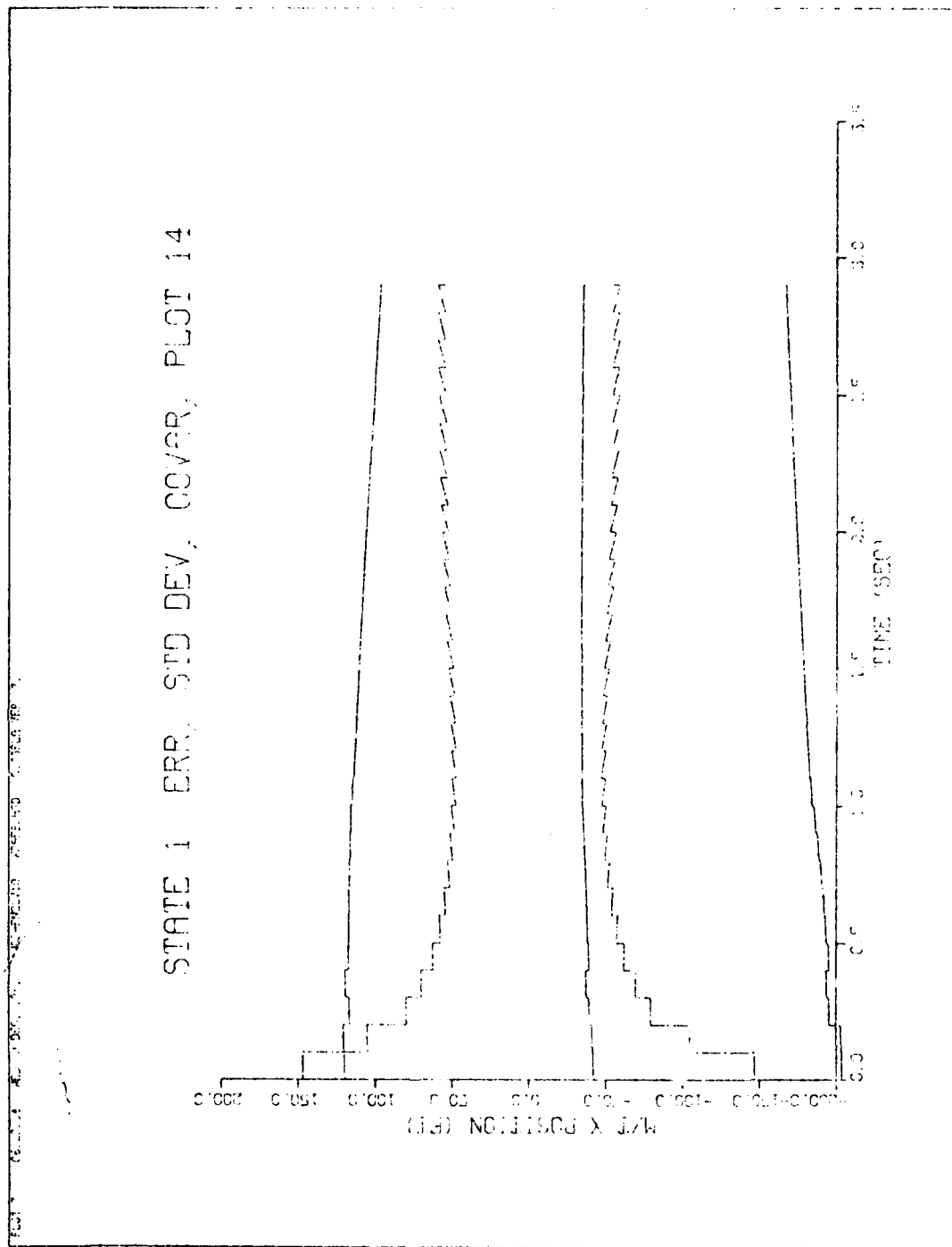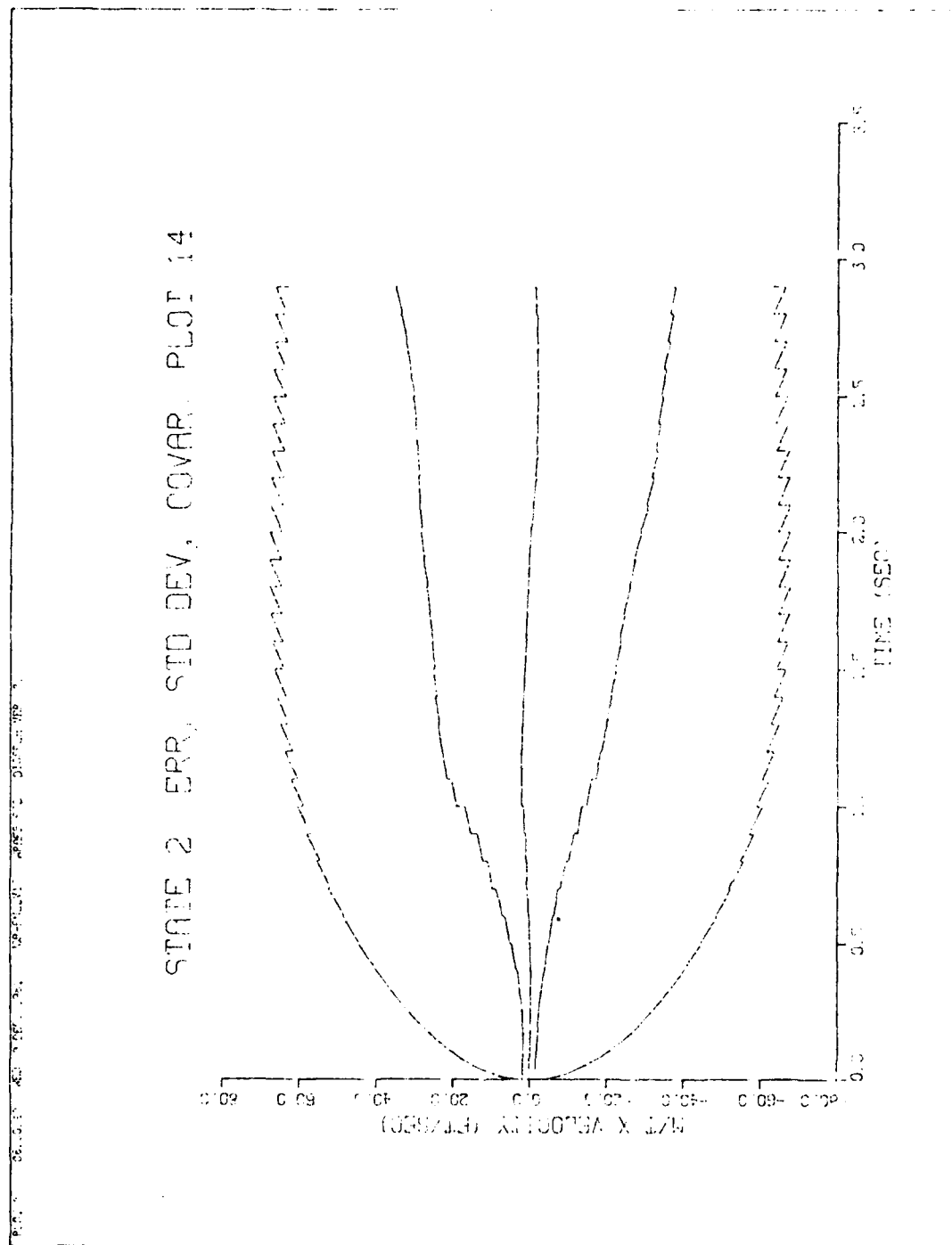Fig F-24. ω Errors and Standard Deviation

F-24
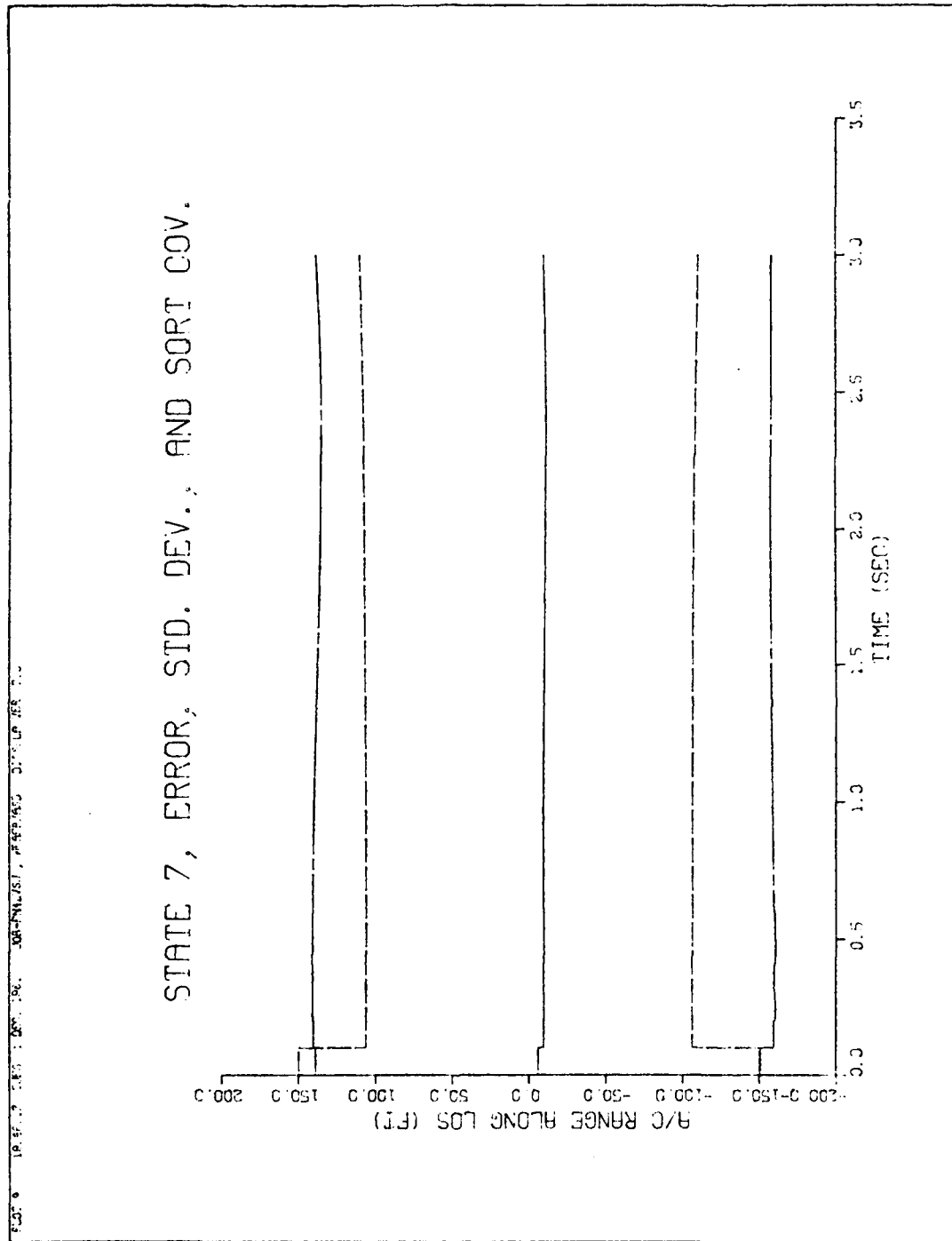
Fig F-25. $R_{A/T}$ State Errors, Standard Deviation, and Filter Covariance

F-25
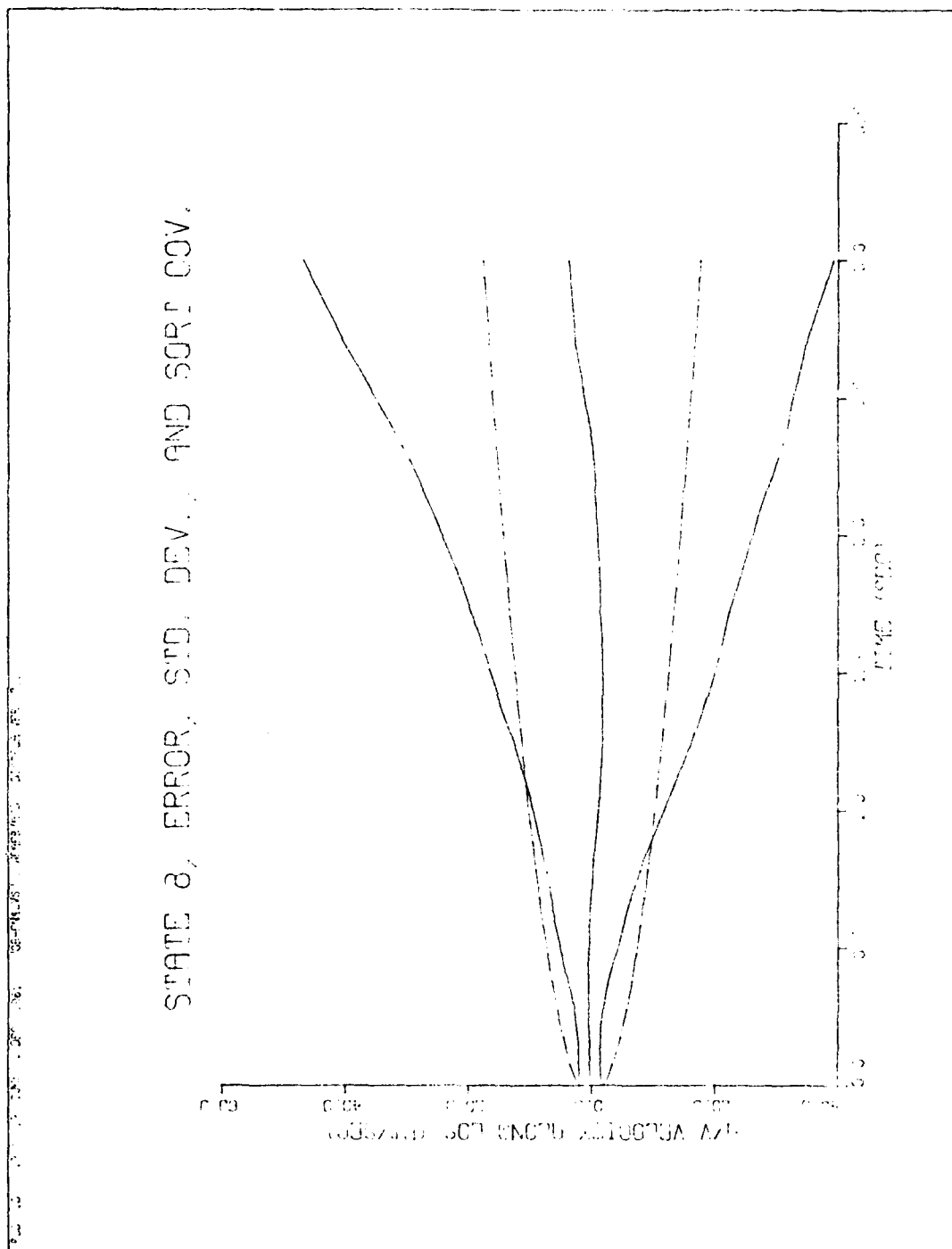
Fig F-26. $V_{A/T}$ State Errors, Standard Deviation, and Filter Covariance

MEASUREMENT RESIDUAL
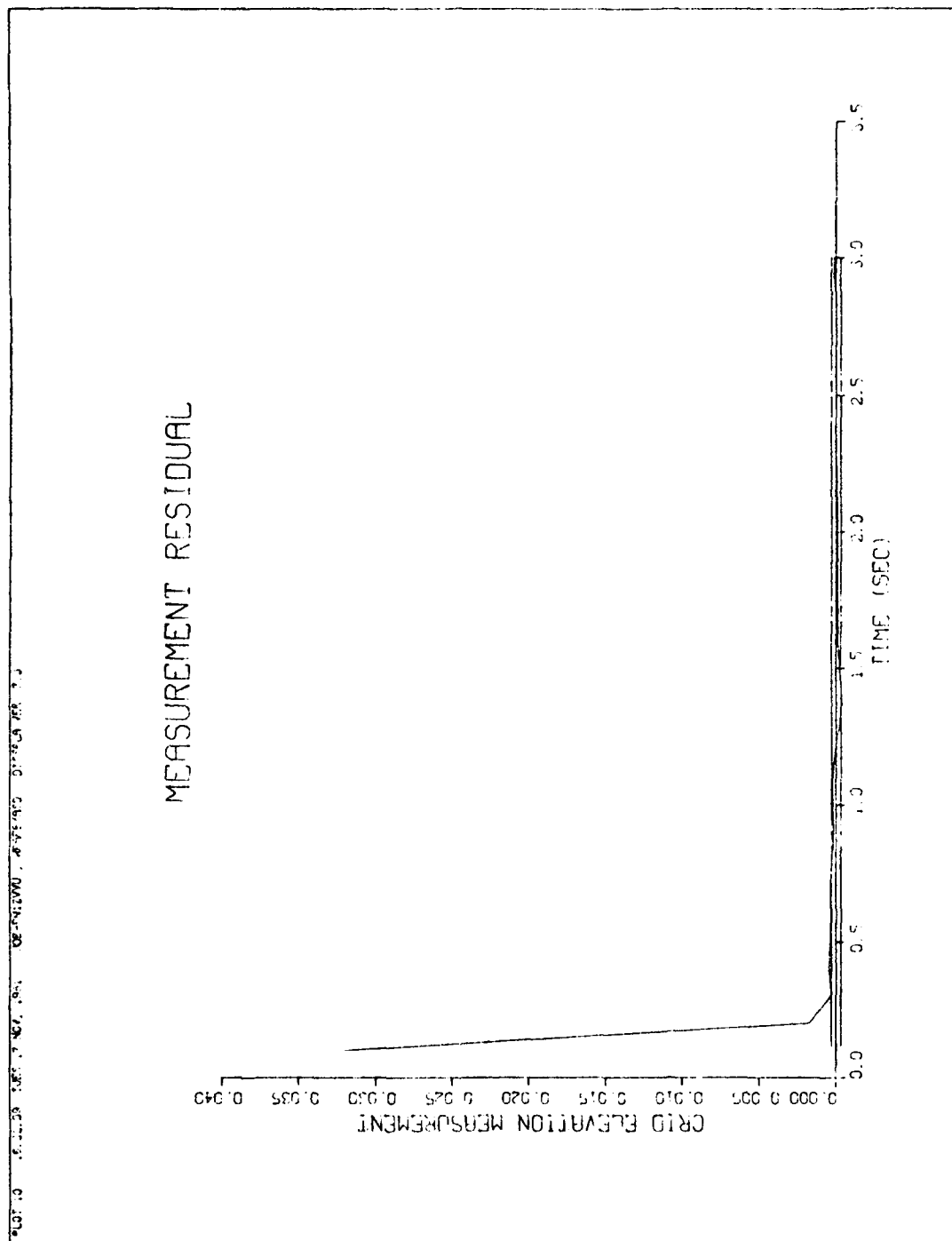
Fig F-27. Measurement Residual With No System Noise

F-27
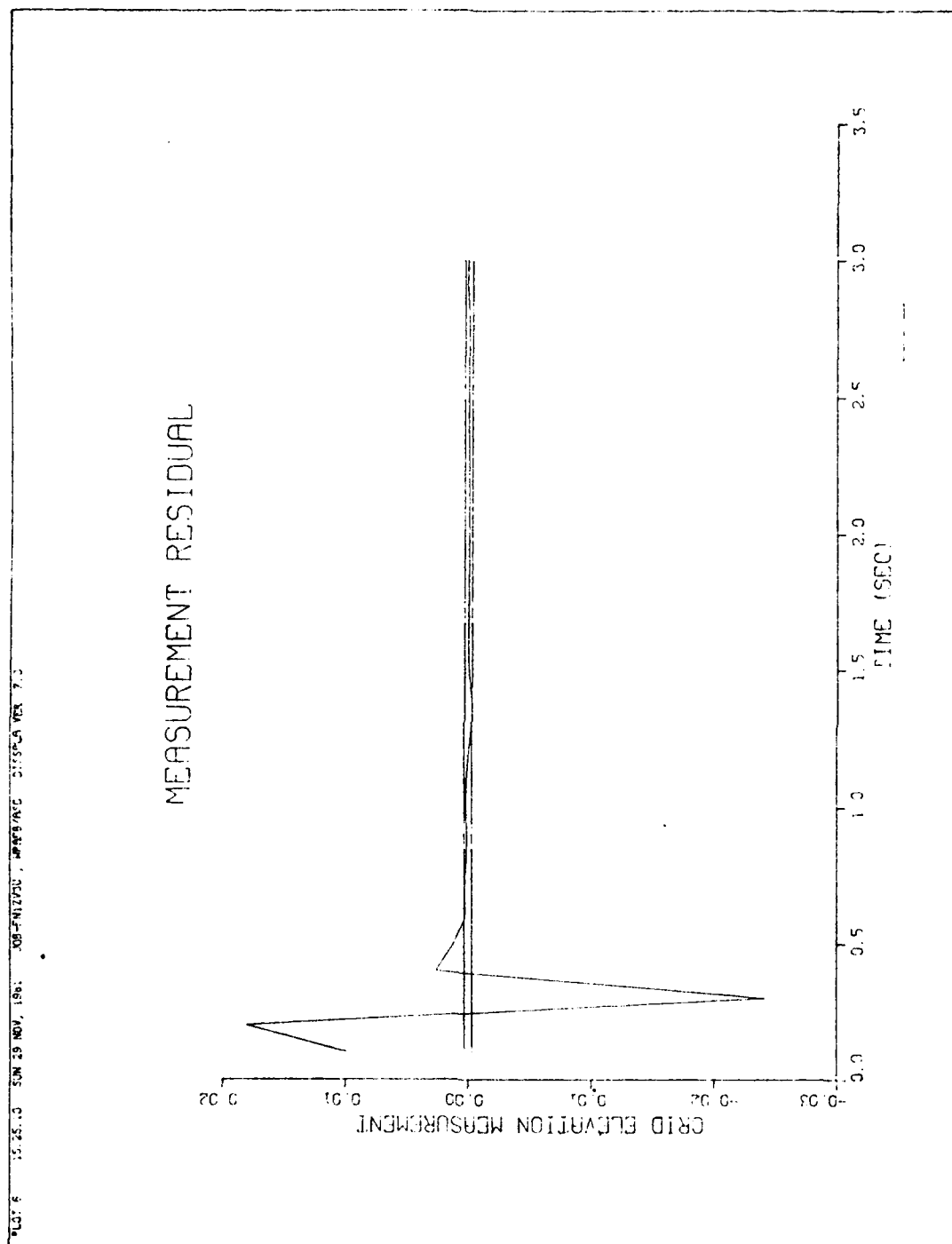
Fig F-28. Measurement Residual With System Noise

STATE 1, ERROR, STD. DEV., AND SORT COV.
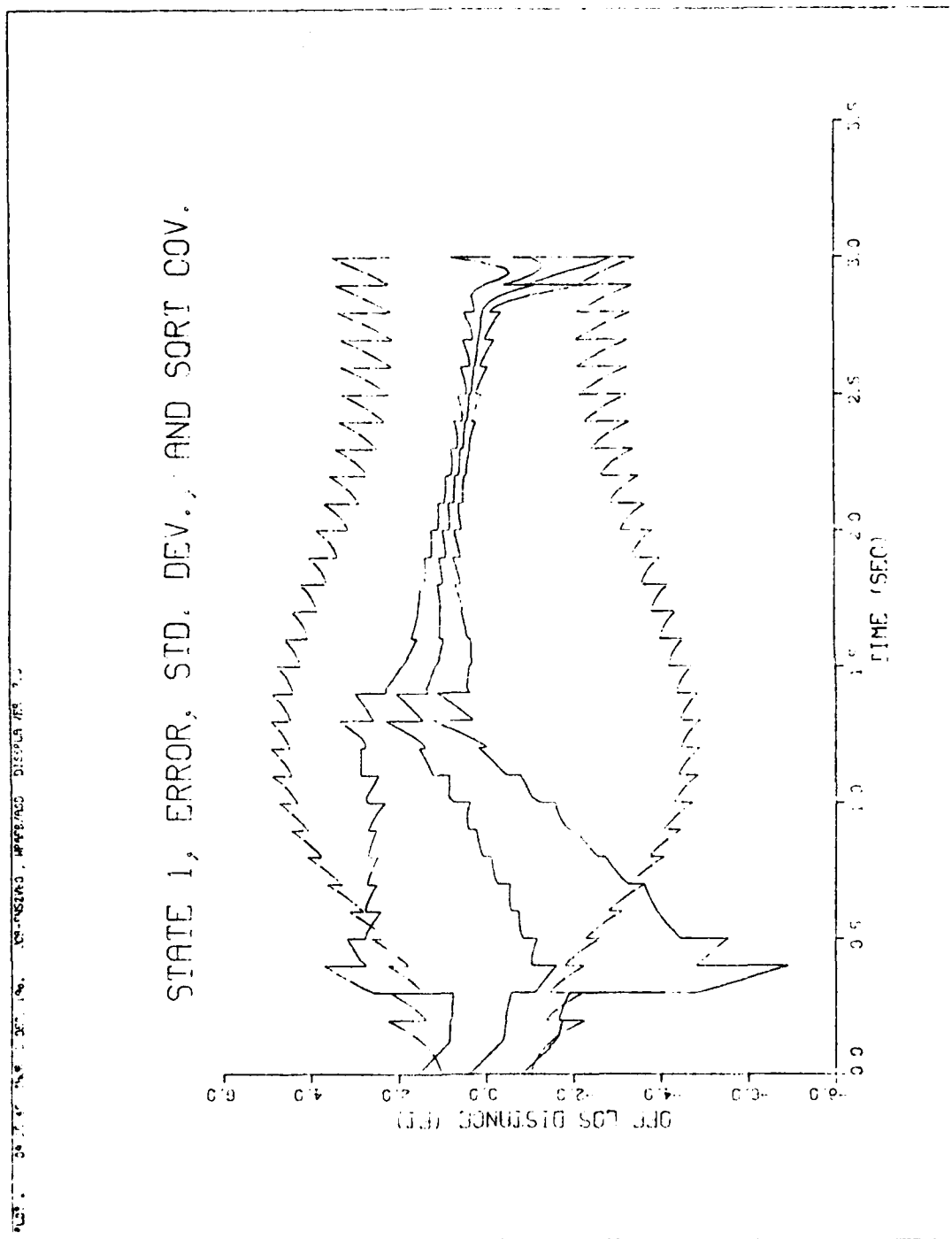
Fig F-29.   Reduced Order Filter, z State Errors

Fig F-30. Reduced Order Filter, ż State Errors
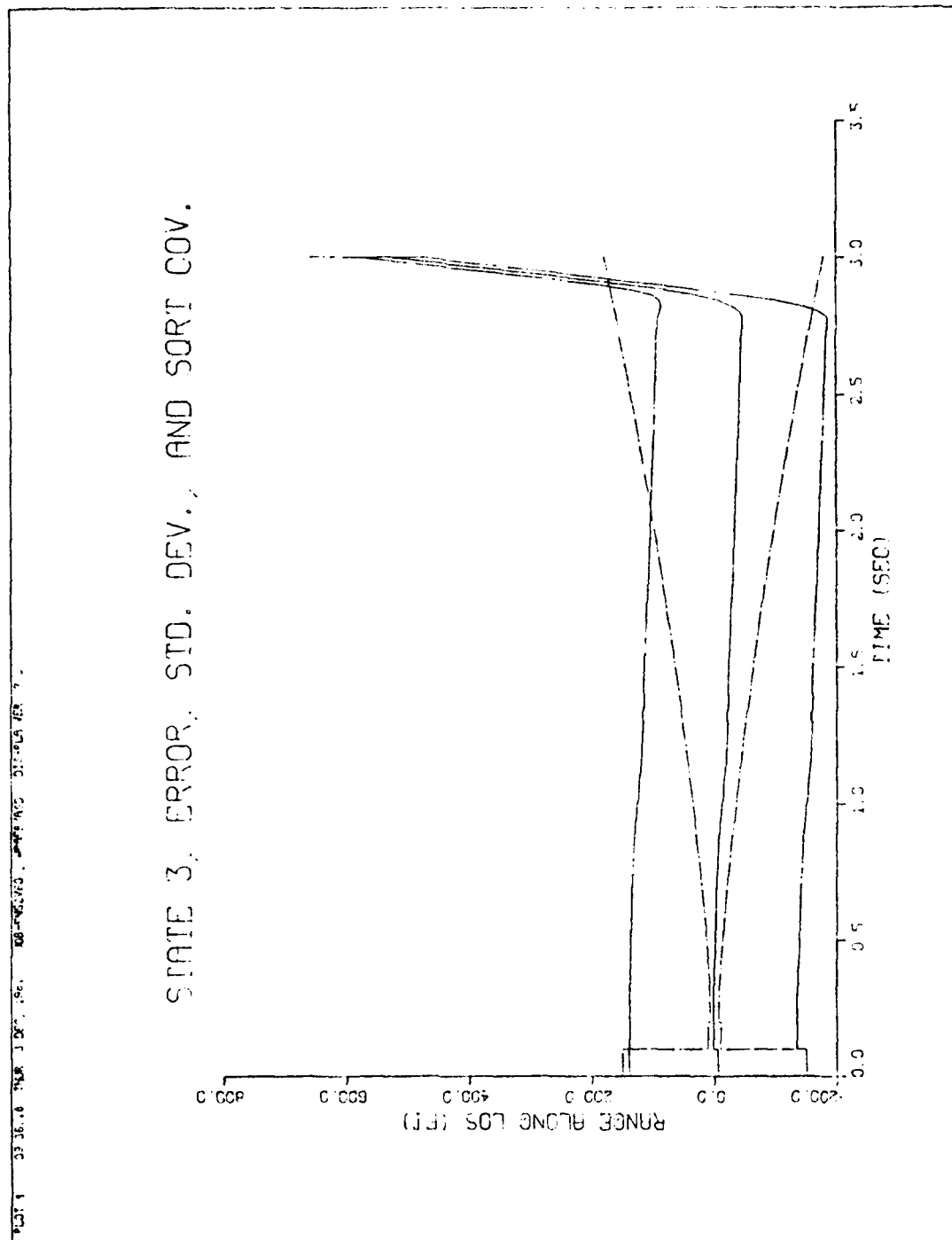
STATE 3. ERROR. STD. DEV., AND SORT COV.

Fig F-31. Reduced Order Filter, $R_{M/T}$ State Errors

F-31

STATE 4, ERROR, STD. DEV., AND SORT COV.
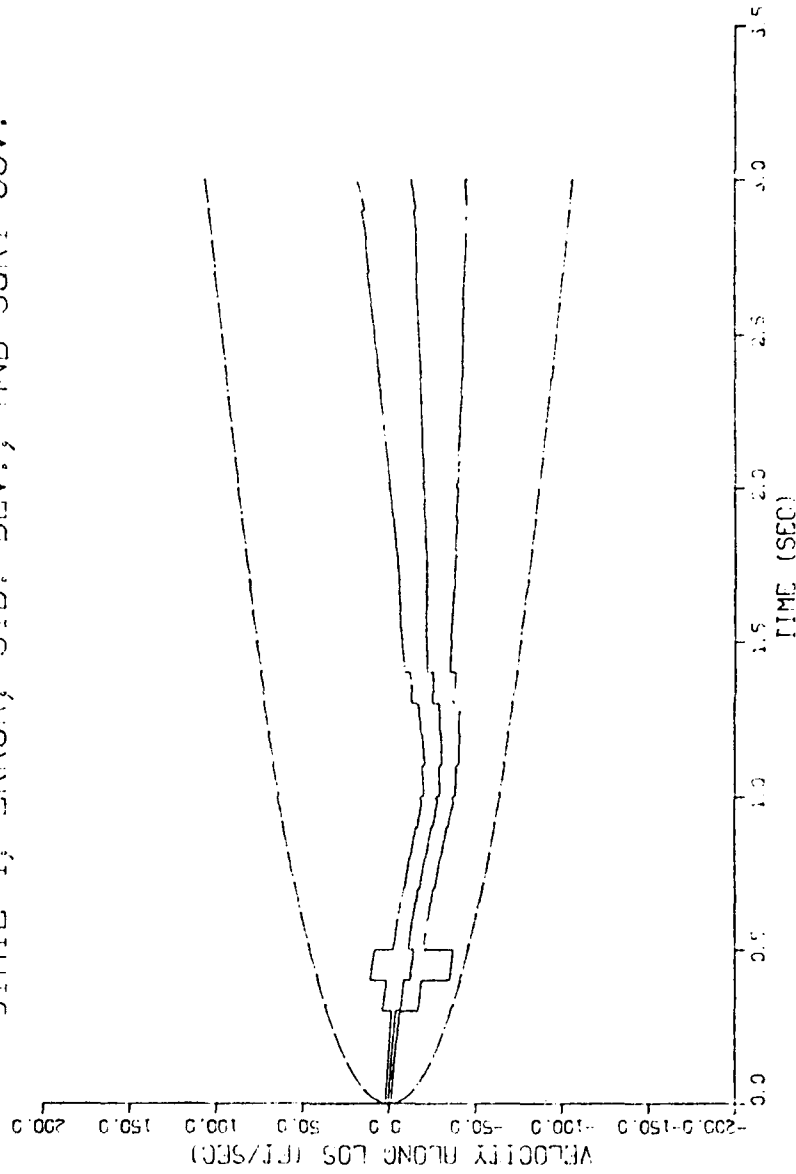
Fig F-32. Reduced Order Filter, $\dot{R}_{M/T}$ State Errors

F-32
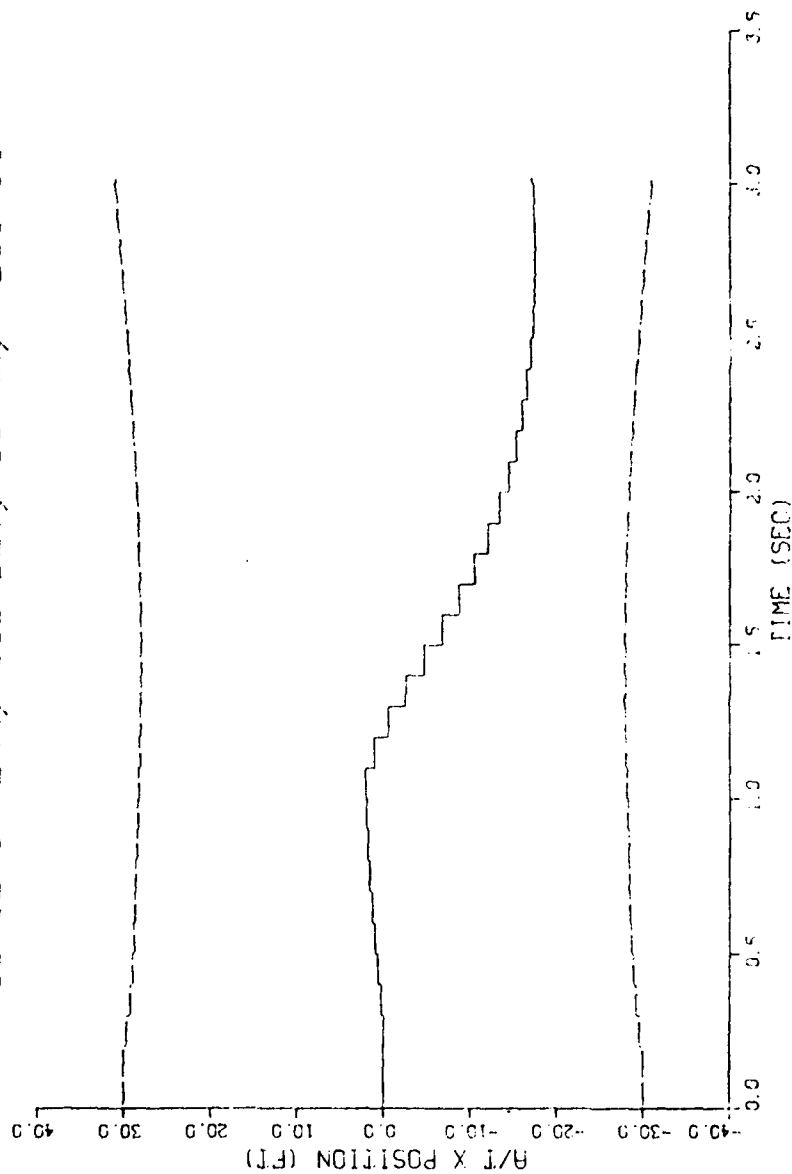
Fig F-33. $x_{A/T}$ Covariance With One Measurement and No System Noise
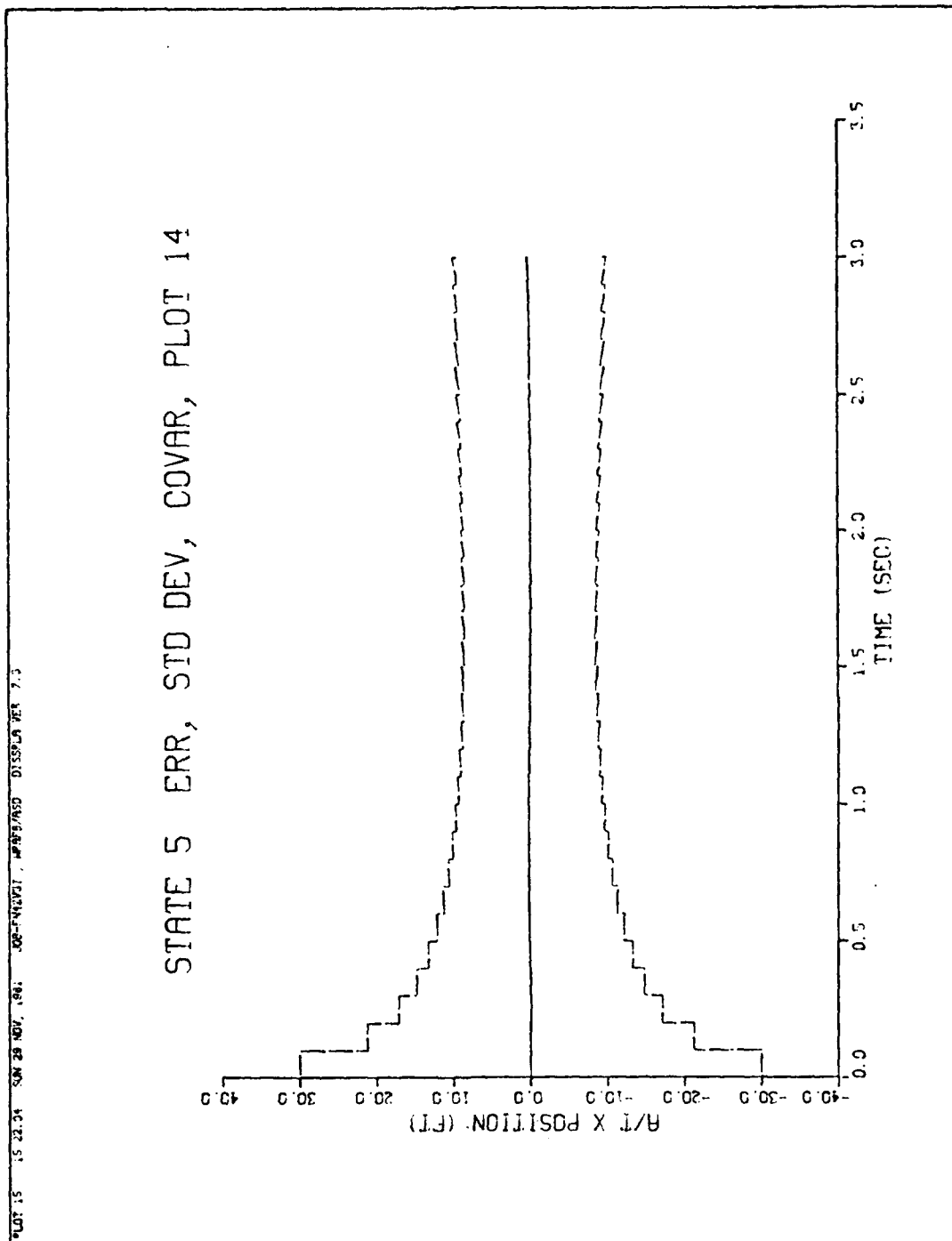
Fig F-34. $x_{A/T}$ Covariance With Three Measurements and No System Noise

F-34
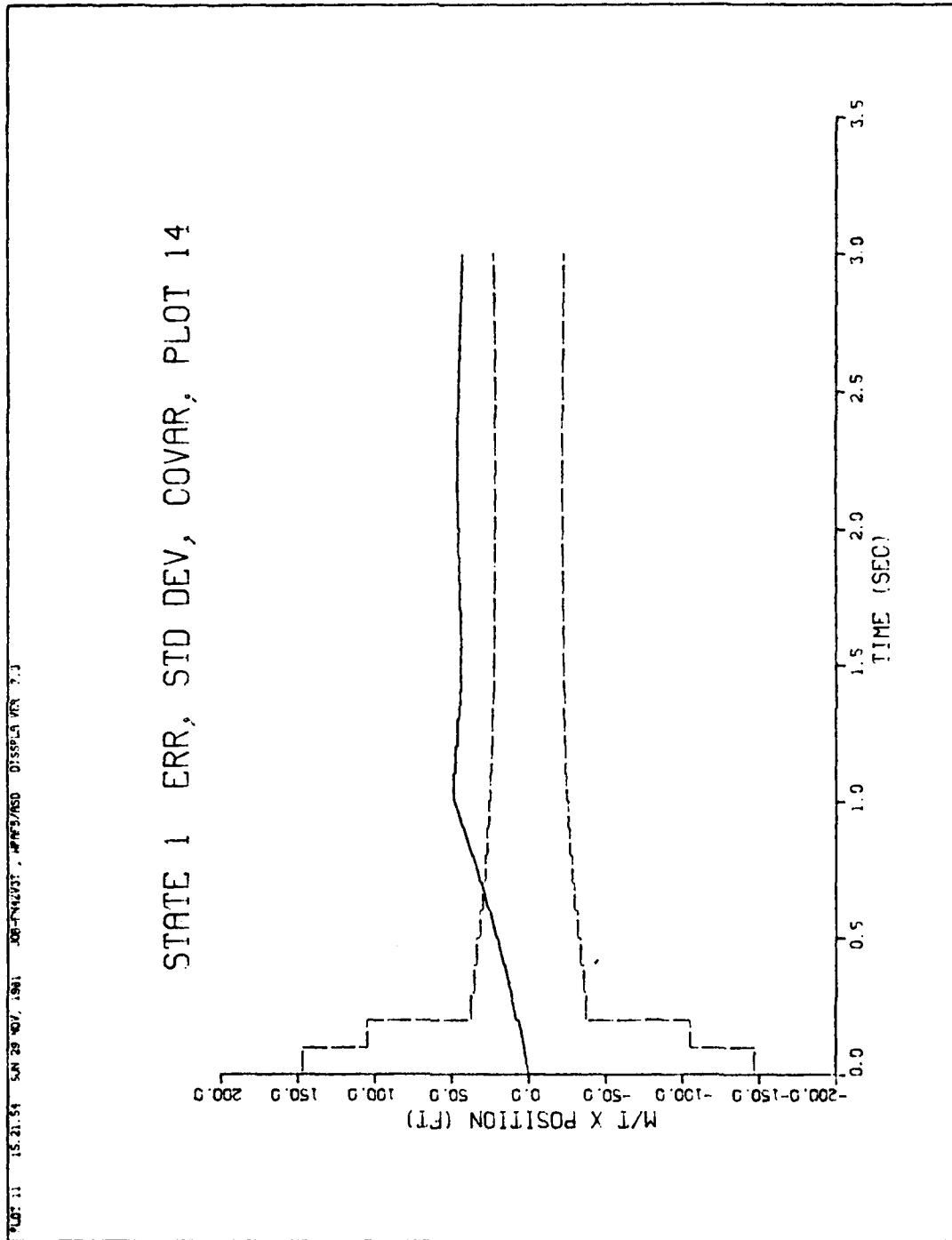
Fig F-35. $x_{M/T}$ State With Euler Integration and No Truth Model Noise

F-35
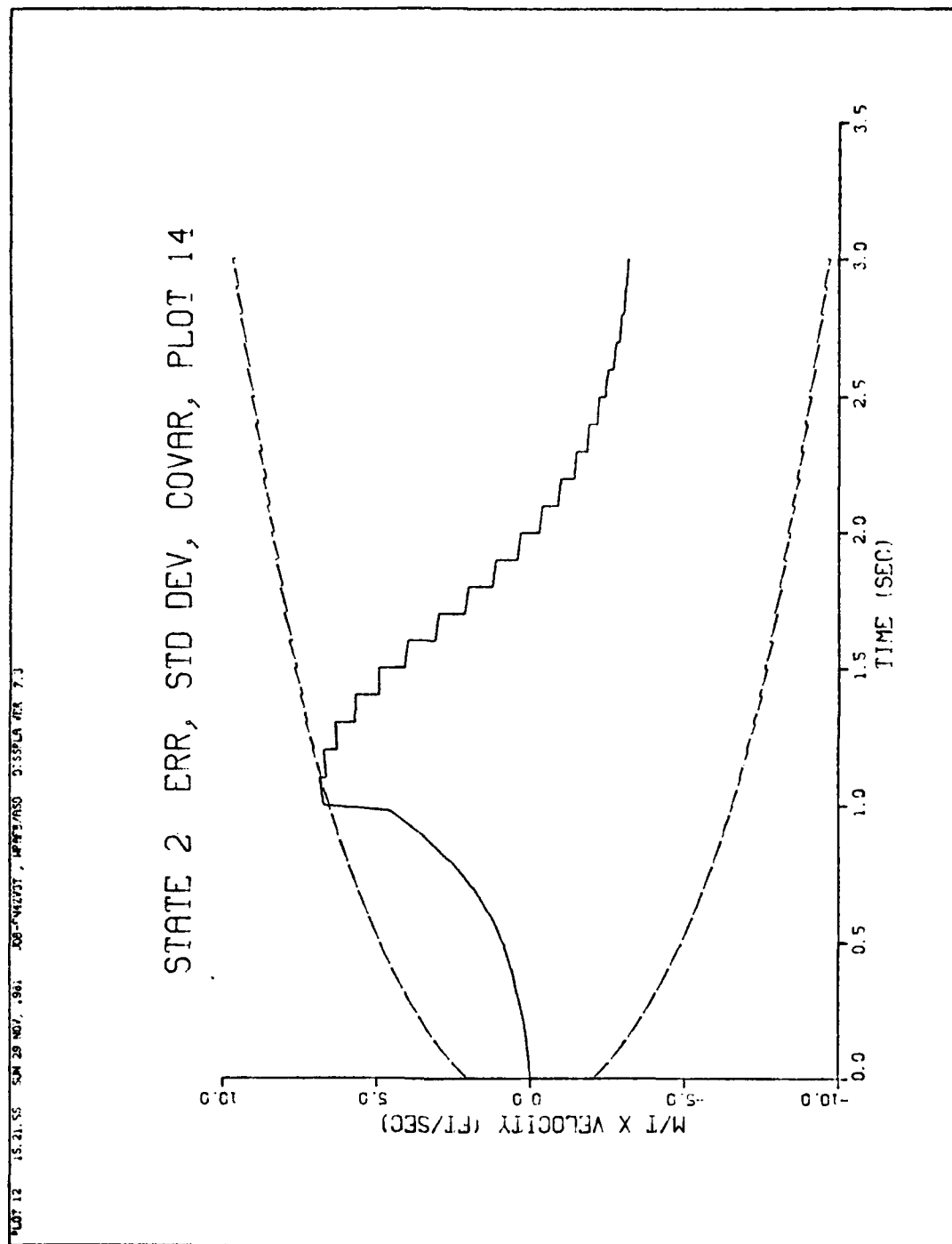
Fig F-36. $\dot{x}_{M/T}$ State With Euler Integration and No Truth Model Noise
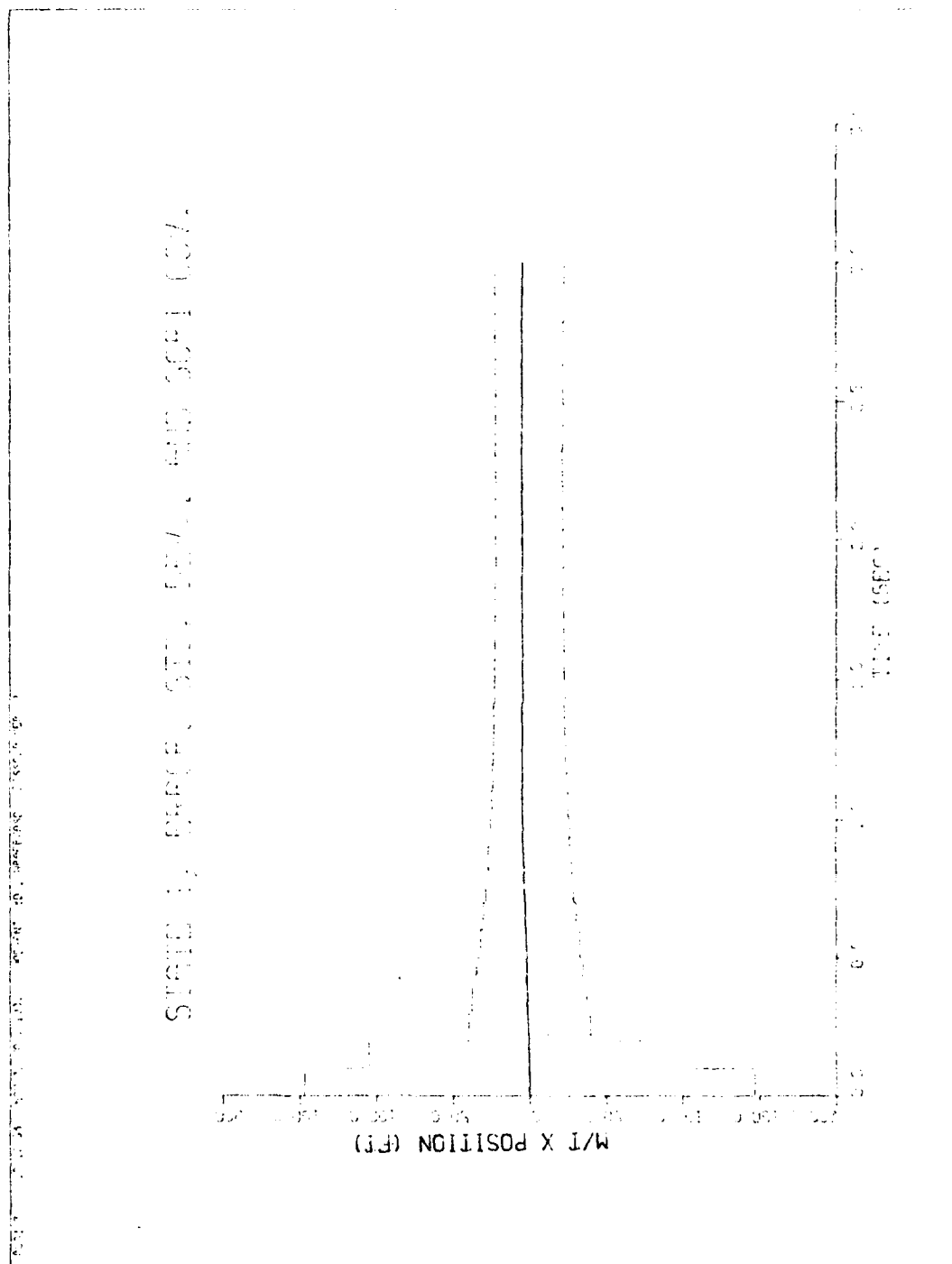
Fig F-37. $x_{M/T}$ State With Decreased Integration Step Size and No Truth Model Noise

STATE 2. EFFC3, STD. DEV., GNL STEP SIZE,

M/T X VELOCITY (FT/SEC)

Fig F-38. $\dot{x}_{M/T}$ State With Decreased Integration Step Size and No Truth Model Noise

STATE 1 ERR, STD DEV, COVAR, PLOT 14
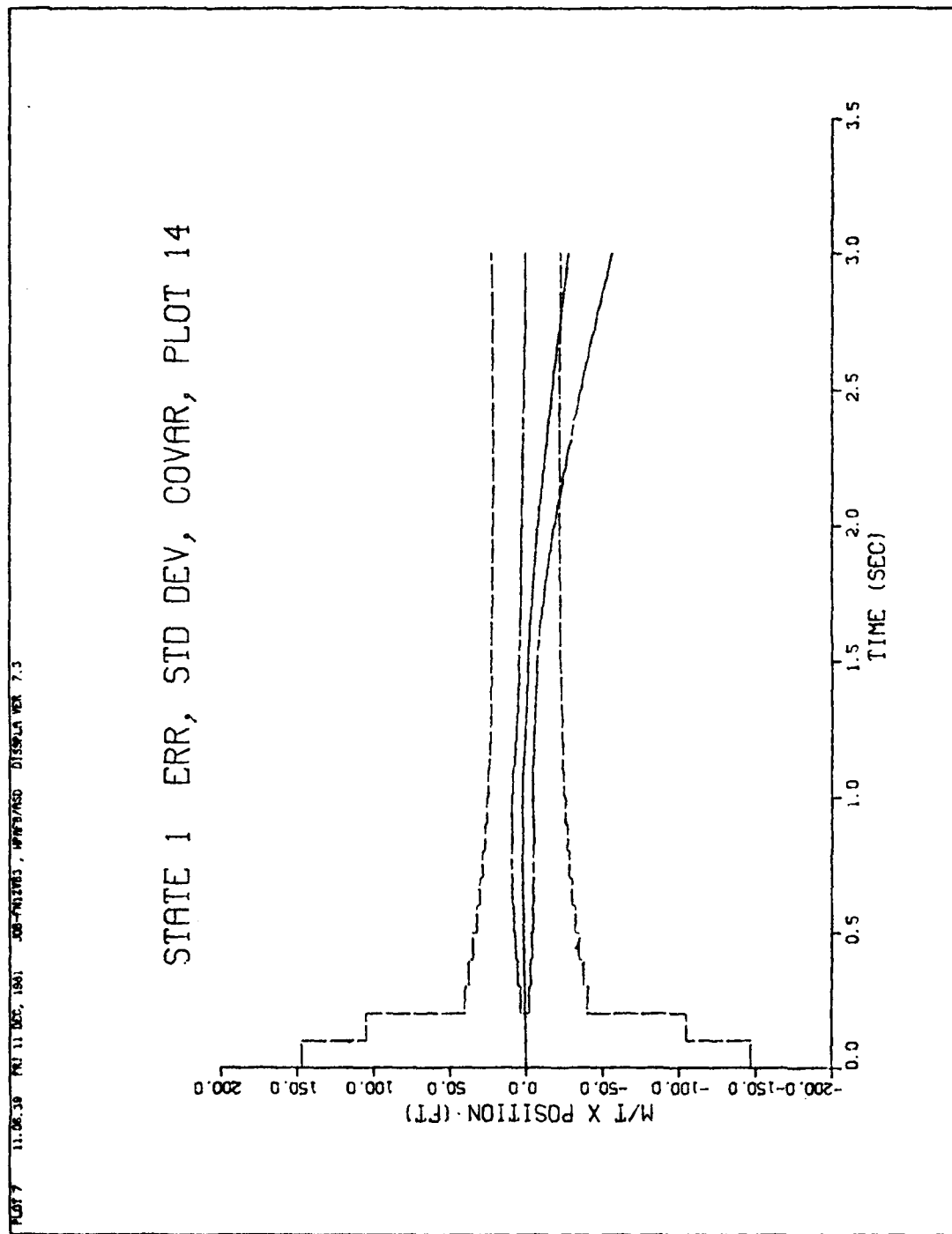
Fig F-39. $x_{M/T}$ State With Computed $\underline{P}$, $\underline{Q}$ and Dynamic Driving Noise
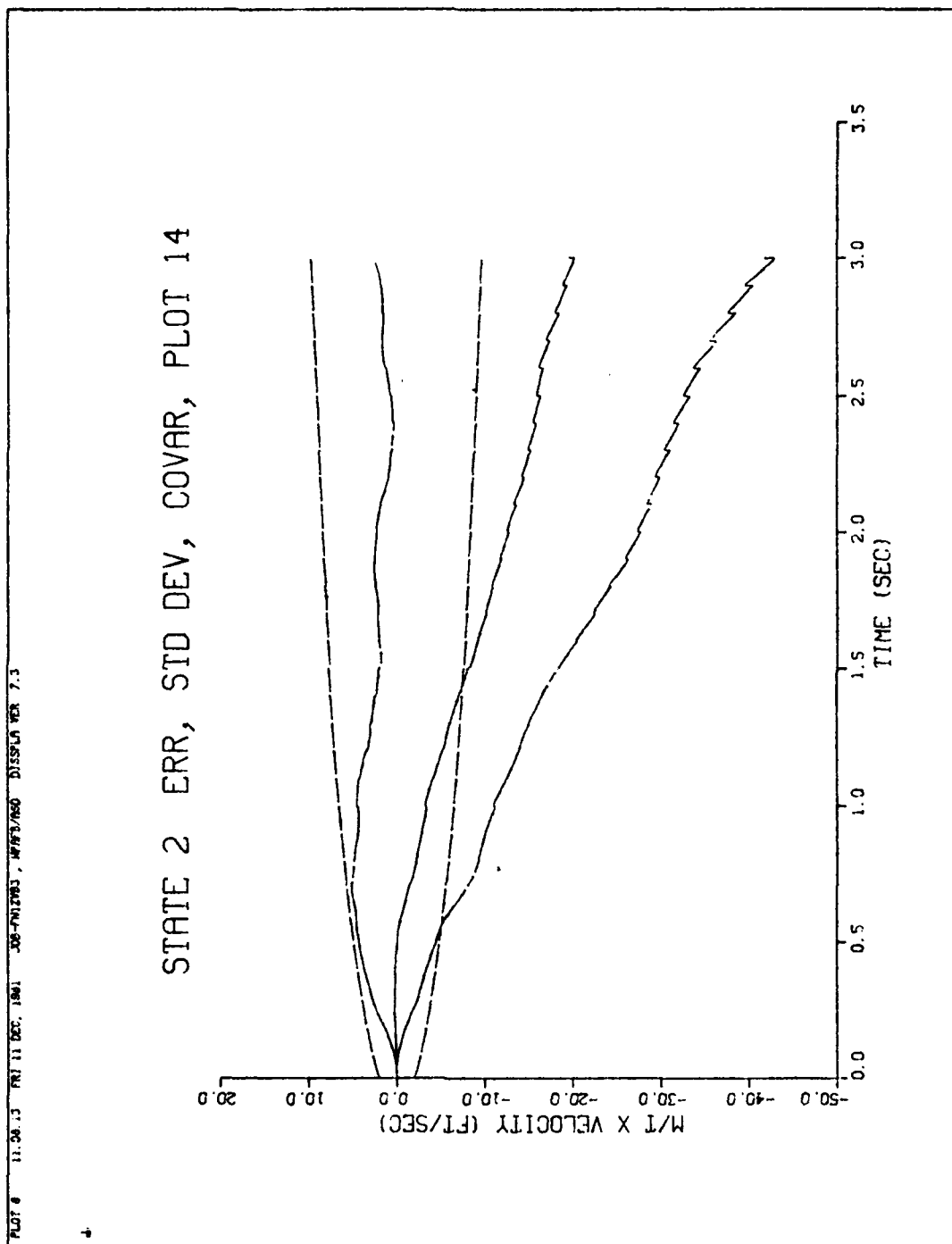
Fig F-40. $\dot{x}_{M/T}$ State With Computed $\underline{P}$, $\underline{Q}$ and Dynamic Driving Noise

F-40
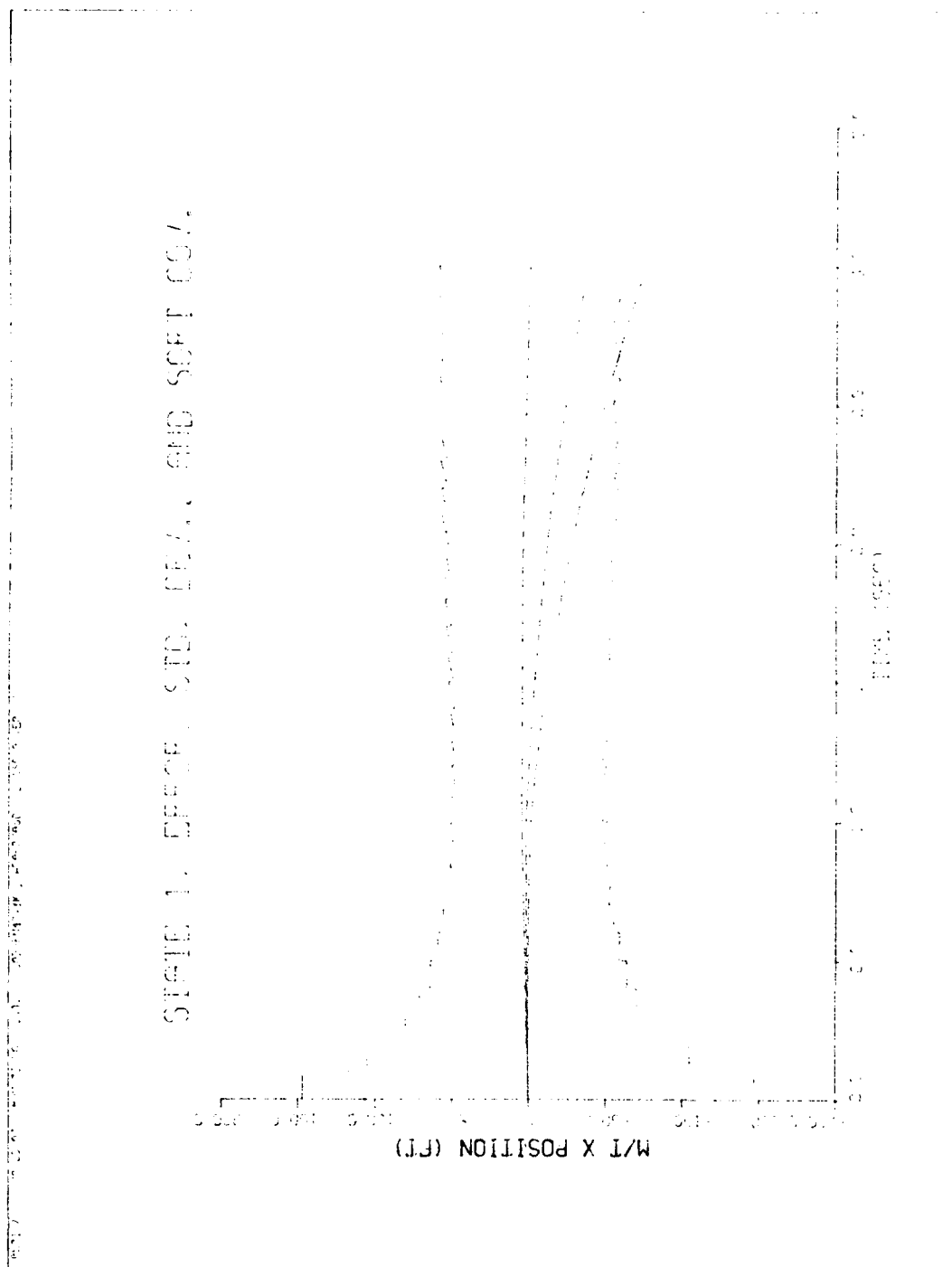
Fig F-41. $x_{M/T}$ State With Tuned Filter $\underline{Q}$ and Dynamic Driving Noise

Fig F-42. $\dot{x}_{M/T}$ State With Tuned Filter Q and Dynamic Driving Noise
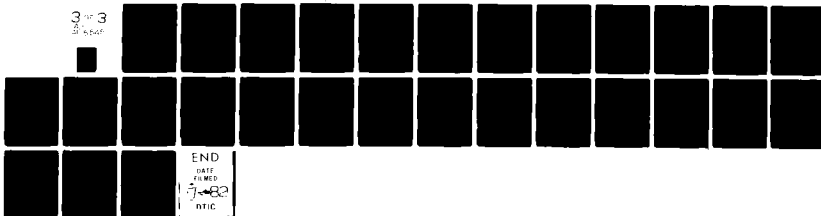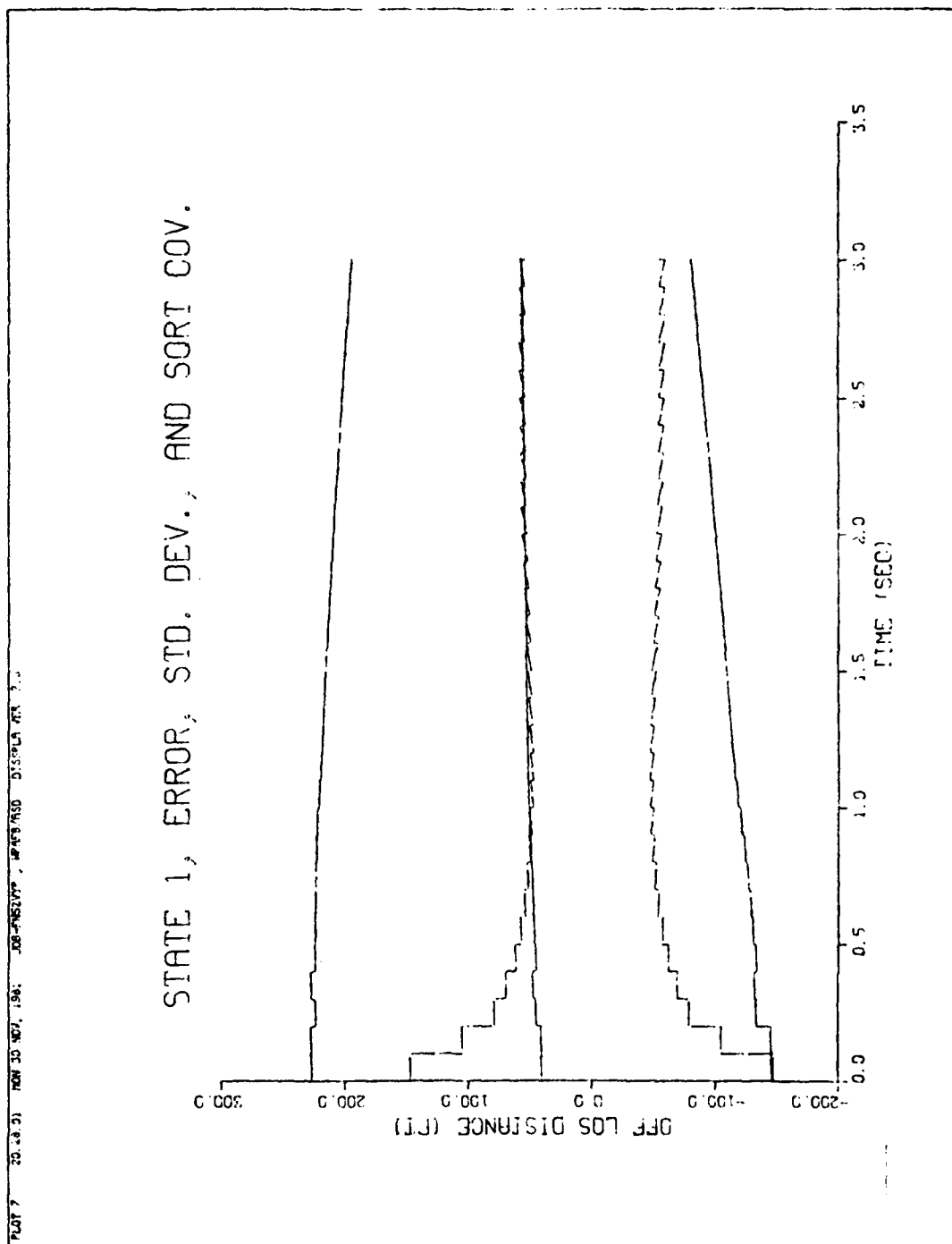
Fig F-43. $x_{M/T}$ State With Tuned Filter Q and Perturbed Initial Conditions
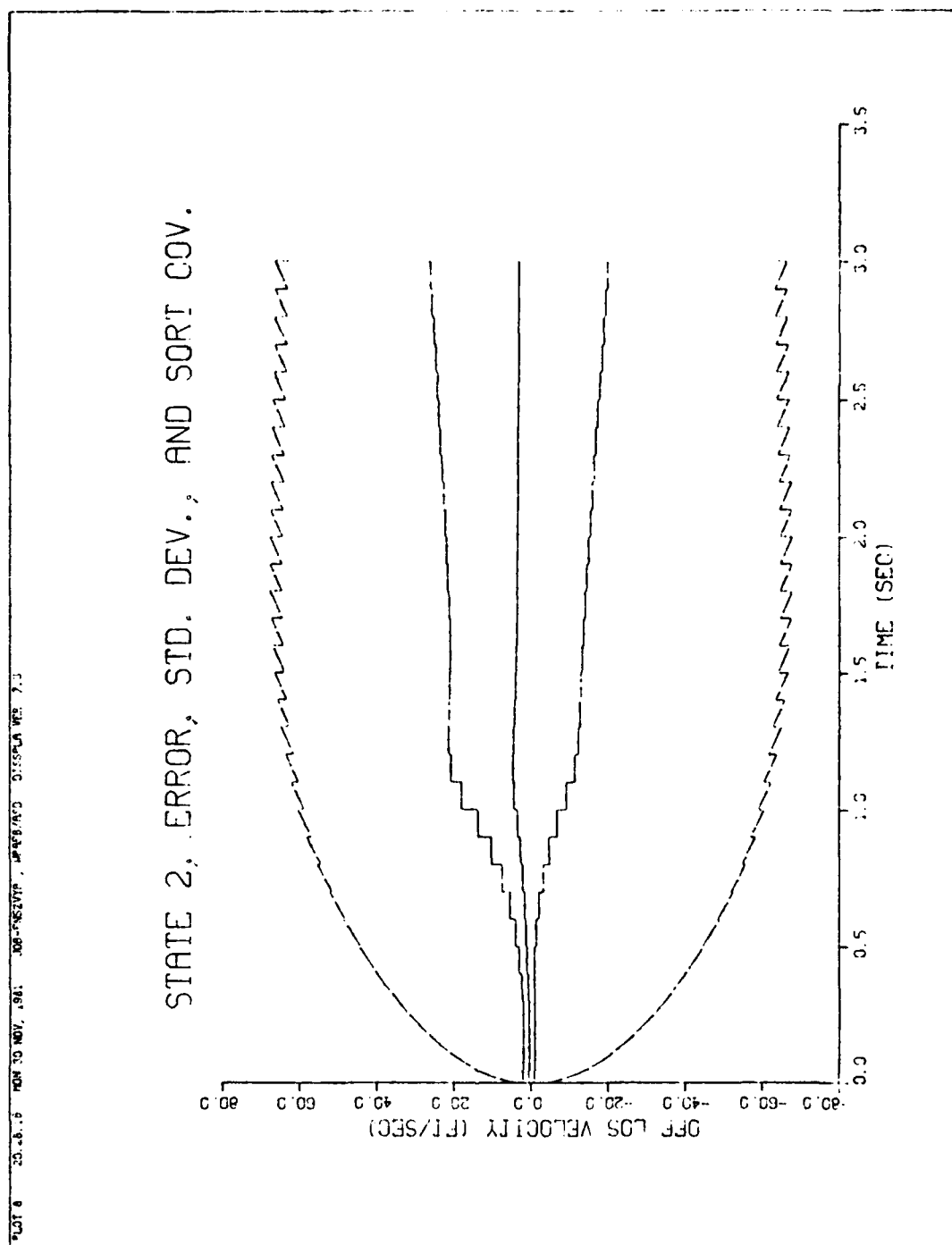
Fig F-44. $\dot{x}_{M/T}$ State With Tuned Filter Q and Perturbed Initial Conditions

Fig F-45. $x_{M/T}$ State Profile With Acquisition and Dynamic Driving Noise

F-45

FILTER STATE 2 AND TRUTH STATE 2, PLOT 3

Fig F-46. $\dot{x}_{M/T}$ State Profile With Acquisition and Dynamic Driving Noise

FILTER STATE 3 AND TRUTH STATE 3, PLOT 3

Fig F-47. $z_{M/T}$ State Profile With Acquisition and Dynamic Driving Noise

FILTER STATE 4 AND TRUTH STATE 4, PLOT 3
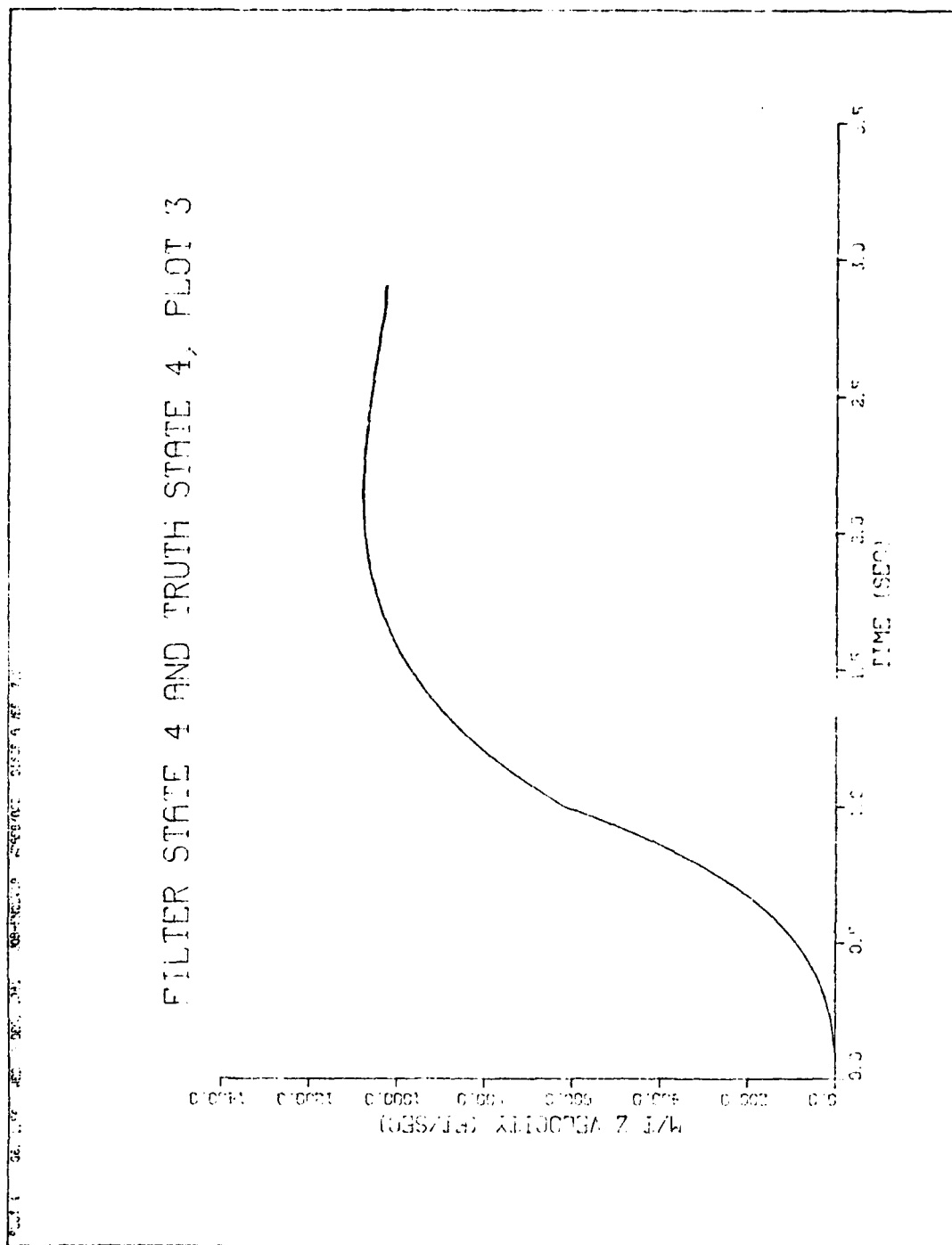
Fig F-48. $\dot{z}_{M/T}$ State Profile With Acquisition and Dynamic Driving Noise
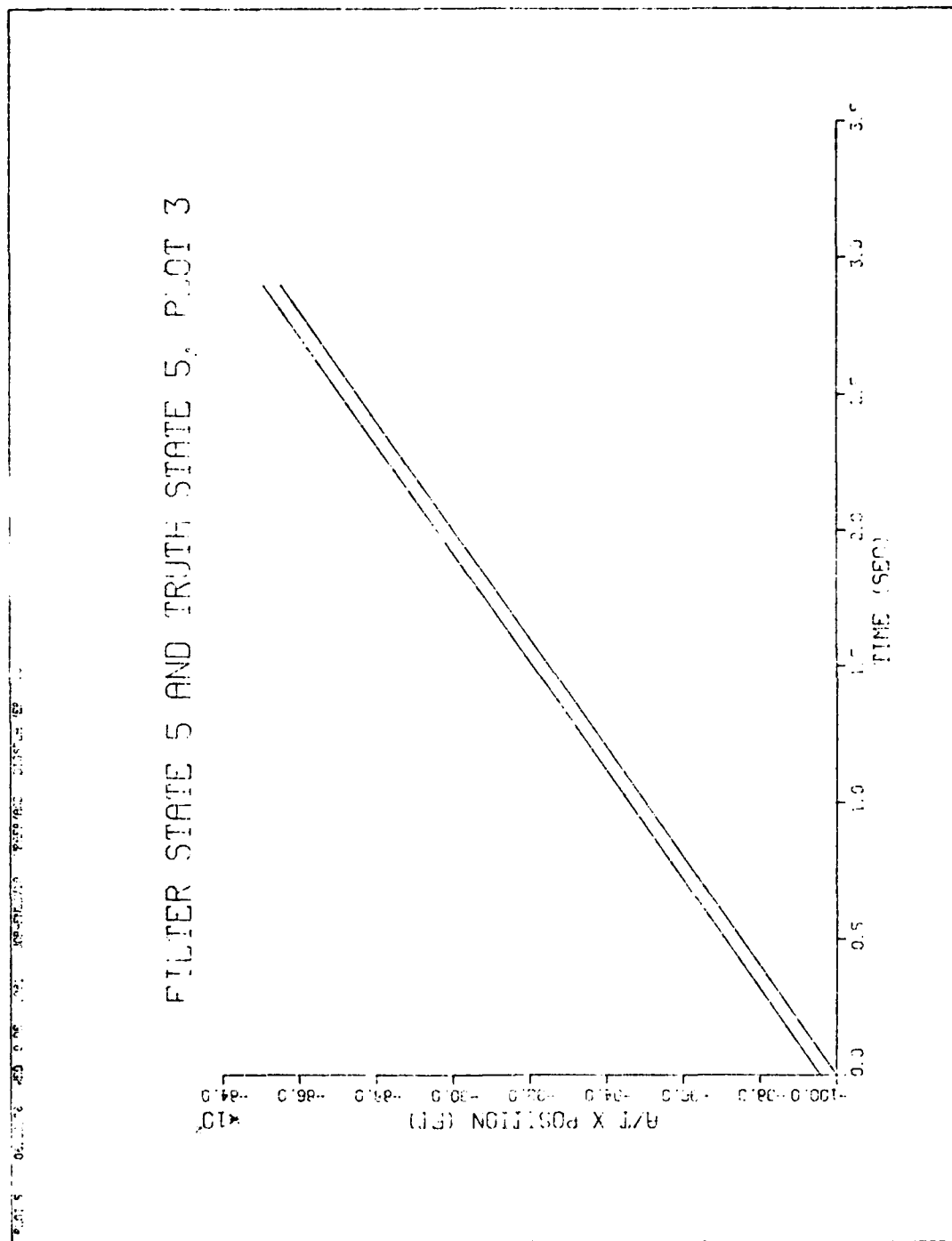
Fig F-49. $x_{A/T}$ State Profile With Acquisition and Dynamic Driving Noise

F-49
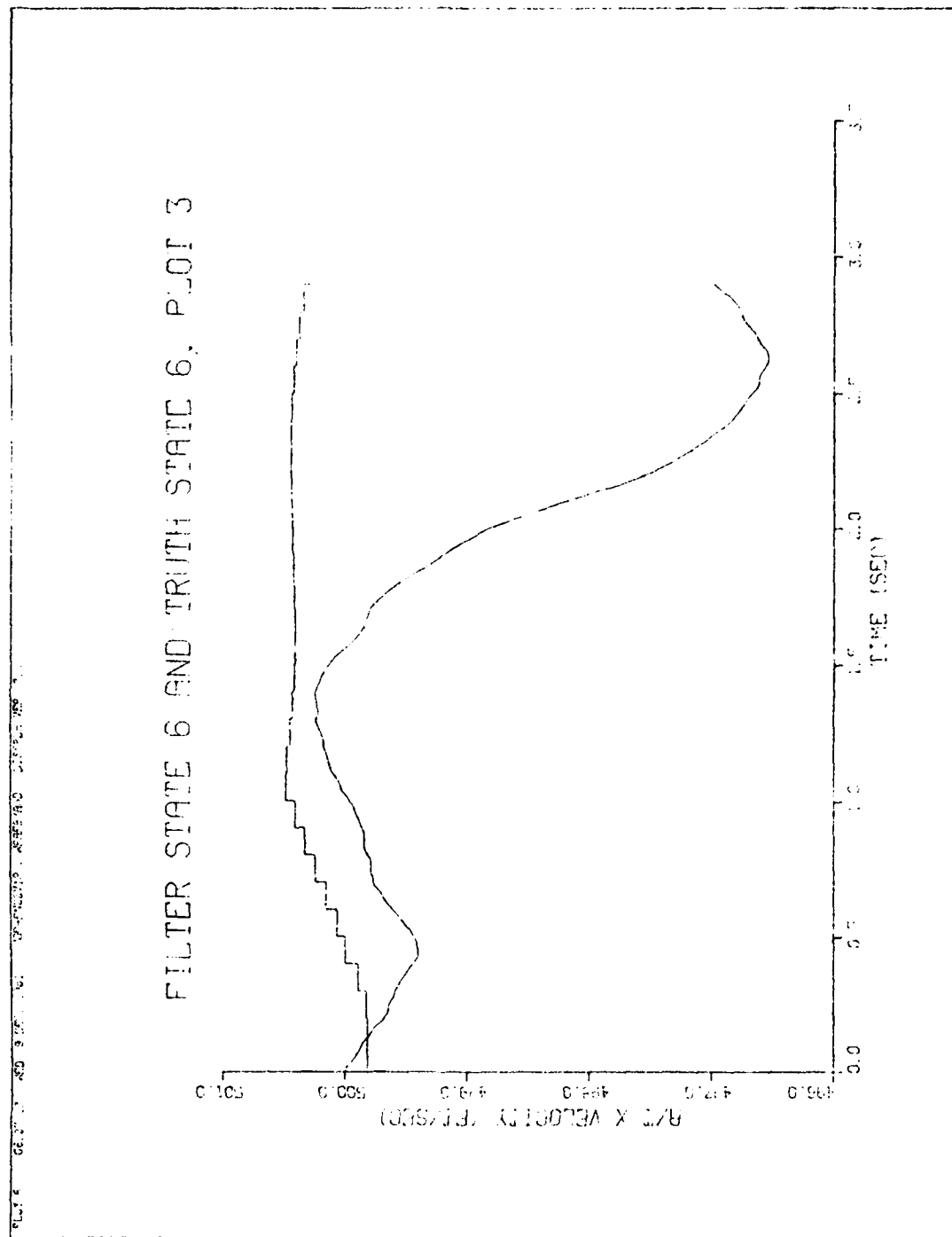
Fig F-50. $\dot{x}_{A/T}$ State Profile With Acquisition and Dynamic Driving Noise

STATE 1 ERR. STD DEV. COVAR. PLOT 14

Fig F-51. $x_{M/T}$ State Errors, Standard Deviation and Filter Covariance

F-51

STAGE 2 ERR. STD DEV. COVAR. PLOT 14

M/T X VELOCITY (FT/SEC)

TIME (SEC)

Fig F-52. $\dot{x}_{M/T}$ State Errors, Standard Deviation and Filter Covariance

Fig F-53. $z_{M/T}$ State Errors, Standard Deviation and Filter Covariance

STATE 4 ERR. STD DEV. COVAR. PLOT 14

M/T Z VELOCITY DEVIATION

TIME (SEC)
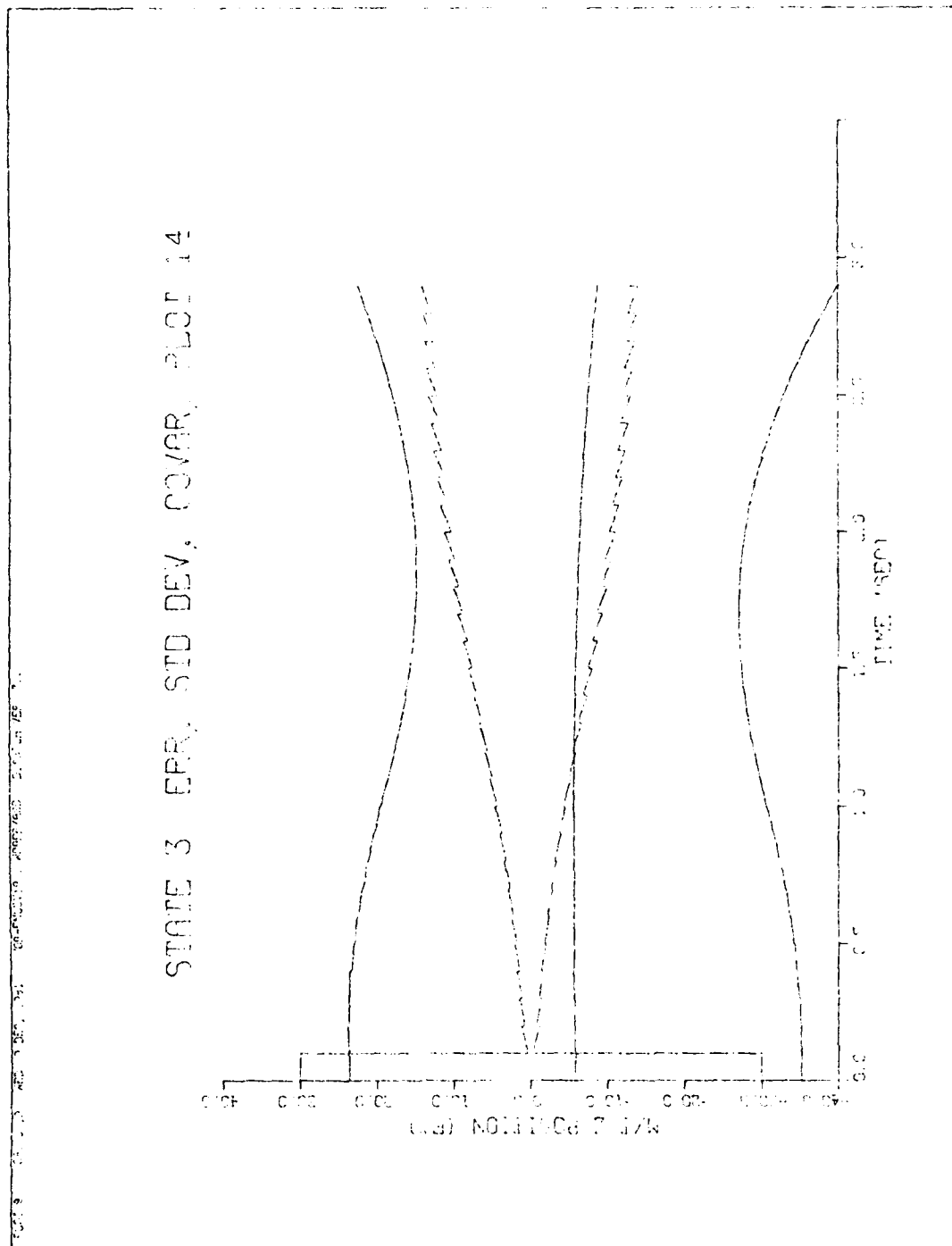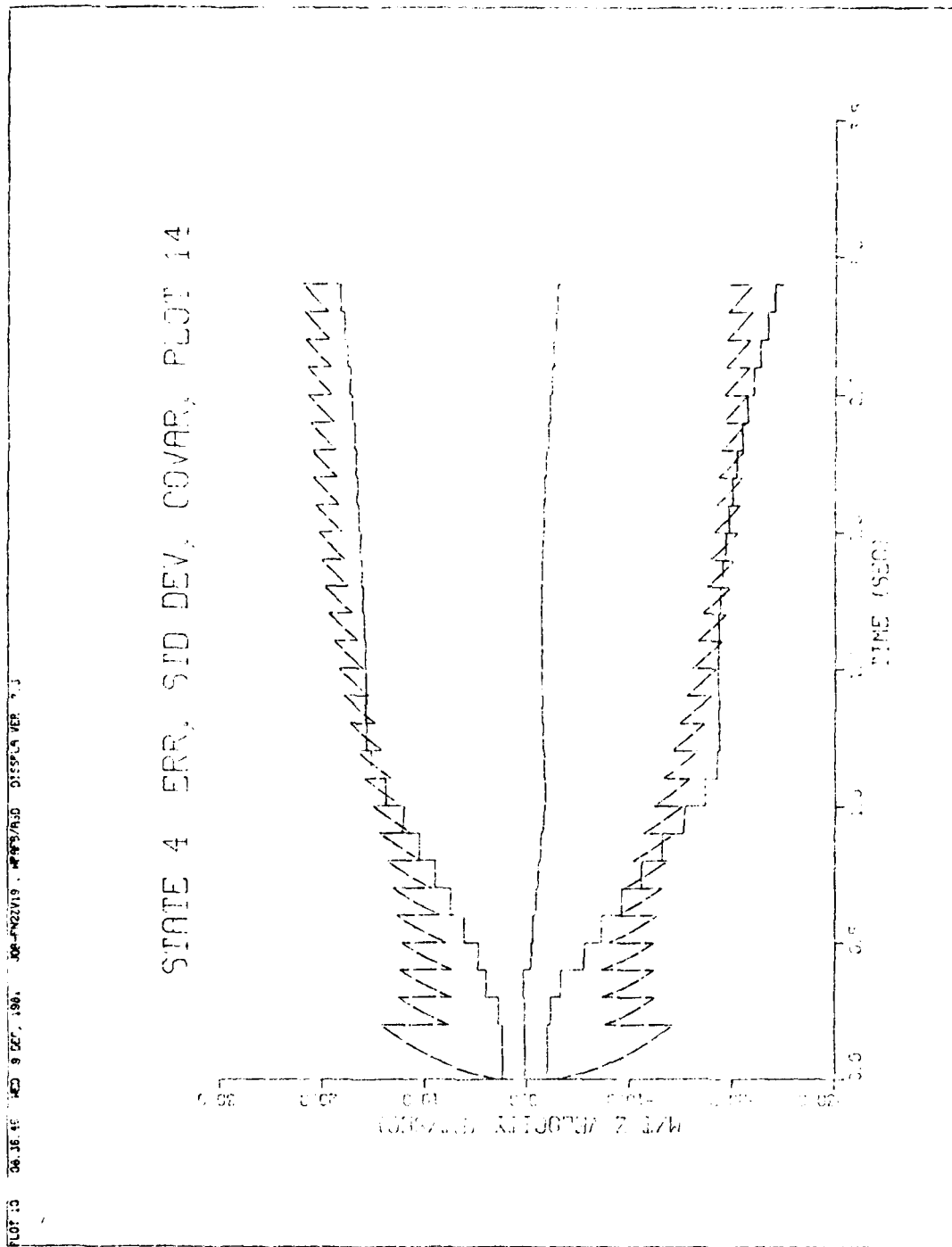
Fig F-54. $\dot{z}_{M/T}$ State Errors, Standard Deviation and Filter Covariance
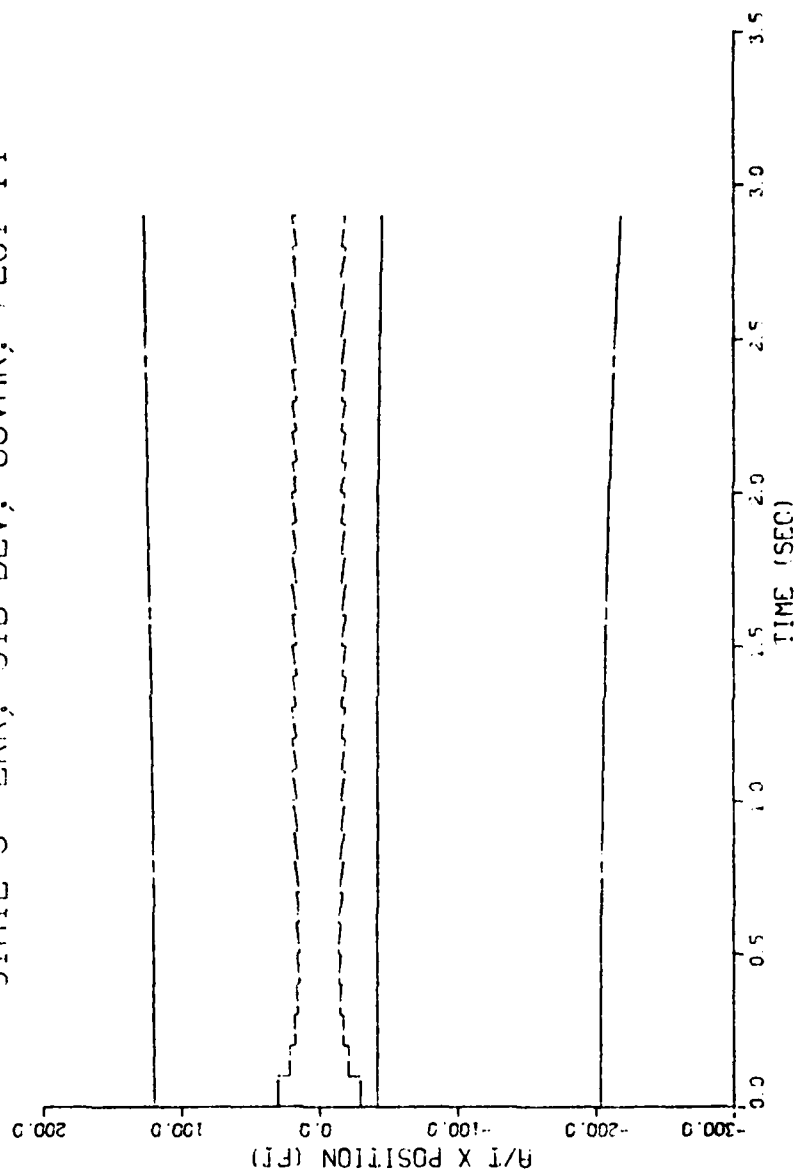
Fig F-55. $x_{A/T}$ State Errors, Standard Deviation and Filter Covariance

STATE 6 ERR, STD DEV. COVAR, PLOT 14

A/T X VELOCITY (FT/SEC)

TIME (SEC)
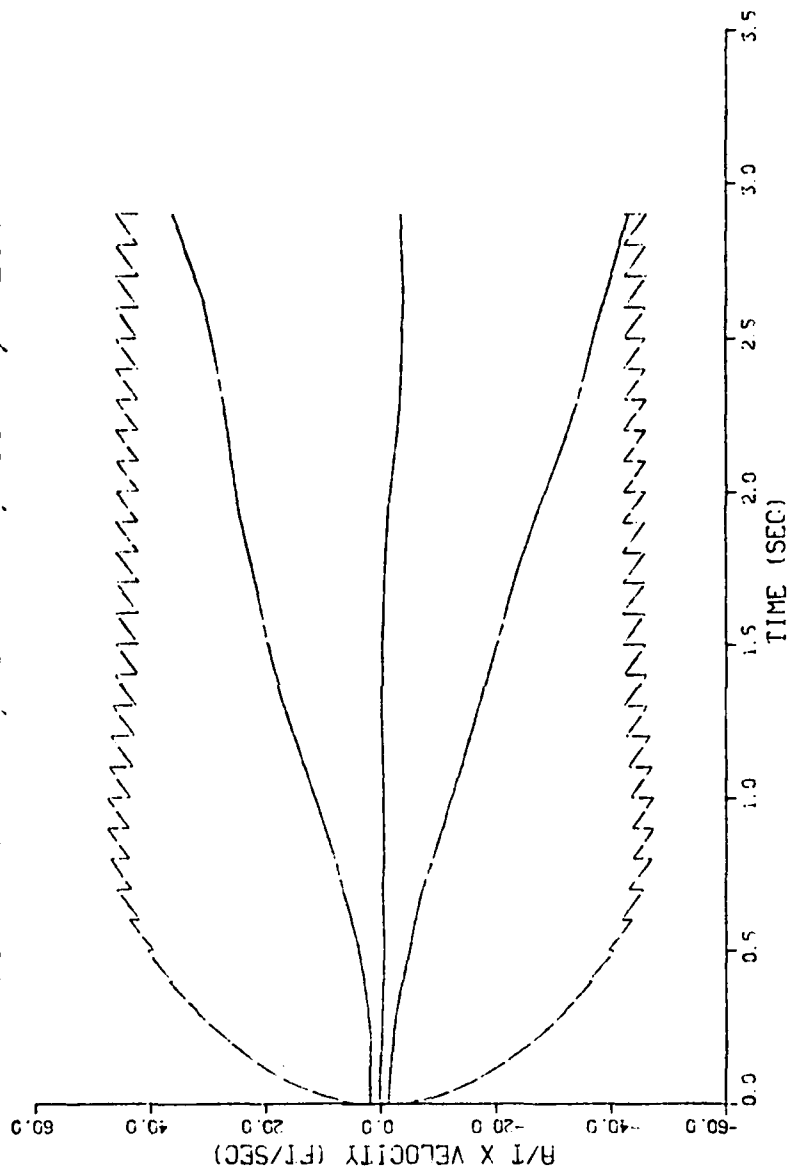
Fig F-56. $\dot{x}_{A/T}$ State Errors, Standard Deviation and Filter Covariance
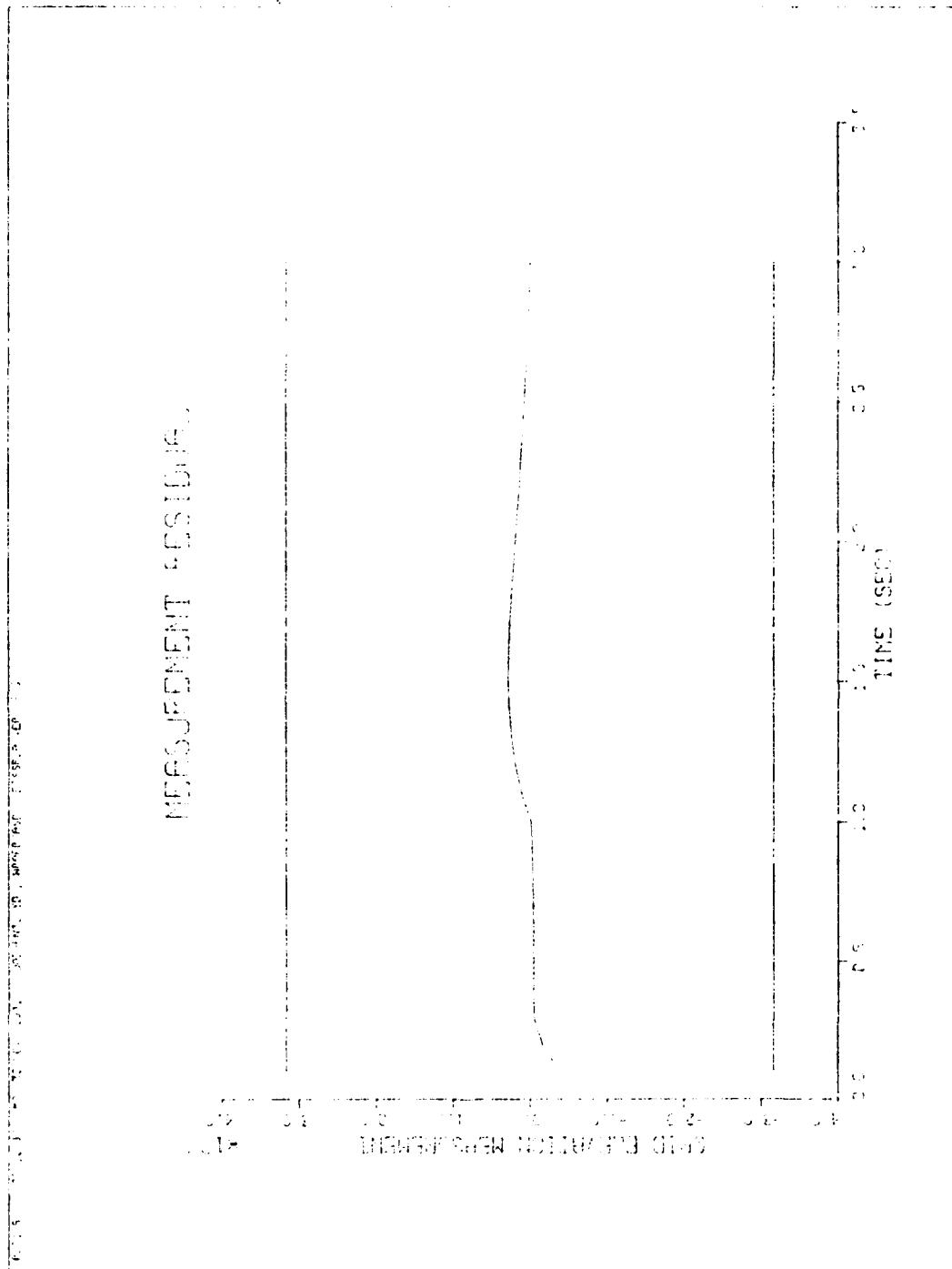
Fig F-57. Elevation Measurement Residual With No System Noise
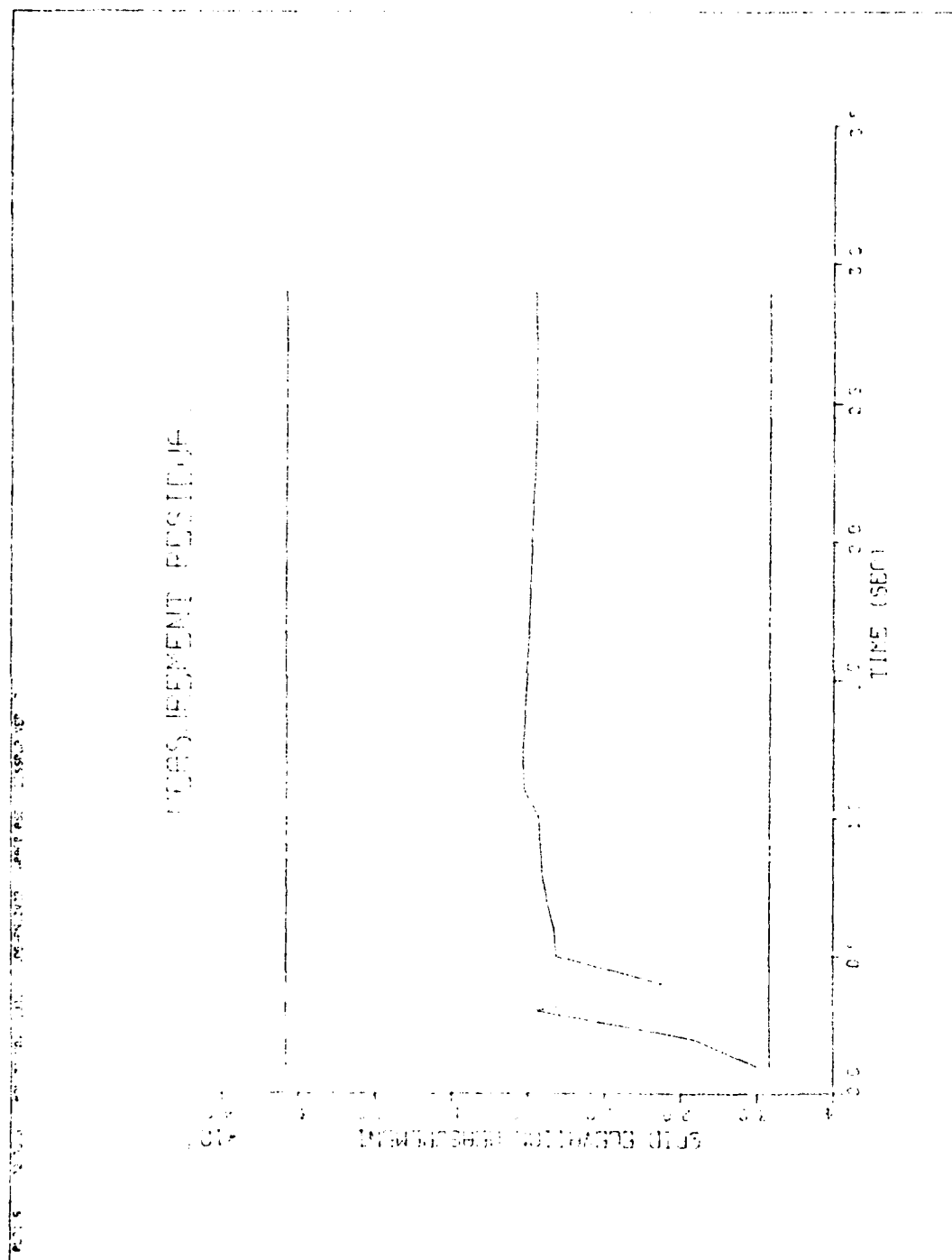
Fig F-58. Elevation Measurement Residual With System Noise

STATE 1 ERR, STD DEV, COVAR, PLOT 14
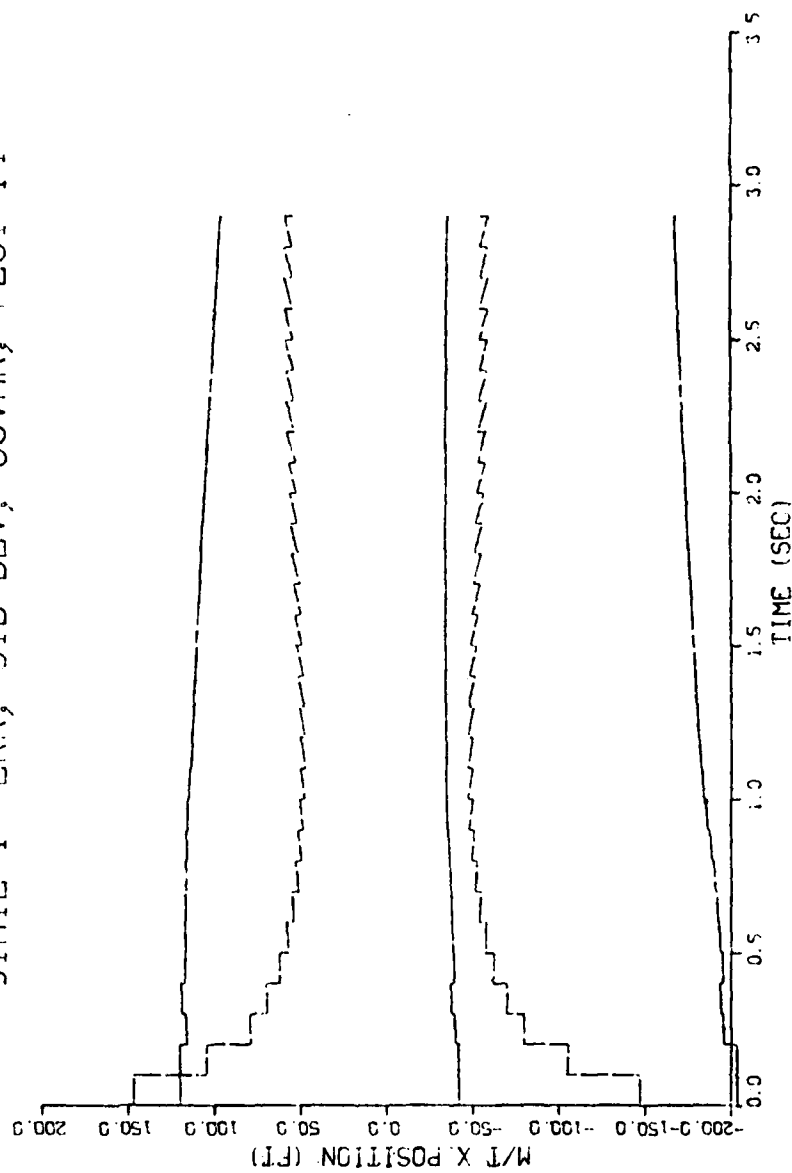
Fig F-59. Reduced Order Filter, $x_{M/T}$ State Errors
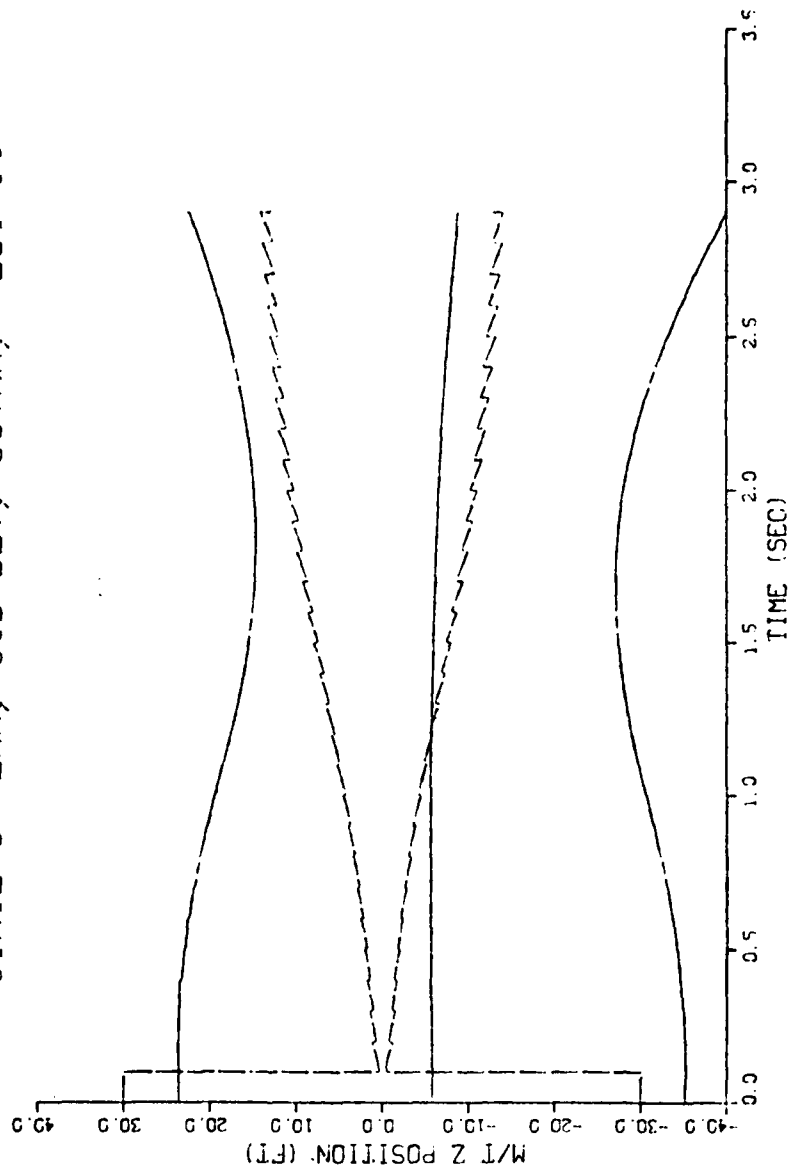
Fig F-61. Reduced Order Filter, $z_{M/T}$ State Errors

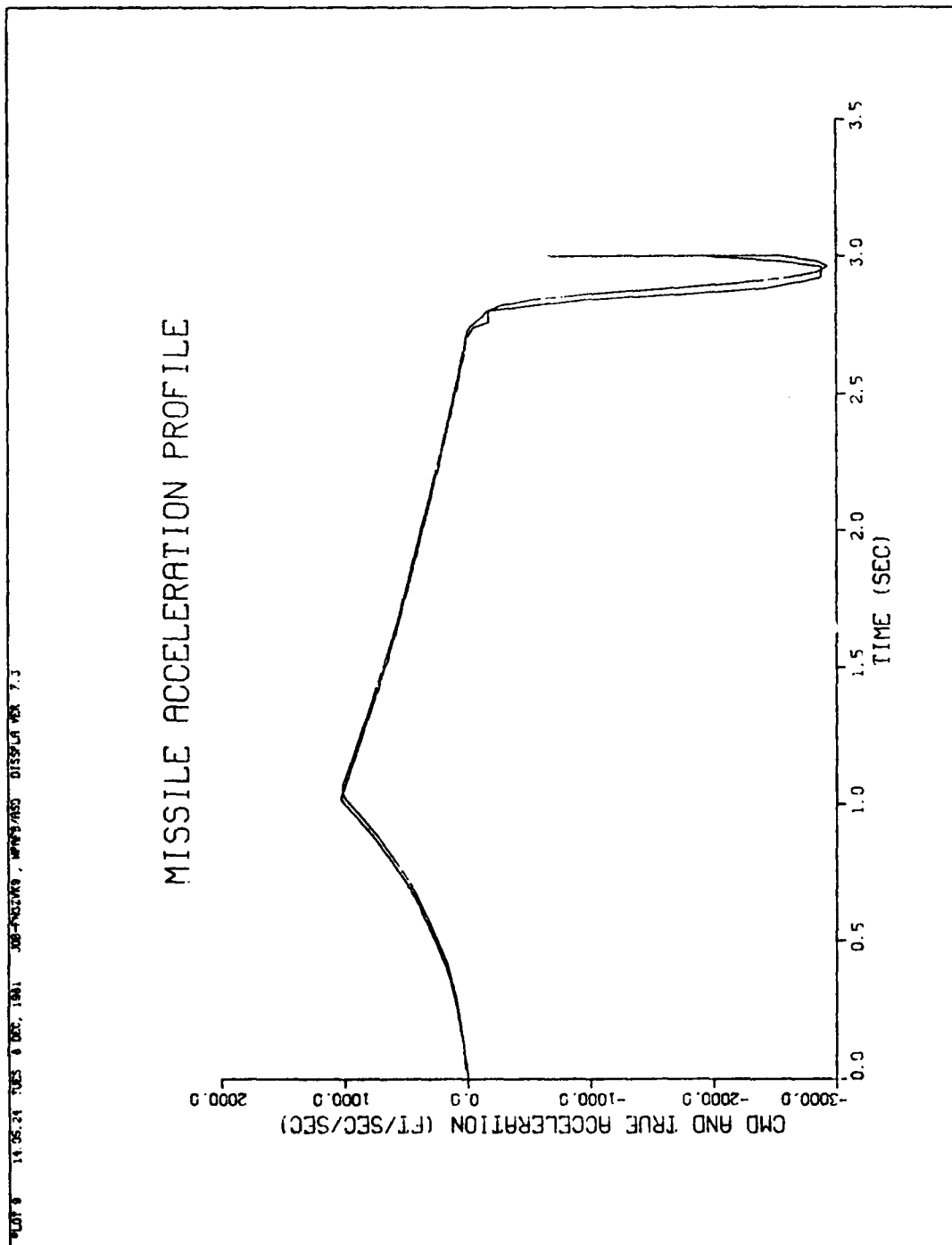Fig F-60. Reduced Order Filter, $\dot{x}_{M/T}$ State Errors

STATE 4 ERR, STD DEV, COVAR, PLOT 14

Fig F-62. Reduced Order Filter, $\dot{z}_{M/T}$ State Errors
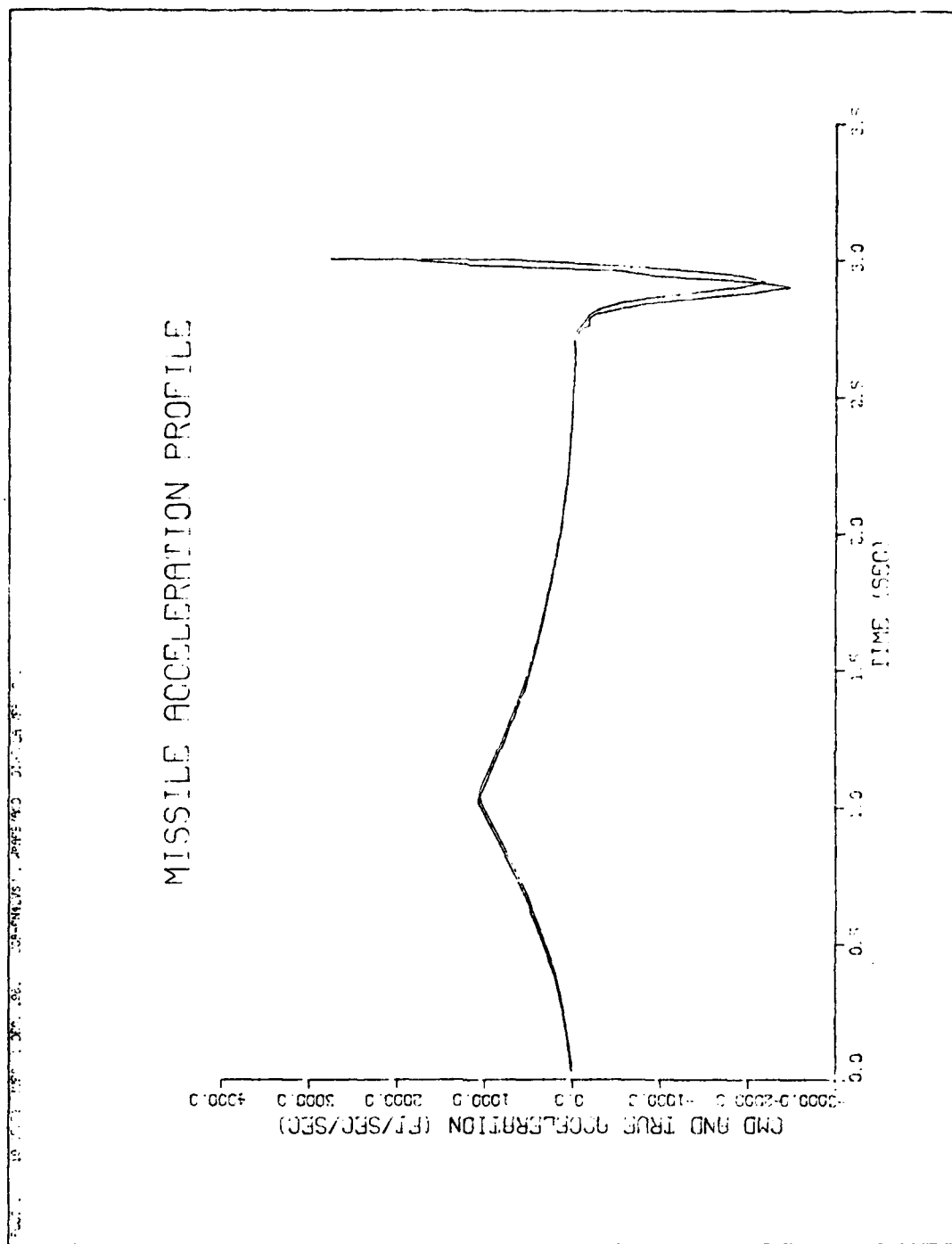
F-62
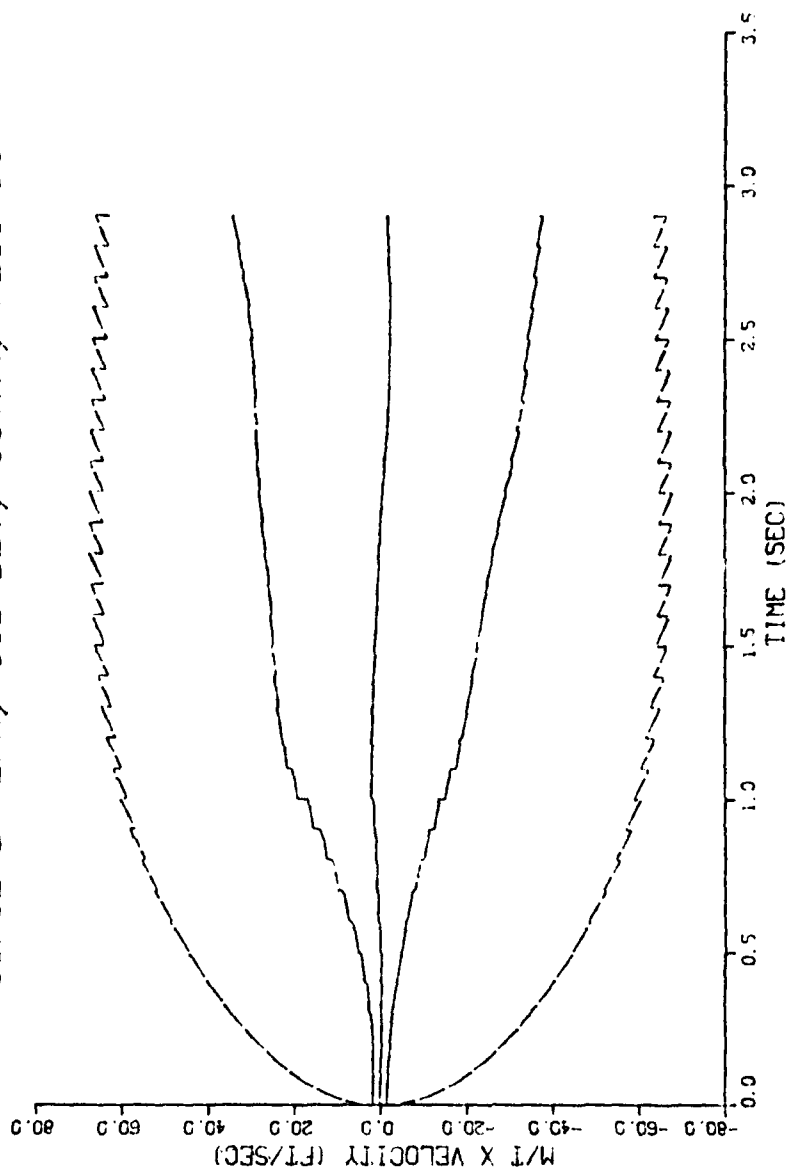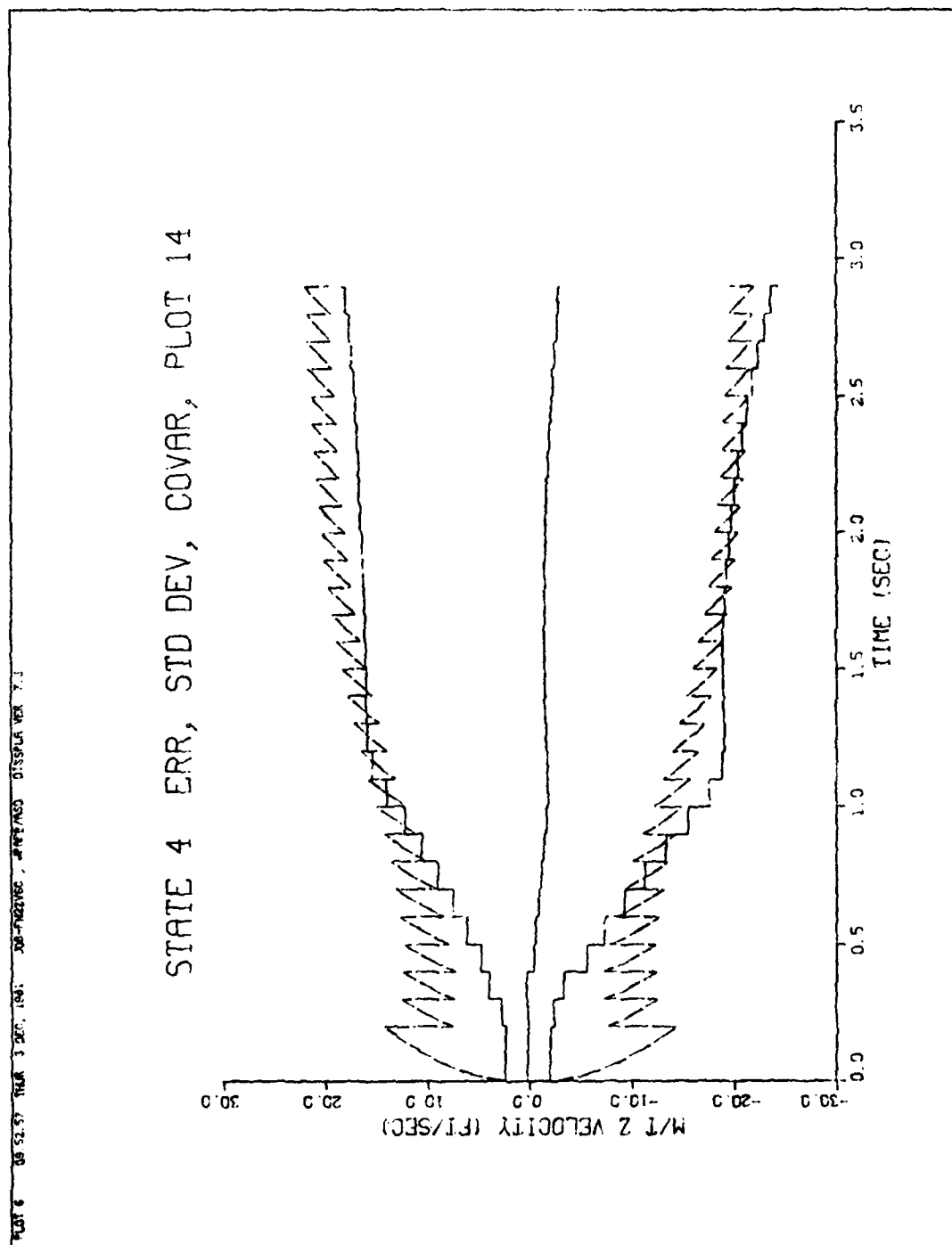
MISSILE ACCELERATION PROFILE

Fig F-63. Acceleration Profile With a Guidance Law Gain of 3

Fig F-64. Acceleration Profile With a Guidance Law Gain of 4
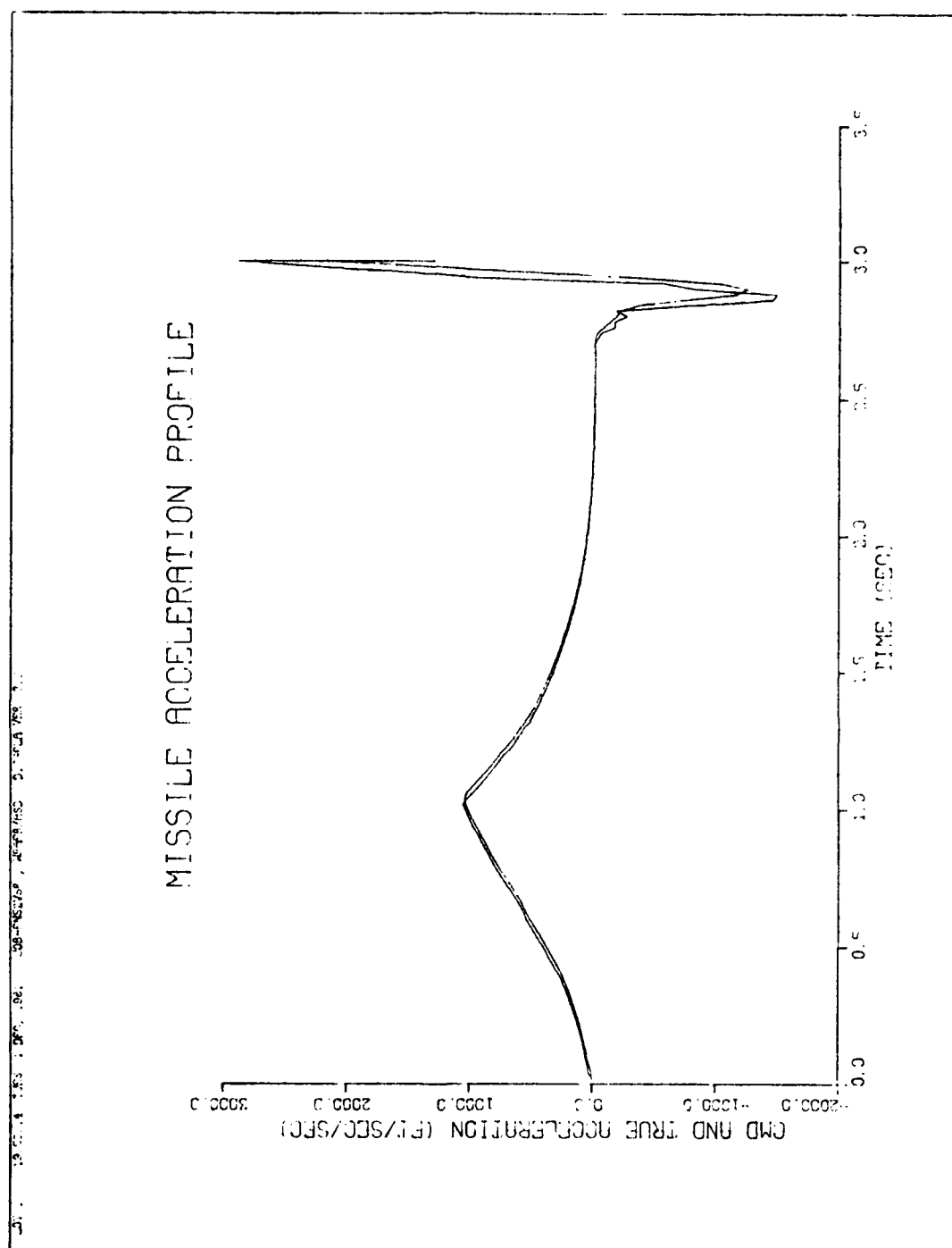
MISSILE ACCELERATION PROFILE

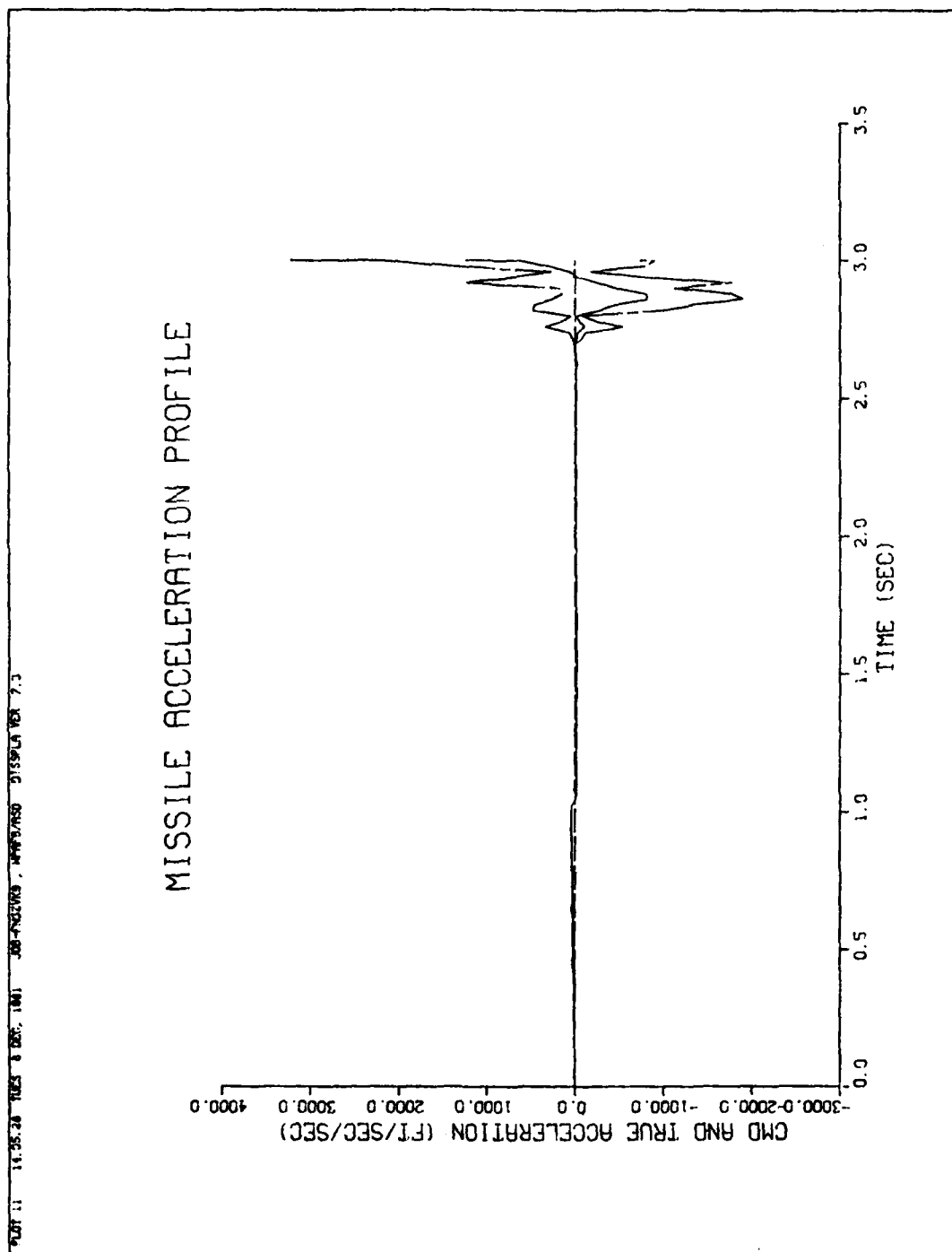Fig F-65. Acceleration Profile With a Guidance Law Gain of 5

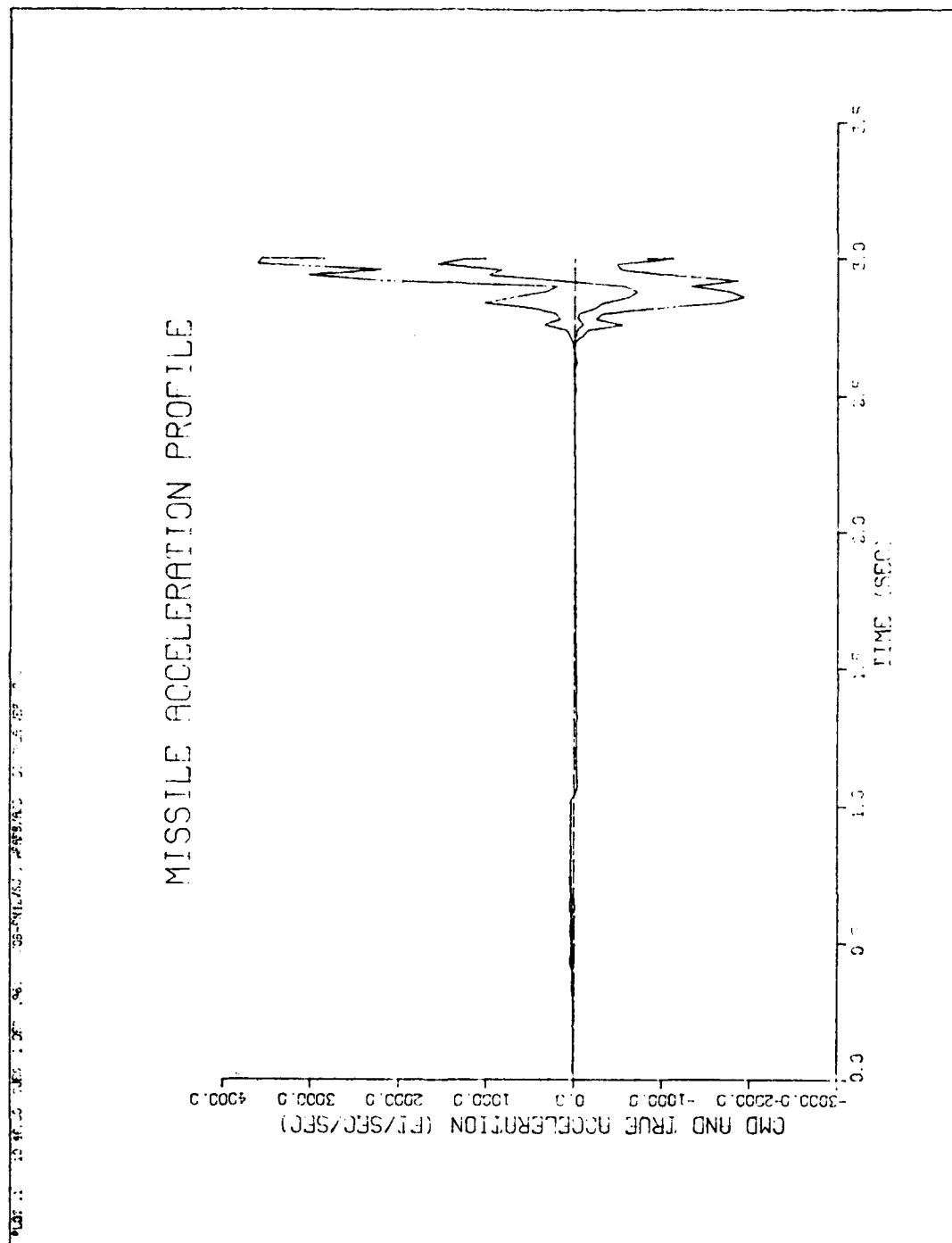Fig F-66. Acceleration Error With a Guidance Law Gain of 3

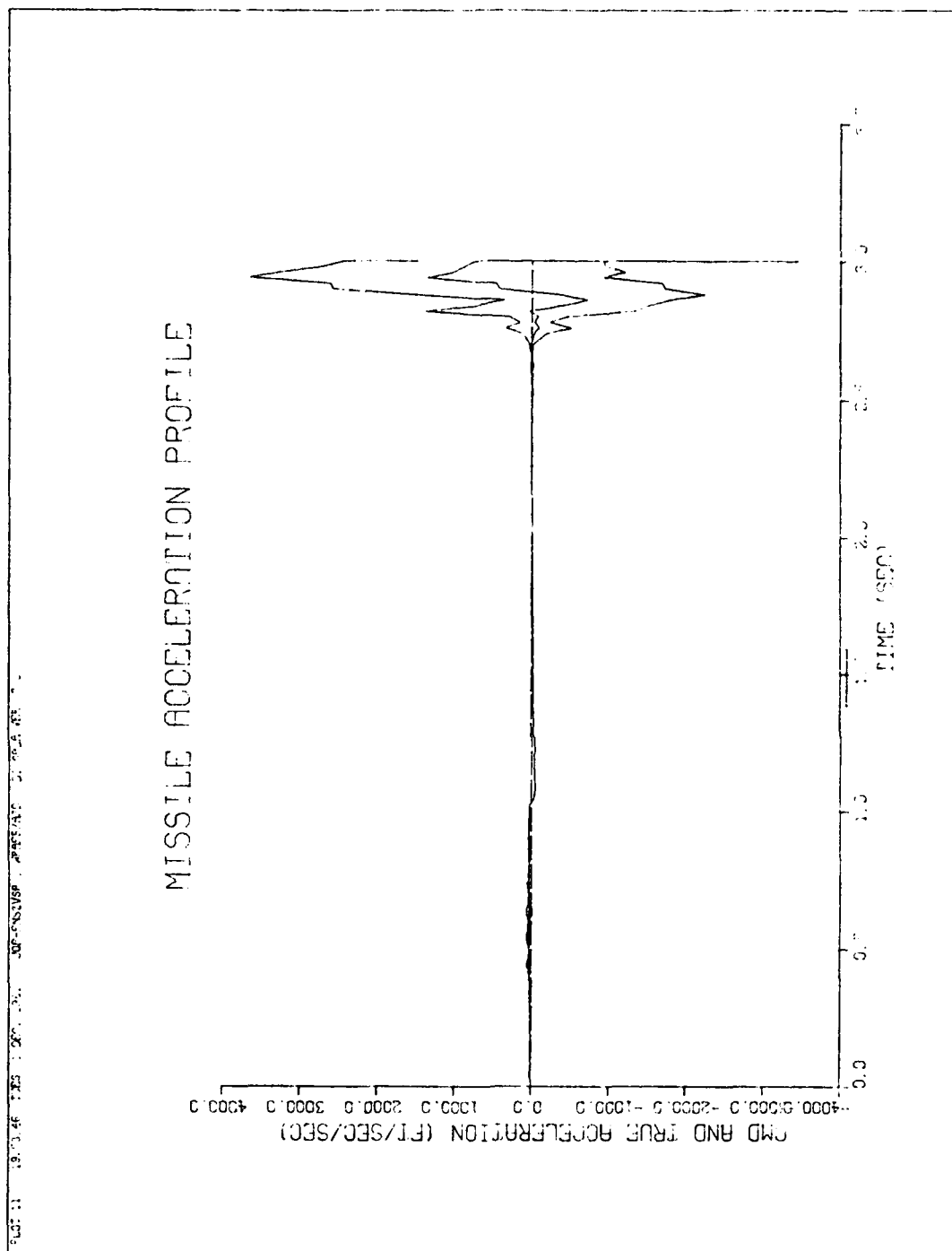Fig F-67. Acceleration Error With a Guidance Law Gain of 4

Fig F-68. Acceleration Error With a Guidance Law Gain of 5

VITA

Donald W. Capps was born on 16 April 1951 in Port St. Joe,
Florida. In 1969, he graduated from Port St. Joe High School. He
enlisted in the Air Force in 1971 and served as a digital data
technician until 1974. In that year, he was accepted into the Airman's
Education and Commissioning Program through which he received a
Bachelor of Science in Electrical Engineering from the University of
Florida at Gainesville, Florida. Upon completion of Officer Training
School in 1976, he was assigned as a project electrical engineer in the
Systems Management Division at Robins AFB, Georgia. In June 1980, he
entered the Graduate Electrical Engineering Program at the Air Force
Institute of Technology. Upon graduation in December 1981, he will be
assigned to the Armament Laboratory at Eglin AFB, Florida.

Donald Chris Nelson was born on 29 September 1948 in Clarkfield,
Minnesota. He graduated from high school in Clarkfield, Minnesota, in
1966 and attended the University of Minnesota, Minneapolis, Minnesota,
from which he received the degree of Bachelor of Electrical Engineering
in July 1971. Upon graduating he entered the Air Force on active duty
in August 1971 and completed technical school in June 1972 as a Special
Electronics Technician. He served as a satellite data analyst and
computer programmer with the Air Force Technical Application Center
first at Sunnyvale AFS, California, until March 1973 and then at
Patrick AFB, Florida, until November 1975. He entered Office Training
School and received his commission in January 1976. He served as an
engineer at the Air Force Armament Laboratory at Eglin AFB, Florida,
until entering the School of Engineering, Air Force Institute of
Technology in June 1980. He is a member of IEEE.

REPORT DOCUMENTATION PAGE	READ INSTRUCTIONS BEFORE COMPLETING FORM

1. REPORT NUMBER AFIT/GE/EE/81D-13	2. GOVT ACCESSION NO. AD-A115 545	3. RECIPIENT'S CATALOG NUMBER

4. TITLE (and Subtitle) A Comparative Analysis of Kalman Filters Using a Hypervelocity MIssile Simulation	5. TYPE OF REPORT & PERIOD COVERED MS Thesis
	6. PERFORMING ORG. REPORT NUMBER

7. AUTHOR(s) Donald W. Capps and Donald C. Nelson Capt USAF Capt USAF	8. CONTRACT OR GRANT NUMBER(s)

9. PERFORMING ORGANIZATION NAME AND ADDRESS Air Force Institue of Technology (AFIT-EN Wright-Patterson AFB, Ohio 45433	10. PROGRAM ELEMENT, PROJECT, TASK AREA & WORK UNIT NUMBERS

11. CONTROLLING OFFICE NAME AND ADDRESS	12. REPORT DATE December 1981
	13. NUMBER OF PAGES 208

14. MONITORING AGENCY NAME & ADDRESS(if different from Controlling Office)	15. SECURITY CLASS. (of this report) Unclassified
	15a. DECLASSIFICATION/DOWNGRADING SCHEDULE

16. DISTRIBUTION STATEMENT (of this Report)

Approved for public release; distribution unlimited.

17. DISTRIBUTION STATEMENT (of the abstract entered in Block 20, if different from Report)

15 APR 1982

18. SUPPLEMENTARY NOTES

Approved for public release IAW AFR 190-17

FREDERIC C. LYNCH, Major, USAF
Director of Public Affairs

Dean for Research and
Professional Development
Air Force Institute of Technology (ATC)
Wright-Patterson AFB, OH 45433

19. KEY WORDS (Continue on reverse side if necessary and identify by block number)

Extended Kalman Filter
Air-to-Surface Missile
Proportional Guidance
Angle-Only Measurements

20. ABSTRACT (Continue on reverse side if necessary and identify by block number)

    A systematic procedure is used to design Kalman filters for a hypervelocity missile system. The procedure includes truth model development, state space model formulation, filter tuning, and Monte Carlo analysis. The study is based upon a planar engagement of highly dynamic missile, a constant-velocity aircraft, and a stationary target. Two line-of-sight filters are developed using the rotating aircraft-to-target line-of-sight frame as a reference and two inertial filters are developed using an inertial frame freference. The

DD FORM 1473 EDITION OF 1 NOV 65 IS OBSOLETE
1 JAN 73

angle between the aircraft-to-target line-of-sight and the aircraft-to-missile line-of-sight is the only physical measurement processed by the filters. Due to observability considerations, the inertial filters also process additional pseudo-measurements of range. The filters are compared by calulation of miss distance statistics, probability of kill, and computational loading.